UNIVERSITY OF SOUTHAMPTON

FACULTY OF ENGINEERING AND THE ENVIRONMENT

Institute of Sound and Vibration Research

The effects of cubic damping on vibration isolation

by

Nuttarut Pananda

Thesis for the degree of Doctor of Philosophy

June 2014

UNIVERSITY OF SOUTHAMPTON

ABSTRACT

FACULTY OF ENGINEERING AND THE ENVIRONMENT

Institute of Sound and Vibration Research

Thesis for the degree of Doctor of Philosophy

THE EFFECTS OF CUBIC DAMPING ON VIBRATION ISOLATION

by Nuttarut Pananda

Vibration isolators are often assumed to possess linear viscous damping which has well known consequences for their performance. However, damping may be designed to be or prove to be nonlinear. This study investigates the effect of cubic damping, as an example of damping nonlinearity, in a single degree of freedom (SDOF) vibration isolation system. The response behaviour due to two excitation types, namely harmonic and broadband excitations, was examined.

For harmonic excitation, the Harmonic Balance Method (HBM) was applied to yield approximate closed form solutions and simplified analytical expressions implicitly show the influence of cubic damping for particular frequency regions. The HBM solutions were verified using direct numerical integration. The presence of cubic damping proves to be beneficial for the force excited case. It reduces response amplitude around the resonance frequency and has similar response to an undamped system in the isolation region. In contrast, for base excitation, the cubic damping is detrimental at high excitation frequencies as the base excitation and isolated mass move almost together. The effect becomes more pronounced for larger excitation amplitudes.

The case of base excitation was then considered for broadband excitation. The responses using direct numerical integration were presented using power spectral densities. In contrast to harmonic excitation, the amplitude of the response does not appear to approach that of the input. Instead, a higher effective cubic damping results in a higher vibration level of the isolated mass at frequencies below the resonance frequency. It also does not reduce explicitly the response amplitude around the resonance frequency unlike the linear viscous damping. For a constant displacement amplitude random excitation, the excitation frequency bandwidth is found to be a significant factor in the level of effective cubic damping. A broader excitation bandwidth results in a higher level of cubic damping force.

The theoretical and numerical results for both harmonic and broadband excitation were validated experimentally. The experimental investigation was performed using a SDOF base excited vibration isolation system possessing a simple velocity feedback control active damper to reproduce the nonlinear damping force. The predictions were shown to be in good agreement with measurements thereby verifying the effects of cubic damping on a SDOF system undergoing harmonic and broadband base excitation.

Contents

List of tables

List of figures

DECLARATION OF AUTHORSHIP

I, NUTTARUT PANANANDA declare that the thesis entitled 'The effects of cubic damping on vibration isolation' and the work presented in the thesis are both my own, and have been generated by me as the result of my own original research. I confirm that:

- this work was done wholly or mainly while in candidature for a research degree at this University;
- where any part of this thesis has previously been submitted for a degree or any other qualification at this University or any other institution, this has been clearly stated;
- where I have consulted the published work of others, this is always clearly attributed;
- where I have quoted from the work of others, the source is always given. With the exception of such quotations, this thesis is entirely my own work;
- I have acknowledged all main sources of help;
- where the thesis is based on work done by myself jointly with others, I have made clear exactly what was done by others and what I have contributed myself;
- parts of this work have been published as:

  Pananda, N., Ferguson, N.S. and Waters, T.P., 2012, The effect of cubic damping in an automotive vehicle suspension model, In *International Symposium on the Computational Modelling and Analysis of Vehicle Body Noise and Vibration, Brighton*, GB, 27-28 March 2012, 10 pp.

  Pananda, N., Ferguson, N.S. and Waters, T.P., 2013, The effect of cubic damping on a base excited isolator: an experimental study for harmonic excitation, In *11th International Conference on Recent Advances in Structural Dynamics (RASD 2013)*, University of Pisa, Italy, 1-3 July 2013, 13 pp.

  Pananda, N., Ferguson, N.S. and Waters, T.P., 2013, The experimental response of a broadband base-excited vibration isolator incorporating cubic damping, In *20th International Congress on Sound and Vibration (ICSV20)*, Bangkok, Thailand, 7-11 July 2013, 8 pp.

Signed: ……..

Date:…….

Acknowledgements

First of all, I would like to express my sincere gratitude to my great PhD supervisors, Dr. Neil Ferguson and Dr. Timothy Waters, for their professional assistance, valuable suggestions and patience throughout my study. They were pushing me from the beginning to success with their encouragement and inspiration.

I would like to extend my thanks to the thesis examiners, Prof. David Thompson and Dr. Jem Rongong, who were not only examining my thesis but they also gave the valuable comments and suggestions on this work. That guided my thesis to perfection.

I am also so thankful to the technical staff, Mr. Phil Oxborrow, Mr. Robert Stansbridge and their teams for their assisting with the experimental rig. My special thanks to all my colleauges in the Dynamics Group, ISVR, especially Ms. Nuthnapa Triepaischajonsak, Ms. Nabilah binti Ramli and Mr. Yung-Sheng Hsu, for their friendship and kindness. Also my special thanks to my Thai friends, especially Mr. Khemapat Tontiwattanakul and Mr. Vorrapath Kokaew for providing very good times during my stay in Unversity of Southampton.

I am deeply indebted and grateful to the National Science and Technology Development Agency, Thailand, and Rajamangala University of Technology Lanna, Thailand, for providing financial support.

Finally, but the most importantly, my deepest gratitude would be extended to my mother, Ms. Jananya Panananda, and my dear wife, Ms. Pimpan Panananda, for their love and extreme support during my study.

List of symbols and abbreviations

English lower case

$a(\tau)$	Shape function
a	Excitation gain
c_1, c_3	Linear viscous damping and Cubic damping coefficients
c_s	Passive damping coefficient of the shaker suspension
c_q	Fourier coefficient of data q
c_p	Damping coefficient
d	Diameter of spring wire
f	Temporal frequency
f_T, f_a	Experimental total and active damping forces from the shaker
f_h	Internal resonance frequency of spring
f_n	Temporal undamped natural frequency
f_s	Temporal sampling frequency
f_d, f_e, f_t	Normalised damping force, excitation force and transmitted force
$\tilde{f}_d$, $\tilde{f}_e$, $\tilde{f}_t$	Dimensional damping force, excitation force and transmitted force
h	Harmonic frequency
k, k_{hs}	Spring stiffness
k_s	Passive stiffness of the shaker suspension
m	Vibrating mass or mass of rigid body
m_{hs}	Mass of helical spring
n	Number of acquisition time periods
$n\Delta$	Discrete time step
$p(x)$	Probability density function
p	Degree of power law damping
q	Number of truncated data
r	Overlap factor

t	Dimensional time
u , u' , u''	Normalised time-dependent relative displacement, velocity and acceleration
$\tilde{u}$, $\tilde{u}'$, $\tilde{u}''$	Normalised time-dependent relative displacement, velocity and acceleration for Zener and two-stage vibration isolation models
w	Waviness for surface roughness
w , w_a	Window function and averaged window function
w , w' , w''	Normalised time-dependent absolute displacement, velocity and acceleration
w_0 , w_0' , w_0''	Normalised time-dependent displacement, velocity and acceleration of the base excitation
x_T	Truncated random data
x , $\dot{x}$, $\ddot{x}$	Dimensional time-dependent absolute displacement, velocity and acceleration
x_0 , $\dot{x}_0$, $\ddot{x}_0$	Dimensional time-dependent displacement, velocity and acceleration of the base excitation
x_r , $\dot{x}_r$, $\ddot{x}_r$	Dimensional time-dependent displacement, velocity and acceleration of the junction between the relaxation spring and damping for the case of Zener model
x_s , $\dot{x}_s$, $\ddot{x}_s$	Dimensional time-dependent displacement, velocity and acceleration of the intermediate mass
z , $\dot{z}$, $\ddot{z}$	Dimensional time-dependent relative displacement, velocity and acceleration

English upper case

A , B , C , D	Simplified dependences for Harmonic Balance Approximation
B	Effective bandwidth of the applied window function
D	Outer diameter of a spring
E_d	Dissipated energy
$E[\ ]$	Expected value of the random data
F_d	Amplitude of normalised damping force
F_{d1} , F_{d3}	Amplitude of normalised linear and cubic damping forces

F_e , F_t	Amplitude of normalised excitation force and transmitted force
$\tilde{F}_e$	Amplitude of dimensional excitation force
G	One sided power spectral density
G	Shear modulus
H , H_0, H_1, H_2	Estimated transfer function
N	Number of simulation data
N_a	Number of spring turn
N_h	Number of window function
N_p	Number of acquisition periods
P	Number of harmonics
$P(x)$	Probability distribution function
S_x	Two sided power spectral density of random data x
S_{xy}	Two sided cross power spectral density of random data x and y
T	Period of acquisition time or truncated time
T_r	Transmissibility for the linear isolation system
T_{re}	Transmissibility for the linear isolation system at the resonance frequency
U	Amplitude of the normalised relative displacement
U_f	Normalised relative displacement for the case of force excitation
U_w	Normalised relative displacement for the case of base excitation
$\tilde{U}$	Amplitude of the normalised relative displacement for Zener model
V_0	Dimensional velocity amplitude of the base excitation
W	Amplitude of the normalised absolute displacement
X	Dimensional displacement amplitude of the isolated mass
X_0	Dimensional displacement amplitude of the base excitation
X_T	Fourier transform of the truncated data
Z	Dimensional amplitude of the relative displacement

Greek lower case

ϕ_f	Phase lag between the excitation and transmitted forces
ϕ_u	Phase lag between the relative motion to the base excitation
ϕ_w	Phase lag between the absolute motion to the base excitation
γ	Coherence function
φ	Discrete frequency
κ_z	Stiffness ratio for the Zener isolation model
κ_t	Stiffness ratio for the two-stage vibration isolation model
λ	Wavelength
μ_t	Mass ratio for the two-stage vibration isolation model
μ_x	Mean value of the random data x
ω	Excitation frequency
ω_n	Undamped natural frequency
ρ	Density
σ_x	Standard deviation of the random data x
τ	Non-dimensional time
$\tau_{\max}$	Maximum of the non-dimensional time range
τ_{sl}	Non-dimensional time for the shape function
ζ	Non-dimensional damping term

Greek upper case

Ω	Frequency ratio
Ω_{re}	Frequency ratio for the resonance frequency
Ω_s	Frequency ratio for the sampling frequency
Ω	Spatial frequency for the surface roughness
Δ	Discrete time/frequency resolution
$\Delta\dot{x}$	Dimensional relative velocity

Abbreviations

CDR	Constant displacement amplitude random excitation
CVR	Constant velocity amplitude random excitation
CPSD	Cross power spectral density
HBM	Harmonic balance method
ODE	Ordinary differential equation
PDF	Probability density function
PSD	Power spectral density
RMS	Root mean square
SDOF	Single degree of freedom
THD	Total harmonic distortion

Chapter 1 Introduction

1.1 Background and motivation

Vibration isolation is typically introduced into a mechanical system in order to reduce the severity of disturbance caused from vibration sources, for example, the application of an automotive vehicle suspension system or a machinery mounting. A simple model of the vibration isolation system is usually considered using a single degree of freedom (SDOF) system which consists of a rigid mass, linear viscous damper and a linear isolation stiffness as shown in figures 1.1 (a) and (b). Vibration can be either the transmission of any dynamic forces from a vibrating mass to a support structure, see figure 1.1 (a), or a motion from the vibrating support structure to the isolated mass, see figure 1.1 (b).

The stiffness and damping represent the physical isolation elements and are commonly both assumed to be massless and linear. However, the assumption of isolator linearity is limited, and in some instances the isolator might exhibit nonlinear characteristics. In some scenarios, the nonlinearity could be triggered by high excitation amplitudes, beyond which the linear assumption breaks down and the predictions obtained from the linear model are not valid.

Nonlinear characteristics of vibration isolation can be found in any practical isolation system. For example, the telescopic shock absorber applied in automotive vehicle suspensions has nonlinear force-velocity characteristic due to the fluid flow through the valves [1]. A rubber mounting is another example with a nonlinear characteristic which has practical application. It is identified to possess a nonlinear restoring force [2]. Therefore, the assumption of linear isolation system is not sufficient to get insight into the characteristic of many practical systems.

In addition, isolation performance can be indicated using transmissibility function. It represents the ratio of the amplitude between two quantities, i.e. the input and the response amplitude, as a function of excitation frequency. The two quantities can be either the ratio between the amplitudes of force-force, force-displacement or displacement-displacement, for example. The nonlinear systems are known to result in

significant differences between the force and motion transmissibility. This is unlike those for a linear isolation system for which force and motion transmissibility are identical. The transmissibility for the linear system can be obtained using various fundamental mathematical approaches, e.g. Laplace transform or Fourier transform. The amplitude of both force and motion transmissibility are well known to be related to the damping ratio.

Figure 1.1 (c) shows the transmissibility function for either the force or base excited linear isolation system which is simply given by

$$|T_r| = \sqrt{\frac{1+\left(2\zeta_1\Omega\right)^2}{\left(1-\Omega^2\right)^2+\left(2\zeta_1\Omega\right)^2}} \tag{1.1}$$

where ζ_1 is a non-dimensional linear viscous damping ratio which is given by $\zeta_1 = \frac{c_1}{2\sqrt{km}}$. Ω is normalised excitation frequency, i.e. $\Omega = \omega/\omega_n$ with ω_n the undamped natural frequency and given by $\omega_n = \sqrt{k/m}$.

At the excitation frequencies well below the resonance frequency, $\Omega \ll 1$ shown by zone (i) in figure 1.1 (c), the system exhibits the so-called quasi-static response where the amplitude and phase of the output coincide with the input. It is seen in zone (ii), around the resonance frequency, $\Omega = 1$, that greater values of damping ratio yield a reduction in the transmissibility amplitude around resonance as given by

$$T_r\big|_{\Omega=1} = \sqrt{1+\frac{1}{\left(2\zeta_1\right)^2}} \tag{1.2}$$

For the linear vibration isolation system, the amplitude of transmissibility at excitation frequency $\Omega = \sqrt{2}$, shown by (iii) in figure 1.1 (c), equals unity. This frequency marks the beginning of the isolation region for the linear systems. The amplitudes of transmissibility in the isolation region, i.e. for excitation frequencies well above $\sqrt{2}$ in zone (iv), are seen to increase directly with the value of damping ratio as given by the following approximation

$$T_r\big|_{\Omega\gg1} \approx \frac{2\zeta_1}{\Omega} \tag{1.3}$$

For some aspects, the assumption of system nonlinearity can reduce the aforementioned disadvantages of the linear damping. Therefore it is essential to introduce the nonlinear characteristics within the theoretical model, in order to understand their effects. Understanding the effect of the nonlinearity could potentially help to improve the isolation performance or avoid any negative effect on the isolation performance.

There have been a variety of nonlinear characteristics previously examined and proposed. The nonlinearities might or might not be identifiable or approximated using a simple or a specific mathematical function. Also the method to get the exact analytical solutions is not generally available. For example, the method of superposition or the application of the frequency domain approaches applied for the linear system are not valid for nonlinear systems. In recent years, new methods for solving nonlinear problems have been proposed. Relevant previous studies and publications on the nonlinear vibration isolation are summarised and reviewed in the following sections. However, this study focuses particularly on a power law damping characteristic. This is one of the most common nonlinear damping characteristics considered and was chosen here as an example nonlinear isolator. Also one particular analytical method, Harmonic Balance Method (HBM), was chosen to solve nonlinear problems throughout this thesis.

1.2 Literature review

The topic of nonlinear vibration isolation has received wide interest in recent years. The isolator can sometimes be considered to possess either nonlinear stiffness, nonlinear damping or both. Some studies are reviewed and summarised here.

1.2.1 A passive nonlinear stiffness vibration isolator

A passive nonlinear stiffness of a vibration isolator can produce undesirable effects. For example, the well-known jump phenomenon can be observed for the harmonically forced Duffing oscillator, as seen in the response curves of the normalised displacement of the mass for a force excited isolation system with cubic stiffness shown in figure 1.2 [3]. The non-dimensional form for the Duffing's equation under harmonic excitation is given by

$$y'' + 2\zeta_1 y' + y + \alpha y^3 = \cos(\Omega\tau) \tag{1.4}$$

where ζ_1 is the linear viscous damping ratio. α is a non-dimensional cubic stiffness and is given by $\alpha = k_3 x_0^2 / k_1$, with k_1 and k_3 the linear and cubic stiffness coefficients and x_0 the amplitude of the isolated mass, defined as $x_0 = F/k_1$ for $k_3 = 0$ and $\omega = 0$. y'', y' and y are functions of non-dimensional time, τ, representing normalised acceleration, velocity and displacement of the system mass respectively.

The jump phenomenon is a result of having a cubic stiffness and is known to occur around the resonance frequency where multiple solutions are obtained. Such a phenomenon can feature jump up or jump down depending on whether excitation frequency is decreasing or increasing, illustrated using the normalized displacement response curve in figure 1.2. The resulting response curve bends towards either the low or high excitation frequency depending on whether a softening or hardening cubic stiffness is applied. This phenomenon is also dependent upon the excitation amplitude. A critical forcing amplitude and the jump frequencies can be determined as reported in [4] where the method of multiple scales was applied. The basic theory, solutions and description of the Duffing oscillator can be found in many text books, e.g. [5-7].

The Duffing oscillator can be examined in different ways. For example, Worden [8] approximated the frequency response curves of the Duffing oscillator using the HBM. The resulting response curves were compared to the exact solutions provided in the study of Friswell and Penny [9]. The occurrence of jump phenomena in [8] and [9] were found to be in very good agreement. Peng et al. [10] solved the Duffing oscillator response using the HBM. The result was compared to that obtained using the method of nonlinear output frequency response functions. The performance of these two approaches was examined by employing the observed difference in the jump phenomena. Carrella et al. [11] included the cubic stiffness in the SDOF force excited isolation model which was considered as possessing a high-static-low-dynamic-stiffness. Analytical expressions for the maximum amplitude and jump frequencies were obtained from their study.

In automotive applications, the linear plus cubic stiffness model has also been of interest. For example, Verros and Natsiavas [12] applied the Duffing type nonlinearity to a tyre model, for which an enhanced accuracy of the model was produced. Litak and

Borowiec [13] also applied the linear plus hardening cubic stiffness to a suspension system of a SDOF quarter-car model to investigate chaotic response.

Apart from nonlinear cubic stiffness, Klein [14] and Kirk [15] introduced the tangent elasticity characteristic as an alternative nonlinear stiffness for which the force-deflection characteristic is given by

$$F(x) = \frac{2k_1 d}{\pi} \tan\left(\frac{\pi x}{2d}\right) \qquad ; -d < x < d \qquad (1.5)$$

where k_1 is the initial spring rate and d is the maximum deflection obtainable with infinite force. Figure 1.3 shows the comparison of the force-deflection characteristic between the cubic hardening and the elasticity stiffness. The force-deflection for the linear stiffness is also plotted as for comparison. The theoretical deflection obtained from a cubic hardening spring can increase indefinitely with force. In reality, the deflection of a spring cannot increase or decrease beyond a certain value. Therefore the tangent stiffness was introduced to present a physical limitation of the spring deflection, shown by the vertical lines at $-d$ and d in figure 1.3.

However, nonlinear stiffness has not been considered here and the focus is on nonlinear damping. Therefore the assumption of linear isolator stiffness has been applied throughout this study. It should be very useful for future work to include other nonlinearities once the effects of nonlinear damping have been determined and understood.

1.2.2 A passive nonlinear damping vibration isolator

A nonlinear damping characteristic can be introduced to an isolation model in many ways. For example, in references [1] and [16], the damping characteristic in the application of an automotive suspension was modelled using piecewise linear damping,. The damping force-velocity characteristic of the piecewise linear damping is unequal between the bounce and rebound strokes. Such a damping characteristic was also mentioned in the studies of Wallaschek [17] and Surace et al. [18]. The asymmetric force-velocity characteristic was realised in practice using different valve sizes for these two strokes.

The application of asymmetric damping in an automotive vehicle suspension in the study of Rajalingham et al. [19] showed that, under harmonic base excitation, the isolated mass oscillates about a new mean value, which shifts the equilibrium position towards the stroke with lower damping. Natsiavas and Verros [20] included Coulomb friction in addition to the piecewise linear damping model. There appeared a discontinuity in the characteristic diagram at the end of each stroke where the velocity across the damper equals zero. The response for such a damping characteristic under harmonic excitation was found to exhibit a so-called stick-slip phenomenon.

The damping component can also be characterised using a polynomial power expansion in terms of the velocity. It is known as power law damping or velocity-*n*th power, i.e. $\tilde{f}_d(\dot{x}) = \sum_{p=0}^{Q} c_p \dot{x}|\dot{x}|^{p-1}$ where c_p is the damping coefficient for the power law damping with exponent p. The force and velocity diagrams for p = 0 to 5 are shown individually in figure 1.4. The absolute amplitude of velocity, $|\dot{x}|$, is introduced to ensure that the direction of the damping force opposes the motion when p is an even value (for $p > 0$). The damping force velocity characteristic for this damping type is anti-symmetric. As such, the damping force for the bounce and rebound strokes are equal.

The damping becomes Coulomb friction when $p = Q = 0$, blue line in figure1.4, and only the one term is included in the series. Coulomb friction is one of the common nonlinear damping characteristics found in mechanical systems. The force generated from the kinetic or sliding friction is a constant amplitude, independent of the relative velocity but in the opposite direction to the velocity. Its magnitude is dependent upon the friction coefficient and the normal force. One well known effect of Coulomb friction is the stick-slip behaviour as mentioned previously. The slip motion is considered when the relative velocity is not equal to zero. It happens when the sum of the inertia, stiffness and external force is sufficient to overcome the static friction force. Otherwise, stick or zero relative motion between two surfaces is considered.

Levitan [21] considered a support-excited isolation system for aircraft-installed equipment. The damping considered comprised linear viscous damping and Coulomb friction. The author assumed that no stick behaviour occurred for steady-state

oscillations due to harmonic excitation. It was apparent that the transmissibility amplitude around the resonance frequency could be reduced by increasing the friction.

The presence of Coulomb friction for base excitation was also reported by Schlesinger [22]. The Coulomb damper was the only damping characteristic present in the model. Two damper mounting configurations were considered, i.e. rigidly and elastically mounted. The author concluded that the amplitude of the resonance peak in the transmissibility at the break-out frequency, the frequency where slipping occurs, was controlled directly by the level of friction. The optimum level of friction could be determined for different values of the intermediate stiffness.

Crede and Ruzicka [23] provided a comparison of the transmissibility for base excitation for four different damping characteristics. The transmissibility with Coulomb friction showed an infinitely high amplitude at the resonance frequency. However, it showed that Coulomb friction worked well at high frequencies as the displacement transmissibility decreased inversely with the excitation frequency squared.

There are also many studies which have considered a combination of nonlinear damping in a model in order to improve the predicted results. For example, Wallaschek [17] and Surace et al. [18] applied Coulomb friction plus linear and quadratic damping to the model of an automotive shock absorber, i.e. the combination of $p = 0$, $p = 1$ and $p = 2$ respectively. However, some of the applied nonlinear damping characteristics were not very accurate compared to experimental results. The characteristics of a real damper exhibit an asymmetric force, whereas the polynomial form characteristic does not provide this in general. Despite this fact, a nonlinear polynomial characteristic for the damping force is still acceptable for study into the effect of nonlinear damping in some instances.

Ravindra and Mallik [24] examined the performance of a nonlinear vibration isolator subjected to both harmonic force and base excitation. The isolator model included both a nonlinear stiffness and nonlinear damping. The stiffness restoring force was considered separately for two different cases, i.e. symmetric and asymmetric. The power exponents of the velocity being 1, 1.5, 2 and 3 were also applied separately to the model. The authors concluded that the bandwidth of the jump phenomenon resulting from the cubic stiffness was narrower for an increasing value of damping coefficient.

In addition, increasing the value of the exponent power of damping could reduce the jump width. Thus the unstable zone was reduced.

Ho et al. [25] also reported that the application of cubic viscous damping, p = 3, on a hardening cubic stiffness Duffing-type force excited isolation reduced the amplitude of force transmissibility around the resonance frequency. As a result, the occurrence of the jump phenomenon could be eliminated without any effect on the isolation performance at high excitation frequencies compared to those with linear viscous damping.

Jing et al. [26] applied a power law damping with p = 1 and 3 into a SDOF force excited isolation model. A frequency domain analysis was carried out using a Volterra series expansion and was verified by simulation. The authors concluded that cubic damping provided a significant reduction in the response at the natural frequency, but has no effect on the response at high excitation frequencies. The results are in accordance with the study of Peng et al. [27] where polynomial type damping with an odd power of velocity with p = 1, 3 and 5 was applied on the same model. The effect of such damping was considered to be beneficial, since the response around resonance was lower whereas the response in the isolation region was not amplified.

Cubic damping was implemented for force isolation by Laalej et al. [28]. Electrodynamic shakers were employed on a hexapod or Stewart platform style subject to force excitation as the experimental rig shown in figure 1.5. The Stewart platform is a six degree of freedom parallel manipulator with variable link length [29]. The experimental results were compared to a theoretical study in [26] and [27]. A beneficial effect of the nonlinear viscous damping was found in and above the resonance region. Increasing the value of cubic damping reduces the level of the force transmissibility when compared to that for linear damping.

Laalej et al. [30] also implemented a nonlinear cubic damping characteristic using a magneto-rheological (MR) damper. The focus was to explore the beneficial effect of the nonlinear cubic damping for a pitch plane suspension system subject to force excitation. The model represented a physical model of a vehicle seat suspension. The authors configured the MR damper as the damping component, rather than the actuator in the feedback control system, so there was no energy input into the system.

The cubic damping characteristic was controlled by the current sent to the MR damper. The results showed a lower level of transmissibility for the system with nonlinear damping compared to that using linear damping. The results were also in a good agreement with the analytical results reported in references [26-28].

Guo et al. [31] applied power law damping in the study of force and displacement transmissibility. The exponent of the velocity was chosen arbitrarily. The analytical results were obtained using the Ritz-Galerkin method. The authors concluded that a different velocity exponent provided different results in both the force and displacement transmissibility. A power of the velocity greater than unity can be beneficial to force transmissibility but be detrimental for the motion transmissibility.

To this end, one might see that power law damping has been beneficial, giving an improvement in the force transmissibility. In this thesis, cubic damping was chosen as an example of power law damping for base excited isolation. Studies into the effect of cubic damping for base excitation isolation are reviewed and reported in the next section.

1.2.3 Cubic damping for base excited vibration isolation

Over recent years, the effect of cubic damping on base excited vibration isolation has been reported in many publications. Shekhar et al. [32] studied a variety of isolator and absorber models. All of the models included linear plus cubic viscous damping. Different shapes of shock base excitations were applied. The authors concluded that the inclusion of cubic damping is beneficial for shock isolation in some of the models considered but not others.

Kovačić et al. [33] were also interested in the displacement transmissibility for harmonic base excited isolation possessing cubic damping. The method of averaging was used to obtain the analytical results. They discovered that pure cubic damping has a detrimental effect on the absolute displacement transmissibility in the isolation region as shown in figure 1.6. The level of absolute displacement transmissibility is higher tending to unity (0 dB) as the excitation frequency increases. Milovanović et al. [34] also examined the displacement transmissibility of the same model. They observed that, for the system with pure cubic damping, the response for high excitation frequencies was greater than that for linear damping indicating a poor isolation performance.

The recent study by Peng et al. [35] examined both the force and base excited isolation model possessing the linear plus cubic damping using the HBM. The influence of cubic damping has been found to be dependent on the amplitude of the excitation input, i.e. constant and independent of the excitation frequency or proportional related to the excitation frequency squared. Regarding the responses in the isolation region, i.e. $\Omega \gg 1$, the authors concluded that the effect of cubic damping on both force and absolute displacement transmissibility is negligible when a constant force is applied. In contrast, for the case which excitation amplitude is proportional to the excitation frequency squared, for example an imbalance force resulting from the rotating machine, increasing cubic damping could increase the level of force transmissibility whereas the displacement transmissibility for such a system could be slightly lowered.

It is seen in general that cubic damping causes a higher vibration amplitude in the isolation region for base excitation. For some systems where cubic damping cannot be eliminated, awareness of the high response amplitude should be raised. Alternatively, the isolation capability might be improved using a higher order vibration isolation model. The Zener vibration isolation and the two-stage vibration isolation models were chosen here to deal with the detrimental effect of cubic damping. Some studies into these higher order models were reviewed and reported in sections 1.2.4 and 1.2.5.

1.2.4 Base excited Zener isolation model

The Zener base excited isolation system is introduced in this thesis in order to reduce the detrimental effects resulting from cubic damping. A brief introduction to the Zener model is given here. It consists of an additional relaxation spring which is working in series with the damping component and in parallel with a primary spring as the model shown in figure 1.7. For the assumed massless springs and damper, the relaxation spring and the damper can be considered as experiencing the same force. There is an additional first order equation of the equilibrium force resulting from these components. The Zener model may therefore be considered as a one and a half degree of freedom system (1½-DOF) [36]. It has also been called many names, for example, an elastically supported damper [23,37,38], a three-element mounting [39,40] or an elastically coupled damping [41]. However, it is referred to here as the Zener isolation model.

Crede and Ruzicka [23] also mentioned the application of the Zener model using linear viscous damping in comparison with three other isolation models. Ruzicka [37] compared the harmonic responses for the passive base excited Zener isolation model having a linear viscous damper to that of a rigidly connected linear viscous damper. It was shown that having a stiffness ratio* close to zero resulted in a higher level for the absolute transmissibility around the resonance frequency. However, it produced a lower level at excitation frequencies well above the resonance frequency. The author concluded that if a relatively small increase around resonance was acceptable, then improved isolation could be obtained using the Zener model.

Snowdon [39] referred to the Zener model as a three-element mounting. The investigation was carried out for the model comprising linear viscous damping subject to harmonic and transient base excitation. The responses for the Zener model were compared to those of the classical SDOF isolation having a rigidly mounted damper. For harmonic excitation, the Zener model produced displacement transmissibility at high frequencies of lower amplitude than that of the rigidly mounted damper. It also reduced the displacement amplitude of the isolated mass due to shock excitation. Snowdon summarised overall that the application of the Zener model provided better vibration isolation.

The performance of the three-element shock isolator was also investigated by Shekhar et al. [32]. The damping component was defined as the combination of linear and cubic viscous damping. For relatively low excitation severity, the presence of cubic damping did not make any significant difference compared to that of SDOF linear or linear plus cubic damping. A better isolation capability of the three-element isolation model possessing linear plus cubic damping was noticeable when the severity of the shock excitation was relatively high. They also concluded that cubic damping should be mounted elastically and the optimum value of stiffness ratio should be about unity.

The performance of the base excited Zener isolation comprising linear viscous damping was also discussed in the study of Ledezma-Ramirez et al. [42]. The level of the displacement transmissibility for the Zener isolation model in the isolation region decreased by 40 dB per decade, whereas that of the SDOF system with a rigidly

* Stiffness ratio refers to the ratio of the stiffness values between the relaxation spring and primary spring.

connected linear damping had a roll off rate at 20 dB per decade. However, it was found that the responses due to shock excitation between the two systems were not different. The authors concluded that the Zener isolation model might be suitable for the system subject to either transient or harmonic excitation.

The free vibration and forced harmonic response of the Zener isolation model were also studied by Brennan et al. [43]. The authors found that critical damping could not be obtained for a stiffness ratio less than a specific value of 8. Therefore, the stiffness of the relaxation spring should be stiffer compared to that of the primary spring. The authors concluded that the application of Zener isolation model does not provide a significant advantage over the SDOF model for the case of free vibration.

In this thesis, the Zener model was applied only for harmonic base isolation. The isolation capability of the Zener model possessing cubic damping was studied alongside the cubically damped SDOF model.

1.2.5 Two-stage base excited vibration isolation

Two-stage vibration isolation is also introduced here in the expectation that is might be applicable to reduce the detrimental effect caused by cubic damping for the SDOF isolation under base excitation. The model consists of two sets of vibration isolators as shown in figure 1.8, i.e. primary and secondary stage isolator. These sets of isolators are separated by an additional mass, known as an intermediate mass. The use of two-stage linear vibration isolators was theoretically shown to reduce the level of the transmissibility in the isolation region, with a steeper roll-off rate compared to the single-stage linear model [44]. However, the presence of the intermediate mass results in a second resonance at a higher frequency.

The two-stage isolation model was introduced as a compound mounting system by Snowdon [40]. Although a second resonance appears because of the presence of the intermediate mass and hence the system becomes a two degree of freedom system, the level of transmissibility at high excitation frequencies was found to reduce at 24 dB per octave independent of the value of stiffness and damping. Snowdon identified that the second resonance frequency should be located as close to the primary resonance as

possible, which can be achieved by choosing the optimum value of the stiffness ratio[†]. This observation is also in agreement with Fu et al. [45] who stated that a stiffness ratio which provides a relatively low secondary resonance should be considered.

Shekhar et al. [32] showed the effect of cubic damping on the two-stage shock isolator, where cubic damping was included in addition to the linear viscous damping on both the first and second stage isolators. The shock response for this model was compared to that for the single-stage isolation possessing linear plus cubic damping. The authors concluded that the two-stage isolation possessing cubic damping on both stages was more preferable for shock isolation than other shock isolations considered in their study.

Similar to the case of the Zener isolation model, the application of two-stage isolation in this thesis concerns only the case of harmonic base excitation. This is to illustrate the possible solution to reduce or eliminate the detrimental effect of cubic damping for base isolation.

1.2.6 Alternative models of nonlinear vibration isolation involving cubic damping

Publications reviewed in this sub-section refer to alternative nonlinear vibration isolation system. For example, Tang and Brennan [46,47] oriented the damping component horizontally, perpendicular to the system's spring as shown in figure 1.9. Such a damper orientation results in the damping force in the moving direction (direction of stiffness) becoming a function of the angle, i.e.

$$F_d = -c_1\left(\frac{d}{dt}\sqrt{a^2 + x(t)^2}\right)\sin\left(\theta(t)\right) \tag{1.6}$$

where c_1 is the linear damping coefficient and a is the length of the damper measured horizontally. It could also be defined geometrically as a function of displacement squared and velocity. As such the equation of motion for the isolated mass is given by

$$m\ddot{x} + c_1\frac{x^2}{a^2 + x^2}\dot{x} + kx = 0 \tag{1.7}$$

[†] Stiffness ratio for the two-stage vibration isolation model refers to the ratio of stiffness between the first and second stage isolators.

where x and $\dot{x}$ are displacement and velocity of the isolated mass. The authors compared the geometrical nonlinear damping to the form of quadratic and cubic damping. The free vibration response and harmonic response were reported in [46] and [47] respectively. The authors concluded that, in general, such a system provided better vibration isolation for base excitation compared to the case of cubic damping.

Sun et al. [48] reported similar work where the damping component was also perpendicular to the stiffness and the motion of the isolated motion. The mass of the base excitation was also considered and was treated as an unconstrained two degree of freedom system. The damping force for the model mentioned was given by $2c_n\left(\frac{|z|}{\sqrt{a^2+z^2}}\right)^{n+1}|\dot{z}|^{n-1}\dot{z}$ where z and $\dot{z}$ are the relative displacement and velocity across the damper in the moving direction and n is the exponent. The averaging method was applied to obtain an approximate solution for the harmonic excitation. The authors concluded that a high isolation performance could be achieved using the optimal value of n, i.e. $0 \le n \le 0.4$.

A more recent study by Xiao et al. [49] proposed a nonlinear damping component which was defined as a product of displacement squared and velocity, i.e. $x^2\dot{x}$. The new damping model was added to the original linear viscous damping for both force and base excited isolation. The responses under harmonic excitation were compared to those having only linear plus cubic damping. The presence of the proposed damping was found to reduce the amplitude of force and displacement transmissibility for both around the resonance and in the isolation regions. The authors concluded that the proposed damping provided better performance over just cubic damping, which is purely dependent on the relative velocity.

Lu et al. [50] studied a nonlinear effect from the stiffness geometry on a two-stage vibration isolation. Two 90 degree oriented springs were added to the sets of vertical stiffness and damping. Each horizontal spring connected the mass for each stage to the supporting structure. The horizontal spring in the second stage was found to provide better isolation. They also found that the force transmissibility at high excitation frequencies can be reduced by the larger intermediate mass.

1.3 Objectives and scope of this study

The application of nonlinear damping reported in the literature was shown to be favourable for harmonic force excitation of a SDOF system. It reduced the transmitted force amplitude so as to be similar to that of an undamped linear system. In contrast, for harmonic base excitation, nonlinear damping resulted in poor isolation performance compared to linear viscous damping. This contrary effect of nonlinear damping motivated the main objective of this thesis, i.e. to investigate and describe the possible reasons behind such effects. Cubic damping was chosen as an example of damping nonlinearity. By understanding the physical cause, it is feasible either to improve the isolation benefits of cubic damping or prevent such a system from poor isolation performance. The base excited Zener and the two-stage vibration isolation models were then introduced in order to eliminate the disadvantages from the presence of cubic damping.

The responses due to harmonic excitation for both base and force excitation are reported separately in comparison to the linear viscous damping case. The examination into the harmonic response is first presented using three methodologies, i.e. a mathematical approximation, numerical simulation and finally experimentally. The effect of cubic damping on a SDOF vibration isolation system subject to broadband base excitation was also investigated and is reported here. The responses due to broadband excitation were carried out using numerical simulation and experimental study with subsequent statistical and spectral post processing. Note that, the experimental investigations were implemented only for the case of a SDOF base excited vibration isolation system.

The numerical simulations carried out here were slightly different from those previously published by others. Most of the studies in the literature assigned the comparable level of nonlinear damping to that for linear viscous damping. This would not be appropriate for some situations. Since the characteristics for linear and nonlinear damping are different, using a comparable damping level for both the linear and cubic damping might result in improper conclusions.

The levels of nonlinear damping considered in this study were determined in order to maintain chosen values of the response amplitude around the resonance frequency. Thus the distinction between linear and nonlinear damping for the excitation

frequencies high above resonance is expected to be observed. A similar strategy of maintaining the response around the resonance frequency was also applied to the experimental study, which has not been found in the literature. The levels of the responses around the resonance frequency for both linear and nonlinear damping were thus comparable for the predictions and the experiments. The latter then was applicable in validating the theoretical and numerical findings.

1.4 The contributions of the thesis

This work has produced some original understanding and knowledge in the area of the effect of nonlinear damping in isolation systems. The original contributions that have been identified are listed as follows:

i) The underlying physical causes for the detrimental effect of cubic damping for base excited isolation are explained.

ii) Approximate closed form solutions for a force and base excited SDOF isolation system possessing cubic damping have been obtained using the Harmonic Balance method. These solutions have been simplified in order to provide insight and understanding into the positive and negative effects of cubic damping for particular frequency regions. Previously the approximate expressions had been obtained using the Averaging Method.

iii) The applications of higher order base isolation models, i.e. the Zener and two-stage isolation models were proposed in order to eliminate the detrimental effects of cubic damping on a SDOF base excited vibration isolation model. The negative effects of the cubic damping have been removed using the application of the Zener isolation model. The application of the two-stage isolation system with cubic damping in the secondary stage isolator produces even better isolation performance than that with linear viscous damping.

iv) Concerning broadband random excitation, the effects of cubic damping for a base excited isolation system have not been found reported in the literature. Distinctive and different response characteristics due to harmonic and broadband excitation were found.

v) The theoretical results showing the detrimental effects of cubic damping were confirmed experimentally. The nonlinear damping was reproduced using a simple velocity feedback for both harmonic and broadband base excitation. In principle, this velocity feedback could be further developed to reproduce any nonlinear damping configuration. The experimental results for both excitation scenarios are in good agreement with theoretical predictions.

1.5 Thesis outline

The study began with the numerical simulation for the application of the integer power law damping. The exponent power was initially ranged from 1 to 5 in order to justify the further examination into the effect of nonlinear damping and is given in Chapter 2. Cubic damping was found to be a good example, showing the beneficial and detrimental effects of power law damping.

The effect of cubic damping on vibration isolation was then examined analytically and numerically and reported in Chapter 3. The key evidence showing the advantages and disadvantages from the presence of cubic damping was found. Chapter 4 reports the application of higher order base excited vibration isolation models, i.e. the Zener and two-stage isolation models. These two models were introduced to minimise the negative effect of cubic damping and to increase the isolation capability. The effect of cubic damping for the broadband excitation was performed only for the case of base excitation, which is reported in Chapter 5 using numerical simulation as no analytical solution is available.

Chapter 6 reports the experimental study, which was performed for both harmonic and broadband excitations on the base excited isolation system for model validation. Finally, a general discussion and conclusions of this work are provided in Chapter 7.

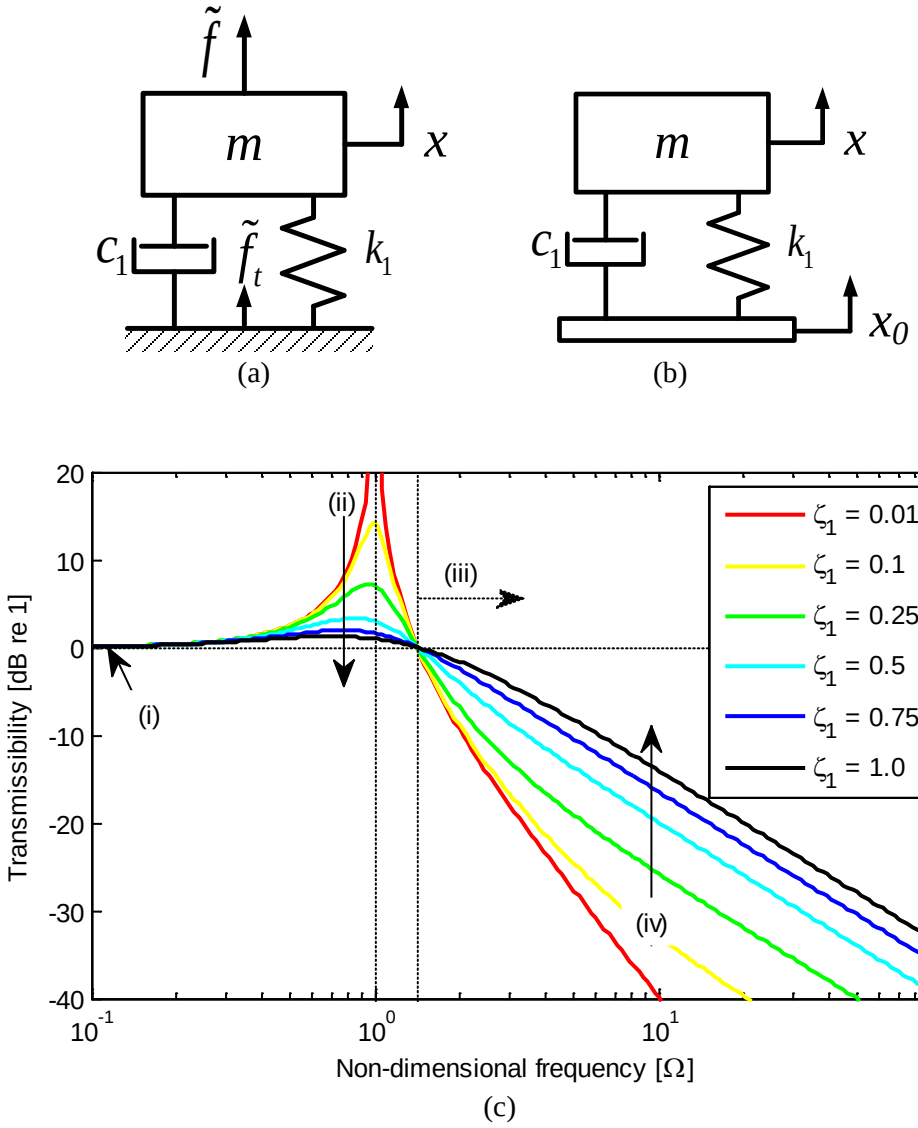

Figure 1.1 SDOF linear vibration isolation models and the corresponding transmissibility function showing the relation between the amplitude and the linear viscous damping ratio.

(a) Force excited vibration isolation model

(b) Base excited vibration isolation model

(c) Transmissibility for either force or base excited linear vibration isolation model with $\zeta_1 = \dfrac{c_1}{2\sqrt{k_1 m}}$.

(i) Quasi static response occurs at excitation frequencies well below the resonance frequency.

(ii) Amplitude decreases as for the greater linear viscous damping.

(iii) The beginning of the isolation region for linear vibration isolation system, i.e. $\Omega = \sqrt{2}$.

(iv) Amplitude increases as for the greater linear viscous damping.

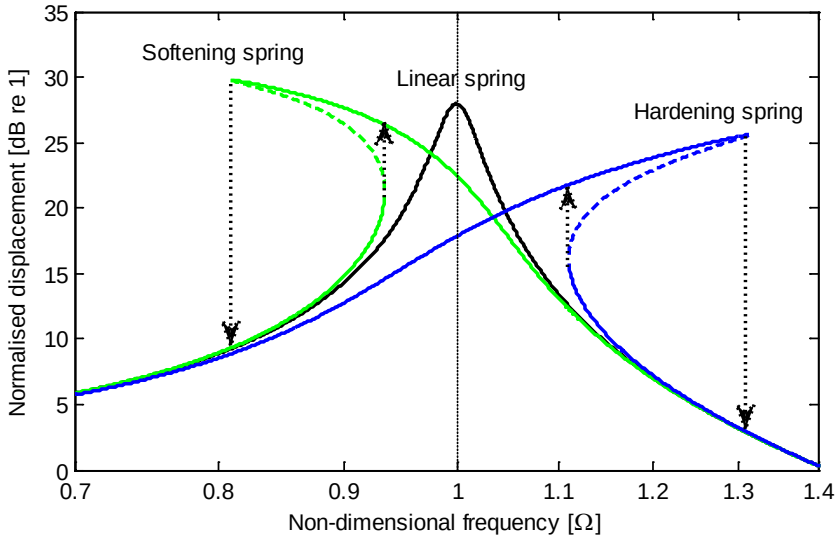

Figure 1.2 The normalised displacement response curves for the system mass of Duffing oscillator subject to harmonic force excitation in comparison to the response for the linear system , figure reproduced from [3].

- Linear spring system
- Softening spring system
- Hardening spring system

Dashed lines denote unstable solutions
Arrows illustrate jump up and jump down phenomena
Note that the horizontal axis is in log scale.

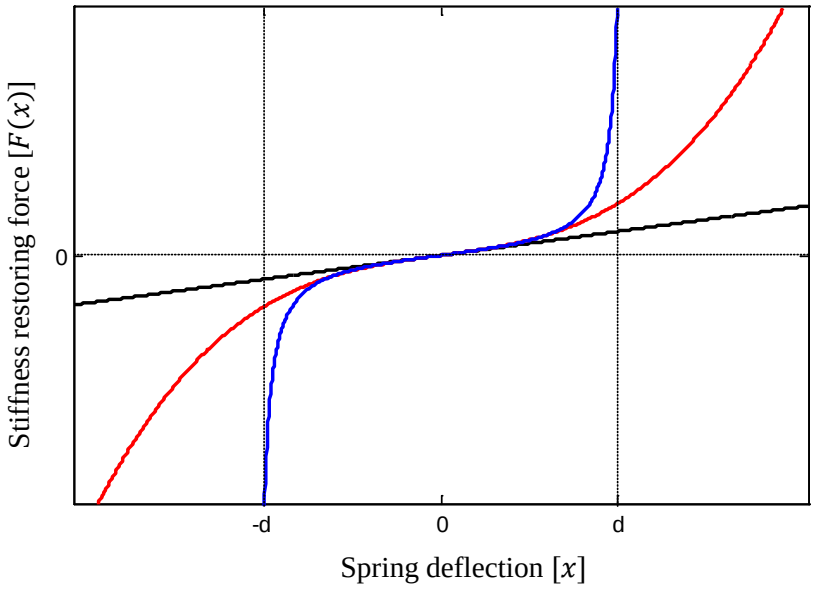

Figure 1.3 Force-deflection diagrams for different stiffness characteristics

- Linear stiffness : $F(x) = k_1 x$
- Cubic hardening stiffness : $F(x) = k_1 x + k_3 x^3$
- Tangent elasticity characteristic : $F(x) = \frac{2k_1 d}{\pi} \tan\left(\frac{\pi x}{2d}\right)$

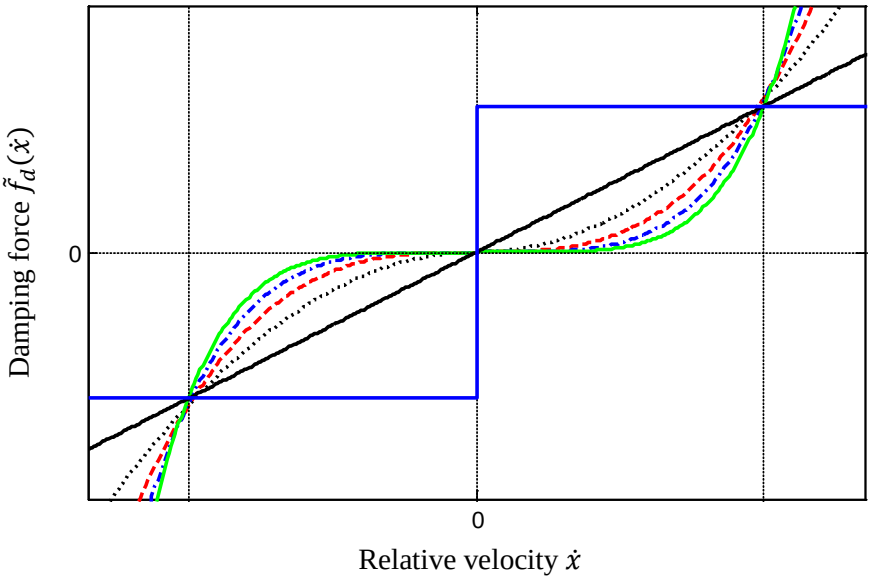

Figure 1.4 Power law damping force characteristics obtained from $\tilde{f}_d(\dot{x}) = c_p \dot{x}|\dot{x}|^{p-1}$.

- Coulomb damping, $p = 0$
- Linear viscous damping, $p = 1$
- Quadratic damping, $p = 2$
- Cubic damping, $p = 3$
- Quartic damping, $p = 4$
- Quintic damping, $p = 5$

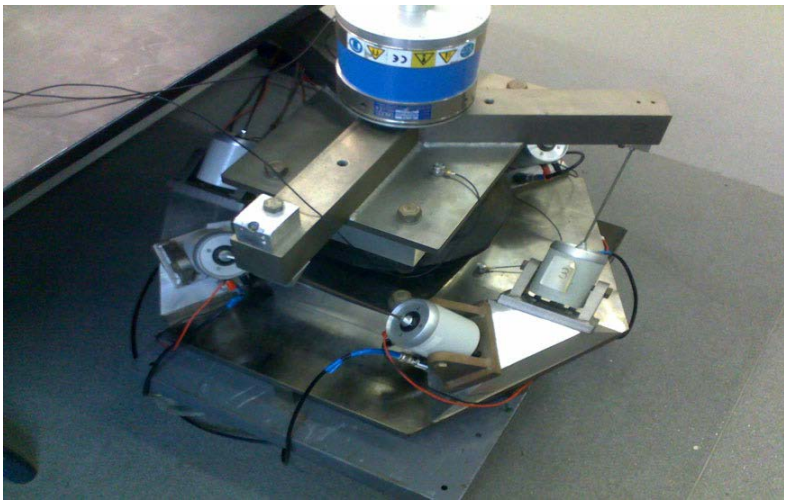

Figure 1.5 Stewart platform style experimental rig employed in the study of Laalej et al. [28]

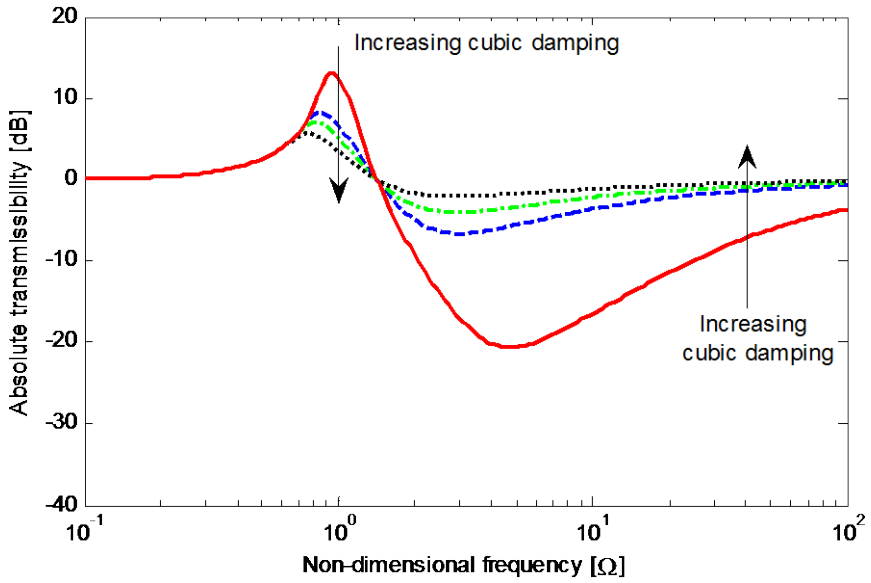

Figure 1.6 Absolute displacement transmissibility for a harmonic base excited vibration isolation system with pure cubic damping ζ_2 ‡, figure reproduced from [33].

$\zeta_2 = 0.01$

$\zeta_2 = 0.1$

$\zeta_2 = 0.2$

$\zeta_2 = 0.5$

Arrows show the level of response amplitudes at around the resonance frequency and high excitation frequencies due to increasing in the level of cubic damping.

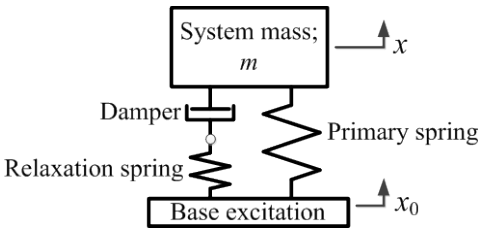

Figure 1.7 Zener base excited isolation.

‡ ζ_2 denotes non-dimensional cubic damping as used in the reference. Non-dimensional cubic damping is denoted later using ζ_3 elsewhere throughout this thesis.

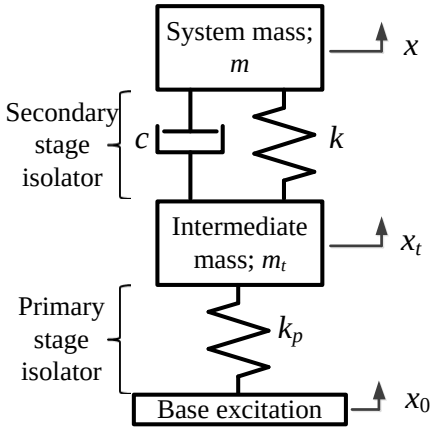

Figure 1.8 Two-stage base excited isolation with undamped primary stage isolator.

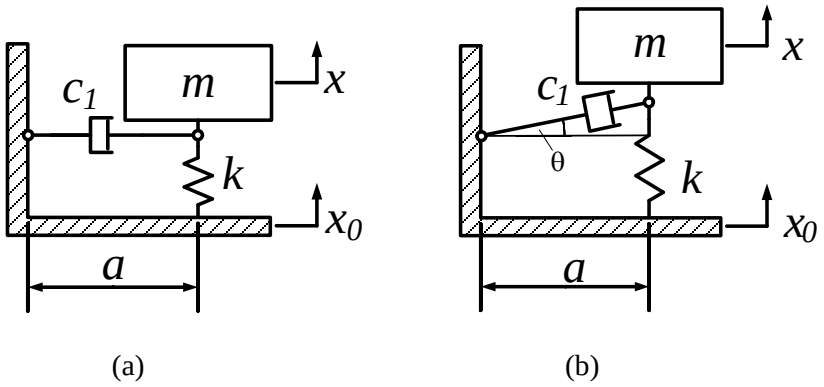

Figure 1.9 Base excited vibration isolation possessing linear viscous damping oriented horizontally and perpendicularly to the system's spring and moving direction of the isolated mass
(a) The isolated mass is at the equilibrium position.
(b) The isolated mass moving upwards results in an angle θ with respect to the horizontal axis.
where a is a length of damper measured horizontally.

Chapter 2 Vibration isolation possessing power-law damping

2.1 Introduction

Damping is often assumed to be linear, either where the response is justifiably small or simply for convenience. However the application of the assumed linear damping is limited for some aspects. This is because the physical damping mechanisms are generally nonlinear, e.g. the automotive vehicle shock absorber etc. The nonlinearity of damping components can be advantageous or disadvantageous. Therefore the consideration of nonlinear damping is required.

The nonlinear damping characteristic is not unique. The attention of this chapter is focused on examining power law damping as an example of damping nonlinearity. This is because applications of power law damping have proved successful, in some cases, for reducing the vibration amplitude in the isolation region. However, it has not been effective for some scenarios and it might exhibit unexpected disadvantages.

This chapter reports the effect of five individual power law damping characteristics on a single degree of freedom (SDOF) isolation system. Two different excitation scenarios, namely force excited and base excited isolation, are applied. The aim of this chapter is to illustrate the effect of the integer exponent power law damping by presenting numerical results. The outcome of this investigation is to provide understanding of the effects produced. It can lead to the further exploration into the basis of such effects whether negative or positive benefits occur.

2.2 Single degree of freedom isolation with nonlinear damping

The model of the SDOF isolation considered here is illustrated in figure 2.1 for two different excitation cases. The isolated mass is assumed to be rigid and is centrally attached to the isolator. As such, only vertical translation from the static equilibrium position is considered. The isolators for both cases comprise a linear stiffness and a

damping component acting in parallel. The damping is assumed to be related to the relative velocity by a power law, the details for which are given in section 2.3.

2.2.1 Equation of motion

Figure 2.1 (a) represents the system subject to force excitation. The excitation force $\tilde{f}_e$ is partly transmitted to the supporting structure via the isolator. The capability of the isolator can be examined in terms of the ratio between the amplitudes of the force being transmitted and the exciting force. A good isolation should transmit less force and so the amplitude ratio is lower. The system in figure 2.1 (b) represents the system undergoing base excitation. The role of the isolator in this scenario is to isolate the motion from the base to the isolated mass. The isolation capability is quantified by the ratio of the motion amplitudes between the isolated mass and the base excitation. This quantity can be considered in terms of displacement, velocity or acceleration. Similarly to the case of force excitation, a lower level of the ratio means a better isolator.

The governing equation of motion for the models shown in figure 2.1 is given by

$$m\ddot{z}(t) + \tilde{f}_d(\dot{z}, t) + kz(t) = \tilde{f}_e(t) \tag{2.1}$$

where m and k are the mass of the rigid body and the assumed linear stiffness. $\tilde{f}_e$ is the dimensional input excitation ($\tilde{f}_e = -m\ddot{x}_0$ is considered for the base motion excitation). $\tilde{f}_d$ is a function representing the dimensional restoring force due to damping. $\ddot{z}$, $\dot{z}$ and z are the relative motions, i.e. acceleration, velocity and displacement as a function of dimensional time t. The relative displacement is given by

$$z = x - x_0 \tag{2.2}$$

where x is the absolute displacement of the rigid body and x_0 is the base displacement excitation. For the case of force excitation, x_0 is equal to zero, therefore $z = x$. However, for simplicity, the relative motion z is applied for both cases as they share the same expression. In addition to the equation of motion, for the case of force excitation the equation for the transmitted force has to be defined, i.e.

$$\tilde{f}_t(t) = \tilde{f}_d(\dot{z}, t) + kz(t) \tag{2.3}$$

2.2.2 Harmonic excitation assumption

The excitation applied in this chapter is assumed to be harmonic excitation, i.e. $\tilde{f}_e = \tilde{F}_e \cos(\omega t)$ for the force case and $\tilde{f}_e = m\omega^2 X_0 \cos(\omega t)$ for the base excitation case. Equations (2.1) and (2.3) can be normalised using the quantity $m\omega_n^2 X$ where X is the displacement amplitude of the rigid body resulting from the excitation at zero frequency and is given by

$$X = \frac{\tilde{F}_e}{k} \text{ and } X = X_0 \tag{2.4}$$

for the case of force and base excitation respectively. The other non-dimensional terms applied for the normalisation are defined as follows.

(a) Frequency ratio

The frequency ratio is defined as the ratio between the angular excitation frequency ω and the undamped natural frequency ω_n, i.e.

$$\Omega = \frac{\omega}{\omega_n} \tag{2.5}$$

The undamped natural frequency is given by $\omega_n = \sqrt{\frac{k}{m}}$ where k is the linear stiffness and m is the mass.

(b) Non-dimensional time

Non-dimensional time is defined by

$$\tau = \omega_n t \tag{2.6}$$

The first and the second derivatives with respect to τ are denoted by $(\bullet)'$ and $(\bullet)''$ respectively. The assumed harmonic excitation also becomes a function of non-dimensional time τ, i.e. $e^{i\omega t} \equiv e^{i\frac{\omega}{\omega_n}\tau} \equiv e^{i\Omega\tau}$.

(c) Normalised response variables

The variable representing relative displacement between the rigid mass and the base excitation is normalised by the amplitude at zero frequency, X. Thus one obtains

the normalised variables for the relative displacement, velocity and acceleration as follows;

$$z = Xu\,,\ \dot{z} = \omega_n X u'\ \text{and}\ \ddot{z} = \omega_n^2 X u'' \tag{2.7}$$

where u'', u' and u are the normalised relative motions with respect to non-dimensional time τ. By substituting these variables into equation (2.1) and dividing by the quantity $m\omega_n^2 X$ one obtains the non-dimensional form as

$$u''(\tau) + f_d(u', \tau) + u(\tau) = F_e \cos(\Omega\tau) \tag{2.8}$$

where f_d is the normalised restoring force due to damping. F_e is the normalised amplitude of excitation force which for force excitation $F_e = 1$ and $F_e = \Omega^2$ for the base excitation. The normalised form for the transmitted force shown in equation (2.3) is given by

$$f_t(\tau) = f_d(u', \tau) + u(\tau) \tag{2.9}$$

The non-dimensional form given in equations (2.8) and (2.9) will be solved later using numerical integration and will be examined in section 2.5.

2.3 Power-law damping and its equivalence

The characteristics of power law damping applied in this study are described here. Its effects are examined in comparison to linear viscous damping, for which the exponent is equal to unity. The equivalent values, under certain assumptions, for linear damping with these nonlinear damping characteristics are also presented.

2.3.1 Power law damping characteristic

The power law damping characteristic considered here can be given in dimensional form by

$$\tilde{f}_d(\dot{z}, t) = c_p \dot{z}(t) \left|\dot{z}(t)\right|^{p-1} \tag{2.10}$$

where c_p is the dimensional damping coefficient assumed constant and p is the exponent of the power law damping which, in this study, ranges from 1 to 5. The linear

viscous damping is considered when $p = 1$ for which the damping force is proportional to the relative velocity with the exponent of unity.

The normalised damping force can also be obtained by dividing equation (2.10) by the quantity $m\omega_n^2 X$, i.e.

$$f_d\left(u',\tau\right) = \frac{c_p}{m\omega_n^2 X}\left(\omega_n X u'\right)\left|\omega_n X u'\right|^{p-1} \tag{2.11}$$

with $\dot{z} = \omega_n X u'$. Equation (2.11) can be rewritten as

$$f_d\left(u',\tau\right) = \zeta_p u'\left|u'\right|^{p-1} \qquad \text{for } p > 1 \tag{2.12}$$

where ζ_p is the non-dimensional power law damping term which is the outcome of equation (2.11) and is given by

$$\zeta_p = \frac{c_p}{m}\omega_n^{p-2} X^{p-1} \tag{2.13}$$

Note that, for p = 1, the normalised linear damping force is given by

$$f_d\left(u',\tau\right) = 2\zeta_1 u' \tag{2.14}$$

as a result of the linear damping ratio, $\zeta_1 = \frac{c_1}{2m\omega_n}$. The further descriptions and the examples for the other types of power law damping are given in the following sub-sections with the damping force characteristics shown in figure 2.2 for exponent p = 0 to 5.

(a) Even exponent power law damping

The even exponent power law damping characteristics applied in this study are quadratic and quartic damping, i.e. p = 2 and 4. The force characteristics for these two damping models are symmetric on the relative velocity by definition. Therefore the use of absolute value or a sign function is needed to convert the damping force characteristic to be anti-symmetric and to ensure that the damping force always opposes the motion.

The quadratic damping, p = 2, is often associated with turbulent fluid flow and is also commonly used in the study of automotive shock absorbers, for example in

references [17,18,38]. It was also examined for the case of base excited isolation, for example [51-53] for which approximate closed form solutions were provided. However, in this study only numerical simulations are considered to enable comparison with the other power law damping types.

The use of quartic damping, $p = 4$, has not been generally found for vibration isolation. However, it is applied in this study to illustrate the effect of the higher power-law damping characteristic in the damping force expression.

(b) Odd exponent power law damping

The effects of odd exponent power law damping with $p = 3$ and 5 are considered here. Cubic damping, $p = 3$, became a damping characteristic of interest in recent years. There have been number of publications considering it, for example those reported in [28,30,32-34]. A cubic damping characteristic produces an anti-symmetric force-velocity diagram, as for linear viscous damping. An example of the application for the quintic damping, $p = 5$, can be found in [27]. The fifth power exponent was considered in combination with both the linear and cubic damping, i.e. $p = 1$ and $p = 3$. In this thesis, the response for each power exponent was examined individually.

To recap, the characteristic diagrams for power law damping are shown here again in figure 2.2. It is seen that the level of power law damping forces with $p > 1$ are much lower than for linear viscous damping at low relative velocity ($|u'| < 1$) and higher for $|u'| > 1$. The force-velocity characteristics of the power law damping with $p = 2$ to 5 are qualitatively similar. So, one might anticipate similar effects from these power law damping types on the isolation performance.

2.3.2 Equivalent linear viscous damping

The equivalent value of the linear damping coefficient for the other types of power law damping can be approximated by equating the energy dissipated over a full cycle of steady-state nonlinear response to that for linear viscous damping. The non-dimensional dissipated energy is calculated by the integral over a cycle of vibration assuming a harmonic response, i.e.

$$E_d = \int_0^{2\pi/\Omega} f_d\left(u', \tau\right) u' d\tau \tag{2.15}$$

where Ω is the excitation frequency ratio. Equation (2.15) can be applied for the steady-state harmonic relative velocity, i.e. $u' = \Omega U \sin\left(\Omega\tau - \phi_u\right)$ where U is a normalised amplitude of the relative displacement and ϕ_u is phase lag of the relative displacement with respect to the base excitation.

The relative velocity for the power law damping with p = 5 subject to force and base excitation at the undamped natural frequency, i.e. Ω = 1, were evaluated as an example of an extreme case. The values of non-dimensional damping ζ_5 = 0.1 and 0.3 were chosen initially. The time histories for the linear viscous damping producing a similar amplitude of the relative velocity were also determined for a comparison. The resulting relative velocity time histories are shown in figure 2.3 for a non-dimensional time period of $T = 2\pi$.

These plots illustrate that the relative velocity for the power law damping p = 5 are distorted. This is known to be a result of the existence of response at other harmonics due to the nonlinearity. Despite the harmonic distortion, the appearance of relative velocity can be considered periodic and dominated by the excitation frequency.

Therefore the non-dimensional damping value for other power law damping models can be estimated using the non-dimensional energy dissipated by a linear viscous damping which is given by

$$E_d = 2\zeta_1 \pi \Omega U^2 \tag{2.16}$$

The non-dimensional damping values for power law damping with p = 2 to 5 for this instance are estimated at Ω = 1 for ζ_1 = 0.1, 0.2 and 0.3. The equivalent values of linear viscous damping are listed in table 2.1. By applying these values the response amplitudes for the power law damping at Ω = 1 are expected to be similar to the linear case. The responses for the power law damping and the existence of the responses at higher harmonics will be discussed in section 2.5.

2.4 ODE solutions and spectral analysis

The ordinary differential equation given in equation (2.8) was solved numerically using direct numerical integration. The ODE45 solver provided in Matlab was chosen as for general purpose ODE solutions. The chosen solver is based on a fourth and fifth order Runge-Kutta method with an automatic step size adjustment [54]. The large or small step-size is applied depending upon the characteristic of the function [55], i.e. the larger step size is applied for low frequency functions and vice versa for the high frequency functions. In order to obtain the time response at a desired time step, it is suggested to apply a one dimensional interpolation, 'interp1', to the obtained result [56]. An example for using ODE45 is given in Appendix A.

The applied numerical time and frequency resolutions are described here as well as the excitation characteristic in the time domain. The time domain numerical results obtained were transformed into the frequency domain and analysed using spectral analysis, which is also described in this section.

2.4.1 Solution procedure

The input for numerical simulations was specified as a set of discrete frequency sinusoidal excitations. The frequency range of interest ranged from $\Omega = 0.1$ to 100. The input excitation amplitude was gradually increased from zero to the maximum of unity for each frequency input considered, i.e.

$$a(\tau) = \begin{cases} \dfrac{\tau}{\tau_{sl}} & ;\tau \le \tau_{sl} \\ 1 & ;\tau_{sl} \le \tau \le \tau_{\max} \end{cases} \tag{2.17}$$

where a is the shape function for the signal amplitude. τ_{sl} is the ramp time which is given by $\tau_{sl} = \tau_{\max}/2$. The response only in the second half of the simulation was employed for subsequent frequency domain analysis. By doing this the effect of any transient response was reduced. However, for the lightly damped systems, the longer duration for the ramp input can be considered. In addition, the application of ramp input can help to avoid transient response resulting from nonlinearity. This is to ensure that only the steady-state response is obtained.

The non-dimensional maximum time length was set at τ_{max} = 256 time units. This τ_{max} allowed four complete cycles of the sinusoidal signal for the lowest excitation frequency considered, i.e. Ω = 0.1. Thus there were two complete cycles at the maximum amplitude at this frequency. The normalised sampling frequency was set at Ω_s = 32768 where $\Omega_s = 2\pi f_s / \omega_n$. The value of Ω_s was set to avoid the occurrence of aliasing from higher harmonics in the response. These harmonic responses are expected to be negligible beyond around five times the maximum excitation frequency for power law damping with p = 5.

2.4.2 Transmissibility and amplitude ratio

The response characteristic of vibration isolation is usually presented as a transmissibility function. It shows the ratio of the amplitude between the response and the input with the same physical quantity [7] as a function of the excitation frequency [57]. For example, the ratio between the force transmitted to the supporting structure and the applied force forms the force transmissibility. The ratio between the motion of the isolated mass and the base excitation is the motion transmissibility [58].

For the linear system, the transmissibility function can represent completely the isolation capability. This is because a single frequency excitation only produces the response at the same frequency and it is independent of excitation amplitude. On the other hand, for nonlinear system, the single frequency excitation can produce response at frequencies other than the excitation frequency. The responses at other frequencies are ignored by means of transmissibility and the term transmissibility is not suitable. Thus, in this study, the term amplitude ratio is used instead which represents the ratio of the amplitude between the input and response at only the fundamental excitation frequency.

The amplitude ratio can usually be constructed using either the ratio of the root mean square (RMS) values or the ratio of the Fourier coefficients at the excitation frequencies between the output and the input. There should be small difference between these two amplitude ratios if the response at the excitation frequency is not strongly affected by the responses at harmonic frequencies. The existence of the responses at other harmonics can distort and affect the time domain response. By using only the

Fourier coefficients at the excitation frequencies, the nonlinear responses at the higher harmonics are disregarded. As such, the amplitude ratio constructed using Fourier coefficients would not in general be the same as that constructed using RMS values. The discussion of amplitude ratios constructed from these two quantities is given in section 2.5.2.

2.4.3 Frequency domain analysis

The frequency domain analysis was carried out by means of the amplitude ratio. The amplitude ratio is constructed using either the Fourier coefficients or the RMS values of the time histories obtained from direct numerical integration of the equation of motion. The discrete value of the Fourier coefficient was calculated using the exponential form of the Fourier series [59], i.e.

$$c_q^{(h)} = \frac{1}{N}\sum_{n=0}^{N-1} q(n) e^{-j\frac{2\pi hn}{N}} \tag{2.18}$$

where $q(n)$ is the discrete time response, h is the harmonic of the excitation frequency and N is the number of discrete data points. The RMS values are calculated from

$$\overline{q^2} = \frac{1}{N}\sum_{n=0}^{N-1} q^2(n) \tag{2.19}$$

The difference in the amplitude ratio constructed from these two quantities is that the amplitude ratio obtained from RMS value includes the effect of higher harmonics whereas that for Fourier coefficient considers only the response at the excitation frequency. The responses at higher harmonics are examined by means of the total harmonic distortion.

However, the application of the RMS value does not provide the phase information. It can be obtained by using Fourier coefficients and can be given by

$$\phi(\varphi) = \angle c_x^{(1)}(\varphi) - \angle c_{x_0}^{(1)}(\varphi) \tag{2.20}$$

where φ is the discrete frequency, $c_x^{(1)}$ and $c_{x_0}^{(1)}$ are Fourier coefficients at excitation frequency for the response and excitation respectively.

2.4.4 Total harmonic distortion

Total harmonic distortion (THD) is a measurement of the distortion of the harmonic signal. The THD indicates the effect of the responses at other harmonics occurring in the signal. It is defined as the ratio or percentage of the sum of the power at all harmonics to the power in the fundamental harmonic and is given by

$$THD(\varphi) = \sqrt{\frac{\sum_{h=2}^{P} \left| c_x^{(h)}(\varphi) \right|^2}{\left| c_x^{(1)}(\varphi) \right|^2}} \tag{2.21}$$

where $c_x^{(h)}$ is the Fourier coefficient of x at the h^{th} harmonic and P is the number of harmonics considered. This expression can be found, for example, in references [60] and [61].

2.5 Numerical results and discussion

The input excitation was taken to be a normalised amplitude for either harmonic force or displacement base excitation, i.e. F_e = 1 for force excitation and $F_e = \Omega^2$ for base excitation. At Ω = 1 the relative displacement for the system with linear damping between these two cases are identical and given by

$$U = \frac{1}{2\zeta_1} \tag{2.22}$$

The calculated relative displacement amplitude for ζ_1 = 0.1, 0.2 and 0.3 obtaining from equation (2.22) are 14 dB, 8 dB and 4 dB. These values were used to estimate the equivalent values of linear viscous damping for the power law damping which are listed in table 2.1.

2.5.1 The response in the isolation region

The numerical results are presented using the amplitude ratio and are shown for both force and base excitation in figure 2.4 for ζ_1 = 0.1, 0.2 and 0.3. It is seen that for every case the level of the peak amplitude can be reduced by increasing the non-dimensional damping term. The difference among the cases occurs in the frequency region well above the resonance frequency, i.e. $\Omega \gg 1$.

For the case of force excitation with an exponent p greater than unity, figures 2.4 (a)-(c) in the first column, the force amplitude ratio at high frequencies is seen to follow the mass line of the undamped system, as shown by the asymptote line of 40 dB per decade. It also appears that the amplitude ratios decrease regardless of either the damping ζ_p or the exponent p. One might presume that the power law damping can produce a behaviour similar to the undamped response in the isolation region.

On the other hand for base excitation, shown in the second column of figure 2.4, the response amplitudes in the high frequency region are considerably higher than that for linear viscous damping. Increasing the value of damping, ζ_p, causes a higher level for the displacement amplitude ratio. The response amplitude in this region for $p = 2$ is constant, whereas the curves for $p > 2$ tend towards the amplitude of the base excitation. It is anticipated that at excitation frequencies well above the resonance frequency the isolated mass is moving almost together with the base excitation.

In addition, figure 2.5 shows the phase between the response and the excitation which is defined from the Fourier coefficients at the excitation frequency. It reveals, for the force case, that the transmitted force in the high frequency region is out of phase with the excitation for power law damping with $p > 1$. This is consistent with an undamped system. In contrast, for the base excitation, the phase information shows a diminishing phase lag between the isolated mass and the base. This supports the argument that the isolated mass is moving almost in unison with the base as the excitation frequency increases. One might assume that at high excitation frequencies the damping component is acting almost like a rigid link.

To this end, one might consider that the application of power law damping with an integer exponent $p > 1$ is beneficial to the case of force excitation and is detrimental for base excitation. Although the application of a greater damping term or higher exponent has provided some noticeable isolation advantages for force isolation, it might produce a negative effect, for example harmonic distortion. Further discussion on harmonic distortion is discussed in the next sub-section.

2.5.2 The response at higher harmonics

The level of total harmonic distortion (THD) shown in figure 2.6 reveals the response amplitude at higher harmonic frequencies other than the excitation frequency. The higher level of THD indicates the higher response amplitude at other harmonics compared to the amplitude at the fundamental frequency. It is seen that either a larger exponent value p or a greater damping value produces a higher THD level for the case of either force or base excitation.

It is noticeable that, for the case of force excitation with $p > 2$, the level of THD is highest around the resonance frequency and is almost zero at higher frequencies. On the other hand, the level of THD for base excitation in the high frequency region is noticeably inversely related to the level of displacement amplitude ratio as shown in figure 2.4. The THD tends to zero as the displacement amplitude ratio tends towards unity. Such behaviour can be thought to be a result of the damping component becoming almost rigid. Since the isolated mass and the base are thought to be moving together the relative velocity across the damper is approaching zero. Hence the effect of nonlinearity is reduced. Thus the response at the excitation frequency becomes dominant.

The THD level for the case of force excitation with $p = 5$ around $\Omega = 1$, see figure 2.6 (c), is highest at about 28%. This high THD level might result in a difference between the force amplitude ratios constructed using the Fourier coefficients and the RMS values around the corresponding frequencies. However, as shown in figure 2.7 (a), comparison of the force amplitude ratios constructed using these two quantities for the power law damping with exponent $p = 5$ and $\zeta_5 = 0.124$ are very slightly different. This result suggests that the nonlinear response amplitude ratio constructed using Fourier coefficients at the excitation frequency is comparable to that using RMS values. Therefore the application of an approximate analytical method which considers only the response at the excitation frequency is suitable, for example the Harmonic Balance method.

2.6 Conclusions

The application of power law damping with an integer exponent p ranging from 1 to 5 has been examined numerically for force and base excitation. The response amplitudes for the power law damping with $p > 1$ were examined in comparison to that with linear damping, $p = 1$. By maintaining the response amplitude around the resonance frequency at a similar level as for the linearly damped response, the distinctive effect of the power law damping can be noticeable in the isolation region. The application of power law damping with $p > 1$ for force excitation results in a lower level of transmitted force. However, the application of a higher integer exponent causes the increasing of response amplitude at higher harmonics when the excitation frequency is around the resonance frequency.

In contrast, for base excitation the power law damping with $p > 2$ causes an increase in the vibration amplitude of the isolated mass compared to linear damping for excitation frequencies well above the resonance frequency. The displacement amplitude of the isolated mass can approach that of the base. At this stage the phase lag is close to zero. One might consider that the damping element locks the isolated mass and base together.

It is interesting to find out the reason why power law damping is beneficial for one excitation but is detrimental for the other. Thus in the next chapter cubic damping, $p = 3$, is chosen as an example to investigate the above mentioned effects. This is because the numerical results obtained in this chapter show that the application of a higher integer exponent in power law damping, i.e. $p = 4$ and $p = 5$, does not significantly change the response characteristics at high frequencies. An analytical investigation will be performed alongside a numerical study.

Table 2.1 Non-dimensional damping coefficients for power law damping and its linear equivalence at undamped natural frequency (Ω = 1).

Non-dimensional damping term	Equivalent values of linear viscous damping		
ζ_1	0.1	0.2	0.3
$\zeta_2 \equiv \zeta_1 \frac{3}{4}\frac{\pi}{U}$	0.047	0.189	0.424
$\zeta_3 \equiv \zeta_1 \frac{8}{3U^2}$	0.011	0.085	0.288
$\zeta_4 \equiv \zeta_1 \frac{15}{16}\frac{\pi}{U^3}$	0.002	0.038	0.191
$\zeta_5 \equiv \zeta_1 \frac{16}{5U^4}$	0.0005	0.016	0.124

(a) (b)

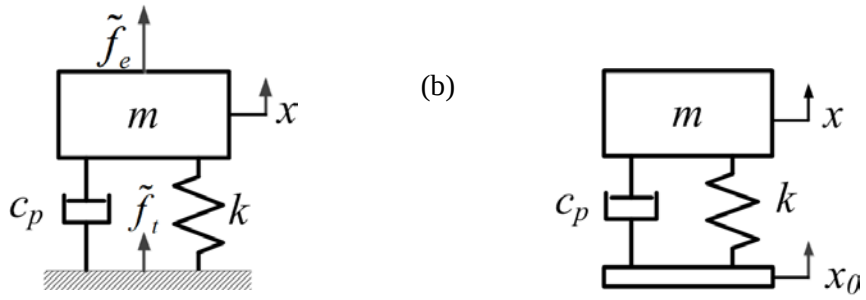

Figure 2.1 Illustrative models for single degree of freedom vibration isolation
(a) Force excited isolation
(b) Base motion excited isolation
where m is a rigid mass. k is an assumed linear stiffness. c_p is a damping coefficient of power law damping. $\tilde{f}_e$ and $\tilde{f}_t$ are the excitation and transmitted forces. x and x_0 are the displacement for the mass and base excitation respectively.

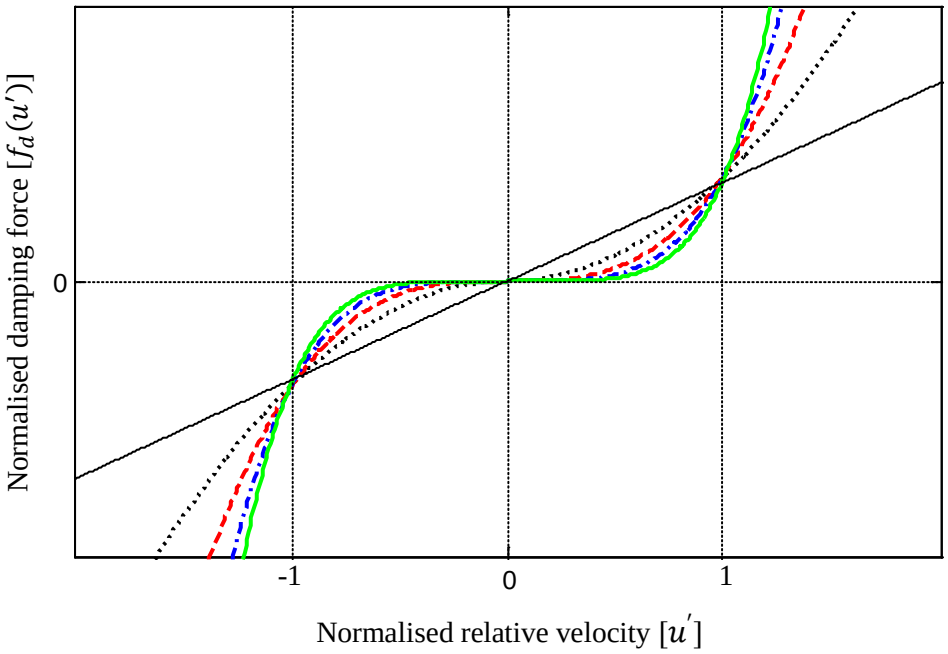

Figure 2.2 Power law damping force characteristics obtained from $f_d(u') = \zeta_p u' |u'|^{p-1}$ in comparison to the linear damping force $f_d(u') = 2\zeta_1 u'$.
—— Linear viscous damping, $p = 1$
····· Quadratic damping, $p = 2$
- - - - Cubic damping, $p = 3$
— · — · Quartic damping, $p = 4$
——— Quintic damping, $p = 5$

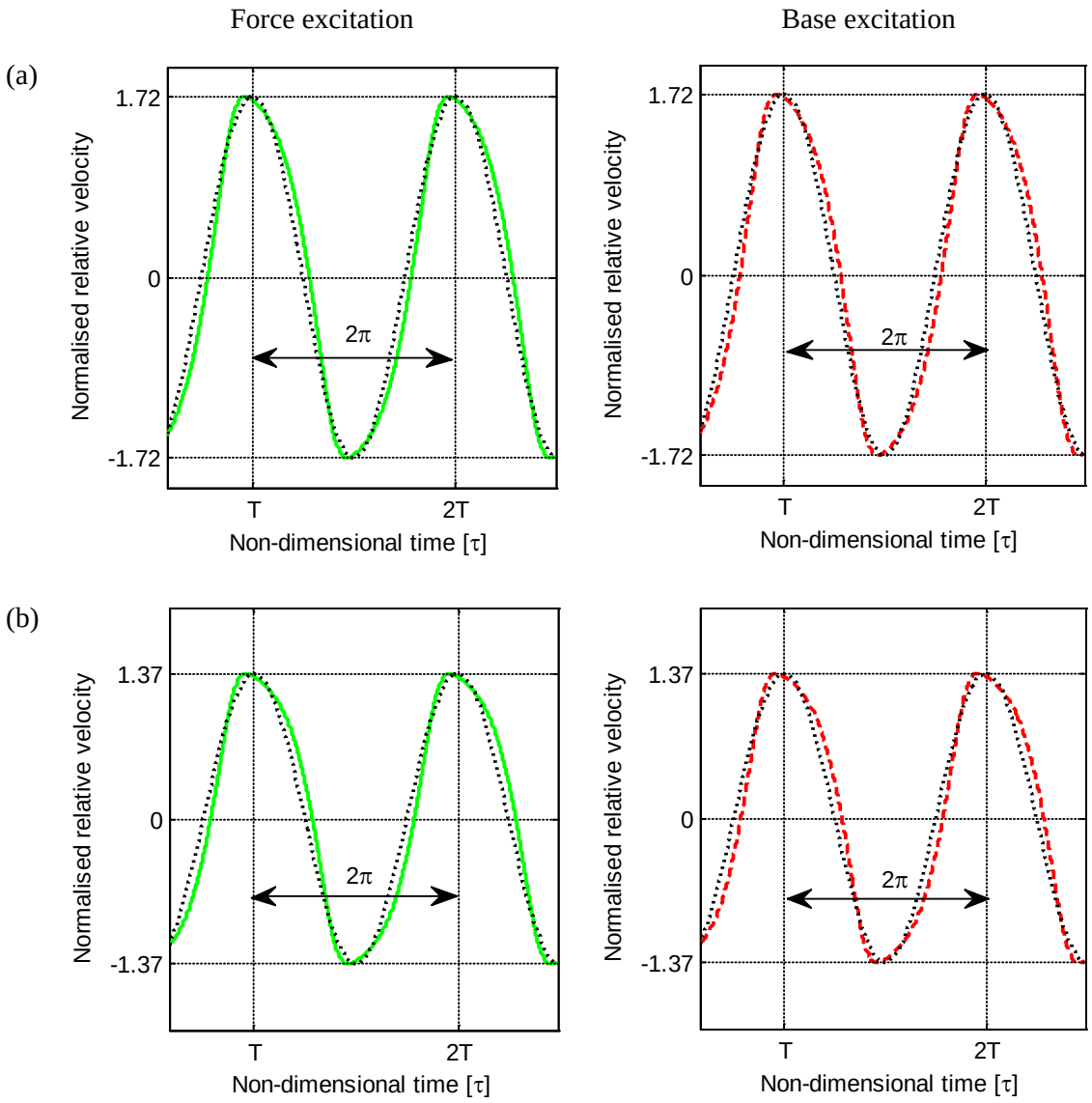

Figure 2.3 Time responses for the relative velocity of the SDOF isolation system possessing power law damping $p = 5$ in comparison to that for linear viscous damping $p = 1$ with a non-dimensional time period of $T = 2\pi$.

(a) $\zeta_5 = 0.1$ and $\zeta_1 = 0.29$

(b) $\zeta_5 = 0.3$ and $\zeta_1 = 0.36$

····· Linear viscous damping

——— Quintic damping force excitation

– – – Quintic damping base excitation

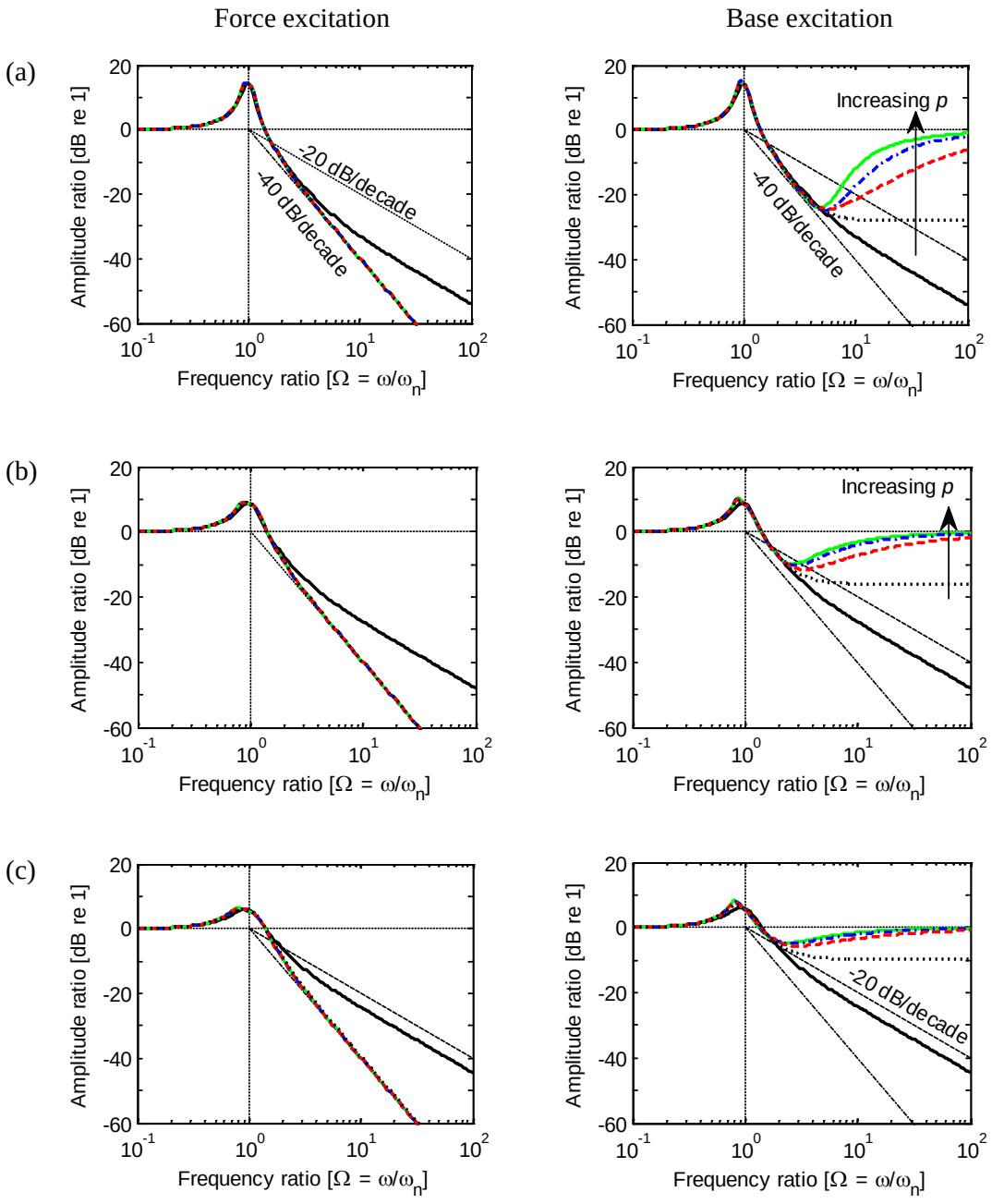

Figure 2.4 The amplitude ratios for a SDOF isolation system possessing power law damping.
(a) ζ_p equivalent to ζ_1 = 0.1
(b) ζ_p equivalent to ζ_1 = 0.2
(c) ζ_p equivalent to ζ_1 = 0.3
Linear viscous damping, p = 1
Quadratic damping, p = 2
Cubic damping, p = 3
Quartic damping, p = 4
Quintic damping, p = 5
-20 dB/decade slope
-40 dB/decade slope

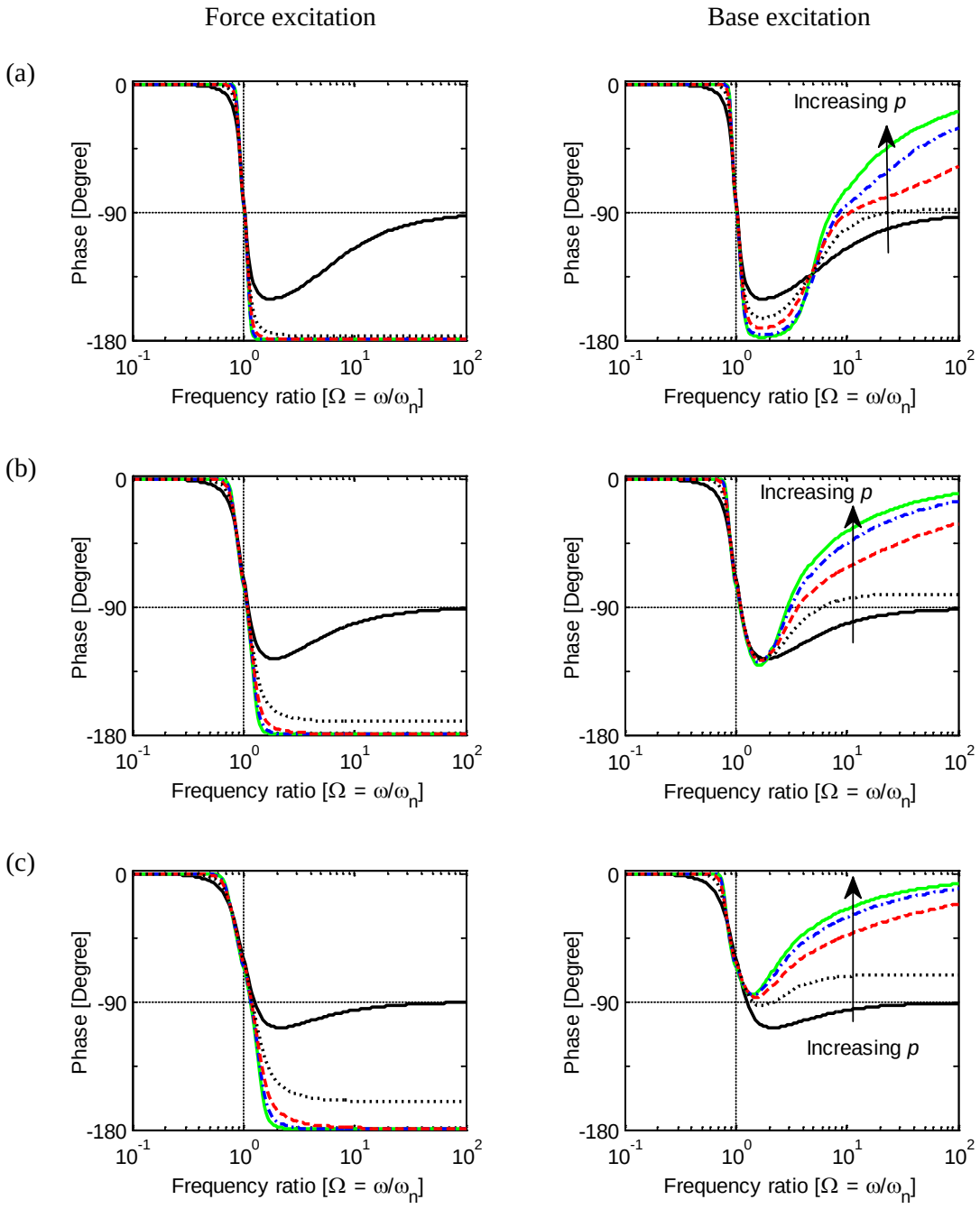

Figure 2.5 The phase lag of the response with respect to the excitation for the SDOF isolation possessing power law damping.

(a) ζ_p equivalent to ζ_1 = 0.1

(b) ζ_p equivalent to ζ_1 = 0.2

(c) ζ_p equivalent to ζ_1 = 0.3

——— Linear viscous damping, p = 1

····· Quadratic damping, p = 2

– – – Cubic damping, p = 3

– · – · Quartic damping, p = 4

——— Quintic damping, p = 5

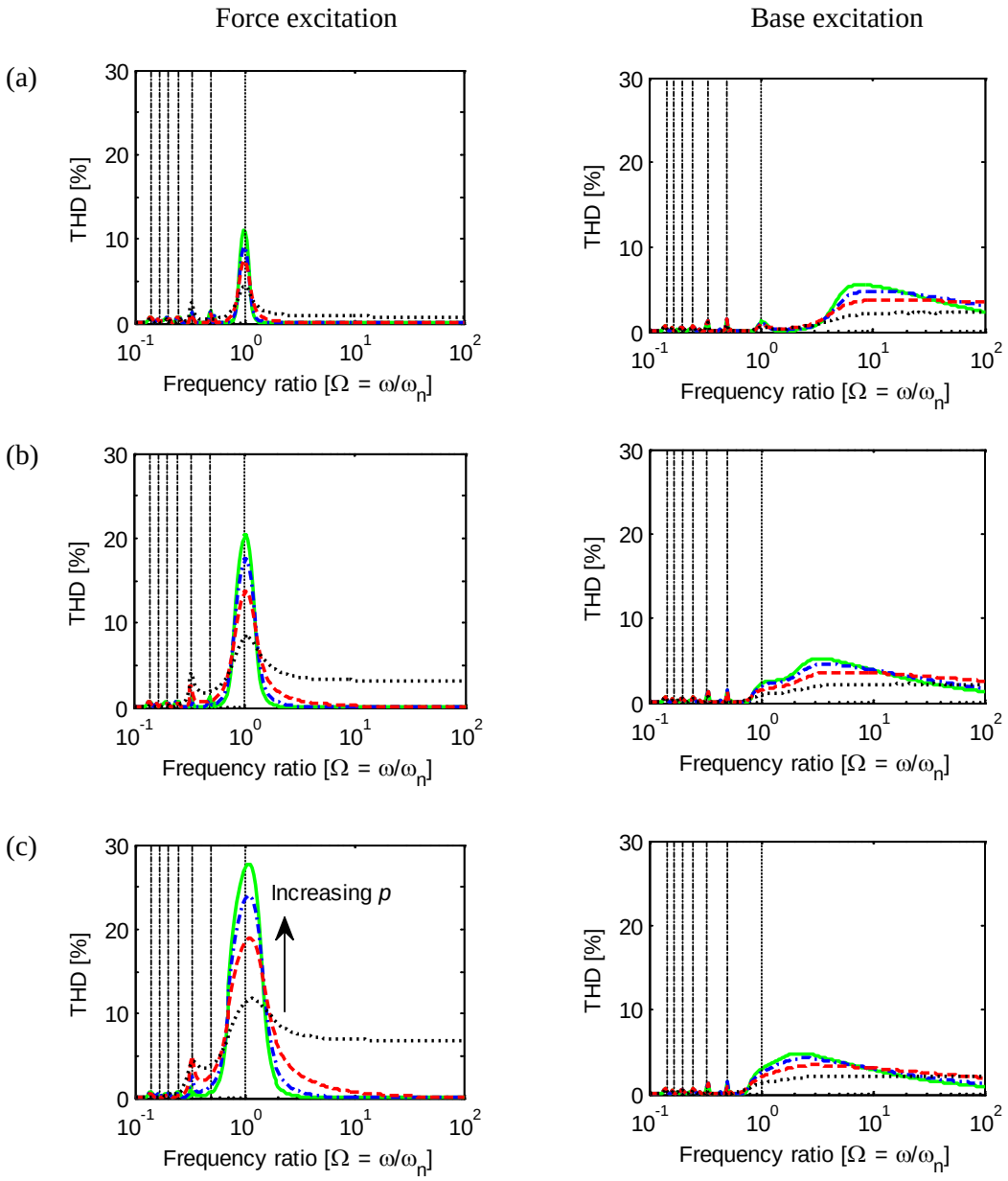

Figure 2.6 The total harmonic distortion for the SDOF isolation possessing power law damping.

(a) ζ_p equivalent to ζ_1 = 0.1

(b) ζ_p equivalent to ζ_1 = 0.2

(c) ζ_p equivalent to ζ_1 = 0.3

—— Linear viscous damping, p = 1

····· Quadratic damping, p = 2

– – – Cubic damping, p = 3

– · – · Quartic damping, p = 4

—— Quintic damping, p = 5

The vertical dash-dot lines represent the excitation frequencies which the resonance frequency, $\Omega = 1$, is one of their harmonics, i.e. $\frac{1}{7}\Omega$, $\frac{1}{6}\Omega$, $\frac{1}{5}\Omega$, $\frac{1}{4}\Omega$, $\frac{1}{3}\Omega$ and $\frac{1}{2}\Omega$ respectively.

(a)

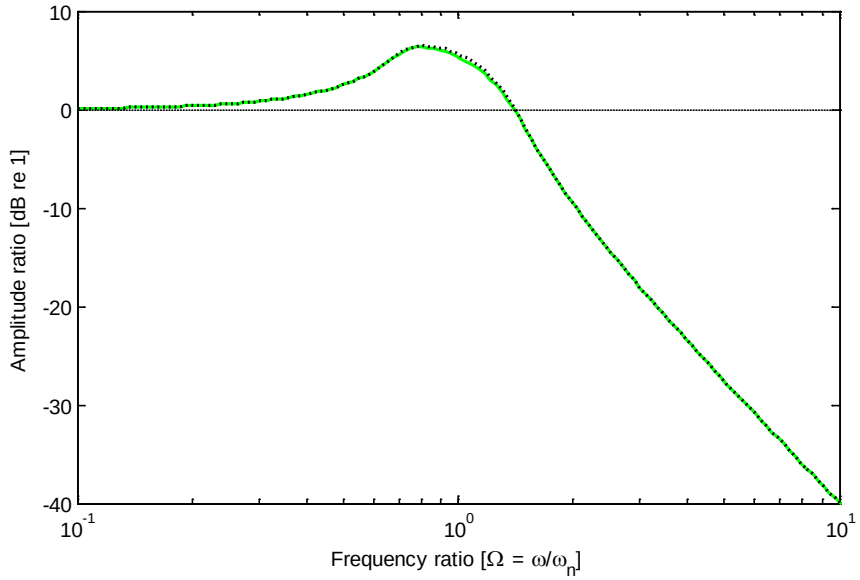

(b)

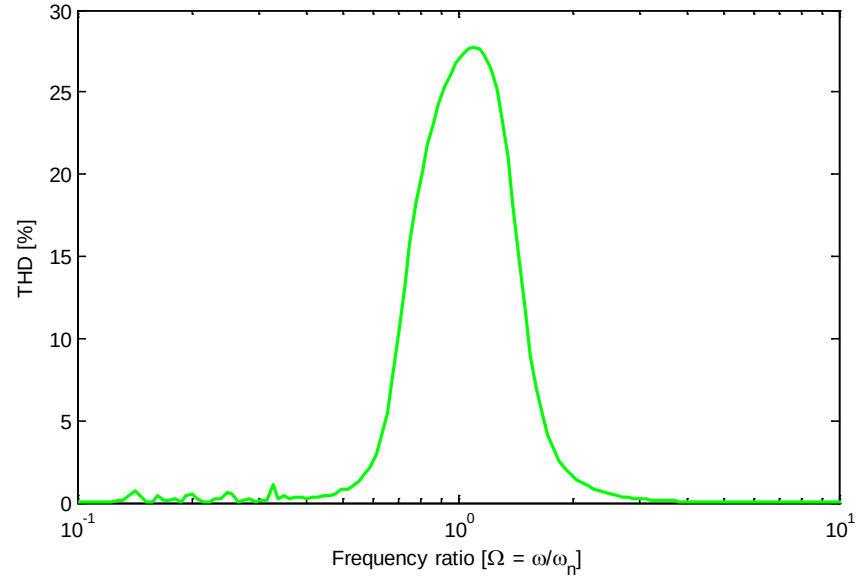

Figure 2.7 Difference of force amplitude ratio due to the total harmonic distortion for the power law damping with $p = 5$ and $\zeta_5 = 0.124$.
(a) Force amplitude ratio
(b) Total harmonic distortion
····· Constructed using RMS values
—— Constructed using Fourier coefficients at excitation frequency

Chapter 3 Analysis of a vibration isolator with cubic damping under harmonic excitation

3.1 Introduction

The numerical simulation results given in Chapter 2 showed that power law damping can be both beneficial and detrimental to isolation. For the case of force excitation, the beneficial effect of the integer power law damping is noticeable when $p = 2$ or higher. On the other hand, the application of power law damping with the integer exponent higher than unity reduces the effectiveness of base isolation.

In this chapter, the analysis will concentrate solely on power law damping with the exponent $p = 3$ (cubic damping). This is because the application of higher integer exponents does not provide any significant difference in terms of the response levels at excitation frequencies well above the resonance frequency, as shown in Chapter 2. This chapter aims to discover the underlying reasons for the conflicting effects on a single degree of freedom (SDOF) system. Two different scenarios were also considered here namely force excited isolation and base excited isolation.

The investigation is conducted using an analytical method in conjunction with the numerical simulation. The former is the Harmonic Balance method (HBM). The HBM is usually applied to obtain approximate closed form solutions for nonlinear systems under harmonic excitation. The results of the method is expected to reveal insights into the effects of cubic damping on the considered isolation model. The application of the numerical approach is expected to validate the analytical examination. The advantageous and disadvantageous effects of cubic damping on the SDOF isolation subject to harmonic excitation will be reported.

Further investigation is performed for base excitation using a harmonic velocity input whose amplitude is constant with frequency. The exploration in the effects of cubic damping on the SDOF isolation might contribute explicit understanding and further consideration to the application of cubic damping in other isolation systems.

3.2 The Harmonic Balance Method

Approximate closed form solutions for the response of nonlinear isolation can be obtained using a variety of approaches. For example, the application of a Volterra series approximation with the concept of Generalised Frequency Response Function (GFRF) was applied in the studies of Jing et al. [26] and Lang et al. [62]. It was applied to analyse the force excitation isolation with third-order polynomial damping. Peng et al. [27] and Lang et al. [63] applied the concept of Output Frequency Response Functions (OFRF), which was proposed by the authors to obtain a frequency domain analysis. Kovacic et al. [33] and Milovanovic et al. [34] approximated the relative displacement and absolute displacement transmissibility for the base excited isolation possessing linear plus cubic damping using the averaging method. Guo et al. [31] applied the Ritz-Galerkin method to evaluate the force and displacement transmissibility for SDOF isolation with nonlinear viscous damping. Among these approaches, the Harmonic Balance Method (HBM) was also applied [24,35] to obtain approximate closed form solutions and is applied here.

For harmonic excitation, the HBM provides comparable theoretical approximations to experimental results [64]. The advantages and limitations of HBM were discussed by Mickens [65]. One useful result of using HBM is that the method is not restricted to weakly nonlinear problems. The limitation for its application is that the response must be dominated by the excitation frequency. In other words, the amplitude of other harmonics of the excitation frequency must be relatively small. From earlier observation in Chapter 2, this shows that it is suitable for solving the problems in this study. The numerical results showed that the level of THD for force excitation with exponent $p = 3$ and damping equivalent to $\zeta_1 = 0.3$ is less than about 20% which is considered relatively small.

The principle of the HBM is to assume a steady-state periodic response for a harmonic input which can be expected in the form of

$$q(t) = \sum_{h=1}^{P} Q_h \cos\left(h\left(\omega t - \phi\right)\right) \tag{3.1}$$

where Q is the amplitude, h is the harmonic of the excitation frequency and P is the number of harmonic frequencies included. The application of the HBM in this study

only determines the amplitude of the response at the excitation frequency, i.e. $h = 1$. This was achieved by integrating the product between the response given in equation (3.1) and the trigonometric functions at excitation frequency over one period, the super harmonics included in the response are eliminated as a result of the orthogonality properties.

3.3 Governing equation of motion and analytical solution

The equations of motion, given in equations (2.8) and (2.9), are employed again, only with $p = 1$ and 3, and are rewritten in non-dimensional form as

$$u'' + 2\zeta_1 u' + \zeta_3 \left(u'\right)^3 + u = F_e \cos\left(\Omega\tau\right) \tag{3.2}$$

$$f_t\left(\tau\right) = 2\zeta_1 u' + \zeta_3 \left(u'\right)^3 + u \tag{3.3}$$

where F_e is the normalised excitation amplitude, $f_t\left(\tau\right)$ is the normalised transmitted force as a function of non-dimensional time τ . u , u' and u'' are normalised relative displacement, velocity and acceleration. The normalised relative displacement is defined by

$$u = w - w_0 \tag{3.4}$$

where w and w_0 are the normalised absolute displacement of the isolated mass and base respectively.

Later the cases of $p = 1$ and 3 are examined separately and discussed comparatively. The non-dimensional damping term for the power law damping given in equation (2.13) is also employed here for $p = 3$. Thus one obtains

$$\zeta_3 = \frac{c_3}{m}\omega_n X^2 \tag{3.5}$$

The expected harmonic responses for the relative motions are given by

$$u = U\cos\left(\Omega\tau - \phi_u\right),\ u' = -\Omega U \sin\left(\Omega\tau - \phi_u\right) \text{ and } u'' = -\Omega^2 U \cos\left(\Omega\tau - \phi_u\right) \tag{3.6}$$

where U is the normalised amplitude of the relative displacement and ϕ_u is the phase lag between the relative displacement and the base excitation. Substituting the harmonic excitation and the responses into equation (3.2) yields

$$\left(1-\Omega^2\right)U\cos\left(\Omega\tau-\phi_u\right)-2\zeta_1\Omega U\sin\left(\Omega\tau-\phi_u\right)-\zeta_3\Omega^3U^3\sin^3\left(\Omega\tau-\phi_u\right)=F_e\cos\left(\Omega\tau\right) \tag{3.7}$$

For simplicity, equation (3.7) is written as

$$AU\cos\left(\Omega\tau-\phi_u\right)-BU\sin\left(\Omega\tau-\phi_u\right)-\frac{4}{3}CU^3\sin^3\left(\Omega\tau-\phi_u\right)=F_e\cos\left(\Omega\tau\right) \tag{3.8}$$

where the expressions for A, B and C are given by

$$A=1-\Omega^2,\ B=2\zeta_1\Omega \text{ and } C=\frac{3}{4}\zeta_3\Omega^3 \tag{3.9}$$

Then apply the orthogonality by integrating the product of the terms in the left and right sides of equation (3.8) with the trigonometric functions at the excitation frequency over a period of $2\pi/\Omega$. This yields

$$\frac{\Omega}{\pi}\int_0^{\frac{2\pi}{\Omega}}AU\cos\left(\Omega\tau-\phi_u\right)\sin\left(\Omega\tau\right)d\tau=AU\sin\left(\phi_u\right) \tag{3.10}$$

$$\frac{\Omega}{\pi}\int_0^{\frac{2\pi}{\Omega}}AU\cos\left(\Omega\tau-\phi_u\right)\cos\left(\Omega\tau\right)d\tau=AU\cos\left(\phi_u\right) \tag{3.11}$$

$$\frac{\Omega}{\pi}\int_0^{\frac{2\pi}{\Omega}}\left[BU\sin\left(\Omega\tau-\phi_u\right)+\frac{4}{3}CU^3\sin^3\left(\Omega\tau-\phi_u\right)\right]\sin\left(\Omega\tau\right)d\tau=\left(BU+CU^3\right)\cos\left(\phi_u\right) \tag{3.12}$$

$$\frac{\Omega}{\pi}\int_0^{\frac{2\pi}{\Omega}}\left[BU\sin\left(\Omega\tau-\phi_u\right)+\frac{4}{3}CU^3\sin^3\left(\Omega\tau-\phi_u\right)\right]\cos\left(\Omega\tau\right)d\tau=-\left(BU+CU^3\right)\sin\left(\phi_u\right) \tag{3.13}$$

$$\frac{\Omega}{\pi}\int_0^{\frac{2\pi}{\Omega}}F_e\cos\left(\Omega\tau\right)\sin\left(\Omega\tau\right)d\tau=0 \tag{3.14}$$

$$\frac{\Omega}{\pi}\int_0^{\frac{2\pi}{\Omega}}F_e\cos\left(\Omega\tau\right)\cos\left(\Omega\tau\right)d\tau=F_e \tag{3.15}$$

As a result, equation (3.8) can be written using terms resulting from equations (3.10), (3.12) and (3.14) to form

$$AU\sin\left(\phi_u\right)-\left(BU+CU^3\right)\cos\left(\phi_u\right)=0 \tag{3.16}$$

and terms resulting from equations (3.11), (3.13) and (3.15) to form

$$AU\cos\left(\phi_u\right)+\left(BU+CU^3\right)\sin\left(\phi_u\right)=F_e \tag{3.17}$$

Squaring and adding equations (3.16) and (3.17) gives

$$C^2U^6+2BCU^4+\left(A^2+B^2\right)U^2=F_e^2 \tag{3.18}$$

The phase lag of the relative motion to the excitation is obtained from equation (3.16) and is given by

$$\phi_u=\tan^{-1}\left(\frac{B+CU^2}{A}\right) \tag{3.19}$$

Later, equation (3.18) is examined separately for linear and cubic damping. For the case of linear viscous damping, with $C = 0$, equations (3.18) and (3.19) are rewritten respectively as

$$\left(A^2+B^2\right)U^2=F_e^2 \tag{3.20}$$

and

$$\phi_u=\tan^{-1}\left(\frac{B}{A}\right) \tag{3.21}$$

For the case of pure cubic damping then $B = 0$, equation (3.18) becomes

$$C^2U^6+A^2U^2=F_e^2 \tag{3.22}$$

The solution of U^2 for equation (3.22) consists of one real and a pair of complex conjugates since the coefficient of U^4 is equal to zero. (see Appendix B for the roots of a cubic polynomial equation.) Therefore only the real solution of U^2 is employed to determine either the force amplitude ratio or absolute displacement amplitude ratio for the system with pure cubic damping. The phase lag given in equation (3.19) becomes

$$\phi_u = \tan^{-1}\left(\frac{CU^2}{A}\right) \tag{3.23}$$

The analytical solutions resulting from solving equations (3.20) and (3.22) are presented respectively in sections 3.3.1 and 3.3.2 for the force and the displacement excitations.

3.3.1 Transmitted force amplitude ratio to the rigid base

For the case of force excitation, the normalised amplitude F_e equals unity thus equations (3.20) and (3.22) become

$$\left(A^2 + B^2\right)U^2 = 1 \tag{3.24}$$

and

$$C^2U^6 + A^2U^2 = 1 \tag{3.25}$$

The frequency response for the transmitted force is obtained by substituting the assumed harmonic responses into equation (3.3) which yields

$$F_t \cos\left(\Omega\tau - \phi_f\right) = U\cos\left(\Omega\tau - \phi_u\right) - BU\sin\left(\Omega\tau - \phi_u\right) - \frac{4}{3}CU^3\sin^3\left(\Omega\tau - \phi_u\right) \tag{3.26}$$

where ϕ_f is the phase lag between the transmitted and the excitation force. The application of orthogonality properties of the excitation frequency and the consequent manipulation of equation (3.26) yields

$$F_t^2 = C^2U^6 + 2BCU^4 + \left(1 + B^2\right)U^2 \tag{3.27}$$

The phase lag between the excitation and transmitted force is obtained from

$$\phi_f = \tan^{-1}\left(\frac{\left(CU^2 + B\right)\Omega^2}{\left(CU^2 + B\right)^2 + A}\right) \tag{3.28}$$

For the case of linear damping system for which $C = 0$, the algebraic manipulation of equations (3.24) and (3.27) yields

$$F_t^2 = \frac{1+B^2}{A^2+B^2} \tag{3.29}$$

The phase lag between the forces for the case of linear damping is given by

$$\phi_f = \tan^{-1}\left(\frac{B\Omega^2}{A+B^2}\right) \tag{3.30}$$

For the case of pure cubic damping, equation (3.27) becomes

$$F_t^2 = C^2U^6 + U^2 \tag{3.31}$$

The force amplitude ratio, F_t, for the case of pure cubic damping can be obtained by substituting the solution of U^2 obtained from equation (3.25) into equation (3.31). The expression of U^2 for force excitation is given by

$$U^2 = \frac{1}{6}\frac{\left(108C + 12\sqrt{12A^6 + 81C^2}\right)^{\frac{2}{3}} - 12A^2}{C\left(108C + 12\sqrt{12A^6 + 81C^2}\right)^{\frac{1}{3}}} \tag{3.32}$$

The resulting closed form solution for the force amplitude ratio is too complicated to understand the effect of cubic damping. Equations (3.25) and (3.31) were simply examined for four specific frequency regions, namely $\Omega \ll 1$, $\Omega \approx 1$, $\Omega \approx \sqrt{2}$ and $\Omega \gg 1$. These frequency regions represent respectively an excitation frequency well below the undamped natural frequency ω_n, around ω_n, the beginning of the isolation region for the linear damping system $\sqrt{2}\omega_n$ and a frequency region much higher than ω_n. The simplified expressions for these frequency regions are examined and discussed in detail later in section 3.5 alongside numerical verification. The details of the simplification for each frequency region are presented in Appendix C.

3.3.2 Absolute displacement amplitude ratio

The absolute displacement harmonic response is determined from the relative motion given in equation (3.4), i.e. $w = w_0 + u$. Equation (3.18) is employed again here with $F_e = \Omega^2$ which yields

$$C^2U^6 + 2BCU^4 + \left(A^2 + B^2\right)U^2 = \Omega^4 \tag{3.33}$$

Using the assumption of harmonic excitation, equation (3.4) can be written as

$$W\cos\left(\Omega\tau - \phi_w\right) = \cos\left(\Omega\tau\right) + U\cos\left(\Omega\tau - \phi_u\right) \tag{3.34}$$

where ϕ_w is the phase lag between the isolated mass and the base excitation. The application of orthogonality and the consequent manipulation transforms equation (3.34) to

$$W^2 = U^2 + 2U\cos\left(\phi_u\right) + 1 \tag{3.35}$$

The phase lag between the base excitation and isolated mass is given by

$$\phi_w = \tan^{-1}\left(\frac{\left(B + CU^2\right)U}{AU + \sqrt{A^2 + \left(B + CU^2\right)^2}}\right) \tag{3.36}$$

Similarly to the case of force excitation, an examination of the case of linear and cubic damping is carried out separately. For the system with linear damping, one sets $C = 0$ thus equations (3.33) becomes

$$\left(A^2 + B^2\right)U^2 = \Omega^4 \tag{3.37}$$

After algebraic manipulation, the absolute displacement amplitude ratio squared is given by

$$W^2 = \frac{1 + B^2}{A^2 + B^2} \tag{3.38}$$

Equation (3.38) is identical to that given in equation (3.29). For simplicity, equations (3.29) and (3.38) are given in a common form, equal to the transmissibility squared for the linear system,

$$T_r^2 = \frac{1+\left(2\zeta_1\Omega\right)^2}{\left(1-\Omega^2\right)^2+\left(2\zeta_1\Omega\right)^2} \tag{3.39}$$

The phase lag between the isolated mass and base excitation for the case of linear viscous damping is given by

$$\phi_w = \tan^{-1}\left(\frac{B\Omega^2}{A+B^2}\right) \tag{3.40}$$

For the case of pure cubic damping, one has $B = 0$ so equation (3.33) becomes

$$C^2U^6 + A^2U^2 = \Omega^4 \tag{3.41}$$

Equation (3.41) has one real solution and a pair of complex conjugates solutions. The only real solution for base excitation is given by

$$U^2 = \frac{1}{6}\frac{\left(108\Omega^4C+12\sqrt{12A^6+81\Omega^8C^2}\right)^{\frac{2}{3}}-12A^2}{C\left(108\Omega^4C+12\sqrt{12A^6+81\Omega^8C^2}\right)^{\frac{1}{3}}} \tag{3.42}$$

The amplitude ratio for the absolute displacement can be obtained by substituting U^2 from equation (3.42) into equation (3.35). Similarly to the case of force excitation, the closed form solution does not explicitly show the effect of cubic damping. Thus equations (3.35) and (3.41) are also examined for four specific frequency regions. The simplification, assumptions and procedure are given in Appendix C.

3.4 Numerical simulations for harmonic excitation

The numerical simulations were carried out by direct numerical integration using the Matlab ODE45 solver [66]. It was applied to the differential equations given in equations (3.2) and (3.3) for force excitation system. For base excitation, equation (3.2) was rewritten using the absolute displacement and the base excitation which is given by

$$w'' + 2\zeta_1 \left(w' - w_0' \right) + \zeta_3 \left(w' - w_0' \right)^3 + \left(w - w_0 \right) = 0 \tag{3.43}$$

The choice in the values of non-dimensional damping terms, i.e. ζ_1 and ζ_3, are described in section 3.4.1. The description of the excitations applied for the simulation is presented in section 3.4.2.

3.4.1 Non-dimensional damping value selection

The values of cubic damping used for the numerical simulation in Chapter 2 were estimated based on the equivalent rate of energy dissipation of linear viscous damping at the undamped natural frequency, $\Omega = 1$. As a result, the levels of the force and absolute displacement amplitude ratios for the nonlinear damping at this frequency were about the same as those for linear viscous damping, see figure 2.4. It is noticed that, for cubic damping (dashed line), the actual resonance frequencies are slightly lower than the undamped natural frequency and are not the same as those for linear damping. This frequency could not be explicitly identified using analysis but could be estimated numerically using the approximate closed form HBM solutions.

The values of non-dimensional linear, ζ_1, and cubic damping, ζ_3, are assigned in the range from 0.01 to 1. The relationship between the peak amplitude and value of non-dimensional damping is shown in figure 3.1 (a), whilst figure 3.1 (b) shows the relationship between the resonance frequency and the value of non-dimensional damping. In order to investigate the effect of cubic damping in the high frequency region, the amplitude ratio at the resonance frequency for the system with cubic damping was fixed at the same level as that for the system with linear damping. Linear viscous damping ratio values of 0.1, 0.2 and 0.3 were used. The levels of the amplitude ratio for the system with linear damping are explicitly obtained from

$$T_{re}^2 = \frac{1 + \left(2\zeta_1 \Omega_{re} \right)^2}{\left(1 - \Omega_{re}^2 \right)^2 + \left(2\zeta_1 \Omega_{re} \right)^2} \tag{3.44}$$

where Ω_{re} is the frequency of resonance and is given by

$$\Omega_{re} = \frac{1}{2\zeta_1} \left(\sqrt{1 + 8\zeta_1^2} - 1 \right)^{\frac{1}{2}} \tag{3.45}$$

for $0 < \zeta_1 < 1$ [7]. The corresponding levels of the absolute displacement amplitude ratios for ζ_1 = 0.1, 0.2 and 0.3 are 14 dB, 9 dB and 6 dB respectively. Considering the peak level of amplitude ratio which linear damping produces, the corresponding non-dimensional cubic damping ζ_3, which produces a similar level of peak response, can be obtained. The corresponding values of ζ_3 are listed in table 3.1 and were applied in the numerical simulations.

The corresponding resonance frequencies could be obtained from the intersection of the lines shown in figure 3.1 (b). It is seen that the resonance frequency with cubic damping is lower than that for linear damping provided one has a similar resonance peak level.

3.4.2 Numerical excitations and responses

The numerical excitations applied have the same characteristics as those in Chapter 2, i.e. harmonic with either constant amplitude of force or constant amplitude of base displacement. The frequency components of the time histories for both cases were found using Fourier coefficients. Only the Fourier coefficients at the excitation frequencies were considered for constructing the amplitude ratios. The Fourier coefficients for the higher harmonics were employed for evaluating the THD.

3.5 Analytical and numerical analyses for specific frequency regions

The analysis into the effect of cubic damping on the vibration isolation is performed using numerical simulation and the HBM. The numerical plots for the HBM are obtained by numerical substitution into equations (3.31) and (3.32) as well as equations (3.35) and (3.42) for the cases of force and base excitation respectively. The numerical values for ζ_3 given in table 3.1 are used for each case.

Figure 3.2 shows comparisons of the force amplitude ratio for the force excited systems with cubic damping. The numerical results obtained using HBM approximation (dashed line) are compared to the results obtained using numerical simulation (cross markers). It is seen that the plots of the force amplitude ratio between the HBM and numerical integration results are similar. The exact solutions of force amplitude ratio for

the system with linear damping (dotted lines) are also shown in figure 3.2 for comparison.

Also, shown in figure 3.3 are the displacement amplitude ratios for the base excited isolation systems with cubic damping. The results obtained using the HBM approximation (solid line) are compared to those obtained using numerical simulation (cross makers). It is noticed that there is almost no difference between these two plots and the approximate HBM expressions are confirmed.

Therefore the subsequent examination given in the following sections are performed based solely on the numerical plots obtained using the HBM solutions and the simplified expressions listed in table 3.2. The examination and discussion present the responses for four frequency regions, i.e. $\Omega \ll 1$, $\Omega \approx 1$, $\Omega \approx \sqrt{2}$ and $\Omega \gg 1$ respectively.

3.5.1 Excitation frequencies well below the undamped natural frequency

The plots of the force amplitude ratios are given in figures 3.2 (a) to (c). The levels of these ratios at $\Omega \ll 1$ for both linear and cubic damping are similar at about unity. The displacement amplitude ratios in this frequency region for base excitation shown in figures 3.3 are also at about the level of unity. The resulting HBM simplifications for both linear and cubic damping listed in row (a) of table 3.2 also are in accordance with this behaviour.

In addition, the plots of phase lag show that the phase in this frequency region is approximately zero. This is typically referred to as quasi-static behaviour. As a result, the relative velocity across the damper is close to zero. Hence there is no contribution to either the transmitted force or motion via the damping component in this frequency region. As such, at this stage, one might conclude that the damper does not have a significant effect at these low frequencies.

3.5.2 The response around the undamped natural frequency

The analysis for this frequency region, i.e. $\Omega \approx 1$, aims to reveal the capability of cubic damping to suppress the amplitude in the amplification zone. Note that the value of non-dimensional cubic damping for either the case of force or base excitation was

chosen to produce the equivalent level of amplitude ratio for the linear system. Therefore, the amplitudes of resonance peaks in either figures 3.2 (a) to (c), for the force case, or figures 3.3 (a) to (c), for the base case, are similar to those for the cases of linear damping systems.

It can be seen that the greater the value of cubic damping for either case results in a lower level of the peak response. These results are consistent with the simplified expressions listed in row (b) of table 3.2. It is apparent that the level of the amplitude ratio contains a term which is inversely related to the value of the damping. Therefore it is in accordance of the numerical results that increasing the level of either linear or cubic damping reduces the level of both the force and displacement amplitude ratio.

One might expect to estimate the value of non-dimensional cubic damping by equating the simplified expressions given in row (b) of table 3.2 for linear and cubic damping. As a result, one obtains

$$\zeta_3 \approx \frac{4}{3}\left(2\zeta_1\right)^3 \tag{3.46}$$

Note that, the value of non-dimensional cubic damping calculated from equation (3.46) will only produce comparable response amplitude to that for linear damping at the undamped natural frequency, i.e. $\Omega \approx 1$. It does not produce comparable response amplitude ratio at the actual resonance frequency. In addition, equation (3.46) gives the same value of non-dimensional cubic damping obtained using equivalent value of linear viscous damping as shown in table 2.1.

3.5.3 The behaviour in lower frequencies of the isolation zone for the linear system

It is commonly known that the start of the isolation region for a SDOF system with linear viscous damping is at the non-dimensional frequency $\Omega = \sqrt{2}$. The level of either force or displacement transmissibility at this frequency can be obtained exactly by substituting $\Omega = \sqrt{2}$ into equation (3.39) and is equal to unity. For the nonlinear system the isolation region might or might not start exactly at $\Omega = \sqrt{2}$ depending on level of nonlinearity. However, the approximate solutions obtained using HBM, as shown in figure 3.2 for force excitation and figure 3.3 for base excitation, are in fairly good

agreement to the numerical simulation results. The figures show that the levels of amplitude ratio at $\Omega = \sqrt{2}$ are about unity.

Further investigation into the response amplitude at higher harmonics of this excitation frequency, figure 3.4, found that the response amplitudes of other harmonics are relatively small compared to that at the excitation frequency. For example, figure 3.4 (c) shows the force amplitude of the third harmonic at around 15 dB lower than that at the excitation frequency (around 17% of the amplitude at the fundamental harmonic) and even smaller for the fifth and seventh harmonics.

So using only the Fourier coefficient at the excitation frequency is acceptable for this instance. For that reason, the HBM approximation is also acceptable. The resulting simplifications for the amplitude ratio for nonlinear systems at this frequency are about unity, as seen in row (c) of table 3.2.

3.5.4 The excitation frequency much above the undamped natural frequency

The isolation zone can be considered as when the excitation frequency is much higher than the natural frequency, i.e. $\Omega \gg 1$. For a SDOF system with linear viscous damping the amplitude ratio is known to reduce inversely proportional to the excitation frequency, i.e. -20 dB per decade. A higher value of linear damping causes a detrimental higher level of response in this frequency region.

The force amplitude ratios for the system with pure cubic damping in this frequency region shown in figure 3.2 are seen to be rolling off at -40 dB per decade. The plots of phase lag between the transmitted and excitation force for the system with cubic damping are constant at around $-\pi$ radians. The plots of force amplitude ratios in this frequency region appear consistent with the simplified expression given in row (d) of table 3.2. For the case of force excitation, it is seen that the force amplitude ratio decreases in proportion to the excitation frequency squared, i.e.-40 dB per decade, independently of the cubic damping value.

One can consider that this is a preferable characteristic for vibration isolation at high frequencies, i.e. less force being transmitted via isolator. These results are also consistent with the results reported in the literature, e.g. [26] and [35], that the cubic

damping is beneficial for the case of force excitation. The reason for this beneficial effect from the cubic damping is discussed in section 3.6.1.

In contrast, the isolator with cubic damping under base excitation does not perform as well as that for the force excitation case. The level of absolute displacement amplitude ratio in this frequency region tends towards the level of unity as shown in figure 3.3. Also the phase lag of the isolated mass with respect to the base excitation tends to zero as excitation frequency increases. As such, for $\Omega \gg 1$, it is not just the equality in the level of displacement amplitude but the isolated mass and the base tend to be moving together. It is also noticeable from figure 3.3 (c) that a greater value of cubic damping causes the level of the amplitude ratio in the isolation region to tend towards 0 dB at a lower frequency compared to that in figure 3.3 (a).

The simplified expression for the displacement amplitude ratio for base excitation given in row (d) of table 3.2 also shows that an increase in excitation frequency results in the level of displacement amplitude ratio being close to unity. Increasing the value of cubic damping increases the amplitude ratio which rises towards unity sooner. This means that the displacement amplitude of the isolated mass is going to be equal to that of the base excitation at high frequencies. This is consistent with the plot shown in figure 3.3.

To this end, the cubic damping on a base excited vibration isolation system can be considered as a rigid connection at high frequencies. As such it does not allow any significant relative motion to occur as seen from the relative displacement amplitude ratio for the base excitation with cubic damping given in row (e) of table 3.2. These results appear to be in accordance with those reported in the literature, e.g. [33] to [35] and [47].

However, the consideration that the damping is acting as a rigid connection is not strictly correct. This is because the damping would never be rigid and the relative velocity across the damper would never be zero. Such consideration is discussed in detail again in section 3.6.1.

3.6 Further discussion and analysis into the effect of cubic damping

The results shown in the previous section are about the outcome in terms of the amplitude ratio and the phase lag. The presence of cubic damping appears useful for force isolation. In the isolation region it produces lower amplitude of the transmitted force than that for linear damping. On the other hand, it would not be preferable for the case of base excitation because the displacement amplitude ratio in the isolation region increases and becomes close to unity. It is interesting to establish the reason why the cubic damping can be beneficial for one system and detrimental for another.

The reason for such occurrences is investigated and reported here in this section by means of the relative velocity and damping force. The existence of the response at higher harmonics is also presented here using the THD. In addition, the effect of cubic damping when the base excitation is specified to have a constant velocity amplitude at all frequencies is examined. This latter case corresponds to the input base displacement having an amplitude inversely proportional to the excitation frequency.

3.6.1 An investigation by means of the damping force

The damping force is the key feature to display the physical influence of the cubic damping since it is a result of a nonlinear function. The amplitude of the damping force can indicate the isolation performance. It should be higher around the resonance frequency in order to suppress the motion of the system mass. On the other hand, for an ideal isolator, it should be minimised in the isolation region, so replicating an undamped system.

The investigation was introduced by considering the level of damping force only in the isolation region, $\Omega \gg 1$, for which the different effect of cubic damping is apparent. The analytical expression for the damping force can be obtained from the corresponding product of the relative displacement and the pre-defined expression B or C, given in equation (3.9). As a result, the damping forces for the case of force excitation are obtained respectively for linear and cubic damping by

$$F_{d1} = BU_{f1} = \frac{2\zeta_1}{\Omega} \tag{3.47}$$

$$F_{d3} = CU_{f3}^3 \approx \frac{3}{4}\frac{\zeta_3}{\Omega^3} \tag{3.48}$$

where U_{f1} and U_{f3} are the relative displacement for linear damping and cubic damping respectively for the force case, listed in row (e) of table 3.2. It is seen that the linear damping force decreases inversely proportionally to the excitation frequency, i.e. at 20 dB per decade, whereas the cubic damping force decreases inversely proportional to the excitation frequency cubed, i.e. at 60 dB per decade. These approximate expressions are included in the numerical plots shown in figure 3.5. The amplitude of the cubic damping force can be considerably lower than the linear damping force for a specific excitation frequency high above ω_n. In other words, there is almost no force transmitted via the damping component. So this is the background reason for the beneficial effect of cubic damping on the force excited system.

The damping forces for base excitation systems possessing separately linear and cubic damping can be determined respectively from

$$F_{d1} = BU_{w1} = 2\zeta_1\Omega \tag{3.49}$$

$$F_{d3} = CU_{w3}^3 \approx \Omega^2 \tag{3.50}$$

where U_{w1} and U_{w3} represent the relative displacement for linear and cubic damping respectively and is given in row (e) of table 3.2 for the base case. The damping forces for this case appear in contrast to those for the case of force excitation. The linear damping force increases directly proportionally to the excitation frequency. The cubic damping force increases proportionally to the excitation frequency squared regardless of the value of cubic damping.

The expressions for damping force for $\Omega \gg 1$ given in equations (3.49) and (3.50) are in agreement with the numerical results and shown in figure 3.6. It is apparent that the cubic damping forces at high excitation frequencies increase by 40 dB per decade. Thus at the very much higher excitation frequencies above ω_n, the damping component becomes responsible for transmitting the motion of the base to the isolated

mass. The level of displacement amplitude ratio approaches unity which is detrimental. Note that the cubic damping force increases with Ω^2 only when $\Omega \gg 1$. As frequency increases then the level of amplitude ratio asymptotes to unity and damping force asymptotes to infinity.

Mitigation of the higher level of cubic damping force at high excitation frequencies might be achieved by alternative higher order isolation models, for example, the Zener or the two-stage base excited isolation system. The effect of cubic damping on these two models is presented in Chapter 4.

In addition, the non-dimensional cubic damping given in equation (3.5) is a function of the excitation amplitude squared. Thus a higher excitation amplitude can result in a higher value of cubic damping. Therefore, awareness should be raised of the effect excitation level applied, especially for the system for which the input amplitude could not be identified.

3.6.2 Total Harmonic Distortion analysis

As mentioned in section 2.4.4, the response of the nonlinear system exhibits harmonic frequencies apart from the excitation frequency. The waveform of the response at the excitation frequency could be distorted due to the appearance of higher harmonics. The harmonics considered here were the 2^{nd} to 7^{th} harmonics. The higher harmonics are neglected because the impact on the distortion of the signal is comparatively small.

Figure 3.7 shows the THD of the 2^{nd} to 7^{th} harmonics obtained from the numerical integration. The highest amplitude of the THD for the case of force excitation, dashed line, is about 20% at around $\Omega = 1$, figure 3.7 (c). It means that increasing the value of ζ_3 increase the transmitted force at the odd harmonics of the excitation frequencies, which could result in the response at the resonance frequency. For example, the response at $\Omega = 1$ is the fifth harmonic for the excitation frequency at $\Omega = 0.2$. Therefore, one should be aware of such instances and should consider the use of cubic damping by regarding the influence of the responses at higher harmonics.

On the other hand, the plots of THD for the case of base excitation at the frequency around resonance are much lower compared to that for the case of force

excitation. Figure 3.7 (c) shows that the value of THD for the case of base excitation is lower than 5% and reduces in inverse proportion to the level of cubic damping force, i.e. the higher cubic damping force corresponds to the lower level of the THD. This occurrence supports the notion that the damping is acting almost rigidly at the high excitation frequencies which results in the lower nonlinearity effect.

Moreover, the analysis of THD does not only inform one about the occurrence of harmonics in the response but also improves the confidence of the analytical and numerical results. These results support the assumptions of the HBM namely that the response is dominated harmonically at the excitation frequency and the use of Fourier coefficients at the excitation frequency is reasonably acceptable.

3.6.3 The effect of cubic damping on a base isolation subject to a constant amplitude harmonic velocity excitation

This section gives a further analysis of the effect of cubic damping on the base excited isolation when the amplitude of displacement base excitation reduces in proportion to the excitation frequency. Such an excitation characteristic can be considered as a harmonic velocity which has a constant amplitude. The velocity of the base displacement excitation for this instance is given by

$$\dot{x}_0(t) = -\omega X_0 \sin(\omega t) \tag{3.51}$$

For the constant velocity amplitude, the product of ωX_0 is kept constant for all frequencies, i.e.

$$\left|\dot{x}_0(t)\right| = \left|\omega X_0 \sin(\omega t)\right| = \omega_n \Omega X_0 \tag{3.52}$$

where $\omega = \omega_n \Omega$. Thus, one has the amplitude of displacement excitation decreases in inverse proportion to the excitation frequency, i.e.

$$X_0 = \frac{\left|\dot{x}_0\right|}{\omega_n \Omega} \tag{3.53}$$

Using the amplitude of displacement excitation given in equation (3.53), the non-dimensional cubic damping term given in equation (3.5) becomes inversely proportional to the excitation frequency squared and is given by

$$\zeta_3 = \frac{c_3}{m}\omega_n X_0^2 = \frac{c_3}{\sqrt{km}}\frac{|\dot{x}_0|^2}{\Omega^2} \tag{3.54}$$

Equation (3.54) shows that for a constant input velocity amplitude the value of cubic damping tends to zero as the excitation frequency increases, $\zeta_3 \to 0$ as $\Omega \to \infty$. The expression of C given in equation (3.9) becomes

$$C = \frac{3}{4}\zeta_3\Omega^3 = \frac{3}{4}\tilde{\zeta}_3\Omega \tag{3.55}$$

where $\tilde{\zeta}_3 = \frac{c_3}{\sqrt{km}}|\dot{x}_0|^2$.

Substituting the expression of C given in equation (3.55) into equation (3.41) results in an approximation of relative displacement at the excitation frequencies well above resonance, $\Omega \gg 1$, becoming $U \approx 1$. As a result, an approximation of the absolute displacement amplitude ratio at this frequency region is given by

$$W \approx \frac{3}{4}\frac{\tilde{\zeta}_3}{\Omega} \tag{3.56}$$

Equation (3.56) reveals that the absolute displacement amplitude ratio at $\Omega \gg 1$ due to harmonic excitation with constant velocity amplitude decreases inversely proportional to the excitation frequency. The analytical approximation for the constant amplitude harmonic velocity excitation is also described in Appendix C.

The numerical responses due to the constant velocity amplitude are shown in figure 3.8. The figure evidently shows a reduction in the displacement amplitude ratio at high excitation frequencies in comparison to those for linear viscous damping. However, the response in the isolation region is directly related with the value of the non-dimensional cubic damping. Thus the system with a very high value of cubic damping does not provide excellent vibration isolation compared to that with lower value. However, the application of cubic damping on the constant velocity base excited vibration isolation model as shown in figures 3.8 (a) and (b) is particularly beneficial. This is because the system with linear damping does not get any benefit from the reduction of the input displacement amplitude. This is one of the possible advantages

obtained from the presence of cubic damping characteristic on the base excitation system for the constant amplitude harmonic velocity input.

3.7 Conclusions

Cubic damping was introduced into the SDOF isolation system which is subject to either force or base excitation. The effect of cubic damping was examined using two techniques, i.e. the HBM analysis and numerical simulations. The effects of cubic damping for each excitation scenario were contrasted as well as being compared to the system with linear viscous damping.

An analytical examination of the amplitude ratio was considered for four specific frequency regions, i.e. $\Omega \ll 1$, $\Omega \approx 1$, $\Omega \approx \sqrt{2}$ and $\Omega \gg 1$. These correspond to excitation frequencies well below ω_n, around ω_n, at the frequency when the isolation occurs for the linear isolation and well above ω_n. The numerical plots obtained from the approximate closed form solutions are in good agreement with the numerical results obtained using ODE45.

The responses in the isolation region were of primary concern, as the cubic damping performed differently for the force and base excitation. It reduces remarkably the level of the force amplitude ratio for the former compared to the level caused by linear damping in the isolation. On the other hand, a high vibration level for the isolated mass occurs with cubic damping for base excitation. This is because the relative velocity across the damper is increasing proportional to the excitation frequency. This is the opposite of what happens for the force excitation. As a result, the damping forces for these two systems appear very different. It is apparent that the level of cubic damping force for the base excited system increases proportionally to the excitation frequency squared. This results in a high vibration amplitude of the isolated mass.

The application of base excited vibration isolation possessing cubic damping is more preferable when the excitation is velocity constant. For some particular values of cubic damping, the system produces better isolation performance over the linear damping system. However, it is important to be reminded that the effect of cubic damping for either case is directly related to the excitation amplitude squared. Therefore, the detrimental effect of cubic damping on the base isolation system could be

more pronounced for the larger excitation amplitude. Thus for the practical situations where cubic damping cannot be eliminated and the excitation amplitude is not known, care must be taken to avoid possible damage to the system.

However, since the source of the detrimental behaviour has been discovered, the isolator modification or improvement can be contributed using this knowledge. As the cubic damping force for the base excited isolation is known to increase proportionally to the excitation frequency squared thus at high frequencies well above undamped natural frequency it locks the isolated mass to the base excitation becoming unity. To isolate such a combined unit using an additional spring could be expected. For example, in next chapter, the application of higher order base excitation models including an additional spring are introduced in order to reduce the detrimental effect caused from the cubic damping or even turn it into a benefit for base isolation.

Table 3.1 The values of non-dimensional cubic damping for the numerical simulation which produce the similar level of peak amplitude to the linear viscous damping.

	$\zeta_1 = 0.1$	$\zeta_1 = 0.2$	$\zeta_1 = 0.3$
Force excitation	$\zeta_3 \approx 0.011$	$\zeta_3 \approx 0.092$	$\zeta_3 \approx 0.325$
Base excitation	$\zeta_3 \approx 0.013$	$\zeta_3 \approx 0.152$	$\zeta_3 \approx 0.787$

Table 3.2 Approximate expressions for the amplitude ratio over four frequency regions for force and base excitation, comparison of the system response with cubic damping to linear damping.

Frequency region	Row index	Linear viscous damping	Cubic damping for the case of force excitation	Cubic damping for the case of base excitation
	Amplitude ratio for the transmitted force and absolute displacement			
$\Omega \ll 1$	(a)	$T_r \approx 1$	$F_t \approx 1$	$W \approx 1$
$\Omega \approx 1$	(b)	$T_r = \sqrt{1+\frac{1}{(2\zeta_1)^2}}$	$F_t \approx \sqrt{1+\left(\frac{4}{3\zeta_3}\right)^{\frac{2}{3}}}$	$W \approx \sqrt{1+\left(\frac{4}{3\zeta_3}\right)^{\frac{2}{3}}}$
$\Omega \approx \sqrt{2}$	(c)	$T_r = 1$	$F_t \approx 1$	$W \approx 1$
$\Omega \gg 1$	(d)	$T_r \approx \frac{2\zeta_1}{\Omega}$	$F_t \approx \frac{1}{\Omega^2}$	$W \approx \sqrt{1-\left(\frac{4}{3\zeta_3\Omega}\right)^{\frac{2}{3}}}$
	Amplitude ratio for the relative displacement between the isolated mass and base at $\Omega \gg 1$			
	(e)	Force excitation: $U_{f1} \approx \frac{1}{\Omega^2}$ Base excitation: $U_{w1} \approx 1$	$U_{f3} \approx \frac{1}{\Omega^2}$	$U_{w3} \approx \left(\frac{4}{3\zeta_3\Omega}\right)^{\frac{1}{3}}$

(a)

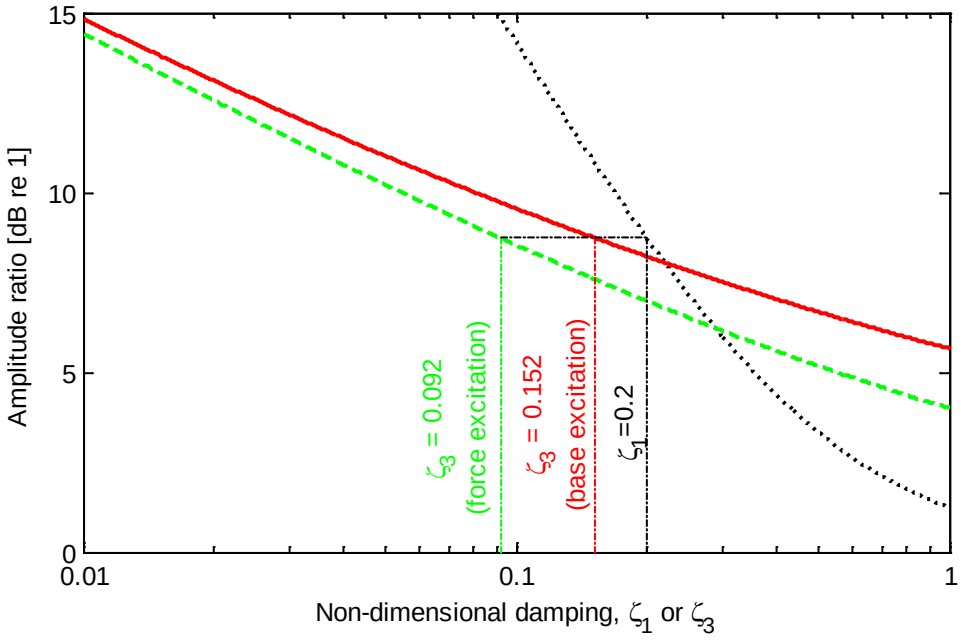

(b)

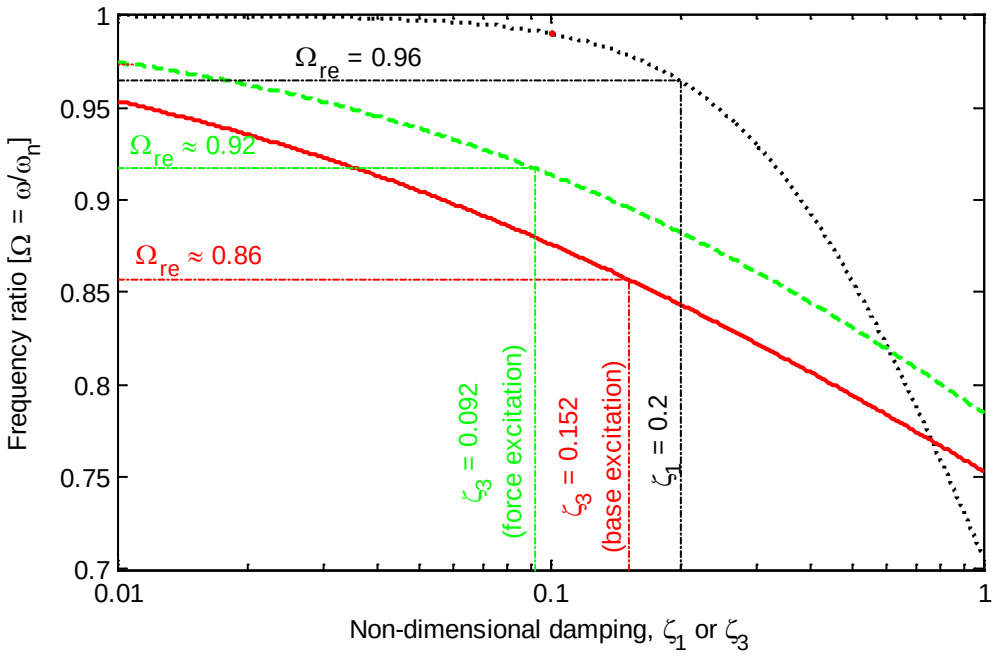

Figure 3.1 The relationship between the non-dimensional damping terms to the corresponding level of amplitude ratio and resonance frequency.
(a) Relationship between Non-dimensional damping and Amplitude ratio
(b) Relationship between Non-dimensional damping and Frequency ratio
····· Linear viscous damping obtained from equations (3.44) and (3.45)
– – – Cubic damping for the force excited isolation model
——— Cubic damping for the base excited isolation model
–·– Linearly damped response with $\zeta_1 = 0.2$
–·– Force excitation with $\zeta_3 = 0.092$
–·– Base excitation with $\zeta_3 = 0.152$

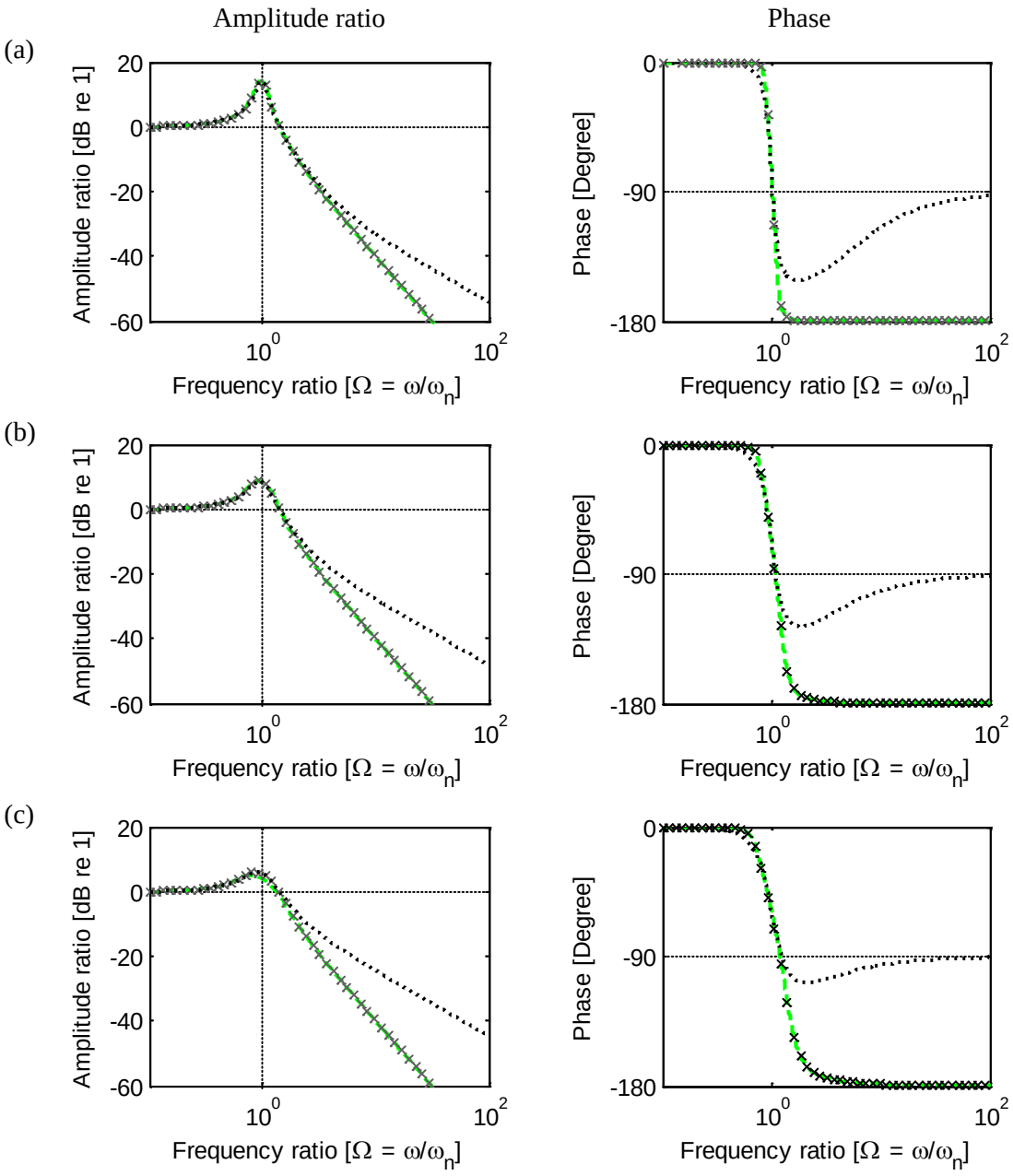

Figure 3.2 Force amplitude ratio and the phase lag for the SDOF isolation possessing cubic damping in comparison to the exact solution of linear viscous damping for the case of force excitation.

(a) ζ_1 = 0.1 and ζ_3 = 0.011

(b) ζ_1 = 0.2 and ζ_3 = 0.092

(c) ζ_1 = 0.3 and ζ_3 = 0.325

····· Linear viscous damping

– – – Cubically damped response obtained using HBM

× Cubically damped response obtained using numerical integration

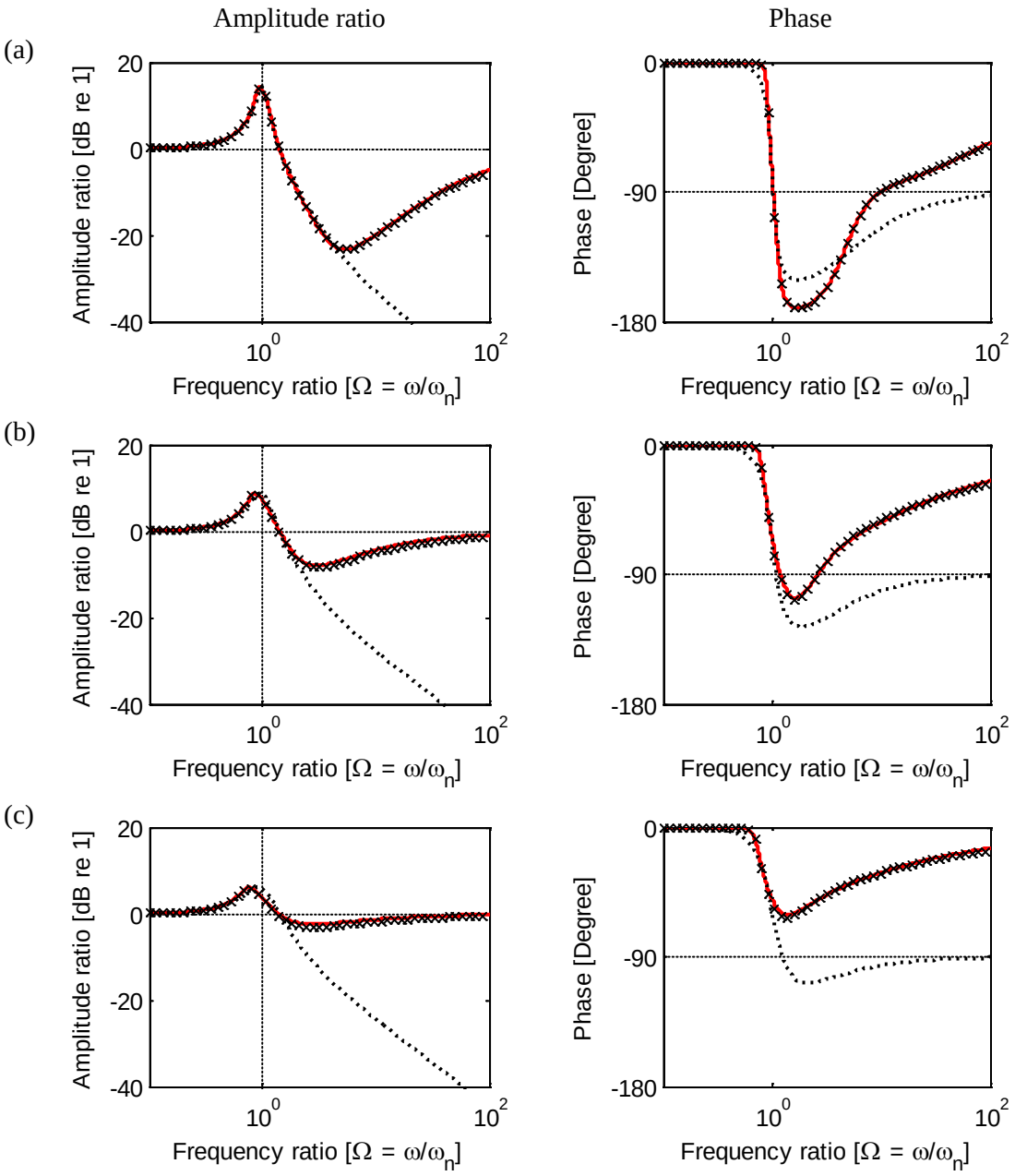

Figure 3.3 Absolute displacement amplitude ratio and the phase lag for the SDOF isolation possessing cubic in comparison to the exact solution of the linear viscous damping for the case of base excitation.

(a) ζ_1 = 0.1 and ζ_3 = 0.013

(b) ζ_1 = 0.2 and ζ_3 = 0.152

(c) ζ_1 = 0.3 and ζ_3 = 0.787

····· Linear viscous damping

—— Cubically damped response obtained using HBM

× Cubically damped response obtained using numerical integration

(a)

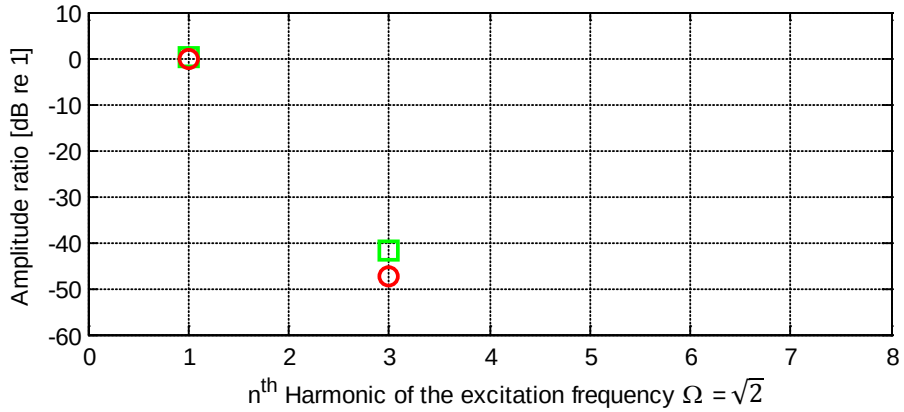

(b)

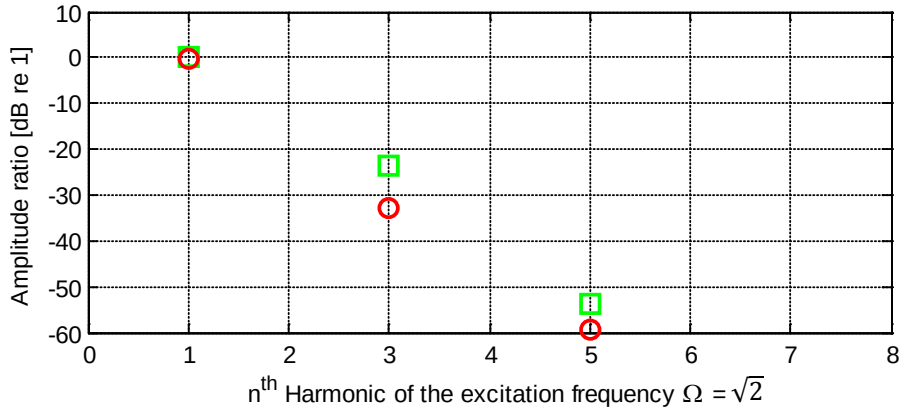

(c)

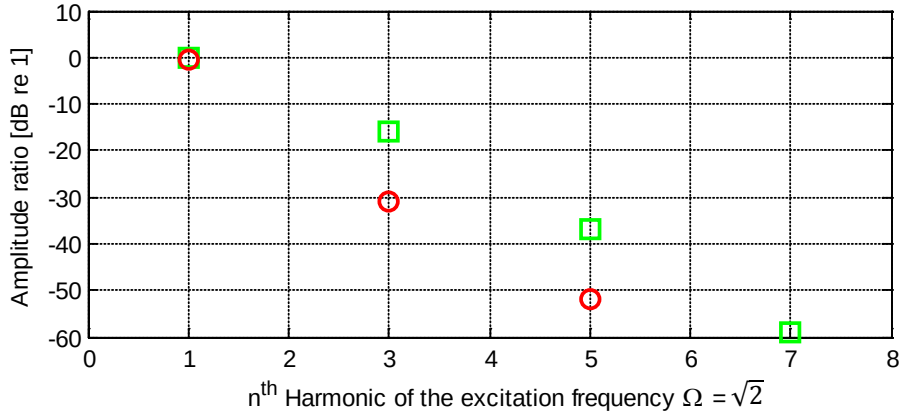

Figure 3.4 Fourier coefficients of the absolute displacement amplitude ratio at $\Omega \approx \sqrt{2}$ obtained from numerical integration for force and base excitation.

(a) $\zeta_3 = 0.011$ for force case and $\zeta_3 = 0.013$ for base case

(b) $\zeta_3 = 0.092$ for force case and $\zeta_3 = 0.152$ for base case

(c) $\zeta_3 = 0.325$ for force case and $\zeta_3 = 0.787$ for base case

□ represents responses due to force excitation

○ represents responses due to base excitation

(a)

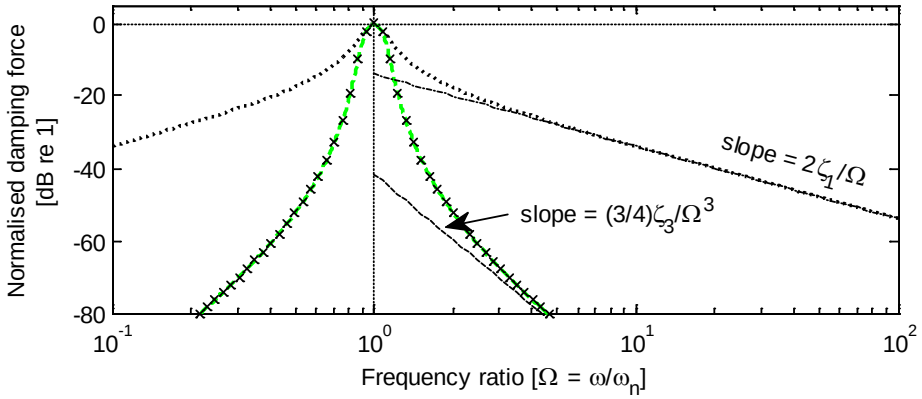

(b)

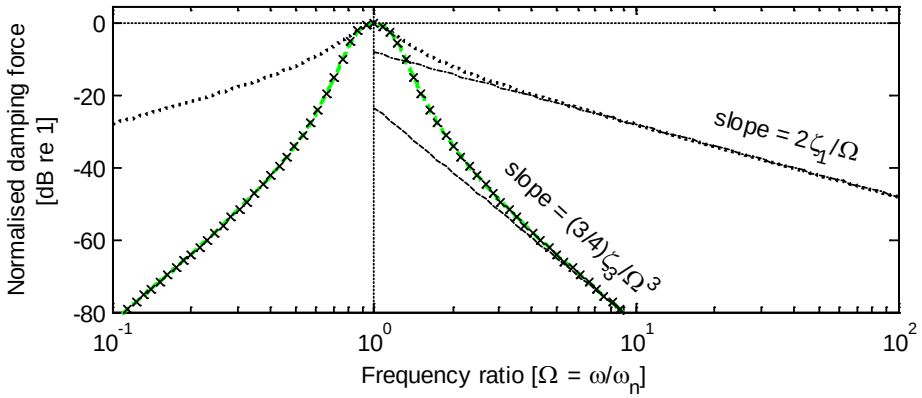

(c)

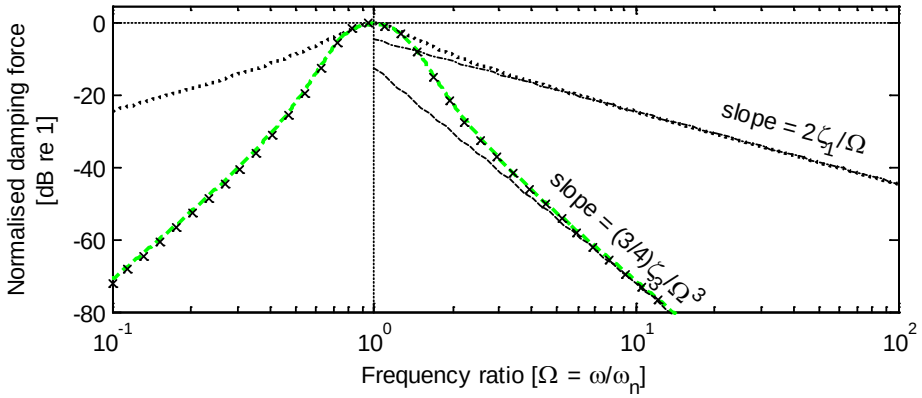

Figure 3.5 Normalised damping force for the case of force excitation.

(a) ζ_1 = 0.1 and ζ_3 = 0.011

(b) ζ_1 = 0.2 and ζ_3 = 0.092

(c) ζ_1 = 0.3 and ζ_3 = 0.325

····· Linear viscous damping force

– – – Cubic damping force obtained using HBM

× Cubic damping force obtained using numerical integration

–·–·– Asymptote line for the slope of $F_{d1} = 2\zeta_1/\Omega$

– – – Asymptote line for the slope of $F_{d3} = 3\zeta_3/4\Omega^3$

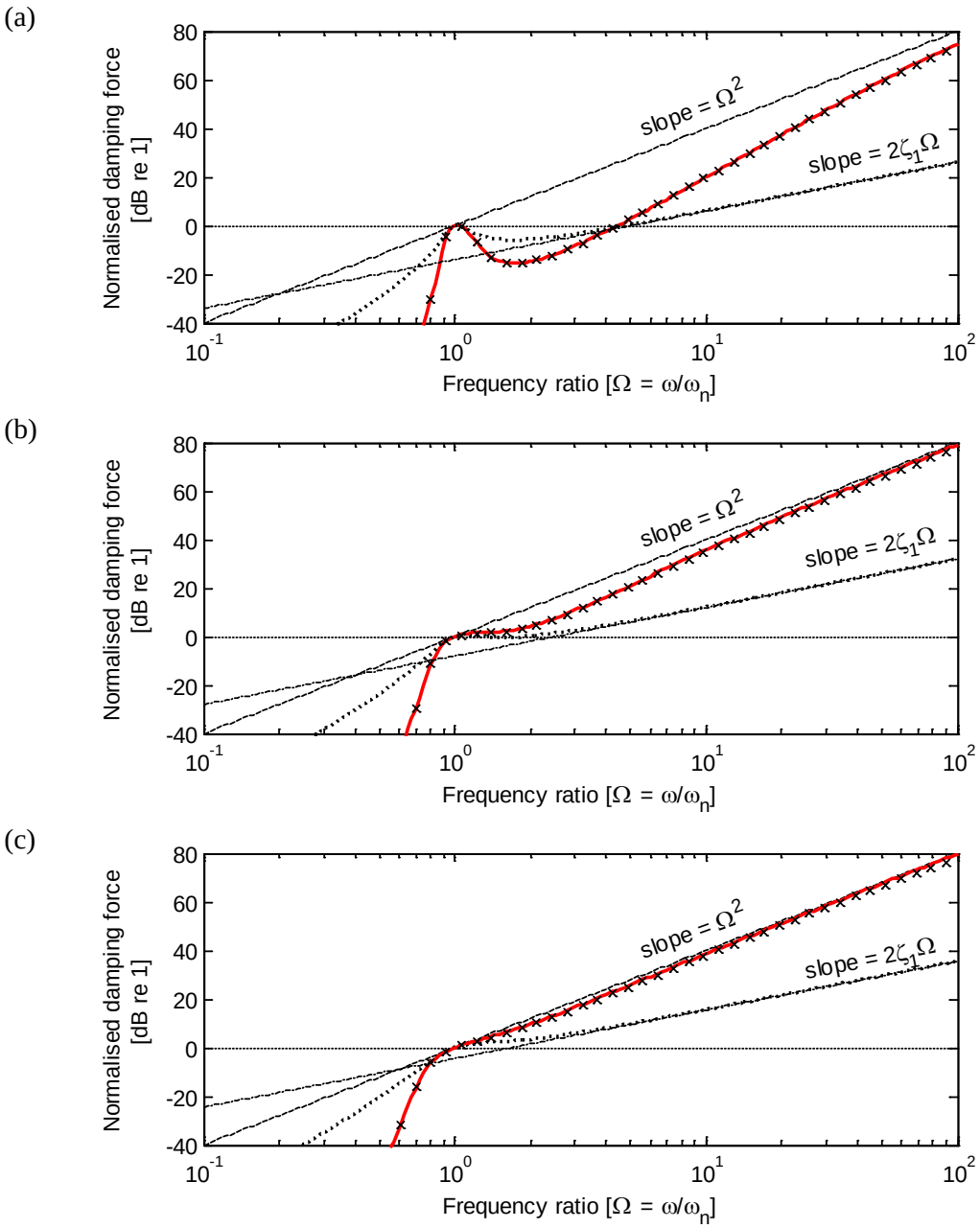

Figure 3.6 Normalised damping force for the case of base excitation.

(a) ζ_1 = 0.1 and ζ_3 = 0.013

(b) ζ_1 = 0.2 and ζ_3 = 0.152

(c) ζ_1 = 0.3 and ζ_3 = 0.787

····· Linear viscous damping force

—— Cubic damping force obtained using HBM

× Cubic damping force obtained using numerical integration

–·–·– Asymptote line for the slope of $F_{d1} = 2\zeta_1\Omega$

– – – Asymptote line for the slope of $F_{d3} = \Omega^2$

(a)

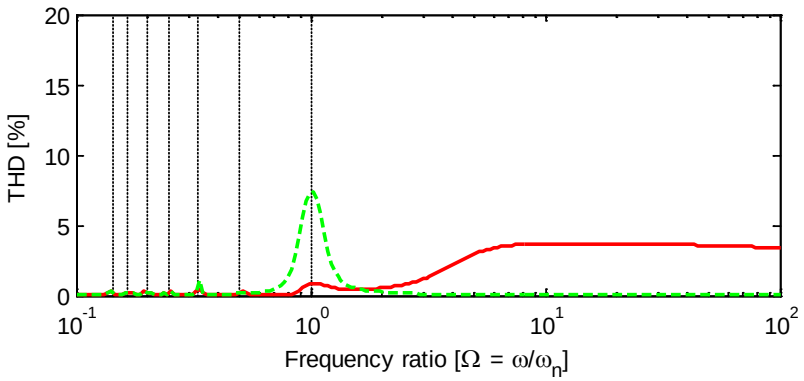

(b)

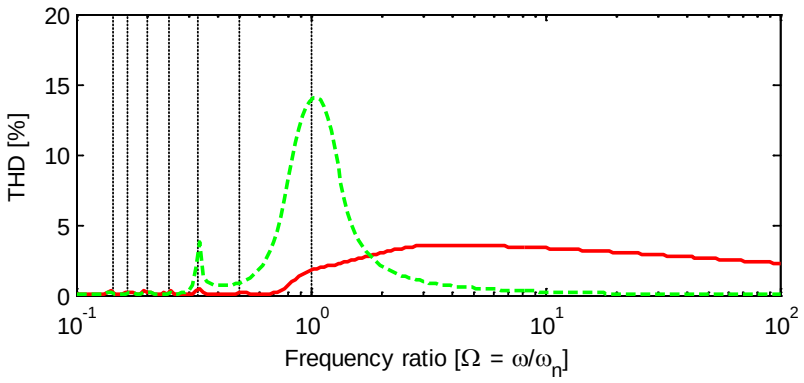

(c)

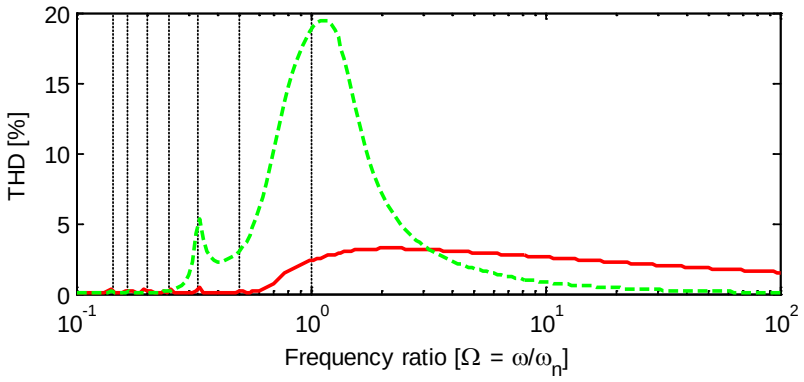

Figure 3.7 Total Harmonic Distortion for the cubically damped responses obtained using numerical integration.

(a) ζ_3 = 0.011 for the force case and ζ_3 = 0.013 for the base case

(b) ζ_3 = 0.092 for the force case and ζ_3 = 0.152 for the base case

(c) ζ_3 = 0.325 for the force case and ζ_3 = 0.787 for the base case

Force excited response

Base excited response

The vertical dotted lines below $\Omega = 1$ represent the excitation frequencies which the resonance frequency, $\Omega = 1$, is one of their harmonics, i.e. $\frac{1}{7}\Omega$, $\frac{1}{6}\Omega$, $\frac{1}{5}\Omega$, $\frac{1}{4}\Omega$, $\frac{1}{3}\Omega$ and $\frac{1}{2}\Omega$ respectively.

(a)

(b)

(c)

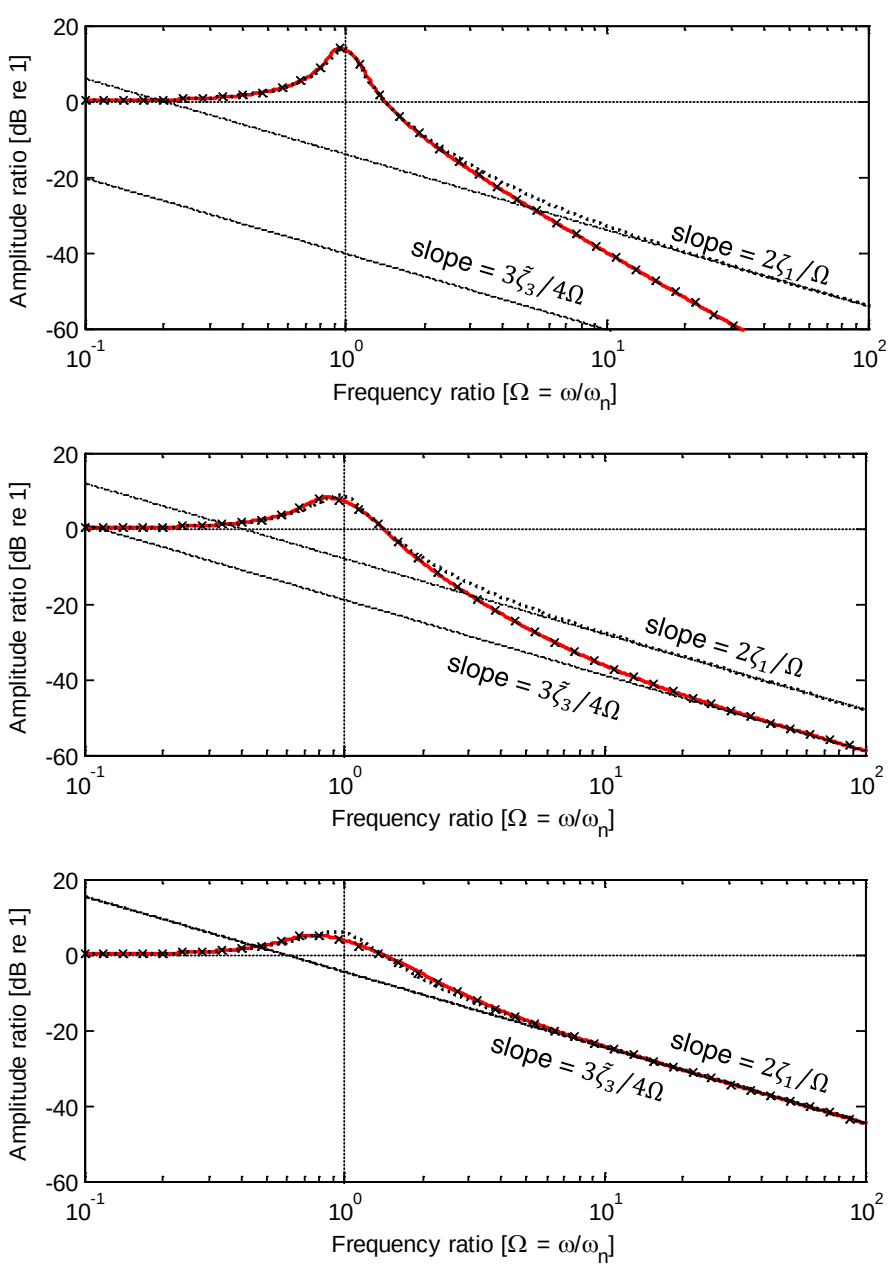

Figure 3.8 Displacement amplitude ratio for the case of base excitation due to constant velocity amplitude excitation.

(a) ζ_1 = 0.1 and $\tilde{\zeta}_3$ = 0.013

(b) ζ_1 = 0.2 and $\tilde{\zeta}_3$ = 0.152

(c) ζ_1 = 0.3 and $\tilde{\zeta}_3$ = 0.787

····· Linear viscous damping response

—— Cubically damped response obtained using HBM

× Cubically damped response obtained using numerical integration

—·— Asymptote line for the slope of $W \approx 2\zeta_1/\Omega$ when $\Omega \gg 1$

— — Asymptote line for the slope of $W \approx 3\tilde{\zeta}_3/4\Omega$ when $\Omega \gg 1$

Chapter 4 Higher order vibration isolation models possessing cubic damping

4.1 Introduction

Theoretical results previously reported in Chapter 3 revealed that the presence of cubic damping in a base excited single degree of freedom (SDOF) isolation system causes high vibration amplitudes of the isolated mass at excitation frequencies high above resonance. This is because the relative velocity amplitude increases with frequency which results in an increase of cubic damping force, unlike the force excited case. The focus of this chapter is to deal with this undesirable effect for only the case of displacement base excitation. The applications of two higher order isolation models are considered here.

Firstly, the one and a half degree of freedom (1 ½-DOF) Zener isolation model subject to the harmonic base excitation is introduced. The damper in this model is supported elastically using a relaxation spring. In previous studies, a linearly damped Zener model has proved to be effective in reducing the response amplitude in the isolation region. The response in the isolation region decreases by ~12 dB per octave (40 dB per decade) [23]. As a result, the levels of displacement transmissibility for the Zener isolation at high frequencies are much lower than that for a system with a rigidly connected linear viscous damper.

The application of the Zener model possessing linear plus cubic damping subject to shock excitation has also shown an impressive shock isolation performance [32]. The severity caused by the presence of cubic damping was reduced by mounting the damping component elastically. Thus one might expect a similar mitigation by elastically mounting a cubic damper for the case of harmonic excitation.

Subsequently another higher order isolation model is considered, namely two-stage isolation. The undamped response due to harmonic excitation at frequencies high above the secondary resonance is well known to decrease by ~24 dB per octave (80 dB per decade) [40]. The roll-off rate is greater than that of the undamped SDOF

system which the roll off rate is 40 dB per decade. Shekhar et al. [32] also reported that the isolation performance of the two-stage shock isolator possessing linear plus cubic damping is better than the SDOF system having linear plus cubic damping and is even better than other isolation models considered in the cited paper. Thus the two-stage vibration isolation has been adopted here, with the expectation of reducing the large vibration amplitude in the isolation region for the case of harmonic excitation.

The effect of cubic damping on these two isolation models is explored analytically using the Harmonic Balance Method (HBM). Numerical integration is also performed using the ODE45 solver under a constant displacement harmonic base excitation. The analytical and numerical analyses are expected to show the advantage of the application of these higher order models. The outcome of the investigation for these isolation models might contribute to improving the isolation capability of systems possessing a cubic damping characteristic.

4.2 A base excited Zener model

The model is shown in figures 4.1 (a) and (b). The damping component is working in series with the relaxation spring, k_r. This spring can either be inserted between the base and the damper, figure 4.1 (a), or inserted between the damper and the isolated mass, as shown in figure 4.1 (b). Theoretically, when the relaxation spring and the damping component are assumed massless, these two components experience the same force in either case. There is no difference in the response of the isolated mass due to the location of the relaxation spring. Thus the model shown in figure 4.1 (a) was chosen here for examination.

4.2.1 Governing equations of motion and non-dimensional quantities

Figure 4.1 (a) shows the series combination of the cubic damper and relaxation spring working in parallel with the primary spring, k. The governing equation of motion for the mass is given by

$$m\ddot{x} + c_1\left(\dot{x} - \dot{x}_r\right) + c_3\left(\dot{x} - \dot{x}_r\right)^3 + k\left(x - x_0\right) = 0 \qquad (4.1)$$

where m is the isolated mass. c_1 and c_3 are the linear and cubic damping coefficients respectively. x, $\dot{x}$ and $\ddot{x}$ are the displacement, velocity and acceleration of the isolated

mass. x_r and $\dot{x}_r$ are the displacement and velocity at the junction of the damper with the relaxation spring. x_0 is the displacement base excitation.

In addition to equilibrium of the mass, the junction between the relaxation spring and the damper must also be in equilibrium. Since the junction is massless the damping force has to balance the spring force, i.e.

$$c_1\left(\dot{x}-\dot{x}_r\right)+c_3\left(\dot{x}-\dot{x}_r\right)^3=k_r\left(x_r-x_0\right) \tag{4.2}$$

This additional first order equation makes the Zener isolation model being considered as a one and a half degree of freedom (1 ½-DOF). Therefore in this chapter, the SDOF system refers to a rigidly connected damping as examined previously in Chapter 3.

There are two frequency limits for the natural frequency, referred to here as lower and upper bound frequencies. The first frequency occurs when both damping coefficients c_1 and c_3 are zero. This is the lower bound on the natural frequency of the system and is defined by

$$\omega_n=\sqrt{\frac{k}{m}} \tag{4.3}$$

It is identical to the undamped natural frequency for the SDOF system. The upper bound on the natural frequency occurs when either of the damping coefficients c_1 or c_3 are infinitely large. Thus the mass is supported on the two springs, primary spring k and relaxation spring k_r. This corresponds to the undamped natural frequency which is given by

$$\omega_u=\sqrt{\frac{k+k_r}{m}} \tag{4.4}$$

The non-dimensional time for the case of the Zener model is defined by considering the lower bound natural frequency, i.e.

$$\tau=\omega_n t \tag{4.5}$$

The frequency ratio is also defined using the lower bound natural frequency, i.e.

$$\Omega=\frac{\omega}{\omega_n} \tag{4.6}$$

It is convenient to define the stiffness ratio which is the ratio of the spring stiffness k_r with respect to the primary spring k, i.e.

$$\kappa_z = \frac{k_r}{k} \tag{4.7}$$

Note that, only a positive relaxation stiffness is considered here, i.e. $\kappa_z \geq 0$. A stiffness ratio of zero corresponds to the undamped SDOF system whereas a stiffness ratio of infinity corresponds to a rigidly connected damper SDOF system.

For harmonic base excitation $x_0 = X_0 \cos(\omega t)$, the normalised variables are defined by

$$w = \frac{x}{X},\ w'' = \frac{\ddot{x}}{\omega_n^2 X},\ \tilde{u} = \frac{x - x_r}{X} \text{ and } \tilde{u}' = \frac{\dot{x} - \dot{x}_r}{\omega_n X} \tag{4.8}$$

where X is the displacement amplitude of the isolated mass and the base excitation at zero frequency. $\tilde{u}$ and $\tilde{u}'$ are the normalised relative displacement and velocity between the isolated mass and the junction of the relaxation spring and damper. w represents the normalised absolute displacement of the isolated mass. $(\bullet)'$ and $(\bullet)''$ are the first and second derivatives with respect to the non-dimensional time τ. Substituting the quantities given in equation (4.8) into equations (4.1) and (4.2), then dividing by quantity $m\omega_n^2 X$ produces

$$w'' + w = w_0 - 2\zeta_1 \tilde{u}' - \zeta_3 (\tilde{u}')^3 \tag{4.9}$$

and

$$2\zeta_1 \tilde{u}' + \zeta_3 (\tilde{u}')^3 + \kappa_z \tilde{u} = \kappa_z (w - w_0) \tag{4.10}$$

The resulting non-dimensional cubic damping term is an outcome and is given by

$$\zeta_3 = \frac{c_3}{m} \omega_n X^2 \tag{4.11}$$

Equation (4.11) is identical to that given in equation (3.5) which is dependent upon the excitation amplitude squared. Later, equations (4.9) and (4.10) will be solved analytically using the HBM and numerically using ODE45. The resulting cubically

damped Zener model will be examined in comparison to the base excitation systems with rigidly connected linear and cubic damping.

In addition, it is also convenient to define the ratio of the lower and upper bound frequencies, i.e.

$$\frac{\omega_u}{\omega_n} = \Omega_b = \sqrt{\kappa_z + 1} \tag{4.12}$$

As the excitation frequency approaches ω_u, large vibration amplitude can occur for a system with high value of viscous damping. It was also reported in Ruzicka [37] that, for a particular value of the stiffness ratio, increasing the value of linear viscous damping from 0 to ∞ results in the resonance peak shifting from ω_n to ω_u as shown in figure 4.2.It is seen that the peak amplitude of absolute displacement transmissibility for the linear viscous damping, ζ_1, of 0.5 is lowest among the others. Thus the optimum value of linear viscous damping, which produces the minimum peak response for a specific value of stiffness ratio, was expected and determined.

However, the study here did not aim to find the optimum value of damping. Instead, the level of damping was kept constant at particular values and the value of stiffness ratio was varied. One might anticipate different amplitudes of the peak response resulting from different values of stiffness ratio. Therefore, in contrast to the previous study, the optimum value of stiffness ratio, which produces the minimum peak amplitude for a particular damping level, was to be determined.

4.2.2 Analytical solution using the Harmonic Balance method

Only the case of pure cubic damping is examined analytically here, i.e. the linear viscous damping ratio ζ_1 is set to zero. Thus equations (4.9) and (4.10) reduce to

$$w'' + w = w_0 - \zeta_3 \left(\tilde{u}'\right)^3 \tag{4.13}$$

and

$$\zeta_3 \left(\tilde{u}'\right)^3 + \kappa_z \tilde{u} = \kappa_z \left(w - w_0\right) \tag{4.14}$$

The normalised harmonic base excitation given by $w_0 = \cos(\Omega\tau)$ is expected to produce harmonic absolute and relative displacements in forms of

$$w = W\cos(\Omega\tau - \phi_w) \text{ and } \tilde{u} = \tilde{U}\cos(\Omega\tau - \phi_{\tilde{u}}) \tag{4.15}$$

where W and $\tilde{U}$ are the normalised amplitudes of the absolute and relative displacement. ϕ_w and $\phi_{\tilde{u}}$ are phase lags of the absolute and relative motion with respect to the base excitation. Note that $\tilde{U}$ is the relative displacement across the damper or between the junction and isolated mass. In other words, it is not the relative displacement between the isolated mass and base excitation.

Substitution of the excitation and responses into equations (4.13) and (4.14) produces respectively

$$\left(1-\Omega^2\right)W\cos(\Omega\tau - \phi_w) = \cos(\Omega\tau) + \zeta_3\Omega^3\tilde{U}^3\sin^3(\Omega\tau - \phi_{\tilde{u}}) \tag{4.16}$$

and

$$-\zeta_3\Omega^3\tilde{U}^3\sin^3(\Omega\tau - \phi_{\tilde{u}}) + \kappa_z\tilde{U}\cos(\Omega\tau - \phi_{\tilde{u}}) = \kappa_z W\cos(\Omega\tau - \phi_w) - \kappa_z\cos(\Omega\tau) \tag{4.17}$$

By integrating the product of the terms in left and right sides of equations (4.16) and (4.17) with the trigonometric functions over a period of $2\pi/\Omega$, the same process as those given in Chapter 3, i.e.

$$\frac{\Omega}{\pi}\int_0^{\frac{2\pi}{\Omega}} g(\tau)\sin(\Omega\tau)\,d\tau \quad \text{and} \quad \frac{\Omega}{\pi}\int_0^{\frac{2\pi}{\Omega}} g(\tau)\cos(\Omega\tau)\,d\tau \tag{4.18}$$

where $g(\tau)$ represents functions of non-dimensional time given in equations (4.16) and (4.17). As a result, equations (4.16) and (4.17) can be rearranged to form

$$AW\sin(\phi_w) = C\tilde{U}^3\cos(\phi_{\tilde{u}}) \tag{4.19}$$

$$AW\cos(\phi_w) = 1 - C\tilde{U}^3\sin(\phi_{\tilde{u}}) \tag{4.20}$$

$$\kappa_z\tilde{U}\sin(\phi_{\tilde{u}}) - C\tilde{U}^3\cos(\phi_u) = \kappa_z W\sin(\phi_w) \tag{4.21}$$

$$\kappa_z\tilde{U}\cos(\phi_{\tilde{u}}) + C\tilde{U}^3\sin(\phi_{\tilde{u}}) = \kappa_z W\cos(\phi_w) - \kappa_z \tag{4.22}$$

where $A = 1-\Omega^2$ and $C = \frac{3}{4}\zeta_3\Omega^3$. Squaring and adding equations (4.19) to (4.22) eliminates W and hence

$$\left(\kappa_z + A\right)^2 C^2 \tilde{U}^6 + \left(\kappa_z A\right)^2 \tilde{U}^2 = \kappa_z^2 \Omega^4 \tag{4.23}$$

Equation (4.23) is a cubic polynomial in $\tilde{U}^2$. The three solutions of equation (4.23) comprise one real and two complex conjugates because the coefficient of $\tilde{U}^4$ is zero. The real solution of equation (4.23) is given by

$$\tilde{U}^2 = \frac{1}{6} \frac{\left(108\kappa_z^2\Omega^4\left(\kappa_z + A\right)C + 12\sqrt{12\left(\kappa_z A\right)^6 + 81\kappa_z^4\Omega^8\left(\kappa_z + A\right)^2 C^2}\right)^{\frac{2}{3}} - 12\left(\kappa_z A\right)^2}{\left(\kappa_z + A\right)C\left(108\kappa_z^2\Omega^4\left(\kappa_z + A\right)C + 12\sqrt{12\left(\kappa_z A\right)^6 + 81\kappa_z^4\Omega^8\left(\kappa_z + A\right)^2 C^2}\right)^{\frac{1}{3}}} \tag{4.24}$$

Equation (4.24) is the square of the amplitude ratio for the relative displacement between the isolated mass and the junction. The square of the absolute displacement amplitude ratio of the isolated mass is given by

$$W^2 = \frac{\kappa_z^2 + \left(\kappa_z + 1\right)^2 C^2 \tilde{U}^4}{\kappa_z^2 A^2 + \left(A + \kappa_z\right)^2 C^2 \tilde{U}^4} \tag{4.25}$$

Equations (4.24) and (4.25) do not explicitly show the effect of cubic damping, thus equation (4.23) is examined for three frequency regions, i.e. $\Omega \ll 1$, $\Omega \approx \Omega_b$ and $\Omega \gg 1$ to obtain approximate simplified expressions for the responses. The frequency ratio at $\Omega \approx \Omega_b$ ($\Omega_b = \sqrt{1+\kappa_z}$) is of interest since it is the upper bound for the natural frequency of the mass vibrating on the two parallel springs. Its relevance was explained previously for the system with high damping level. The detailed derivations of the approximations for the three frequency regions are given in Appendix C. The resulting simplified expressions are listed in table 4.1 in comparison to those for the SDOF system with pure cubic damping reported in Chapter 3.

4.2.3 Numerical procedure and solutions

Numerical simulations were carried out to solve equations (4.9) and (4.10) for the case of linear and cubic damping. The values of non-dimensional damping chosen were the same as those applied for the SDOF system presented in Chapter 3, i.e. ζ_1 = 0.1, 0.2,0.3 and ζ_3 = 0.013, 0.152, 0.787.

The values of the stiffness ratio κ_z chosen were 1, 8, 48 and 99. These stiffness ratios correspond to the frequency ratio of $\Omega_b = \sqrt{2}$, 3, 7 and 10. The responses for these stiffness values are shown in comparison to those for the SDOF base excitation as in Chapter 3, which corresponds to the limit as $\kappa_z \to \infty$.

The Fourier coefficients at the excitation frequencies were estimated to construct the amplitude ratios between the isolated mass and the base excitation. The motion of the junction between the damping and relaxation spring is not presented here. The numerical results for the cubically damped system is examined and discussed later in conjunction with the analytical results.

4.2.4 Performance of a linearly damped Zener model

The performance of the linearly damped Zener model is briefly provided here to illustrate the basic idea. The numerical results for the amplitude ratios are shown in figure 4.3 for different values of stiffness ratio with a specific value of damping. The responses for the SDOF system ($\kappa_z = \infty$) with the same value of damping are also plotted in the figure using a solid thin line.

It is seen that a softer stiffness ratio and heavier damping, see figures 4.3 (b) and (c), result in the peak response shifted to the right, which is noticeable clearly from the response for $\kappa_z = 1$ (blue solid lines). The softer relaxation spring also produces the lower displacement amplitude ratio at high frequencies. The response in the isolation region for $\kappa_z = 1$ follows the mass line of the undamped SDOF system, i.e. 40 dB per decade. As such, the detrimental effect of the linear damper in the isolation region can be circumvented by increasing the flexibility of the relaxation spring. Therefore, one might hypothesise that employing a relaxation spring in series with a cubic damper might produce a similar effect.

4.2.5 Performance of a cubically damped Zener model and discussion

A numerical examination is conducted using figure 4.4, which shows numerical integration results for the amplitude ratios for the Zener model with cubic damping. Also shown are results for the cubically damped SDOF system ($\kappa_z = \infty$) using a solid

thin line. These plots show that the application of the heavy damping results in a higher peak at the excitation frequency around $\omega/\omega_n = \Omega_b$ as shown in figure 4.4 (c). It shows that the level of the peak for κ_z = 8 is the lowest amongst the chosen values of stiffness ratio. The peak in the amplitude ratio appears highest for κ_z = 1 and 99. The chosen values of stiffness ratio also shift the frequency of resonance for the system with high damping level corresponding to the frequency given in equation (4.12). However, the numerical results show that the application of the Zener model can reduce the detrimental effect of cubic damping in the isolation region compared to the SDOF response.

An analytical examination is conducted using the simplified expressions for the absolute displacement amplitude ratio given in table 4.1, which provide insight into the effect of cubic damping in the Zener model. The simplified expressions for the cubically damped SDOF system are also listed for comparison. Considering firstly the low frequency region, for which $\Omega \ll 1$, the levels of estimated amplitude ratios for both systems are about unity. This is due to the so-called quasi-static behaviour. It indicates that the neither type of damping affects the response at these frequencies.

When the excitation frequency is around $\Omega \approx \Omega_b$, the isolated mass will experience a high vibration amplitude. Figures 4.4 (b) and (c), for which the responses with high damping level are presented, show the high response amplitude at the excitation frequency corresponding to $\Omega_b = \sqrt{\kappa_z + 1}$. The corresponding simplified expression for the amplitude ratio, given in row (b) of table 4.1, is given by

$$W \approx \left(\frac{3}{4}\zeta_3\right)\frac{(\kappa_z+1)^{\frac{9}{2}}}{\kappa_z^4} \tag{4.26}$$

In order to explicitly show the influence of stiffness ratio on the level of absolute displacement amplitude ratio, one might assume that the stiffness ratio is large and finite, i.e. $\kappa_z \gg 1$. Thus the level of absolute displacement amplitude ratio is directly dependent upon the values of the damping and square root of stiffness ratio. Therefore the higher value of either damping or stiffness ratio can result in higher response amplitude at Ω_b. This is in better agreement with numerical results for the responses for higher damping, shown in figures 4.4 (b) and (c) using the circle markers.

An optimum value of κ_z which produces a minimum amplitude ratio at the corresponding Ω_b can be obtained numerically for fixed values of damping as shown in figure 4.5. It shows the relationship between the level of the amplitude and stiffness ratios obtained from the solution given in equation (4.25). The minimum level of the amplitude ratio for different value of cubic damping can be found at the intersection of the dot-dashed blue line. At this point, the optimum value of stiffness ratio for different value of cubic damping can be found. For high cubic damping, the minimum level of amplitude ratio can be obtained for a stiffness ratio of around $\kappa_z \approx 8$.

The optimum value of κ_z for high cubic damping, for which resonance occurs at Ω_b, can also be obtained by taking the derivative of the simplified expression given in equation (4.26) with respect to κ_z and equating it to zero, i.e.

$$\frac{d}{d\kappa_z} W = \frac{d}{d\kappa_z}\left(\left(\frac{3}{4}\zeta_3\right)\frac{(\kappa_z+1)^{\frac{9}{2}}}{\kappa_z^4}\right) = 0 \tag{4.27}$$

After solving equation (4.27) for κ_z, one obtains $\kappa_z = 8$ which produces the minimum amplitude irrespective of the level of cubic damping. Thus for the high cubic damping Zener model using $\kappa_z = 8$, the resonance peak at an upper bound frequency of $\Omega_b = 3$ is anticipated.

The value of stiffness ratio also controls the amplitude ratio at high excitation frequencies, i.e. $\Omega \gg 1$. Figure 4.4 also shows that the response amplitude ratio at these frequencies reduces as excitation frequency increases whereas that for the SDOF increasing towards unity. The simplified expression for the Zener model given in row (c) of table 4.1 shows that the level of amplitude ratio decreases proportionally to the excitation frequency squared (40 dB per decade) regardless of the value of damping but dependent on the stiffness ratio, i.e.

$$W \approx \frac{\kappa_z + 1}{\Omega^2} \tag{4.28}$$

The asymptotes obtained from equation (4.28) are plotted in figure 4.4 using dashed lines which are colour-coded according to the stiffness ratio. These asymptotes are in good agreement to the numerical results.

Also notice that a larger value of κ_z not only increases the level of the amplitude ratio but also shifts the isolation region higher in frequency. Thus the stiffness ratio should be kept low to maximise the bandwidth of the isolation region. In addition, the expression given in equation (4.28) can be compared to the simplified expression of the SDOF system with rigidly connected cubic damping which is given by

$$W \approx \sqrt{1-\left(\frac{4}{3\zeta_3\Omega}\right)^{\frac{2}{3}}} \tag{4.29}$$

As seen previously in Chapter 3, at high excitation frequencies, cubic damping produces a response of the mass in the SDOF system similar to the base input. Therefore, supporting the cubic damping elastically helps to reduce the mass response in the isolation region.

To this end, one might conclude that it is preferable to mount the damping component in series with a relaxation spring. The flexibility of the relaxation spring can be chosen to maximise the isolation capability for the base isolation system exhibiting a cubic damping characteristic.

4.3 A two-stage passive isolation possessing cubic damping

The two-stage base excited vibration isolation is the other higher order vibration isolation model discussed in this study. Its isolation effectiveness is reported to be better than the single stage or SDOF system in the case of a linear damper [40,44]. The model of two-stage passive vibration isolation for this study is shown in figure 4.1 (c). It comprises two sets of isolators which are separated by an intermediate mass. In this study, the damping component is inserted only between the isolated mass m and the intermediate mass m_t which is referred to here as the second stage isolation. There is only an assumed linear isolator stiffness k_p present between the intermediate mass and the base. This stiffness forms the first or the primary stage isolation.

4.3.1 Governing equations of motion and non-dimensionalisation

The governing equations of motion for the mass m and the intermediate mass m_t are given respectively by

$$m\ddot{x} + c_1\left(\dot{x} - \dot{x}_t\right) + c_3\left(\dot{x} - \dot{x}_t\right)^3 + k\left(x - x_t\right) = 0 \tag{4.30}$$

and

$$m_t\ddot{x}_t + c_1\left(\dot{x}_t - \dot{x}\right) + c_3\left(\dot{x}_t - \dot{x}\right)^3 + k\left(x_t - x\right) + k_p\left(x_t - x_0\right) = 0 \tag{4.31}$$

where k_p is the linear stiffness of the primary stage isolator. x_t, $\dot{x}_t$ and $\ddot{x}_t$ are the displacement, velocity and acceleration of the intermediate mass.

By considering the model as two uncoupled isolation systems, one can define the uncoupled undamped natural frequencies which are given by

$$\omega_n = \sqrt{\frac{k}{m}} \text{ and } \omega_p = \sqrt{\frac{k_p}{m_t}} \tag{4.32}$$

where ω_n is the uncoupled undamped natural frequency of the second stage isolation. ω_p is the uncoupled undamped natural frequency of the mass m_t supported on the stiffness k_p. The non-dimensional time and the frequency ratio for this case are defined based on ω_n, i.e. $\tau = \omega_n t$ and $\Omega = \omega/\omega_n$. The non-dimensional parameters introduced for this model are the mass ratio,

$$\mu_t = \frac{m_t}{m} \tag{4.33}$$

and the stiffness ratio,

$$\kappa_t = \frac{k_p}{k} \tag{4.34}$$

In the case when m_t is negligible compared to the mass m, and/or k_p is infinitely stiff compared to k, the two-stage system reduces to a simple SDOF isolation model.

The disadvantage of the two-stage vibration isolation is the appearance of a secondary resonance above the primary resonance [44]. It is a result of having the intermediate mass. To obtain the isolation benefit from this model, the secondary resonance should be located as close to the primary resonance as possible to broaden the isolation zone despite the impracticality for some applications. This can be achieved using the optimum value of the stiffness ratio, introduced in references [40,67] and given by

$$\kappa_t = \mu_t + 1 \tag{4.35}$$

It is seen from equation (4.35) that the mass ratio μ_t and the stiffness ratio κ_t become interdependent when chosen in this optimal way.

One might normalise the response variables using the amplitude of the harmonic base excitation X and the natural frequency ω_n. The normalised variables chosen are

$$w_0 = \frac{x_0}{X},\ w = \frac{x}{X},\ w'' = \frac{\ddot{x}}{\omega_n^2 X},\ \tilde{u} = \frac{x - x_t}{X},\ \tilde{u}' = \frac{\dot{x} - \dot{x}_t}{\omega_n X},\ \text{and}\ \tilde{u}'' = \frac{\ddot{x} - \ddot{x}_t}{\omega_n^2 X} \tag{4.36}$$

where w_0 is the normalised base displacement. w and w'' are the normalised absolute displacement and acceleration of the isolated mass. $\tilde{u}$, $\tilde{u}'$ and $\tilde{u}''$ are the normalised relative displacement, velocity and acceleration between the isolated mass m and the intermediate mass m_t across the second-stage isolator.

Substituting the normalised variables and dividing by the quantity $m\omega_n^2 X$ produce

$$w'' + 2\zeta_1\tilde{u}' + \zeta_3\left(\tilde{u}'\right)^3 + \tilde{u} = 0 \tag{4.37}$$

$$\mu_t w'' + \kappa_t w = \mu_t\tilde{u}'' + 2\zeta_1\tilde{u}' + \zeta_3\left(\tilde{u}'\right)^3 + \left(\mu_t + 2\right)\tilde{u} + \kappa_t w_0 \tag{4.38}$$

Similarly to the previous cases, the non-dimensional cubic damping obtained from the normalisation is given by

$$\zeta_3 = \frac{c_3}{m}\omega_n X^2 \tag{4.39}$$

It is also identical to that for the SDOF isolator given in equation (3.5).

The isolation capability of the two-stage model is also examined analytically using the HBM and numerically using direct integration. The capability of a two stage isolation system with cubic damping is compared to the corresponding linear damping system.

4.3.2 Analytical solution using the Harmonic Balance method

The harmonic responses due to the harmonic base excitation, $w_0 = \cos(\Omega\tau)$ are expected as

$$w = W\cos(\Omega\tau - \phi_w) \text{ and } \tilde{u} = \tilde{U}\cos(\Omega\tau - \phi_{\tilde{u}}) \tag{4.40}$$

where ϕ_w and $\phi_{\tilde{u}}$ are the phase lags for the isolated mass m and the relative motion with respect to the base excitation.

After substitution of these quantities into equations (4.37) and (4.38), and the application of orthogonality, see the application as shown in equation (4.18), this yields four equations as follows:

$$\Omega^2 W\sin(\phi_w) = \tilde{U}\sin(\phi_{\tilde{u}}) - B\tilde{U}\cos(\phi_{\tilde{u}}) - C\tilde{U}^3\cos(\phi_{\tilde{u}}) \tag{4.41}$$

$$\Omega^2 W\cos(\phi_w) = \tilde{U}\cos(\phi_{\tilde{u}}) + B\tilde{U}\sin(\phi_{\tilde{u}}) + C\tilde{U}^3\sin(\phi_{\tilde{u}}) \tag{4.42}$$

$$AW\sin(\phi_w) = D\tilde{U}\sin(\phi_{\tilde{u}}) - B\tilde{U}\cos(\phi_{\tilde{u}}) - C\tilde{U}^3\cos(\phi_{\tilde{u}}) \tag{4.43}$$

$$AW\cos(\phi_w) = D\tilde{U}\cos(\phi_{\tilde{u}}) + B\tilde{U}\sin(\phi_{\tilde{u}}) + C\tilde{U}^3\sin(\phi_{\tilde{u}}) + \kappa_t \tag{4.44}$$

where $A = (1-\Omega^2)\mu_t + 1$, $B = 2\zeta_1\Omega$, $C = \frac{3}{4}\zeta_3\Omega^3$ and $D = (1-\Omega^2)\mu_t + 2$.

Algebraic manipulation of equations (4.41) to (4.44) produces

$$\Omega^4 W^2 = C^2\tilde{U}^6 + 2BC\tilde{U}^4 + (1+B^2)\tilde{U}^2 \tag{4.45}$$

and

$$(A - \Omega^2 D)^2\tilde{U}^2 + (A-\Omega^2)^2(B\tilde{U} + C\tilde{U}^3)^2 = \kappa_t^2\Omega^4 \tag{4.46}$$

For the case of linear viscous damping, i.e. $C = 0$, the solutions of equations (4.45) and (4.46) are given by

$$\tilde{U}^2 = \frac{\kappa_t^2 \Omega^4}{\left(A - \Omega^2 D\right)^2 + \left(A - \Omega^2\right)^2 B^2} \tag{4.47}$$

$$W^2 = \frac{\kappa_t^2 \left(1 + B^2\right)}{\left(A - \Omega^2 D\right)^2 + \left(A - \Omega^2\right)^2 B^2} \tag{4.48}$$

For the case of pure cubic damping, i.e. $B = 0$, equations (4.45) and (4.46) become

$$C^2 \tilde{U}^6 + \tilde{U}^2 = \Omega^4 W^2 \tag{4.49}$$

$$\left(A - \Omega^2\right)^2 C^2 \tilde{U}^6 + \left(A - \Omega^2 D\right)^2 \tilde{U}^2 = \Omega^4 \kappa_t^2 \tag{4.50}$$

The amplitude ratio for the relative displacement amplitude ratio squared, $\tilde{U}^2$, can be obtained by solving equation (4.50), which is a cubic polynomial in $\tilde{U}^2$. The coefficient of $\tilde{U}^4$ is zero so the solutions for $\tilde{U}^2$ are one real and two complex conjugates. The real solution for this case is too complicated to gain any insight into the effects of cubic damping. Thus it has been omitted here. The absolute displacement amplitude ratio for the isolated mass can be obtained by substituting for $\tilde{U}^2$ in equation (4.49).

For simplicity, the solution of the two-stage vibration isolation model is analysed for two frequency regions, i.e. $\Omega \ll 1$ and $\Omega \gg 1$. These frequency regions represent the excitation frequency much lower and much greater than the uncoupled undamped natural frequency ω_n respectively. The region of excitation frequency well above the resonance frequency, $\Omega \gg 1$, is also considered to be much greater than the secondary resonance. The simplified expressions for the absolute displacement are listed in table 4.2 for both linear and cubic damping. The detailed description for the simplification is given in Appendix C.

4.3.3 Numerical simulation procedure and solutions

The numerical integration for the two-stage isolation system was carried out to illustrate the response for different values of the mass ratio μ_t, by solving

equations (4.37) and (4.38). Values of linear viscous damping ζ_1 of 0.1, 0.2 and 0.3, and values of non-dimensional cubic damping ζ_3 of 0.013, 0.152 and 0.787 were considered.

Three values of the mass ratios, i.e. μ_t = 0.1, μ_t = 0.5 and μ_t = 1.0 have been investigated. For particular aspect, a system where a value of mass ratio greater than unity, i.e. the intermediate mass bigger than the isolated mass, is not considered in this study. Therefore only these lower values of mass ratios were chosen to investigate its effect of it on the displacement amplitude ratio.

4.3.4 Isolation performance for linear and cubic damping

The performance of the two-stage vibration isolation is examined first using the numerical results shown in figure 4.6. The responses for different mass ratios are plotted for comparison. It is seen that, for both the linear and cubic damping systems, the smaller μ_t shifts the frequency of the secondary resonance further from the primary resonance. The occurrence of the secondary resonance can be observed more easily when damping is low, e.g. in figure 4.6 (a).

One might also notice that the magnitude of the primary resonance can be reduced by increasing the value of either the linear or cubic damping. However, in the response for high cubic damping, shown in figure 4.6 (c) with μ_t = 1 (green dashed-dotted line), it is noticeable that the primary resonance for the system with cubic damping moves towards a frequency ratio of unity. This can be a result from that the isolated mass and the intermediate mass move almost as a combined unit $m + m_t$ on a spring k_p and the relative velocity across the damper tends to zero. The undamped frequency for the combined mass on a spring k_p can be given by

$$\omega_{new}^2 = \frac{k_p}{m_t + m} \tag{4.51}$$

Considering the definitions of the stiffness ratio and the mass ratio, i.e. $\kappa_t = k_p / k$ and $\mu_t = m_t / m$, equation (4.51) can be given by

$$\omega_{new}^2 = \frac{k\kappa_t}{m\left(\mu_t + 1\right)} \tag{4.52}$$

Strictly for the optimum value of stiffness ratio given in equation (4.35), i.e. $\kappa_t = \mu_t + 1$, equation (4.51) becomes

$$\omega_{new}^2 = \frac{k}{m} = \omega_n^2 \tag{4.53}$$

This means that, once the isolated mass and the intermediate mass are joined together, the system behaves like undamped vibration at the uncoupled undamped natural frequency of the second stage isolator ω_n.

The analytical examination is achieved using the simplified expressions listed in table 4.2. The expressions for the cubically damped system are compared to those for linear viscous damping. Consider the low frequency region, i.e. $\Omega \ll 1$. In both cases the amplitude ratios are about unity, i.e. quasi-static behaviour, similar to the SDOF and Zener models. As such the effect of any damping is negligible in this frequency region.

At frequencies well above the primary and secondary resonance, i.e. $\Omega \gg 1$, the approximate expressions are listed in row (b) of table 4.2. The cubically damped response is more interesting in that the approximate expression for displacement amplitude decreases by 80 dB per decade independent of the value of cubic damping. Its roll-off rate is much steeper than that for linear viscous damping, which is 60 dB per decade. The levels of amplitude ratio in the isolation region obtained from the analytical expressions are shown by the asymptote lines in figure 4.6, which are in good agreement with the numerical results.

The rolling-off in the isolation region ($\Omega \gg 1$), can be investigated using the relative displacement between the isolated and intermediate mass, which is listed in row (c) of table 4.2 for linear and cubic damping. The expressions for both damping systems at $\Omega \gg 1$ are identical and are given by

$$\tilde{U} \approx \frac{\mu_t + 1}{\Omega^2 \mu_t} \tag{4.54}$$

Thus one might expect similar plots of the relative velocity in this frequency region as shown in figure 4.7 in which the relative velocity decreases inversely proportional to the

excitation frequency, i.e. 20 dB per decade. By having a similar level of the relative velocity, the level of cubic damping force is expected to be lower than for linear damping force for small relative velocity much less than unity. This is because it is a result of the relative velocity cubed.

The damping forces are obtained by multiplying the relative velocity and relative velocity cubed by the terms B and C given in section 4.3.2 respectively. The dependences B and C are given here again, i.e.

$$B = 2\zeta_1\Omega \text{ and } C = \frac{3}{4}\zeta_3\Omega^3 \tag{4.55}$$

The linear damping force for $\Omega \gg 1$ is then

$$F_{d1} = \left(2\zeta_1\Omega\right)\frac{\left(\mu_t + 1\right)}{\Omega^2\mu_t} = 2\zeta_1\frac{\left(\mu_t + 1\right)}{\Omega\mu_t} \tag{4.56}$$

whereas the corresponding cubic damping force is

$$F_{d3} \approx \left(\frac{3}{4}\zeta_3\Omega^3\right)\left(\frac{\mu_t + 1}{\Omega^2\mu_t}\right)^3 = \frac{3}{4}\zeta_3\frac{\left(\mu_t + 1\right)^3}{\Omega^3\mu_t^3} \tag{4.57}$$

By considering that the linear and cubic damping produce a similar level of peak response, then it is considerable that the cubic damping force given in equation (4.57) is much lower than the linear damping force given in equation (4.56). The damping force can become negligible at the very high excitation frequencies as shown in figure 4.8. Therefore the mass of the rigid body is isolated with the negligible restoring force due to stiffness k at high frequencies as presented by $\tilde{U}$ given in equation (4.54).

Since the relative displacement between the intermediate and isolated mass tends to zero as excitation frequency increases, one might expect a reduction in absolute displacement for the intermediate mass at high frequencies similar to the isolated mass. Figure 4.9 shows the absolute displacement for the intermediate and isolated mass for both linear and cubic damping. Note that only the responses for $\zeta_1 = 0.3$ and $\zeta_3 = 0.787$ are chosen to be shown in figure 4.9. Figure 4.9 (b) shows that the absolute displacement for the intermediate mass for both linear and cubic damping decreases as excitation frequency increases by 40 dB per decade.

The relative displacement between the intermediate mass and the base excitation is also shown in figure 4.9 (c). It is seen in the high frequency region that the amplitude of relative displacement at high frequency is constant at the magnitude of unity which is the amplitude of base excitation. This means that at the high excitation frequencies, the intermediate mass is almost not moving. As a result there is almost no transmitted motion via the secondary stage isolation.

To this end, one can conclude that supporting the SDOF cubic damping system in a two-stage configuration can reduce the detrimental effect seen previously in the SDOF model. In addition, the isolation capability for the cubically damped system is much better than that for the linearly damped two-stage system.

4.4 Conclusions

In this chapter cubic damping was applied to two higher order isolation models, namely Zener and two-stage models. The analysis shows that the application of higher order isolation models possessing cubic damping can significantly remove the detrimental effect of the cubic damping under base excitation in the isolation region compared to the cubically damped SDOF system.

For the Zener model, the cubic damping element is supported elastically on a relaxation spring. The cubically damped response in the isolation region decreases by 40 dB per decade as the excitation frequency increases. It is also found that the value of the stiffness ratio equal to 8 is optimal for a system with high cubic damping. It produces a minimum level for the second resonance peak at the corresponding frequency $\Omega = 3$, especially for systems with high damping. One can conclude that it is preferable to elastically support the cubic damping component for a vibration isolation system exhibiting a cubic damping characteristic.

The isolation performance for the cubically damped two-stage isolation is more effective than that of the Zener model. The two-stage isolation is arranged by supporting the SDOF cubically damped isolation system on an undamped mass-spring system which forms the primary stage isolation. The SDOF cubic damping isolation then becomes a second stage isolation. The mass of primary stage or intermediate mass is considered as a ratio with respect to the isolated mass or secondary stage mass. It is found that a larger mass ratio provides a lower isolation frequency whereas the smaller

mass ratio shifts the isolation frequency further towards high frequencies. However, the application of the smaller mass ratio for the system with high value of cubic damping can result in high level of peak amplitude. Therefore the mass ratio should be chosen carefully to optimise the limitations. .

The existence of cubic damping in the second stage isolation is also found to improve the isolation capability compared to the linear damping. The level of the isolated mass response, e.g. the amplitude ratio, in the isolation zone decreases dramatically compared to the linear damping system. Therefore, it is more desirable to apply the cubic damping in the second-stage isolator of the two-stage model, strictly with the optimum stiffness ratio.

To this end, it can be concluded that these two higher order base excited vibration isolation models eliminate the detrimental effect of cubic damping as present in the SDOF system. The application of these two models also increases the isolation performance, especially for the two-stage vibration. Therefore, it is recommended to apply either model in preference to the SDOF isolation system under harmonic excitation where a cubic damping characteristic is incorporated.

Table 4.1 Approximate expressions for the amplitude ratio for base excited Zener isolation possessing cubic damping in comparison to those for the SDOF rigidly connected cubic damping.

	Frequency region	Cubic damping SDOF system $\kappa_z \approx \infty$	Cubic damping Zener model $\kappa_z \ll \infty$
(a)	$\Omega \ll 1$	$W \approx 1$	$W \approx 1$
(b)	$\Omega \approx \sqrt{\kappa_z + 1}$	-	$W \approx \left(\frac{3}{4}\zeta_3\right)\frac{(\kappa_z+1)^{\frac{9}{2}}}{\kappa_z^4}$
(c)	$\Omega \gg 1$	$W \approx \sqrt{1-\left(\frac{4}{3\zeta_3\Omega}\right)^{\frac{2}{3}}}$	$W \approx \frac{(\kappa_z+1)}{\Omega^2}$

Table 4.2 Approximate expressions of the absolute displacement amplitude ratio for two-stage base excited isolation model possessing cubic damping in comparison to linear viscous damping.

	Frequency region	Linear viscous damping	Cubic damping
Absolute displacement amplitude ratio			
(a)	$\Omega \ll 1$	$W \approx 1$	$W \approx 1$
(b)	$\Omega \gg 1$	$W \approx (2\zeta_1)\frac{(\mu_t+1)}{\mu_t}\frac{1}{\Omega^3}$	$W \approx \frac{(\mu_t+1)}{\mu_t}\frac{1}{\Omega^4}$
Relative displacement amplitude ratio at high frequencies			
(c)	$\Omega \gg 1$	$\tilde{U} \approx \frac{(\mu_t+1)}{\mu_t}\frac{1}{\Omega^2}$	$\tilde{U} \approx \frac{(\mu_t+1)}{\mu_t}\frac{1}{\Omega^2}$

Note that $\tilde{U}$ represents the relative motion between the isolated mass and intermediate mass.

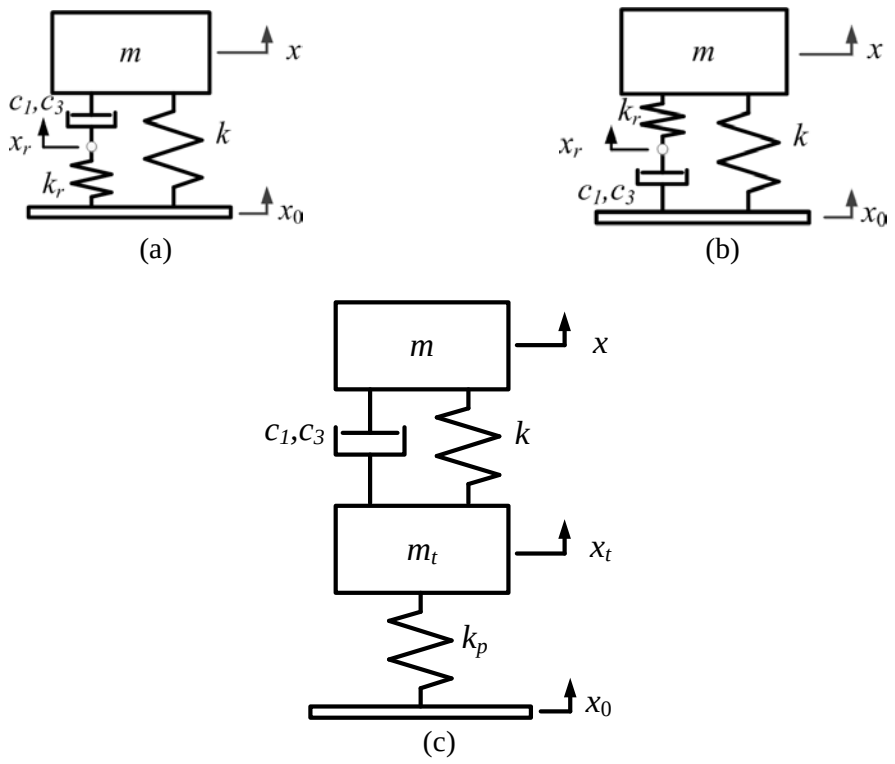

Figure 4.1 The higher order isolation models possessing cubic damping.
(a) Zener isolation with relaxation spring inserted between the damping and base excitation
(b) Zener isolation with relaxation spring inserted between the damping and isolated mass
(c) Two-stage isolation with undamped primary stage isolator

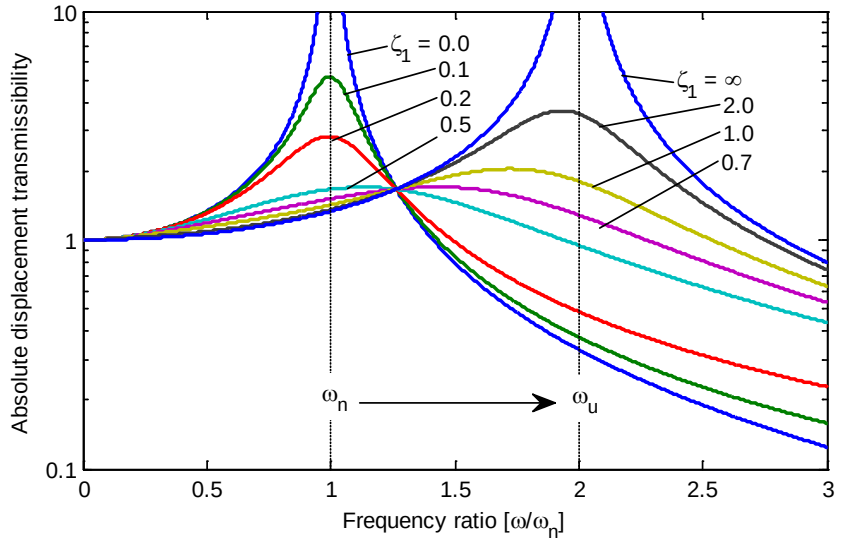

Figure 4.2 Absolute displacement transmissibility for Zener isolation model with stiffness ratio, $\kappa_z = 3$, and different levels of linear viscous damping, figure reproduced from [37].
Arrow illustrates that the natural frequency shifts from ω_n to ω_u as value of viscous damping increases.

(a)

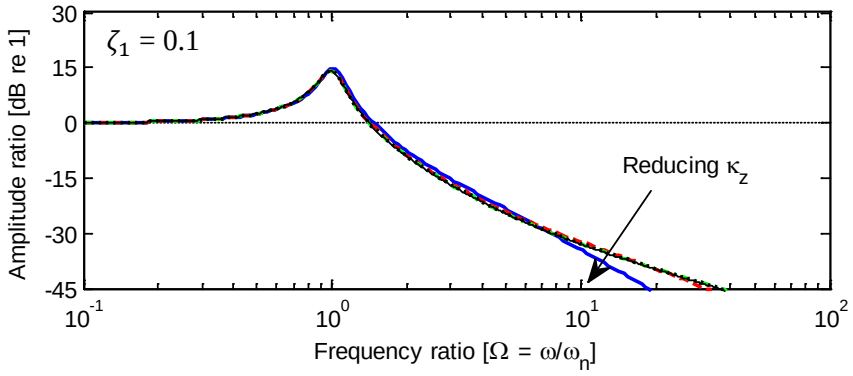

(b)

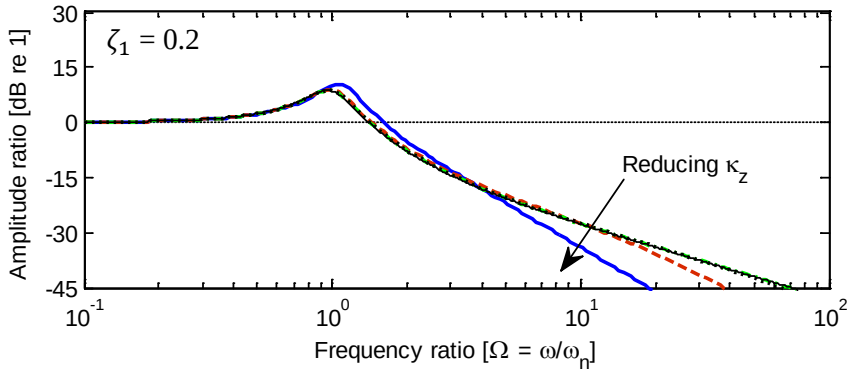

(c)

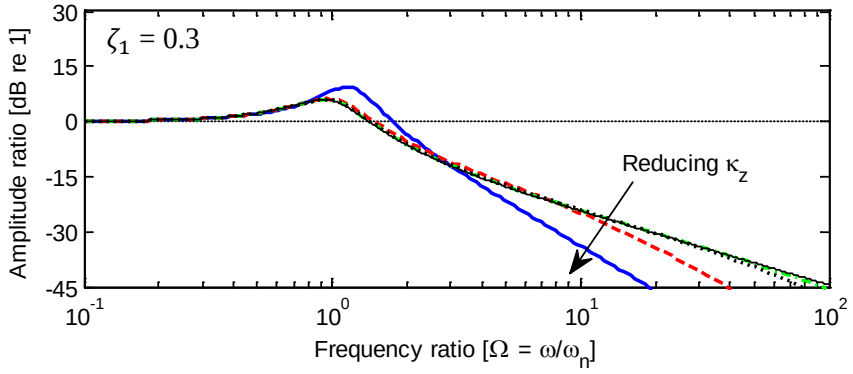

Figure 4.3 Absolute displacement amplitude ratio of the isolated mass for the Zener base excited isolation possessing linear viscous damping obtained from numerical integration.

(a) ζ_1 = 0.1, (b) ζ_1 = 0.2 and (c) ζ_1 = 0.3.

κ_z =1, κ_z = 8, ····· κ_z = 48 and κ_z = 99.

—— response for the SDOF model ($\kappa = \infty$)

(a)

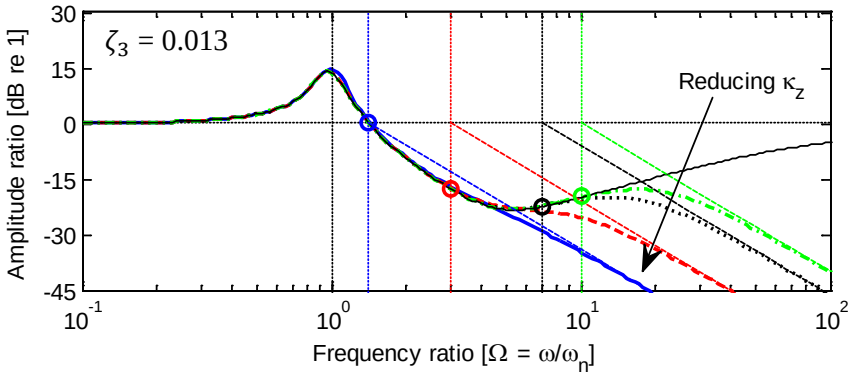

(b)

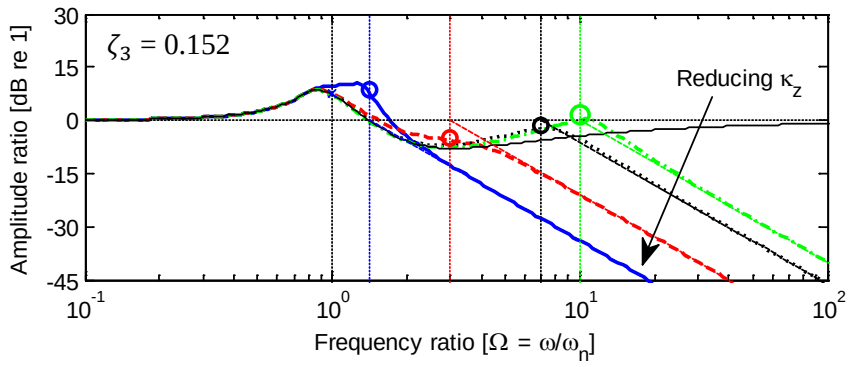

(c)

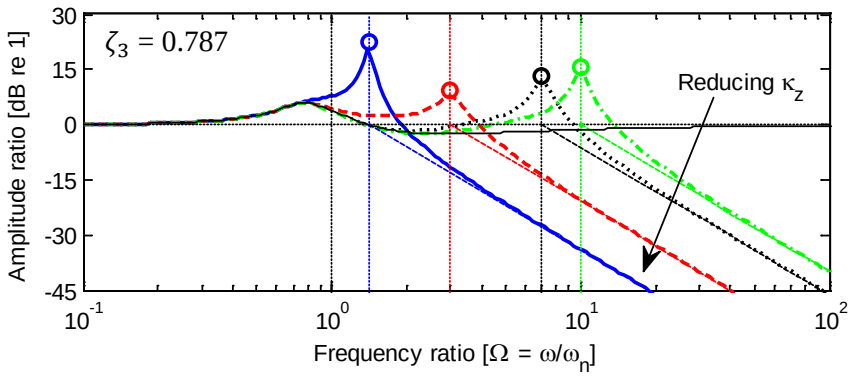

Figure 4.4 Absolute displacement amplitude ratio of the isolated mass for the Zener base excited isolation possessing cubic damping
(a) ζ_3 = 0.013, (b) ζ_3 = 0.152 and (c) ζ_3 = 0.787.
—— κ_z = 1, - - - - κ_z = 8, ····· κ_z = 48 and — · — κ_z = 99.
—— Cubically damped SDOF model ($\kappa = \infty$)
○ Markers respectively represent the amplitude ratio at $\Omega = \Omega_b = \sqrt{\kappa_z + 1}$ which are listed in row (b) of table 4.1
– – – The asymptote lines with the slope of $\frac{(\kappa_z + 1)}{\Omega^2}$ for cubic damping at $\Omega \gg 1$ with colours corresponding to the stiffness ratios

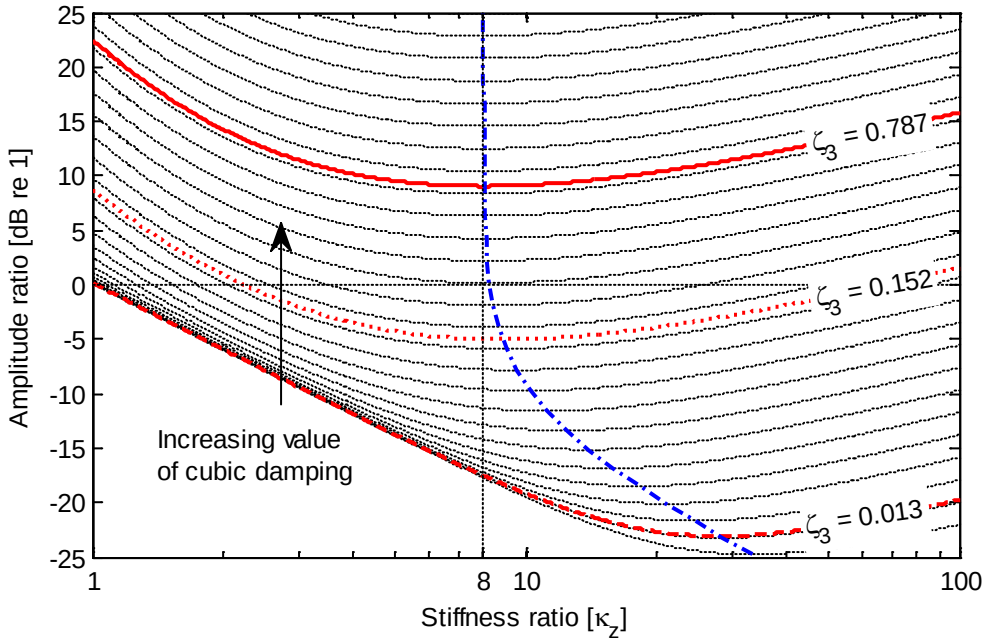

Figure 4.5 Relationship between the value of the stiffness ratio κ_z and the absolute displacement amplitude ratio, W, for the cubic damping Zener isolation model at a particular frequency ratio of $\Omega = \sqrt{\kappa_z + 1}$ using HBM approximation.
– · – · – indicates the optimum value of stiffness ratio which produces the minimum level of the amplitude ratio resulting from the application for each value of ζ_3

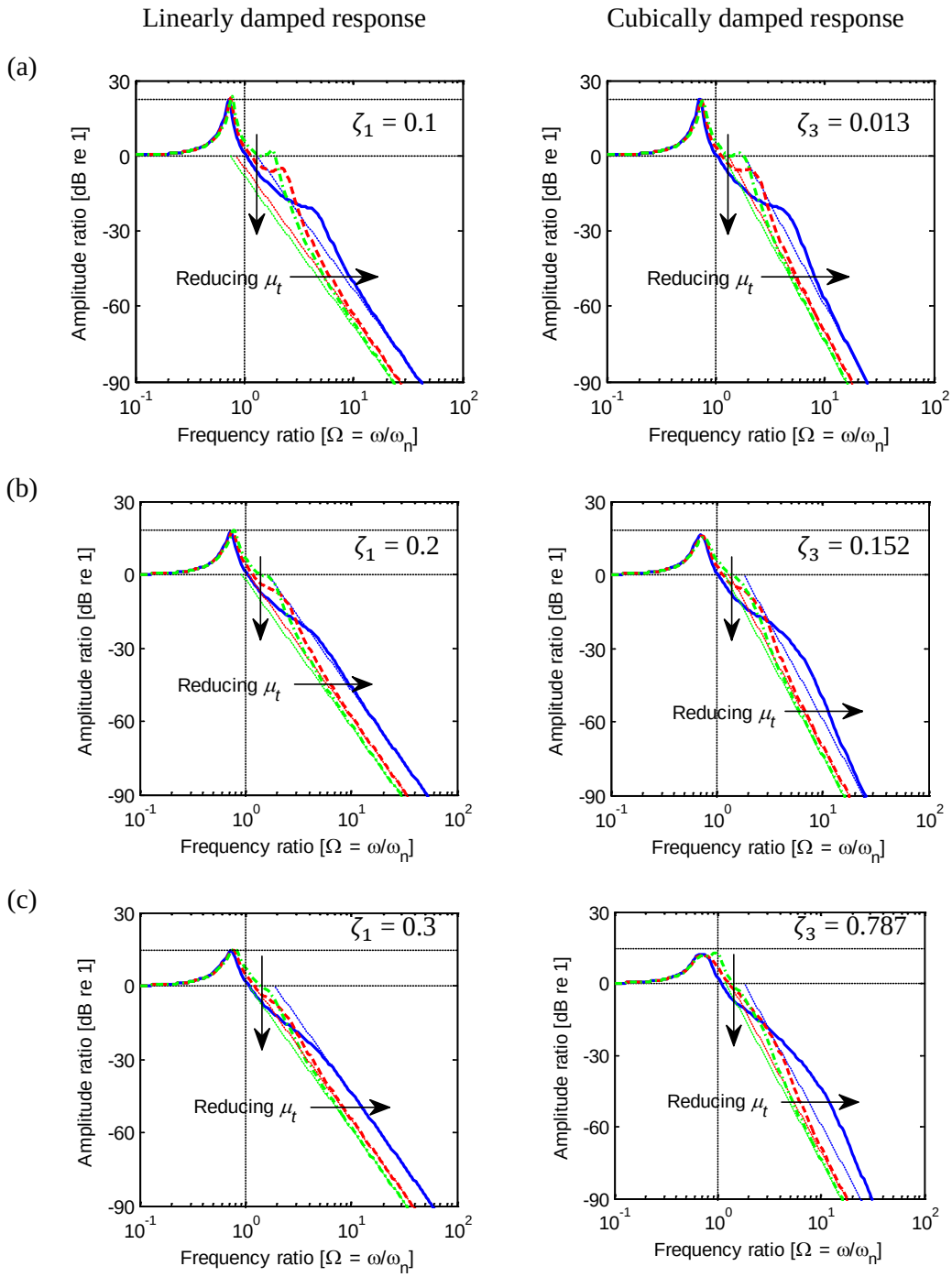

Figure 4.6 Absolute displacement amplitude ratio of the isolated mass for the two-stage base excited isolation obtained from numerical integration.

(a) $\zeta_1 = 0.1, \zeta_3 = 0.013$, (b) $\zeta_1 = 0.2$, $\zeta_3 = 0.152$ and (c) $\zeta_1 = 0.3$, $\zeta_3 = 0.787$

$\mu_t = 1$, $\mu_t = 0.5$, $\mu_t = 0.1$

○ Markers represent the cubically response levels at $\Omega \approx \Omega_r$

Asymptote lines for the slope given in row (c) of table 4.3

→ Arrows show the direction of reducing the value of μ_t

Note that the colours of markers and lines corresponding to μ_t

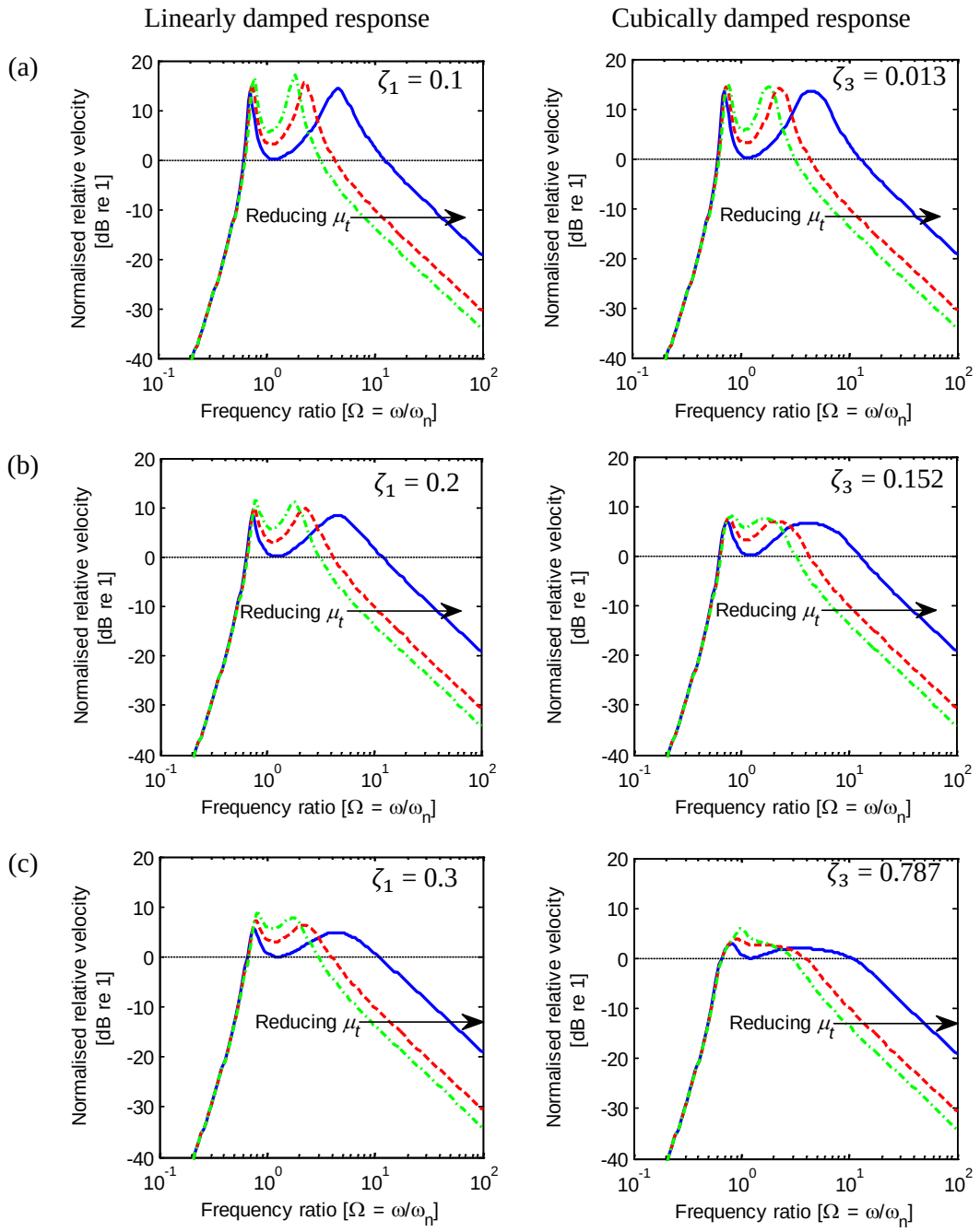

Figure 4.7 Normalised relative velocity across the damper for linearly and cubically damped responses obtained from numerical integration.

(a) ζ_1 = 0.1 and ζ_3 = 0.013

(b) ζ_1 = 0.2 and ζ_3 = 0.152

(c) ζ_1 = 0.3 and ζ_3 = 0.787

μ_t = 1, μ_t = 0.5, μ_t = 0.1

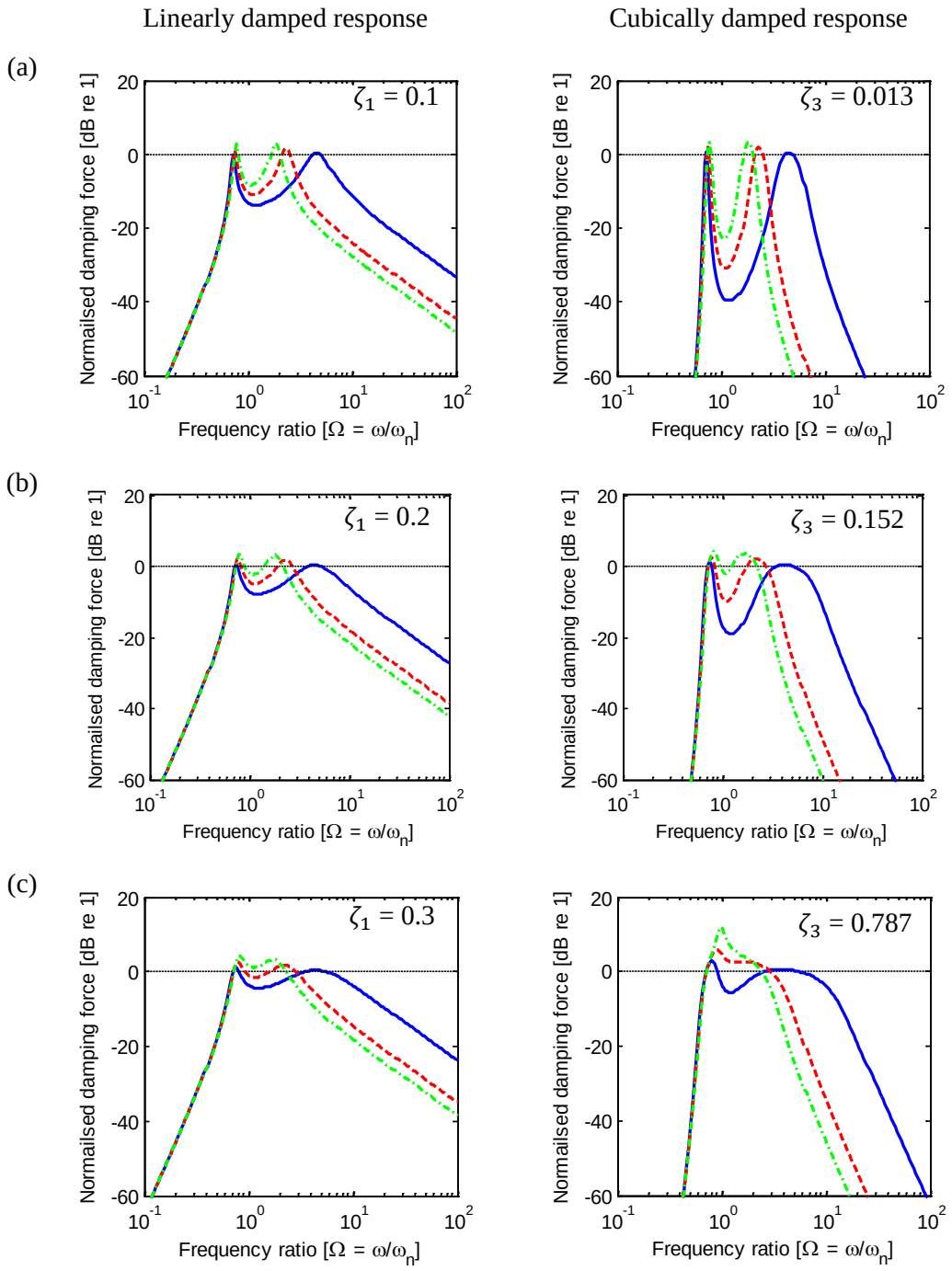

Figure 4.8 Normalised damping force for the secondary stage isolation.
(a) ζ_1 = 0.1 and ζ_3 = 0.013
(b) ζ_1 = 0.2 and ζ_3 = 0.152
(c) ζ_1 = 0.3 and ζ_3 = 0.787
μ_t = 1, μ_t = 0.5, μ_t = 0.1

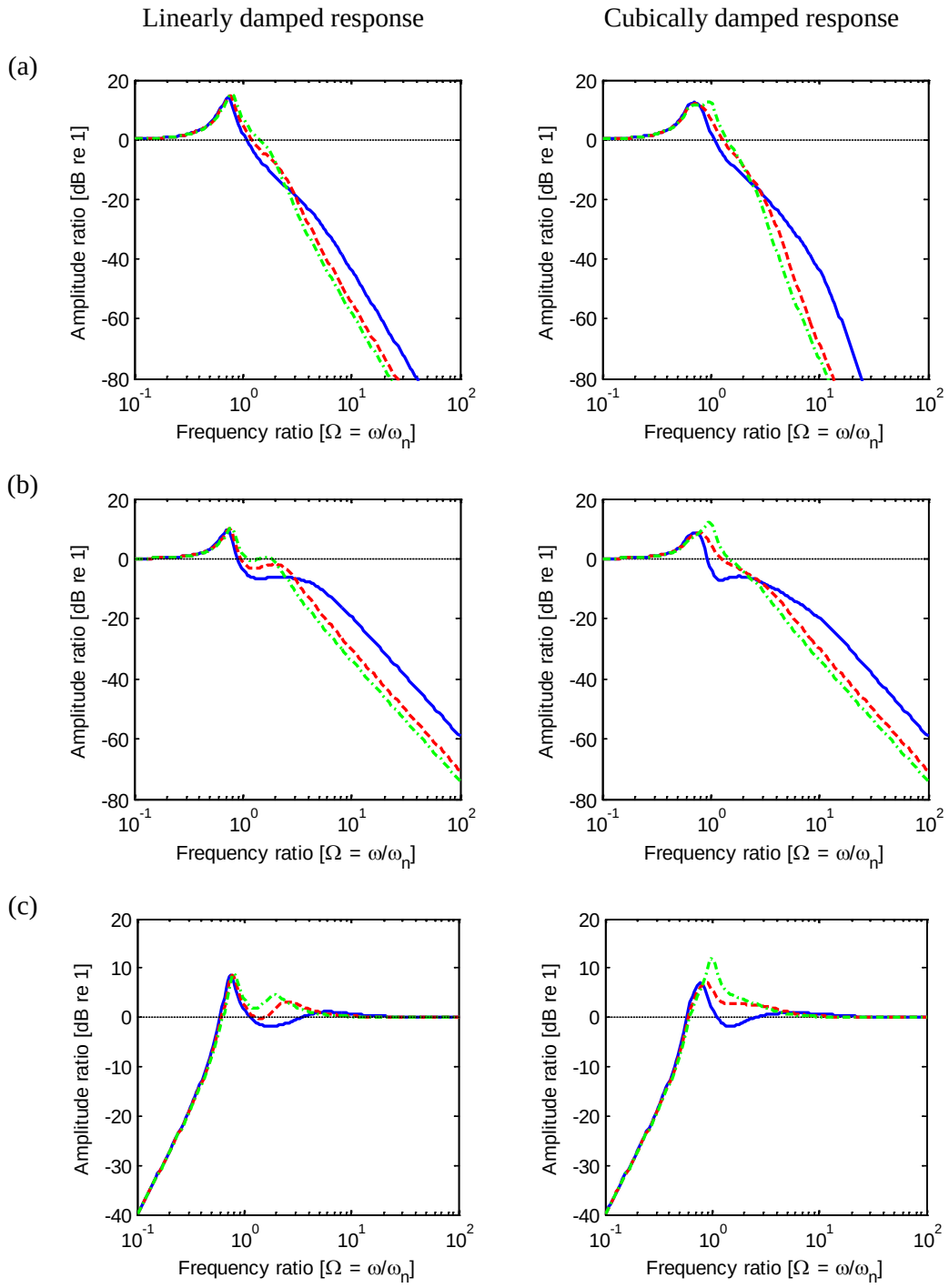

Figure 4.9 Displacement amplitude ratios for the two-stage isolation in comparison between the linear damping system with ζ_1 = 0.3 and cubic damping system with ζ_3 = 0.787.

(a) Absolute displacement for the isolated mass, $|W|$

(b) Absolute displacement for the intermediate mass, $|W_t|$

(c) Relative displacement between the intermediate mass and the base excitation, $|1-W_t|$

μ_t = 1, μ_t = 0.5, μ_t = 0.1

Chapter 5 Simulation of a cubically damped vibration isolation system subject to broadband excitation

5.1 Introduction

Previously a theoretical examination into cubically damped isolation subject to harmonic excitation was given in Chapter 3. The cubic damping proved to be beneficial in reducing the transmitted force from the excited structure to a supporting structure for excitation frequencies well above resonance. On the other hand, for base excitation, cubic damping causes an increased transmitted displacement at the same frequency region, unless a relaxation spring or an intermediate mass is introduced, as seen in Chapter 4.

In this chapter, the focus is on broadband random base excitation for the single degree of freedom (SDOF) system. It aims to explore whether the same detrimental effect happens as for harmonic excitation. In many practical instances broadband excitation can occur, e.g. road vehicles travelling over rough surfaces, ground vibration from railways, etc. The road surface roughness, for example, can usually be assumed as broadband excitation. Any unevenness of the road surface causes a base input to the automotive vehicle suspension. Such roughness is transmitted as vertical vibration to the passengers. The characteristic of the broadband random excitation for typical road vehicles applications is described later in section 5.4. Automotive dampers are nonlinear by design. One possibility is that the isolation system could be modelled as, or designed to exhibit, a cubic damping characteristic.

Generally, the nonlinear response due to broadband excitation cannot be easily predicted using analytical approaches. Instead, numerical integration is typically applied and this has been employed here. Numerical integration provides results in terms of time histories, which can be processed by means of statistical analysis or spectral analysis. The simulations produced in this chapter were mainly obtained using the ODE45 routine provided in Matlab [66].

This chapter reveals that cubic damping also produces the detrimental effects on the SDOF broadband base excitation. However, the effects are different from those resulting from harmonic excitation. The possible physical reasons for such effects are reported in this chapter. The obtained results show that the existence of nonlinear cubic damping on the broadband base excited isolation system has detrimental effects. Having this information can lead to further improvement of the SDOF broadband base excitation vibration isolation system in order to minimise possible severity.

5.2 Governing equation of motion

The model under investigation in this chapter was previously given in figure 2.1 (b) for which the governing equation of motion is equation (2.1) and given here again, i.e.

$$m\ddot{z}(t)+\tilde{f}_d(\dot{z},t)+kz(t)=\tilde{f}_e(t) \tag{5.1}$$

where m and k are the mass of the rigid body and the assumed linear stiffness. $\tilde{f}_e$ is the dimensional base excitation for which $\tilde{f}_e=-m\ddot{x}_0$. $\tilde{f}_d$ is a function representing the dimensional restoring force due to damping and given by

$$\tilde{f}_d(\dot{z},t)=c_p\dot{z}(t)\left|\dot{z}(t)\right|^{p-1} \tag{5.2}$$

$\ddot{z}$, $\dot{z}$ and z are the relative motion, i.e. acceleration, velocity and displacement as a function of dimensional time t. p is the exponent of the power law damping.

However, it is more convenient in this chapter to solve the equation of motion using the absolute displacement of the isolated mass, x, for which is obtained from

$$z=x-x_0 \tag{5.3}$$

where x_0 is the base displacement excitation. Linear and cubic viscous damping are only the damping components considered here, i.e. p = 1 and 3. Thus, equation (5.1) can be rewritten as

$$m\ddot{x}+c_1(\dot{x}-\dot{x}_0)+c_3(\dot{x}-\dot{x}_0)^3+k(x-x_0)=0 \tag{5.4}$$

where $\dot{x}_0$ and x_0 are the corresponding broadband base excitation velocity and displacement. $\ddot{x}$, $\dot{x}$ and x are the random responses.

The effects of cubic damping are evaluated by comparison with the case of linear viscous damping. Thus the system and the equation of motion given in equation (5.4) is considered for two separate cases, i.e.

(i) linear viscous damping :

$$m\ddot{x} + c_1\left(\dot{x} - \dot{x}_0\right) + k\left(x - x_0\right) = 0 \tag{5.5}$$

(ii) pure cubic damping:

$$m\ddot{x} + c_3\left(\dot{x} - \dot{x}_0\right)^3 + k\left(x - x_0\right) = 0 \tag{5.6}$$

Note that the numerical simulations for the case of broadband excitation are carried out using dimensional quantities, as stated in the governing equations of motion given in equations (5.5) and (5.6). This is unlike the case of harmonic excitation, where a non-dimensional set of quantities were defined. This is because for broadband excitation there is no single appropriate choice of non-dimensionalisation and introducing several forms would be unhelpful and ambiguous.

5.3 Analysis approaches

The broadband excitations applied here were assumed to be Gaussian random processes and stationary, i.e. mean and variance are independent of time. The response is anticipated to have the same property. An assumed stationary random time variable can usually be represented in terms of a statistical approach using either time domain or spectral analysis. Since the statistical properties for the assumed stationary random process do not change with time it is possible to investigate the effect of nonlinearity present in the broadband response using the time average instead of ensemble average [68]. Some relevant analysis approaches applied in this study are briefly described here.

5.3.1 Probability density function

A probability density function (PDF) is defined by a first order derivative of a probability distribution function, i.e.

$$p\left(x\right) = \frac{dP\left(x\right)}{dx} \tag{5.7}$$

where $P(x)$ is the probability distribution function. Some useful properties of the PDF are that it is always equal or greater than zero, $p(x) \geq 0$, and the area under its curve equals unity, $\int_{-\infty}^{\infty} p(x)\,dx = 1$ [69].

The assumed input PDF used in this study was the Gaussian or Normal distribution which is given by

$$p(x) = \frac{1}{\sigma_x \sqrt{2\pi}} e^{-(x-\mu_x)^2/(2\sigma_x^2)} \tag{5.8}$$

where μ_x, σ_x and σ_x^2 are mean value, standard deviation and variance of the random variable x respectively. The PDF of the Gaussian distribution has a bell shape as shown in figure 5.1.

5.3.2 Expected values and moments of random variables

An expected value of a random variable x is written as $E[x]$. It is sometimes called a mean or an average value of x, μ_x. The mean value is usually defined as a first moment of random variable and is given by

$$\mu_x = E[x] = \int_{-\infty}^{\infty} x p(x)\,dx \tag{5.9}$$

A second moment of random variables refers to the mean square value which is given by

$$E[x^2] = \int_{-\infty}^{\infty} x^2 p(x)\,dx \tag{5.10}$$

The second moment about the mean value is referred to as a central moment. It is called the variance and is given by

$$\sigma_x^2 = E\left[(x-\mu_x)^2\right] = \int_{-\infty}^{\infty} (x-\mu_x)^2\, p(x)\,dx \tag{5.11}$$

The positive square root of the variance is called the standard deviation. For an assumed zero mean signal, μ_x = 0, the standard deviation is equivalent to the root mean square (RMS) value.

5.3.3 Histogram and distribution

A histogram is one of the statistical methods used to represent the distribution of random data. It represents the random data by counting the number of times that a particular value, x_i, was found and putting that number into an interval or a bin. The width and the number of bins are interdependent. A greater number of bins can be obtained as a result of using narrower bins which produces a smoother curve for the histogram as shown in figure 5.1. Therefore the selection of the width and the number of bins depends upon the amount and quality of the data.

In addition, the height of the histogram is proportional to the amount of data in the bin. Therefore, to obtain a histogram which is comparable to that using PDF, the area underneath the histogram should be equal to unity. This can be achieved by normalising the area of the bins with the total area of the histogram. Thus the total normalised area of the histogram is equal to unity and the height of the histogram is comparable to the PDF of a Gaussian distribution as also shown in figure 5.1.

5.3.4 Spectral analysis

The analysis of broadband random can also be achieved using spectral analysis i.e. the power spectral density (PSD). The PSD can be estimated from the Fourier transformed [59], i.e.

$$S_{xx}(\varphi) = \frac{1}{T_s}\left|X(\varphi)\right|^2 \tag{5.12}$$

where $X(\varphi)$ is the discrete Fourier transform (DFT) of a sequence data $x(n)$ and is given by

$$X(\varphi) = \sum_{n=0}^{N-1} x(n) e^{-j\frac{2\pi n\varphi}{N}} \tag{5.13}$$

Similarly, the cross power spectrum density (CPSD) between the time signals x and y can also be estimated using the Fourier transformed of these two signals. The time histories of two signals are processed in the same way. The CPSD for truncated data can be obtained from

$$S_{xy}(\varphi) = \frac{1}{T_s} X(\varphi) Y^*(\varphi) \tag{5.14}$$

where asterisk $*$ denotes the complex conjugate.

5.3.5 Window function and data overlapping

The estimated PSD can also be obtained using the application of the so called Welch's method [70]. The method requires sets of truncated time histories. There might be discontinuities at the beginning and the end of the truncated data as a result of assumed periodicity. The discontinuity in the time domain signal can cause leakage in the frequency domain analysis.

To eliminate leakage, the time domain signal should be smoothly increased and decreased from and back to zero. This can be achieved by applying a window function to the truncated time data. A Hanning window is one of commonly applied windows. One of the advantages of the Hanning window is a rapidly decreasing side lobe in the frequency domain compared to the others. The rate of decreasing is about 60 dB per decade [68].

The application of the Hanning window results in lost or discounted data. However, it can be recovered by overlapping windows. The overlap is considered as a percentage of a period of the acquisition time. Figure 5.2 shows the plot of the Hanning window and its averaged power with an overlap of 0%, 50%, 66.67%, 75% and 80% of the period T. There are r sets of Hanning window in the length of T. r also represents the overlap factor, i.e.

$$\%_{Overlap} = \left(1 - \frac{1}{r}\right) \times 100 \tag{5.15}$$

In the acquisition period of $N_p T$, the number of complete sets of Hanning windows can be determined from

$$N_h = \left(N_p - 1\right) r + 1 \tag{5.16}$$

where N_p is a number of acquisition periods, N_h is the number of the complete window(s) in the period $N_p T$. The averaged power of the Hanning window as shown in figure 5.2 is given by

$$w_a^2(t) = \frac{1}{r}\sum_{i=1}^{N_h} w_i^2(t) \tag{5.17}$$

where w is the Hanning window.

It is seen from figures 5.2 (a) and (b) that an overlap of 50 % or lower produces a non-uniform weighting for the averaged power. There appears a ripple of about half (3 dB) of the maximum power [59]. A uniform weighting for the averaged power can be obtained for integer values of $r \geq 3$ [68] regarding equation (5.15) as shown in figures 5.2 (c) to (e). The overlap with $r = 4$ was chosen here, i.e. 75% overlap.

Finally, the estimated PSDs of the truncated data are averaged and given by

$$S_x(\varphi) = \frac{1}{q}\sum_{i=1}^{q} S_{x_{T_i}}(\varphi) \tag{5.18}$$

where q is the number of averaging PSDs and S_{x_T} is the estimated PSD of the truncated data x_T which is calculated using equation (5.12).

5.4 Generation of broadband random excitation

Broadband random excitation applied in this study was defined by referring to a displacement PSD. Two displacement base excitation characteristics were employed for the numerical examination, namely a white and a non-white random excitation. The displacement PSD for the white random is defined ideally to be constant over all frequencies. As a result, the ideal white random process has an infinite mean square value and the signal is not realistic. Therefore the term white random does not reflect the excitation characteristic applied here. This is because a finite frequency bandwidth was applied. Later, the term constant displacement amplitude random (CDR) excitation is used instead. The CDR excitation characteristic is introduced for comparison to the harmonic responses obtained from Chapter 3, for which a constant displacement amplitude was applied.

The other applied excitation for the base isolation is a white-velocity random excitation [71]. It is so called because the PSD level of the excitation velocity is constant for all excitation frequencies. Thus a corresponding displacement PSD is inversely proportional to the frequency squared. This excitation characteristic represented the non-white displacement broadband excitation applied here. Similarly to

the CDR excitation a limited frequency range was applied, so the term white-velocity random is also not suitable here. It is termed a constant velocity amplitude random (CVR) excitation as a substitute.

5.4.1 Constant displacement amplitude random excitation

A time history of the CDR excitation was generated by taking an inverse discrete Fourier transform (IDFT) [72] of

$$X_0(\varphi) = X_\varphi e^{j(2\pi f_\varphi t + \phi_\varphi)} \qquad ;\ \varphi = 1, 2, \ldots\ N \qquad (5.19)$$

where $X_0(\varphi)$ is a complex number representing the signal at the discrete frequency, X_φ is a constant real number representing the displacement amplitude in terms of discrete frequency. f_φ is the discrete frequency and is defined by $f_\varphi = \Delta f\, \varphi$ with Δf the frequency resolution. ϕ_φ is a uniformly distributed random phase and has a value between 0 and 2π. The constant amplitude of X_φ can be chosen in order that the excitation signal has the required displacement PSD level, i.e.

$$X_\varphi = \sqrt{T_s S_{xx}} \qquad (5.20)$$

where S_{xx} is the constant level of displacement PSD in the frequency bandwidth of interest. T_s is the period of acquisition time length and is defined by

$$T_s = \frac{1}{\Delta f} = \frac{N}{f_s} \qquad (5.21)$$

where N is the total number of data and f_s is the sampling frequency. The time history for the corresponding velocity can also be determined using the IDFT of

$$V_0(\varphi) = j\omega_\varphi X_0(\varphi) \qquad (5.22)$$

The implementation of the CDR is described in detail in section 5.6.

5.4.2 Constant velocity amplitude random excitation

The CVR excitation considered in this study has a PSD of the corresponding displacement that decreases inversely proportional to the frequency squared. The example for such excitation characteristic is sometimes representative of the surface

roughness excitation. The displacement PSD of a surface roughness is usually considered in terms of the wavenumber, i.e. spatial circular frequency, and is given by [59,73]

$$G(\Omega) = G(\Omega_0)\left(\frac{\Omega}{\Omega_0}\right)^{-w} \tag{5.23}$$

where G is a one-sided PSD. Ω denotes a spatial frequency and is given by $\Omega = \frac{2\pi}{\lambda}$ with λ a wavelength. Ω_0 is a reference wave number value. w is the waviness of the road surface for which the value recommended in ISO 6808 is equal to 2 [71,73]. Therefore, by having the displacement PSD inversely proportional to the excitation frequency squared, the excitation considered here has the same displacement spectral shape as the commonly adopted surface roughness model. However, its amplitude has not been chosen to be comparable to typical road roughness levels. The definition of surface roughness is given here only an example and is not included in the study.

The time domain signal for the CVR excitation applied in this study is obtained by taking the IDFT of the frequency domain amplitude given by

$$V_0(\varphi) = V_\varphi e^{j\left(2\pi f_\varphi t + \phi_\varphi\right)} \tag{5.24}$$

where V_φ is a constant real number representing a velocity amplitude at the discrete frequency f_φ. The constant velocity amplitude V_φ can also be obtained using equation (5.12) similarly to the constant displacement. The frequency domain amplitude for the corresponding displacement excitation is determined by

$$X_0(\varphi) = \frac{1}{j\omega_\varphi} V_0(\varphi) \tag{5.25}$$

By taking the IDFT of equation (5.25), one obtains the displacement based excitation time history for the CVR excitation. The detailed description for this excitation is also given in section 5.6.

5.5 Numerical simulation implementation and system parameters

The numerical examination was implemented using numerical integration obtained from the ODE45 solver in Matlab. One needs to specify the time and frequency resolutions to cover the investigating conditions. The physical parameters for

the isolation system are also required. The parameters assumed in this section are only for illustrative purpose of the effect of cubic damping on a SDOF base excited isolation system subject to the specified broadband random excitation.

5.5.1 Time and frequency resolution

The choice of time and frequency resolutions for the numerical integration is discussed here. The frequency resolution was determined using the application of a half power bandwidth criterion. For a SDOF system with known value of linear viscous damping, the half power bandwidth can be obtained from the transmissibility function, i.e.

$$T_r^2 = \frac{1+\left(2\zeta_1\Omega\right)^2}{\left(1-\Omega^2\right)^2+\left(2\zeta_1\Omega\right)^2} \tag{5.26}$$

where Ω is a frequency ratio and is given by $\Omega = \omega/\omega_n$ with ω_n the undamped natural frequency.

In this instance the frequency resolution was chosen to be sufficient for a system with linear viscous damping of $\zeta_1 = 0.01$. The transmissibility for such the system is shown in figure 5.3. A bandwidth of 0.02 f_n was obtained after the application of a half power bandwidth criterion as shown in figure 5.3 (b), where f_n is the natural frequency in Hz . To ensure an accurate reproduction of the peak response, the half power bandwidth was divided into 20 spectral lines which yielded a frequency resolution $\Delta f = 0.001\ f_n$.

The frequency bandwidth of the excitation for the simulation was initially chosen to range from 1–1000 Hz. The lowest excitation frequency of 1 Hz was set to avoid an extremely low frequency oscillation due to nonlinearity. The maximum frequency of 1000 Hz was set to ensure that the effects of cubic damping at high frequencies become apparent. The undamped natural frequency of the system was chosen as $f_n = 10$ Hz. Thus the excitation range covered one decade lower and two decades higher than the natural frequency. Therefore ideally, for the linear case at least, from the given information that $f_n = 10$ Hz and $\Delta f = 0.001\ f_n$, the frequency resolution should not be bigger than 0.01 Hz, i.e. $\Delta f \le 0.01$ Hz .

The discrete FFT was applied to analyse a set of sampled data. The frequency resolution can also be specified using the number of data points N and sampling frequency f_s as given in equation (5.21), i.e. $\Delta f = N/f_s$. It is also recommended to assign N and f_s in the base-2 format for the calculation of the Fourier transform using the FFT algorithm, i.e. 2^n where n is a positive integer. For the maximum frequency resolution of 0.01 Hz, the lower nearest base-2 value is 2^{-7}or 0.0078 Hz which produces a single sample time interval of 128 s.

Since the maximum excitation frequency, $f_{\max}$, was set at 1000 Hz, there responses are expected at the odd harmonics resulting from the nonlinear cubic damping at frequencies higher than 1000 Hz. To avoid possible signal aliasing, the sampling frequency was set at 2^{14} Hz (16384 Hz or 0.016 ms). This yields the total number of data points to be 2^{21} points for the time interval of 2^7 s.

However, for the analysis of a random process, averaging is needed in order to reduce the variance in the level of the estimated PSD when it is assumed stationary. An appropriate time length can be determined from an effective bandwidth (B) and total acquisition time length (T) product or BT product. It is recommended that the BT product should be much greater than unity [68]. The effective bandwidth is determined from the bandwidth of an applied spectral window [68]. It is sometimes called the 3 dB bandwidth. For instance, the 3 dB bandwidth for the Hanning window is given by [59]

$$B = 1.44\frac{1}{T_s} \tag{5.27}$$

The effective bandwidth B for this instance was approximately equal to $1.44/128 \approx 0.011$ Hz. In this instance, the total acquisition time was extended to 2048 s, 2^4 times the original set of data. This yields a total number of data point of 2^{25} points, i.e. $N = f_s\Delta f = (2^{14}\text{ Hz})(2^{11}\text{ s})$. Thus the BT product is approximately equal to 22.5 and is high enough to expect that the statistical variation in the estimated PSDs would be minimal and not significant.

5.5.2 System mass and stiffness

There are choices in the values of mass and stiffness to match the chosen natural frequency, i.e. 10 Hz. The value of the mass also influences the effective system

damping. This can be seen from the definitions of the linear viscous damping ratio and the non-dimensional cubic damping parameters for the case of harmonic excitation which are respectively given by , $\zeta_1 = \frac{c_1}{2m\omega_n}$ and $\zeta_3 = \frac{c_3}{m}\omega_n X^2$.

For simplicity, the mass m was chosen to be unity, i.e. m = 1 kg. This yields the corresponding value of isolator stiffness equal to 3.95 kNm^{-1}. The selected values of the damping coefficients c_1 and c_3 are given in the next section.

5.5.3 Damping coefficients

The value of cubic damping coefficient was defined referring to the linearly damped response for ζ_1 = 0.2. The dimensional linear damping coefficient (c_1) can be obtained from $c_1 = 2m\zeta_1\omega_n$. According to the specified natural frequency, f_n = 10 Hz and the mass m = 1 kg, the resulting value of c_1 is equal to 25.13 Nsm^{-1}. The resulting level of peak response around resonance for the normalised absolute displacement transmissibility is about 9 dB.

The corresponding value of c_3 which provides a similar level of peak response for the CDR base excitation was 0.33 Ns^3m^{-3} and c_3 = 133 Ns^3m^{-3} was applied for the CVR excitation. Note that the values for the damping coefficients chosen here are only to demonstrate the effect of cubic damping for this numerical study. The procedure to obtain the value of c_3 is omitted.

5.6 Influence of broadband excitation on the level of effective damping

The responses due to four excitation characteristics are reported and examined in this section. The descriptions of the applied excitation characteristics are given as follows.

(i) The CDR excitation with fixed excitation bandwidth of 1-1000 Hz.
The displacement PSD, S_{x_0}, level was varied to achieve displacement RMS values of 0.25 mm, 1.25 mm and 2.5 mm, see figure 5.4 (a).

(ii) The CDR excitation with fixed displacement PSD level.

The level of S_{x_0} was fixed so as to give an RMS value of 1.25 mm for an excitation bandwidth of 1-1000 Hz. Two additional frequency bandwidths were introduced, i.e. 1-500 Hz and 1-100 Hz, see figure 5.4 (b). As a result, the displacement RMS value was reduced to 0.88mm and 0.39 mm respectively.

(iii) The CDR excitation with fixed displacement RMS value at 1.25 mm.

Three excitation bandwidths were introduced, i.e. 1-1000 Hz, 1-500 Hz and 1-100 Hz each with a displacement RMS value fixed at 1.25 mm. Thus the level of S_{x_0} is higher as a result of the narrower bandwidth, see figure 5.4 (c).

(iv) The CVR excitation with fixed <u>velocity PSD</u> level.

The velocity PSD, $S_{x_0'}$, level was fixed whilst the excitation bandwidth was varied, i.e. 1-1000 Hz, 1-500 Hz and 1-100 Hz as shown in figure 5.4 (d). The corresponding level of estimated displacement excitation PSD, S_{x_0}, decreases with excitation frequency squared as shown in figure 5.4 (e). It is seen from figure 5.4 (e) that the level of S_{x_0} at high frequencies is considerably lower than that at low frequencies. As a result it is mostly low frequency excitation that contributes to the displacement RMS value. Thus the displacement RMS for narrower bandwidths applied in this study is not significantly different from that of 1-1000 Hz and it is around 1.25 mm. However, the difference in the velocity RMS values is significant.

These excitations were introduced in order to investigate the response characteristics due to different excitations. One might expect to synthesise and distinguish the influence of the broadband input on the effect of cubic damping.

The examination for the first three excitation scenarios given in this section will be carried out using the absolute displacement PSD for the isolated mass. The responses due to the last excitation scenario, case (iv), are examined using the absolute velocity PSD for the isolated mass. The linear and cubic damping force PSDs are also considered in conjunction with the estimate PSDs of the motion of the isolated mass.

The corresponding standard deviations of the mentioned quantities are also presented for some examinations.

Later, for the linear damping case, the displacement PSD, the velocity PSD and the linear damping force PSD are represented by S_{x_1}, $S_{x_1'}$ and $S_{f_{d1}}$ respectively. Those for the cubically damped response are denoted respectively by S_{x_3}, $S_{x_3'}$ and $S_{f_{d3}}$. The corresponding standard deviations for the absolute displacement for the isolated mass and damping force are denoted by σ_{x_1} and $\sigma_{f_{d1}}$ for the linear case, σ_{x_3} and $\sigma_{f_{d3}}$ for the cubic case.

5.6.1 Different displacement PSD level with fixed bandwidth

The responses due to CDR excitations with fixed bandwidth of 1-1000 Hz, case (i), are examined. The estimated input displacement PSD, S_{x_0}, is shown again in figure 5.5 using dashed lines. The levels of S_{x_0} shown in figures 5.5 (a) to (c) are about -22 dB, -28 dB and -42 dB respectively. The response displacement PSDs and damping force PSDs for both linear and cubic damping are also shown in figure 5.5.

Considering first the linearly damped responses (dotted lines), the estimate PSDs of the displacement responses, S_{x_1}, as shown in figures 5.5 (a) to (c), are seen to scale simply with excitation level. This is also noticeable from the values of displacement standard deviation, σ_{x_1}, annotated in the graphs, which scale with the RMS of the displacement excitation.

In contrast, in the same figures, the plots of the estimate displacement PSDs for the cubically damped response, S_{x_3}, (solid lines) are totally different among the cubic damping cases and also different from the linear responses. The difference in excitation level does not only affect the level of the response but also changes the response characteristic. In the case of a high excitation amplitude, figures 5.5 (a) and (b), the presence of cubic damping causes significant amplification to the response especially at low frequencies. It contributes significantly to the standard deviation value for the system with cubic damping, σ_{x_3}. For the system with lower excitation level, figure 5.5 (c), the response at low frequencies is similar to the input, as is also the case for a linearly damped system.

The appearances of peak responses are also noticeably different. The higher excitation level, figure 5.5 (a), causes the response characteristic of a linearly heavily damped system, i.e. there is no obvious frequency which the peak occurs. The peak response due to the lower excitation level, figure 5.5 (c), is more obvious and is consistent with a linearly lightly damped system.

By considering the estimate damping force PSDs as shown in figures 5.5 (d) to (f), the estimated linear damping force PSDs, $S_{f_{d1}}$, are also seen to scale by the level of excitation. The amplitude of excitation only effects the level of $S_{f_{d1}}$ and not the spectrum characteristic. In contrast, the excitation level has significant influence on both the level and characteristic of estimated cubic damping force PSDs, $S_{f_{d3}}$. The cubic damping force for the low excitation level, figure 5.5 (f), is considerably negligible compared to the linear damping force. This occurrence results in the very lightly damped response as seen in S_{x_3}.

From the given results, the level of the effective cubic damping is shown to be dependent upon the level of displacement excitation which can be related to the excitation RMS value. However, the excitation RMS value is in turn dependent upon the excitation bandwidth. In the next section, the effect of cubic damping is investigated for different excitation bandwidths whilst the level of S_{x_0} is fixed.

Note that the occurrence of the responses outside the excitation bandwidth at low and high frequency regions for both S_{x_3} and $S_{f_{d3}}$ is examined and discussed later in section 5.8.

5.6.2 Fixed displacement PSD level but different bandwidth

Figure 5.6 show the estimated PSDs of the displacement and damping force when the excitations have a fixed level of displacement excitation PSD at about -28 dB and different bandwidths (case ii). The PSDs of the displacement excitation are also shown in the figure using dashed lines and the corresponding RMS values are annotated in the figures, simply denoted by σ_{x_0}. It is seen that a reduction in the excitation bandwidth yields a reduction in the excitation RMS value. As such, considering the

knowledge obtained from the examination in section 5.6.1, one might anticipate a reduction in the effective cubic damping for the excitation with a smaller RMS value.

Figures 5.6 (a) to (c) show that the characteristics of the displacement response PSDs for the system with linear damping are not significantly different due to the reduction of the excitation bandwidth. It is noticeable only the absence of the response at high frequencies which corresponds directly to the excitation frequency. This is in contrast with the displacement response PSDs for the system with cubic damping, S_{x_3}. The characteristics of S_{x_3} are totally different. The effect of cubic damping can be noticeable from the level of S_{x_3} at low frequencies below the resonance frequency. It is more profound for the excitation with broader bandwidth. The S_{x_3} is consistent to the very lightly damped system for the narrower excitation bandwidth.

The standard deviation of the displacement response for the system with linear damping, σ_{x_1}, is essentially constant at 0.26 mm. This can be interpreted that the linear response at high frequencies produces a negligible contribution to the overall value. Therefore, the value of σ_{x_1} is contributed to mostly by the response at frequencies below and around the resonance frequency. The reduction of the excitation bandwidth does not affect the absolute displacement for linear system provided that the excitation frequencies around the resonance frequency are included.

In contrast, the value of σ_{x_3} is neither constant nor changing monotonically with the change in excitation RMS. The plots of S_{x_3} in figures 5.6 (a) to (c) show that σ_{x_3} can be contributed to by the response at either the low frequencies, figure 5.6 (a), or around the resonance frequency, figure 5.6 (c).

For the linear damping force, it is well-known for the linear isolation system that the excitation at one particular frequency can only produce a response at that frequency. Therefore there exhibit the linear damping force PSDs, displayed by the dotted lines in figure 5.6 (d) to (e), corresponding to the excitation bandwidth. However, the value of $\sigma_{f_{d1}}$ is influenced mostly by the damping force at high frequencies.

Although the cubic damping force standard deviation, $\sigma_{f_{d3}}$, is also directly related to the excitation bandwidth, the cubic damping force at a particular frequency

can be influenced by excitation at other frequencies. Thus the estimated cubic damping force PSDs are very different for both levels and characteristics. The excitation with narrower bandwidth results in almost negligible level of damping force compared to that for the broader excitation bandwidth.

Therefore, given the results obtained from this and previous simulation scenarios, the reduction in the cubic damping force is believed to be a result of the reduction in the excitation RMS value. However, the presence or absence of displacement excitation at high frequencies might also be a contribution in the cubic damping force. So the next investigation scenario was conducted by maintaining the RMS value of excitation whilst the excitation bandwidth is reduced.

5.6.3 Fixed displacement excitation RMS but different bandwidth

The excitations applied in this section were introduced in order to investigate whether the reduction in cubic damping force is influenced by the displacement excitation at high frequencies. The displacement excitation RMS was kept constant at 1.25 mm whilst the bandwidth was altered (case iii). As a result of these two constraints, the level of estimate displacement excitation PSD, S_{x_0}, for the narrower excitation bandwidth is higher as previously shown in figure 5.4 (c). The levels of S_{x_0} for excitation bandwidth of 1-1000 Hz, 1-500 Hz and 1-100 Hz are about -28 dB, -25 dB and -18 dB respectively. These excitations are shown here again in figures 5.7 (a) to (c) using dashed lines.

The results obtained from section 5.6.1 lead one to believe that a higher excitation level results in a lower peak response, whilst the observations in section 5.6.2 show that narrowing the excitation bandwidth reduces the effective damping. As such one might expect opposing effects on the level of damping from the increased level of S_{x_0} and the reduced bandwidth.

Unexpectedly, figures 5.7 (a) to (c) show that the estimated displacement PSDs for the system with cubic damping, solid lines, are similar to those reported in section 5.6.2. The response for the excitation with reduced bandwidth still has the lightly damping response characteristic as shown in figure 5.7 (c), despite the increased

excitation level. The estimate cubic damping force PSDs in figure 5.7 (f) also decreases unevenly similar to that in the previous section,

One might set the hypothesis from these results that the effect of cubic damping is partially influenced by the excitation RMS value but mostly affected by the frequency content of the excitation, especially the high frequencies. To verify this hypothesis and continue the investigation into the influence of the displacement amplitude at high frequencies, the level of S_{x_0} for the next simulation was reduced in proportion to the excitation frequency squared or in other words constant velocity PSD or the CVR excitation.

5.6.4 Fixed excitation velocity PSD level but different bandwidth

The plots of the excitation with constant velocity PSD (case iv) are shown again in figure 5.8 using dashed lines. It is understood for the excitation with constant velocity PSD that the level of displacement PSD reduces with the excitation frequency squared. The excitation displacement RMS value is mostly contributed to by the displacement excitation amplitude at low frequencies. For this instance, it was approximately equal to 1.25 mm for different excitation bandwidth.

The estimated velocity PSDs are shown in figures 5.8 (a) to (c). The response characteristics for the system with linear damping (dotted lines) are similar. Also the values of velocity standard deviation, $\sigma_{\dot{x}_1}$, are similar at about 52.4 mm/s. This is because it is mostly contributed to by the response at low frequencies and around the resonance frequency. The amplitudes of response at excitation frequencies high above the resonance frequency are considerably negligible.

The estimated velocity PSDs for the system with cubic damping, shown by solid lines in figures 5.8 (a) to (c), are seen to be influenced by excitation bandwidth similarly to those reported in sections 5.6.2 and 5.6.3. The narrower excitation bandwidth results in a lightly damped response. However, the response amplitude at excitation frequencies below the resonance frequency is different from those subject to the CDR excitation. It has similar amplitude with the excitation. This is believed to be a result of lower amplitude displacement excitation at high frequencies. The level of estimated cubic damping force PSD in figures 5.8 (f) is also considered very low compared to the linear

damping force. This is similar to previous two scenarios that, for the cubic damping system, the excitation with the absence of high frequencies results in a lightly damped response.

In addition, figures 5.8 (a) to (c) reveal that the low displacement excitation amplitude at high frequencies of the CVR also results in a lower level of the response outside the excitation bandwidth compared to those due to the CDR excitation. This occurrence also supports the argument that the displacement amplitude at high frequencies has a significant influence on the level of the cubic damping force.

However, one might not be able to conclude firmly that the excitation at high frequencies is the main contributor to the effect of cubic damping. Therefore, the next section reports the effect of cubic damping due to the special broadband excitation characteristics.

5.7 Influence of two pass-band excitation

In addition to the excitations applied in section 5.6, input excitations in this section were considered that have two pass bands. Whilst idealistic, it was introduced in order to verify that displacement excitation at high frequencies is the most significant contribution to the effect of cubic damping.

The first pass band was 1-250 Hz in all cases; the second pass band was chosen as 250-500 Hz (i.e. one continuous pass-band), 500-750 Hz and 750-1000 Hz as shown in figure 5.9. For the CDR excitation, figures 5.9 (a) to (c), the displacement RMS values for these excitations are similar at about 1.25 mm. This is because the level of estimated displacement excitation PSD was fixed and the total frequency bandwidth for every case was the same. The estimated excitation with constant velocity PSDs are shown figures 5.9 (d) to (f) whereas those in figures 5.9 (g) to (i) are the corresponding excitation displacement PSDs. The displacement RMS value for the CVR excitation, figure was also approximately equal to 1.25 mm since it was contributed to mostly by the excitation at low frequencies.

Figure 5.9 shows that these excitations include different frequency contents whilst sharing other characteristics, i.e. the total frequency bandwidth, the PSD level (either displacement or velocity) and the displacement RMS value. Therefore, any

difference in the broadband response can be identifiable as a result from the frequency content of the excitation.

The responses due to these excitations are examined separately for the case of constant displacement and constant velocity. Similarly to the previous section, the examination will be carried out using the estimate PSDs of the absolute motion of the isolated mass (either displacement or velocity) and the damping force. The results obtained in this section will also be studied to highlight the influence of displacement amplitude excitation at high frequencies later discussed in section 5.8.2.

5.7.1 Constant displacement amplitude random excitation

The displacement PSDs for these excitations are shown again in figure 5.10 using the dashed lines. The displacement PSDs for the responses are shown in figures 5.10 (a) to (c) and cubic damping force PSDs are also shown in figures 5.10 (d) to (f). It reveals the noticeable difference especially at low frequencies below resonance. The excitation with the absence of high frequency content produces a lower response level at this frequency region, figure 5.10 (a). The response levels at these frequencies are higher when excitation contains the higher frequency content, figure 5.10 (c).

The estimated cubic damping force PSDs show that the existence of high excitation frequencies produces a higher level of damping force across all frequencies. The value of $\sigma_{f_{d3}}$ is contributed to mostly by the damping force at high frequencies. This occurrence is investigated and reported in detail in section 5.8 where the possible reason for the effect on the level of damping is discussed. From the provided information, the existence of displacement amplitude at high frequencies plays a significant role in the effect of cubic damping. However, the next excitation scenario with the same pass bands but using constant velocity was introduced in order to ensure that this hypothesis is true.

5.7.2 Constant velocity amplitude random excitation

The estimated excitation velocity PSDs are shown in figure 5.11 using the dashed lines. The estimated response velocity PSDs for the system with linear and cubic damping are shown in figures 5.11 (a) to (c). The differences in the levels of velocity PSDs and the values of response velocity standard deviation, $\sigma_{\dot{x}_1}$ and $\sigma_{\dot{x}_3}$, are

considerably negligible. There is also no significant difference in the level of the estimated linear and cubic damping force PSDs as shown in figures 5.11 (d) to (f). There is no change in the response level due to the change of excitation bandwidth. There is also no noticeable difference for the level of cubic damping forces and the corresponding standard deviation among the cases.

This shows that, when the excitation is a constant velocity spectrum, changing the bandwidth of high excitation frequencies does not significantly affect the overall response. This is because the influence of displacement excitation at high frequency is very small compared to those at low frequencies. This is in contrast to that for the CDR excitation, where the displacement amplitude at high excitation frequencies plays a vital role in the level of damping. A further examination and discussion into the effect of cubic damping is also given in detail in section 5.8.

5.8 Analysis and further discussion on the effect of cubic damping due to broadband excitation

There are two main concerns regarding the presence of cubic damping. The first is the influence of the excitation displacement at high frequencies on the level of the cubic damping force. The investigation for this is presented in sections 5.8.1 and 5.8.2. The second is the occurrence of either the displacement response or damping force at low frequencies outside the excitation bandwidth. This issue is presented in section 5.8.3.

5.8.1 The response due to a displacement excitation at high frequencies

The examination in this section is introduced to verify that the displacement excitation at high frequencies is a significant contribution to the level of effective cubic damping. It is performed by using some results obtained from the previous sections which include the responses due to:

(i) the CDR having fixed RMS with bandwidth of 1-100 Hz (section 5.6.3),
(ii) the CDR with bandwidth of 1-250 Hz and 750-1000 Hz (section 5.7.1) and
(iii) the CDR having the bandwidth of 1-1000 Hz and RMS of 1.25 mm.

The responses due to these excitations are chosen because the excitations share the same RMS value of 1.25 mm whereas the frequency contents are different. The displacement PSD and the damping force PSD for both linearly and cubically damped responses due to these excitations are shown together again in figure 5.12. Note that the estimated displacement excitation PSDs are different in level as a result of having the same RMS value.

The figure shows that the frequency content in the excitation influences the peak amplitude of estimate displacement response PSDs at around the resonance frequency. The excitation with less frequency produces response similarly with the linearly lightly damped response disregarding the excitation RMS value. It is clearer by considering the estimate cubic damping PSD. It appears that the level of cubic damping force is directly related with frequency content in the excitation. The excitation with high frequencies and higher level, figure 5.12 (e), results in higher value of $\sigma_{f_{d3}}$ compared to that with an absence of high frequencies, figure 5.12 (d), or with high frequencies but lower level, figure 5.12 (f).

Time histories for the responses due to the mentioned excitations are shown in figure 5.13. The oscillations of both linearly and cubically damped response are seen majorly at around the resonance frequency of 10 Hz, illustrated by dashed line. The cubically damped responses are at a higher amplitude compared to the linearly damped responses. The excitation with narrower bandwidth is found to produce negligible amplitude of cubic damping force compared to the linear damping force, figure 5.13 (d). It is in contrast to those due to excitations having broader frequency range, figures 5.13 (e) and (f).

To this end, one can conclude that the effective cubic damping is mainly influenced by the displacement excitation at high frequencies. The absence of excitation at high frequencies results in weak cubic damping. A possible reason for this phenomenon is examined and reported in the next sub-section.

5.8.2 Analysis of the influence of high frequency content in the excitation

An examination into the influence of high frequencies carried out in this sub-section was conducted into two parts. The first part was carried out using the numerical responses due to the two pass bands excitations obtained from sections 5.7.1 and 5.7.2.

Statistical analysis was employed to examine the relative velocity. The second part was performed using theoretical expressions for the assumed random time response. Insight into the effect of excitation at high frequencies is expected.

The responses from sections 5.7.1 and 5.7.2 are chosen for the first examination because the excitation amplitude for each case was fixed to be the same, only the excitation bandwidth was modified. The total number of frequencies in the excitation is also comparable. Then the influence of excitation amplitude and number of frequencies can be removed and only the influence of the frequency content can be observed.

The responses for the case of CDR are first examined. The significance of the displacement excitation at high frequencies can be seen from the histograms shown in figure 5.14. The difference of high frequencies results in different distribution and the standard deviation for the relative velocity, $\sigma_{\Delta\dot{x}}$. The excitation with lower frequencies produces a higher peak and histogram with narrower tails, figure 5.14 (a), compared to that having higher frequencies, figure 5.14 (c). It can be implied that the existence of displacement excitation at high frequencies causes a higher amplitude of relative velocity. As a result, the density around the mean value is reduced and the tails are wider.

In contrast, when an excitation with constant velocity spectrum is applied, there is almost no difference in the histograms of the relative velocity, see figure 5.15. The values of $\sigma_{\Delta\dot{x}}$ are similar and constant for this latter case. The distribution of relative velocity is denser around the mean value with narrower tails compared to those for the CDR excitation. This is identifiable as a result of the low amplitude of the displacement excitation at high frequencies compared to those at low frequencies. As such, for the CVR excitation, the presence or absence of displacement excitation at high frequencies is not so important and does not cause any difference to the value of $\sigma_{\Delta\dot{x}}$. However, this is strictly valid only when the low frequency content is the same and produces the comparable displacement excitation RMS value.

In addition, it is noticeable that the histograms for relative velocity are very similar for the cases of linear and cubic damping, for the same excitation bandwidth and characteristic, as shown in figures 5.14 and 5.15. Therefore, it is possible to determine the relative velocity at which the linear and cubic damping forces are at the same level.

By considering that the relative velocity for linear damping is equivalent to that for cubic damping, one obtains

$$\Delta\dot{x} = \pm\sqrt{\frac{c_1}{c_3}} \tag{5.28}$$

The relative velocity given in equation (5.28) is plotted in figures 5.14 and 5.15 using the vertical dashed lines. These lines are also displayed for both cases, CDR and CVR in figure 5.16 which shows the force-velocity characteristics.

The force-velocity characteristic shows that the amplitude of cubic damping force resulting from the CDR excitation is much higher than that for the CVR excitation. The cubic damping for the broader bandwidth CDR excitation is even higher as seen in figure 5.16 (c). This can imply that the broader excitation bandwidth results in a higher level of cubic damping force. This can also cause the high amplitude of spike as shown in figure 5.13 (e).

One can see that, when the CDR excitation was applied, the displacement amplitudes at high frequencies play the vital role to the value of $\sigma_{\Delta\dot{x}}$. The presence or absence and the amplitude of displacement excitation at high frequencies are important consideration. However, the histogram does not clearly show how the existence of displacement amplitude at high frequencies results in the different level damping especially for cubic damping.

Therefore, for the second part, one can examine the effect of high frequencies on the expression of relative velocity. The relative velocity resulting from the broadband frequency excitation can be given by

$$\Delta\dot{x} = \sum_{i=1}^{N} \omega_i Z_i \sin\left(\omega_i t + \phi_i\right) \tag{5.29}$$

where Z is the amplitude of the relative displacement as a function of frequency and ϕ is the phase lag of the relative response. N represents the number of frequencies inside the excitation bandwidth.

The linear damping force at a particular excitation frequency can be obtained directly from the product of c_1 and $\Delta\dot{x}$. Therefore the amplitude of the linear damping force is a scaled quantity of the relative velocity. In addition, the damping force at one

particular frequency is only produced by excitation at the same frequency. The cubic damping force can be obtained from the product of c_3 and $\left(\Delta\dot{x}\right)^3$. The expansion of the relative velocity cubed can be given by

$$\begin{aligned}\left(\Delta\dot{x}\right)^3 = \sum_{i=1}^{N}\left(\frac{3}{2}\omega_i Z_i\left(\sum_{j=1}^{N}\omega_j^2 Z_j^2\right)-\frac{3}{4}\omega_i^3 Z_i^3\right)\sin\left(\omega_i t+\phi_i\right)\\ -\frac{1}{4}\sum_{i=1}^{N}\omega_i^3 Z_i^3\sin\left(3\omega_i t+3\phi_i\right)+\varepsilon\left(t\right)\end{aligned} \tag{5.30}$$

where $\varepsilon\left(t\right)$ represents the responses at other frequencies resulting from the cubic exponent apart from the first two frequency orders ω_i and $3\omega_i$.

The first term on the right hand side of equation (5.30) shows that the amplitude of the relative velocity at a frequency i is contributed to by the amplitude of the relative velocity at all N frequencies inside the bandwidth. The amplitude of cubic damping force at a particular frequency is a consequence of this summation. The greater number of high frequency content can cause a much higher level for the cubic damping force. This is the difference from what happens for linear damping force.

To this end, one can conclude in general for cubic damping system that the amount and amplitude of high frequency content can result in significant differences in the level of the relative velocity cubed. The cubic damping force is as a result obtained from this expansion. This is in contrast to the linear damping case where the linear damping force amplitude at a particular frequency is obtained directly from the product of $c_1\omega_i Z_i$. Thus the appearance of the cubic damping force for each excitation bandwidth is noticeably different.

5.8.3 The response at low frequencies outside the excitation bandwidth

The occurrence of high amplitudes of the response outside the excitation bandwidth for the cubic damping system is more noticeable when the broader excitation bandwidth was applied. A result of exciting with the broader bandwidth is the significantly higher amplitude of damping force as discussed in the previous section. This high level of damping force can occur in the form of spikes or impulsive forces as seen by the red lines in figures 5.13 (e) and (f).

It is well known that an impulsive force can produce a broadband frequency characteristic which reasonably flat over all frequencies. A shorter duration of pulse produces a broader frequency spectrum and vice versa. The pulses occurring can have different durations which can give different high frequency responses but always the same or similar low frequency response. Therefore, large spikes of damping force can result in the vibration response at low frequencies outside the excitation bandwidth.

Figures 5.17 (a) and (b) show levels for the relative velocity PSDs between the linear and cubic damping responses due to the CDR and CVR excitation with the excitation bandwidth of 1-1000 Hz respectively. The differences at the lower frequencies below resonance inside the excitation bandwidth are apparent. This occurrence can be identifiable as a result of impulsive force resulting from relative velocity cubed. The occurrence of forces at these additional frequencies can be acting on the isolated mass apart from the force from base excitation. These forces yield the higher amplitude of isolated mass which results in response amplitude greater than the amplitude of excitation at these frequencies. As a result, the velocity amplitude of isolated mass is higher than that for excitation. It also yields the higher relative velocity at low frequency region.

5.9 Conclusions

In this chapter the effect of cubic damping on a SDOF base excited vibration isolation system was investigated using a variety of broadband excitations. Two different random excitation characteristics, namely constant displacement amplitude (CDR) and constant velocity amplitude (CVR) excitations were applied. The numerical results were carried out using direct numerical integration. The excitation characteristics were altered in terms of the amplitude and bandwidth.

The responses for the base excited vibration isolator possessing cubic damping subject to either the CDR or CVR excitation is clearly dominated mainly by the input displacement amplitude at high frequencies. Greater displacement amplitude at high frequencies produces a higher level of damping force. Therefore, the base excited vibration isolator with the cubic damping characteristic can encounter a detrimental effect. It is considered detrimental since the result of cubic damping can cause higher vibration amplitude for the isolated mass at low frequencies below the resonance as well

as in the expected isolation region. The absence of displacement input at high frequencies also results in the low level of cubic damping force which also results in a high peak amplitude around resonance.

Although the existence of displacement at high frequency increases the level of cubic damping force, it does not significantly reduce the peak response around resonance but increases the response at lower frequencies as mentioned earlier. The high vibration response level at low frequencies outside excitation bandwidth is identifiable as being a result of impulsive damping force. Such the force is a consequent result of taking the relative velocity to the power of three. It can be concluded that the occurrence of responses at low frequencies outside the excitation bandwidth are due to these impulsive damping forces.

To this end, the investigation into the effect of cubic damping due to broadband excitation reflects some behaviour that might happen for the nonlinear damping base excited vibration isolation. Therefore, consideration of the amplitude and bandwidth of the input excitation has to be taken into account.

The effect of cubic damping has proved theoretically detrimental on the base excited isolation system due to either harmonic or broadband excitation. The level of cubic damping force has been found to be a possible reason. However, to ensure that the theoretical results are acceptable and reliable, the next chapter is about to report the experimental results for both harmonic and broadband random excitation.

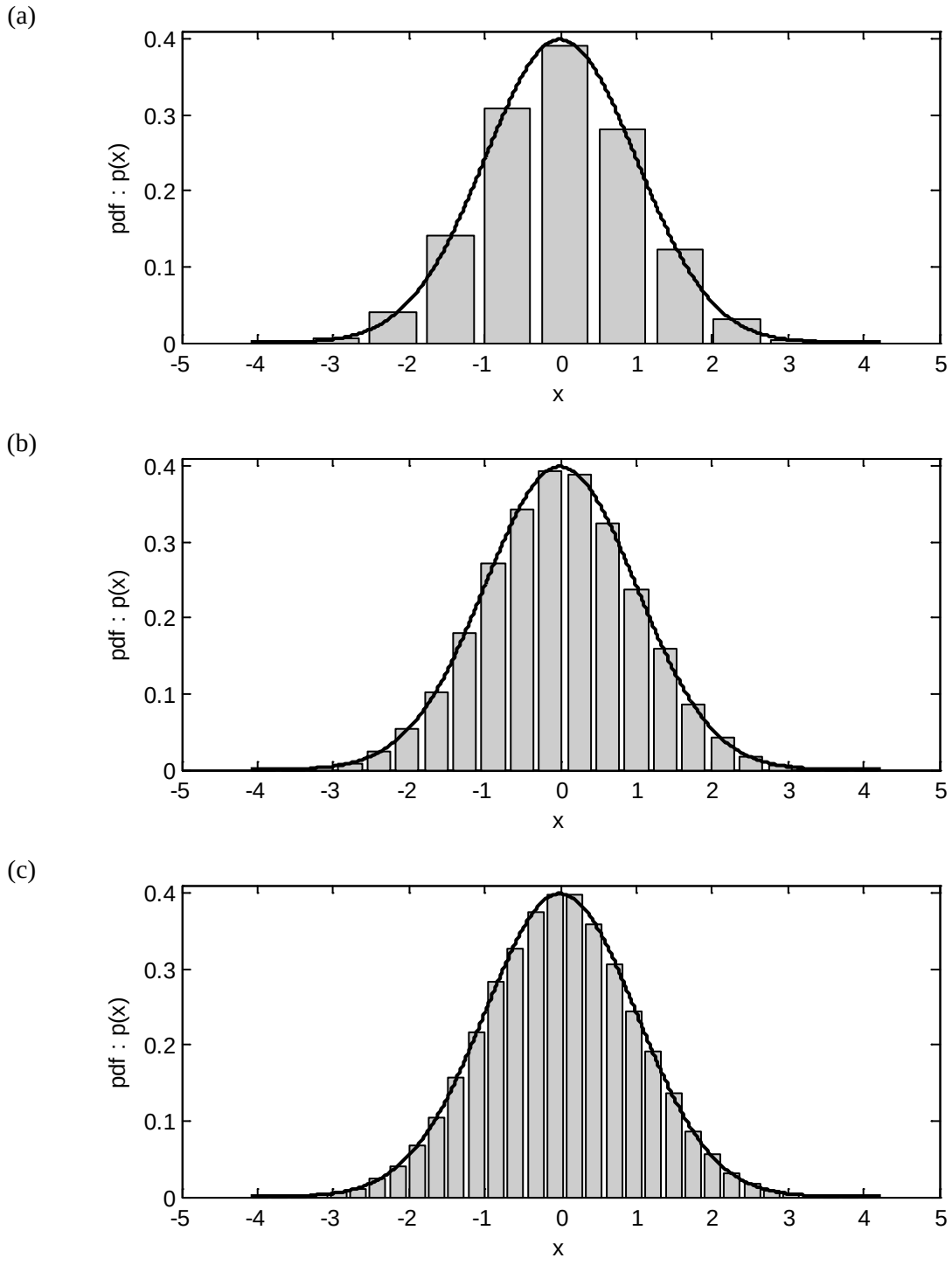

Figure 5.1 Probability distribution functions of the Gaussian distribution with $\mu_x = 0$ and $\sigma_x = 1$.
(a) 10 bins, (b) 20 bins and (c) 30 bins
—— Gaussian distribution

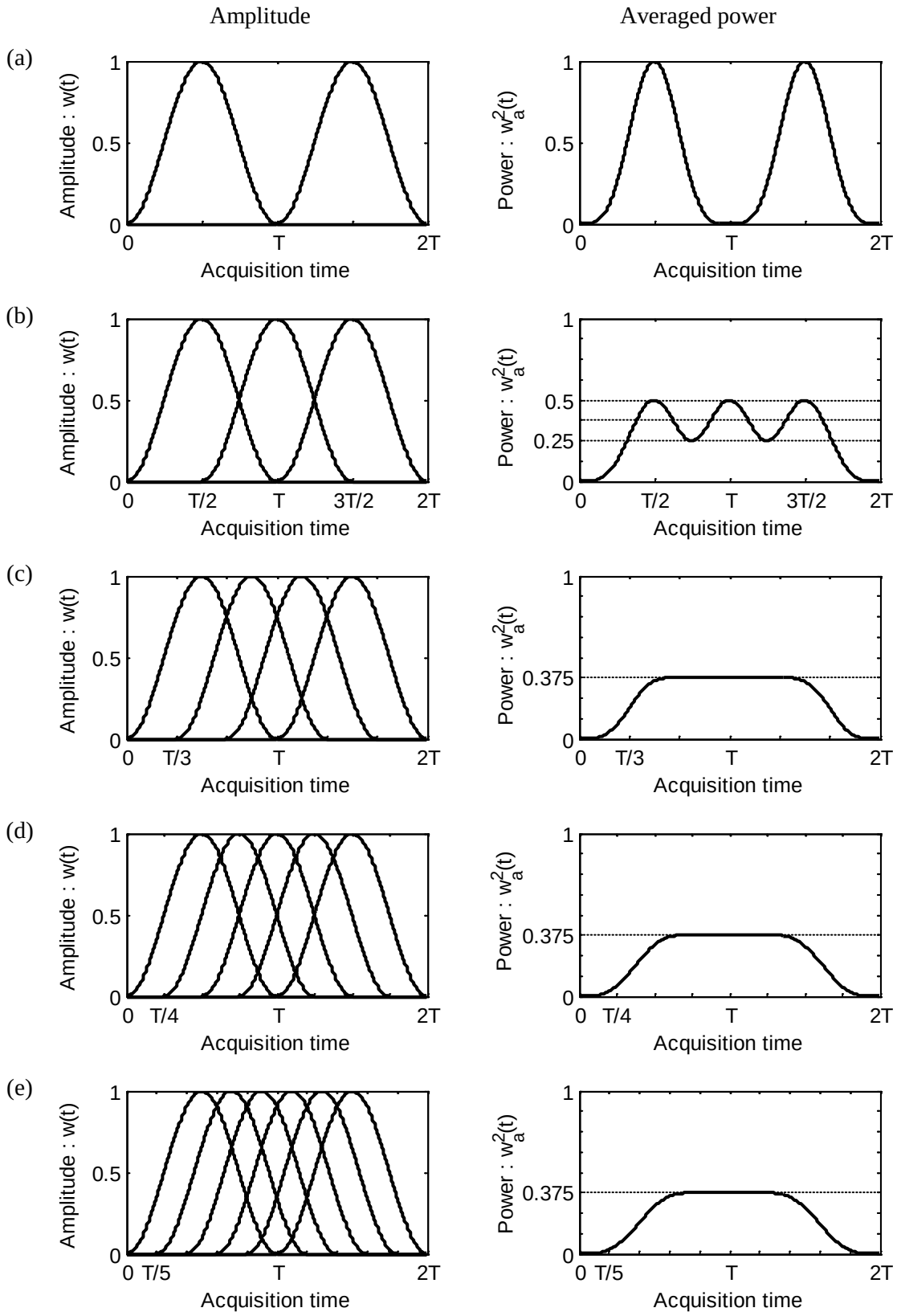

Figure 5.2 Amplitude and the resulting averaged power of overlapping Hanning windows in the period of acquisition time of $2T$.
(a) 0% overlap, (b) 50% overlap, (c) 66.67% overlap, (d) 75% overlap and (e) 80% overlap.

(a)

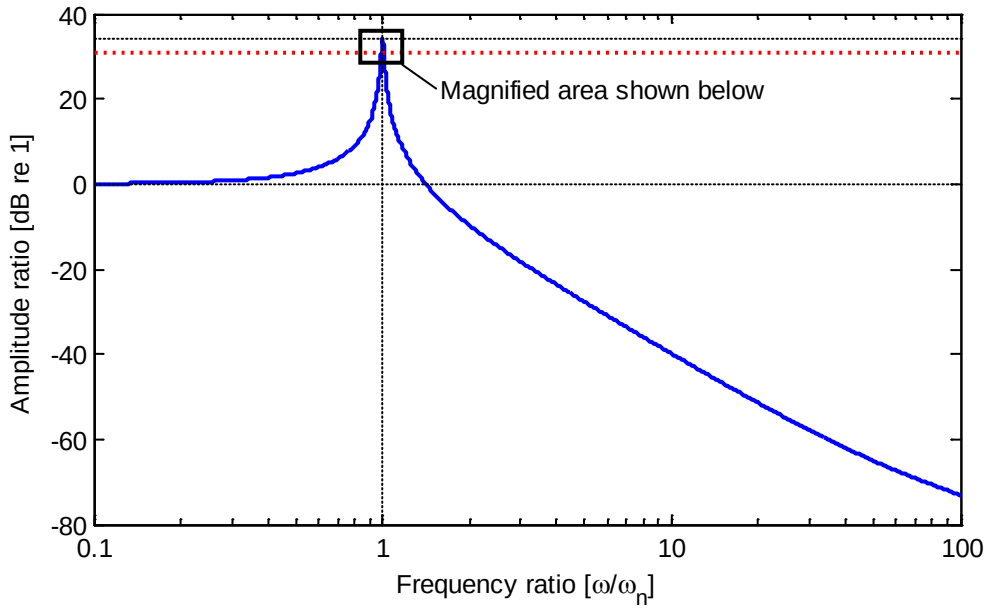

(b)

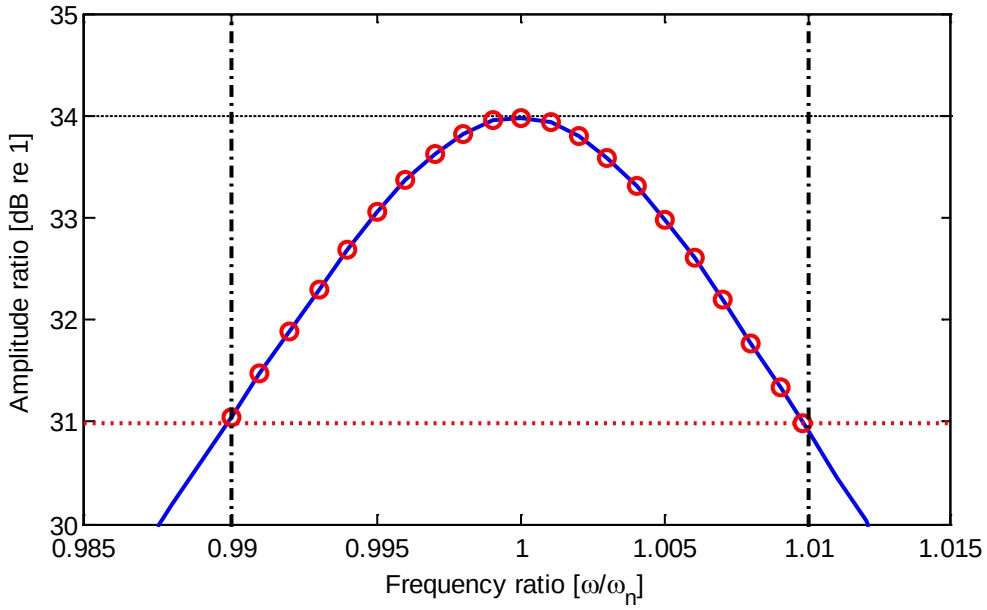

Figure 5.3 Transmissibility function for a lightly linearly damped base excited vibration isolation model with $\zeta_1 = 0.01$.
(a) A frequency range of 0.1- 100 times the natural frequency and
(b) around the resonance frequency.
- - - - - peak response level
····· half power level
– · – half power frequencies
——— transmissibility function
O spectral lines at intervals of 0.001 f_n

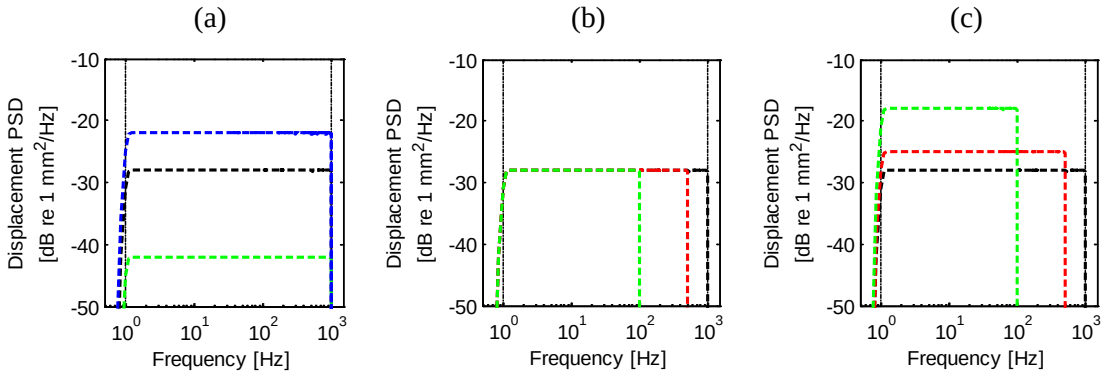

Displacement estimated PSD for the constant displacement random excitation (CDR)

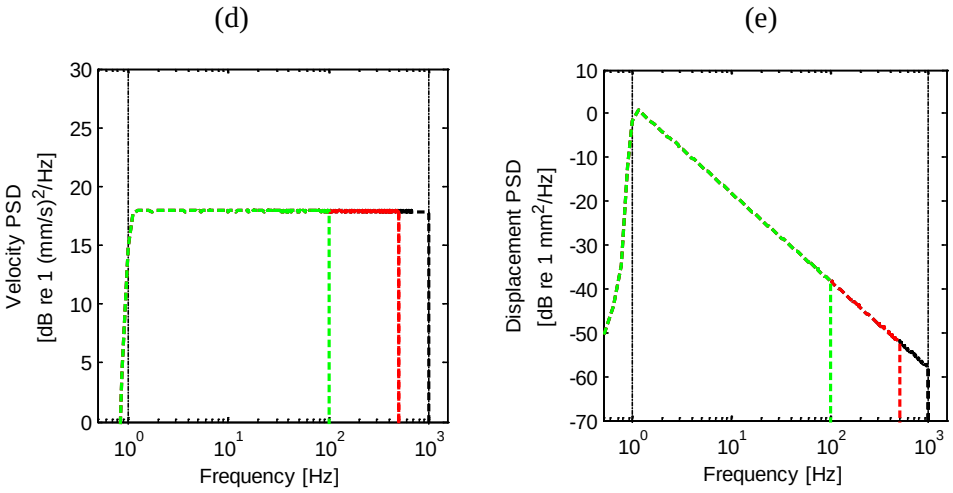

Constant velocity random excitation (CVR)

Figure 5.4 Estimate PSD for the applied broadband random excitation
(a) A CDR excitation with fixed bandwidth at 1-1000 Hz
(b) A CDR excitation with fixed displacement PSD level
(c) A CDR excitation with fixed displacement RMS at 1.25 mm
(d) A velocity PSD for the CVR excitation
(e) A corresponding displacement PSD for the CVR excitation
---- Excitation PSD level
–·–·– Excitation bandwidth of 1-1000 Hz

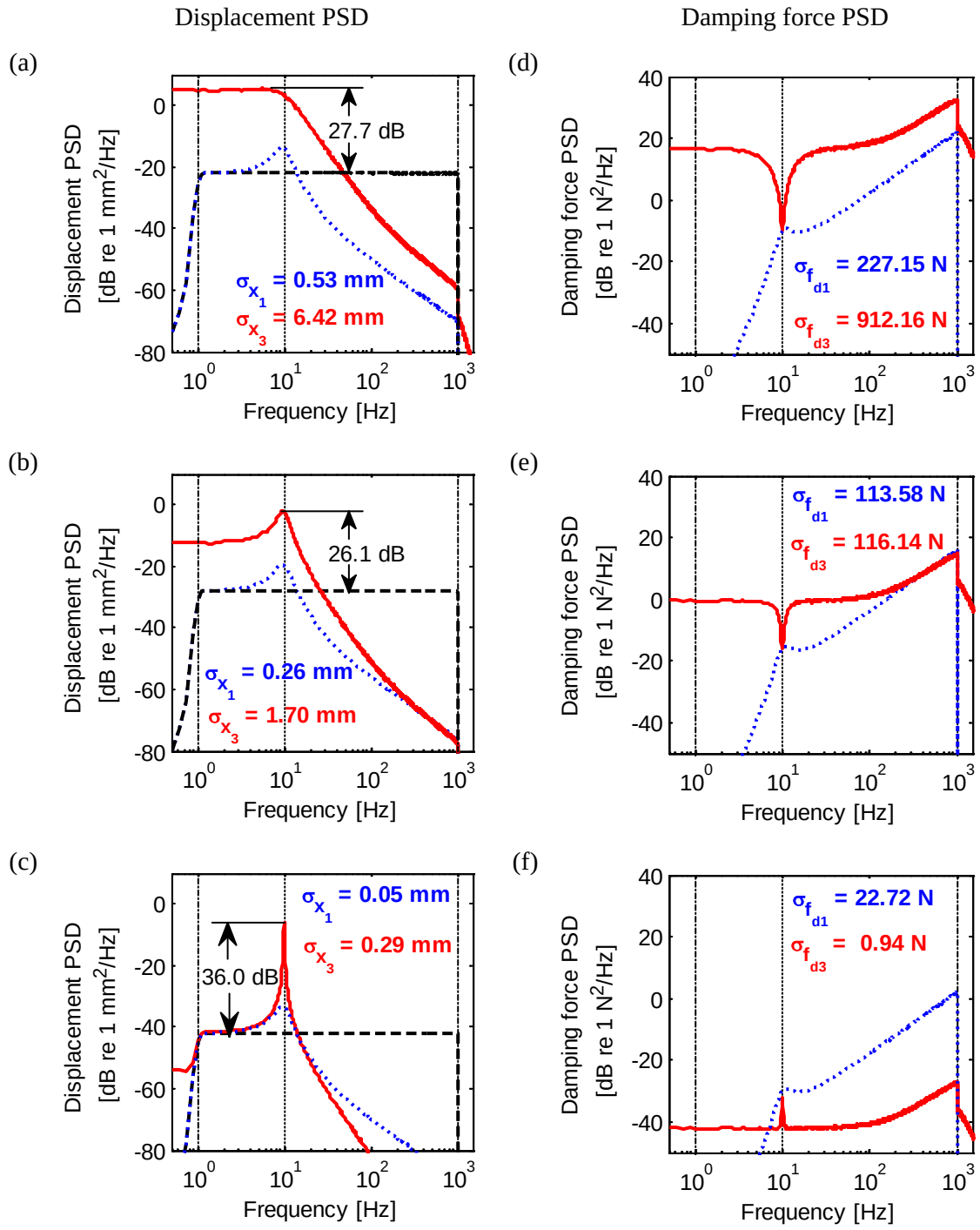

Figure 5.5 Responses for linear viscous damping and cubic damping subject to different excitation levels of a constant displacement amplitude random excitation with bandwidth of 1-1000 Hz.
(a) and (d) response for displacement excitation RMS = 2.5 mm
(b) and (e) response for displacement excitation RMS = 1.25 mm
(c) and (f) response for displacement excitation RMS = 0.25 mm
Linearly damped response
Cubically damped response
Displacement excitation
Excitation bandwidth of 1-1000 Hz

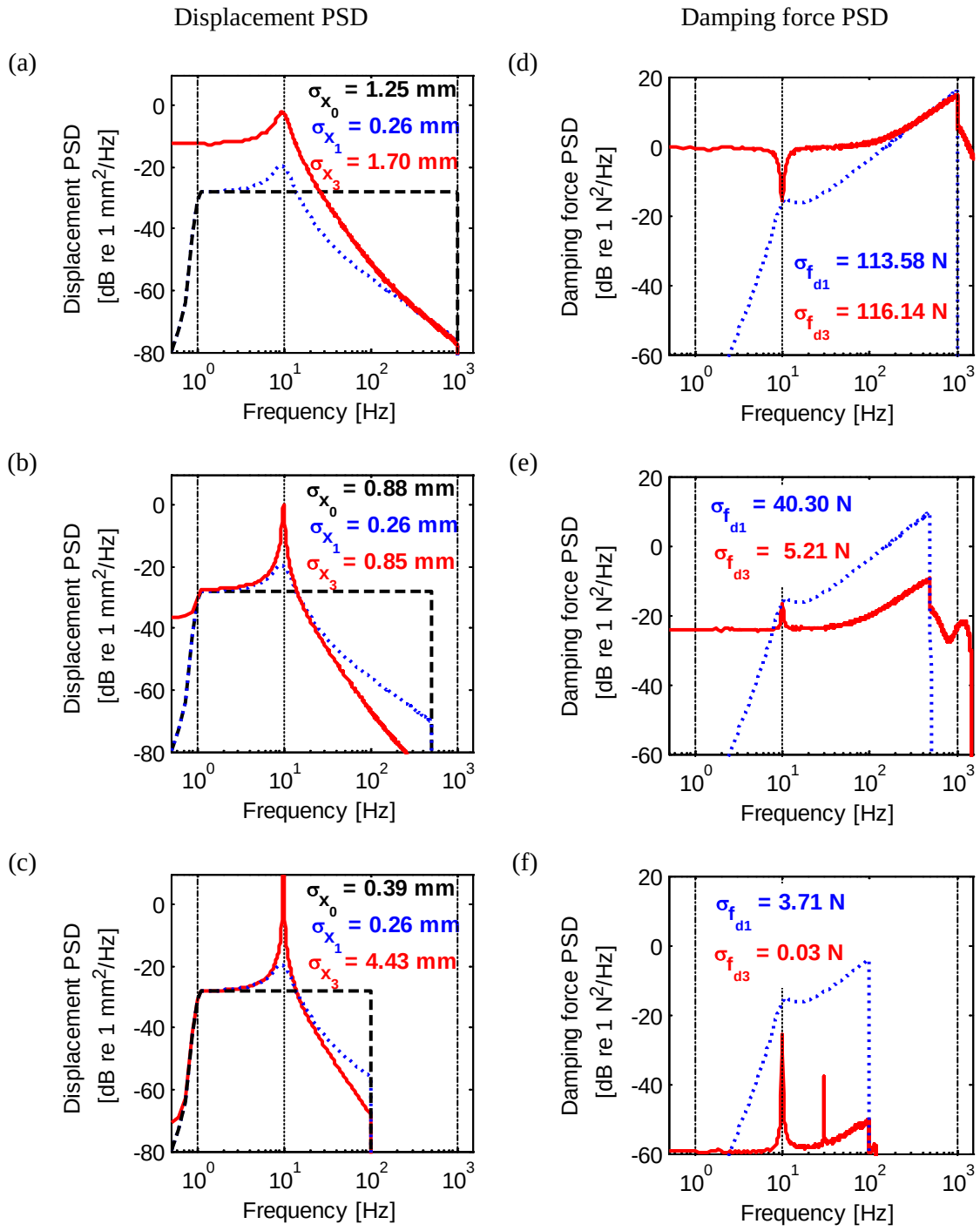

Figure 5.6 Responses for linear viscous damping and cubic damping subject to different excitation bandwidth of a constant displacement amplitude random excitation with fixed excitation levels.
(a) and (d) response for excitation bandwidth = 1-1000 Hz
(b) and (e) response for excitation bandwidth = 1-500 Hz
(c) and (f) response for excitation bandwidth = 1-100 Hz
Linearly damped response
Cubically damped response
Displacement excitation
Excitation bandwidth of 1-1000 Hz

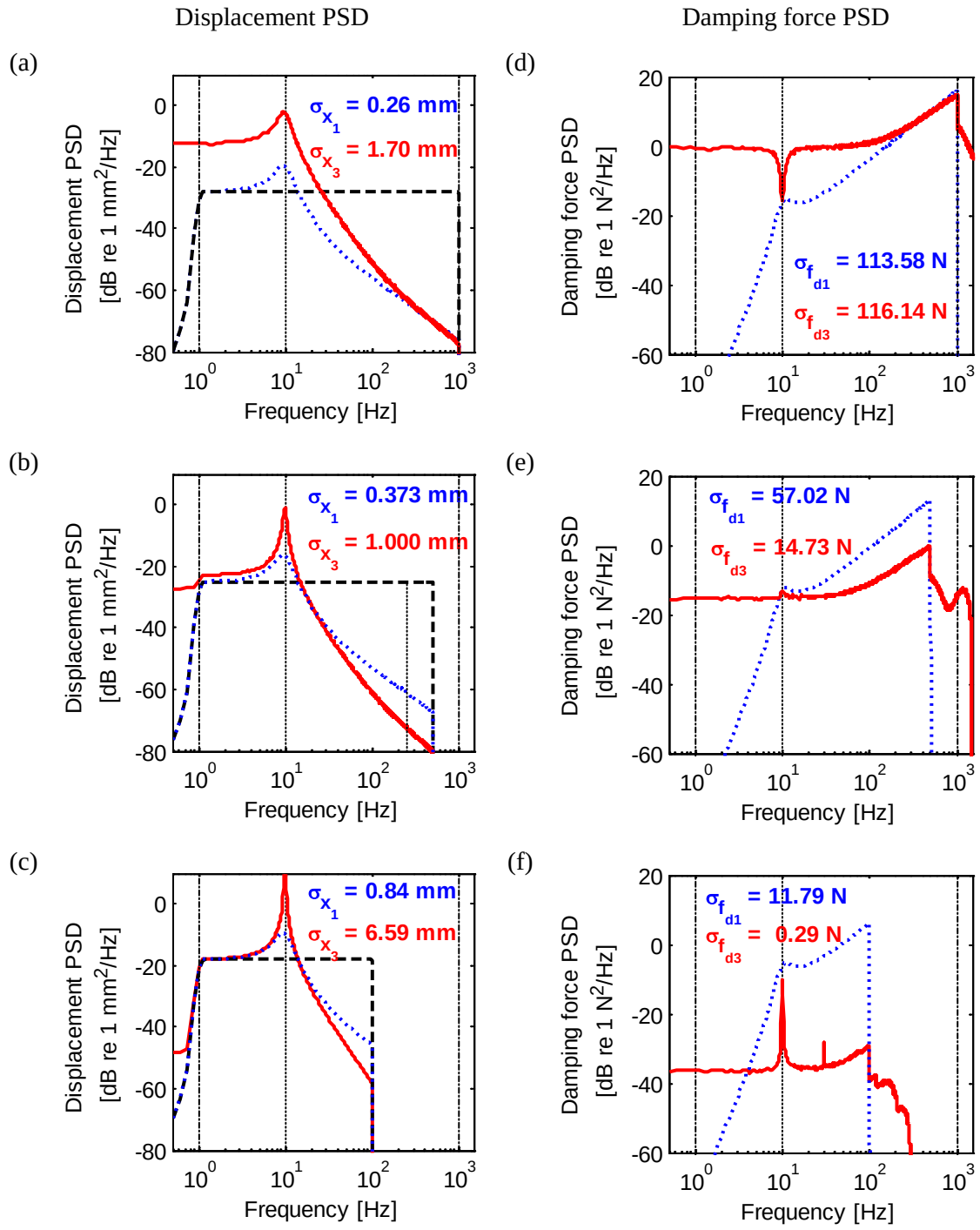

Figure 5.7 Responses for linear viscous damping and cubic damping subject to different excitation bandwidth of a constant displacement amplitude random excitation with fixed displacement excitation RMS of 1.25 mm.
(a) and (d) response for excitation bandwidth = 1-1000 Hz
(b) and (e) response for excitation bandwidth = 1-500 Hz
(c) and (f) response for excitation bandwidth = 1-100 Hz
Linearly damped response
Cubically damped response
Displacement excitation
Excitation bandwidth of 1-1000 Hz

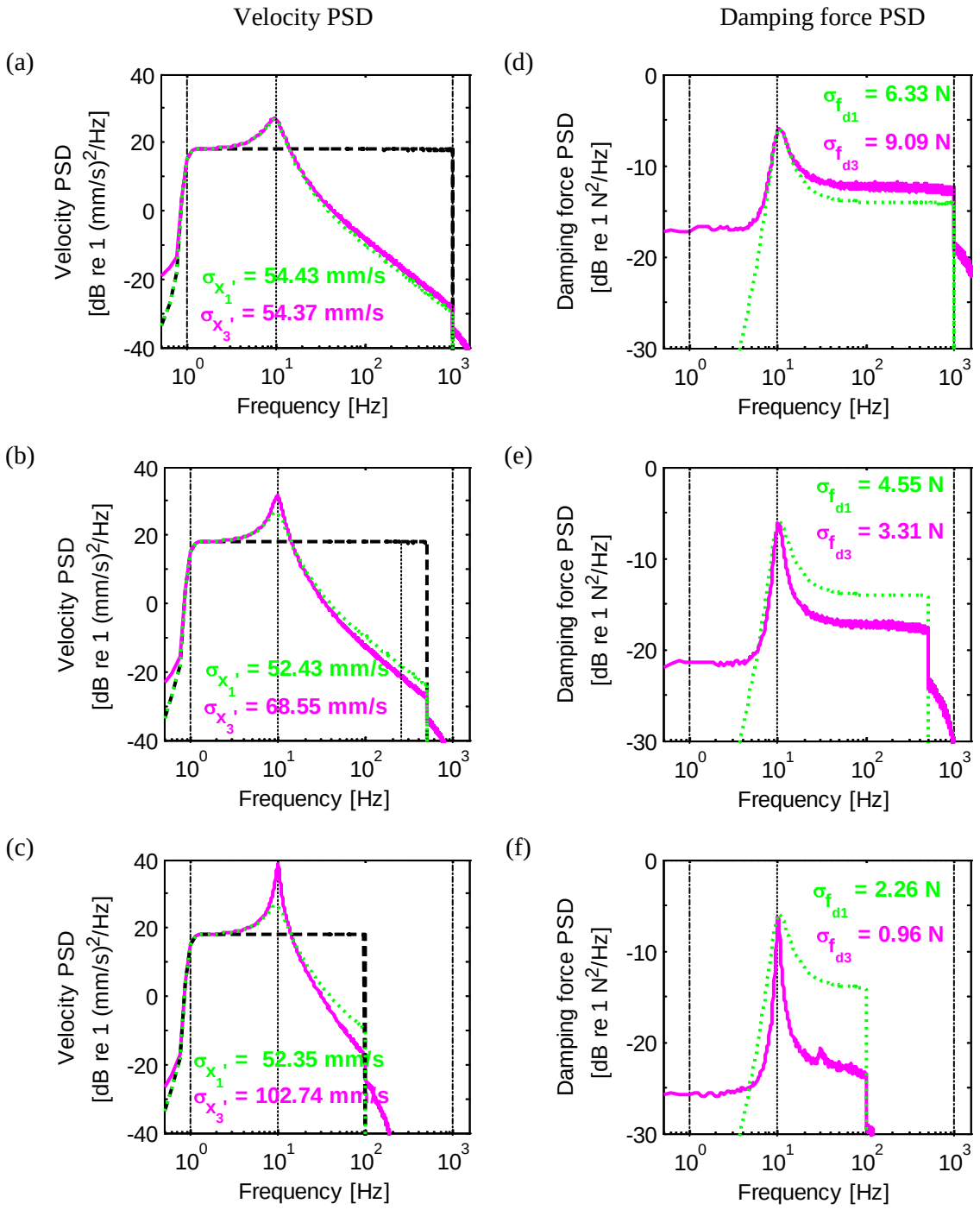

Figure 5.8 Responses for linear viscous damping and cubic damping subject to different excitation bandwidth of a constant velocity amplitude random excitation with fixed displacement excitation RMS of about 1.25 mm and fixed velocity PSD.
(a) and (d) response for excitation bandwidth = 1-1000 Hz
(b) and (e) response for excitation bandwidth = 1-500 Hz
(c) and (f) response for excitation bandwidth = 1-100 Hz
Linearly damped response
Cubically damped response
Displacement excitation
Excitation bandwidth of 1-1000 Hz

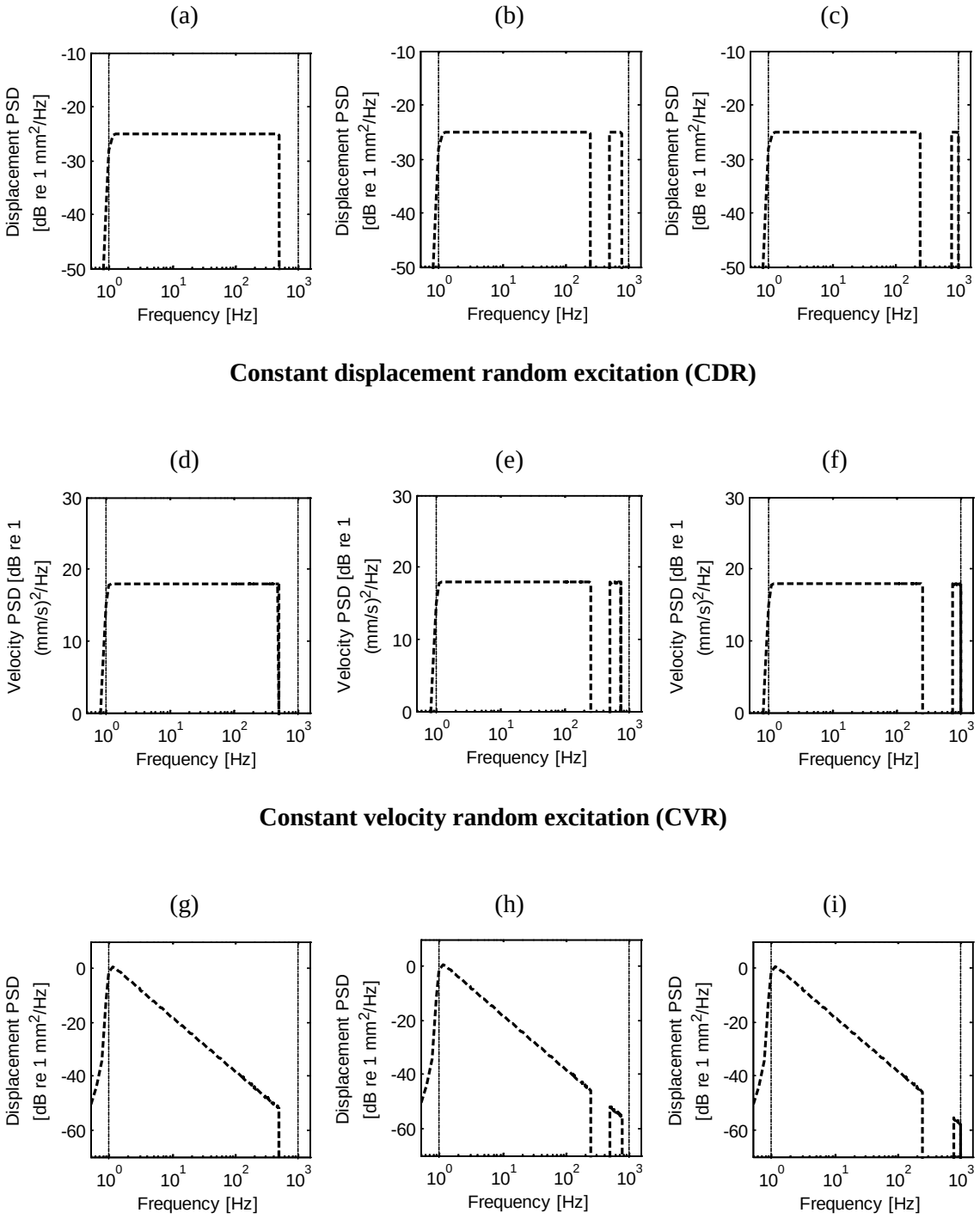

Figure 5.9 Estimate PSD for the two pass-band excitations.
Bandwidths for the constant displacement amplitude excitation are (a) 1-500 Hz, (b) 1-250 Hz plus 500-750 Hz and (c) 1-250 Hz plus 750-1000 Hz. The similar bandwidths are also applied to the constant velocity amplitude excitation which are presented using velocity PSD in figure (d) to (f) respectively. Figures (g) to (i) respectively present the corresponding displacement PSD for the CVR excitations.

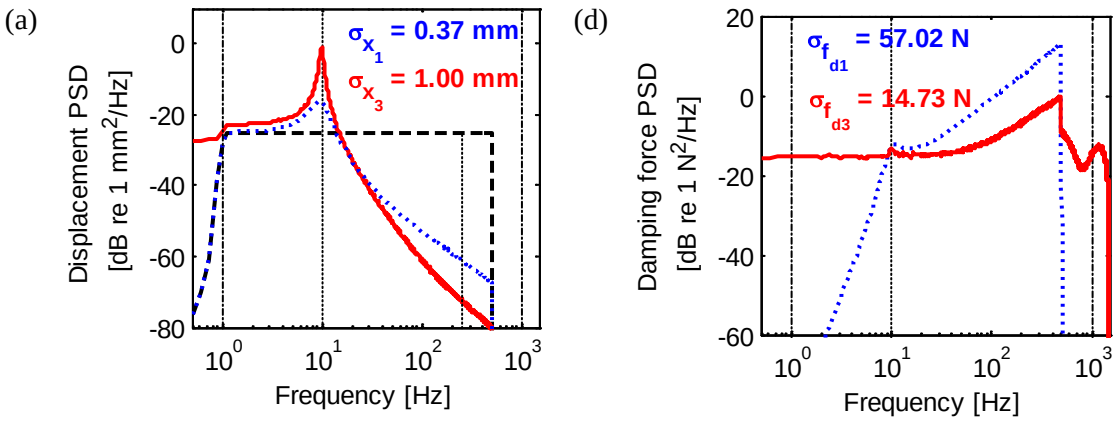

Bandwidth 1-250 Hz and 250-500 Hz

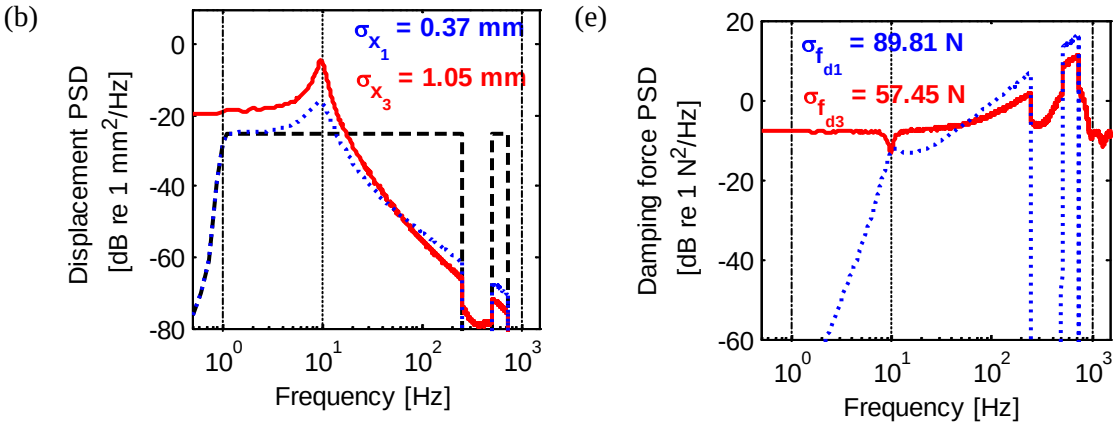

Bandwidth 1-250 Hz and 500-750 Hz

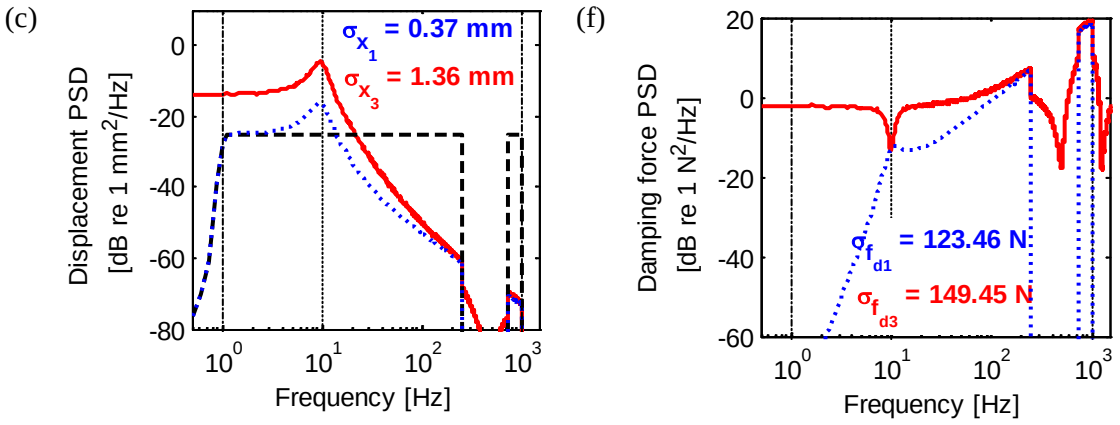

Bandwidth 1-250 Hz and 750-1000 Hz

Figure 5.10 Responses for linear viscous damping and cubic damping subject to two pass-band random excitation having constant displacement amplitude.
- Linearly damped response
- Cubically damped response
- Displacement excitation
- Excitation bandwidth of 1-1000 Hz

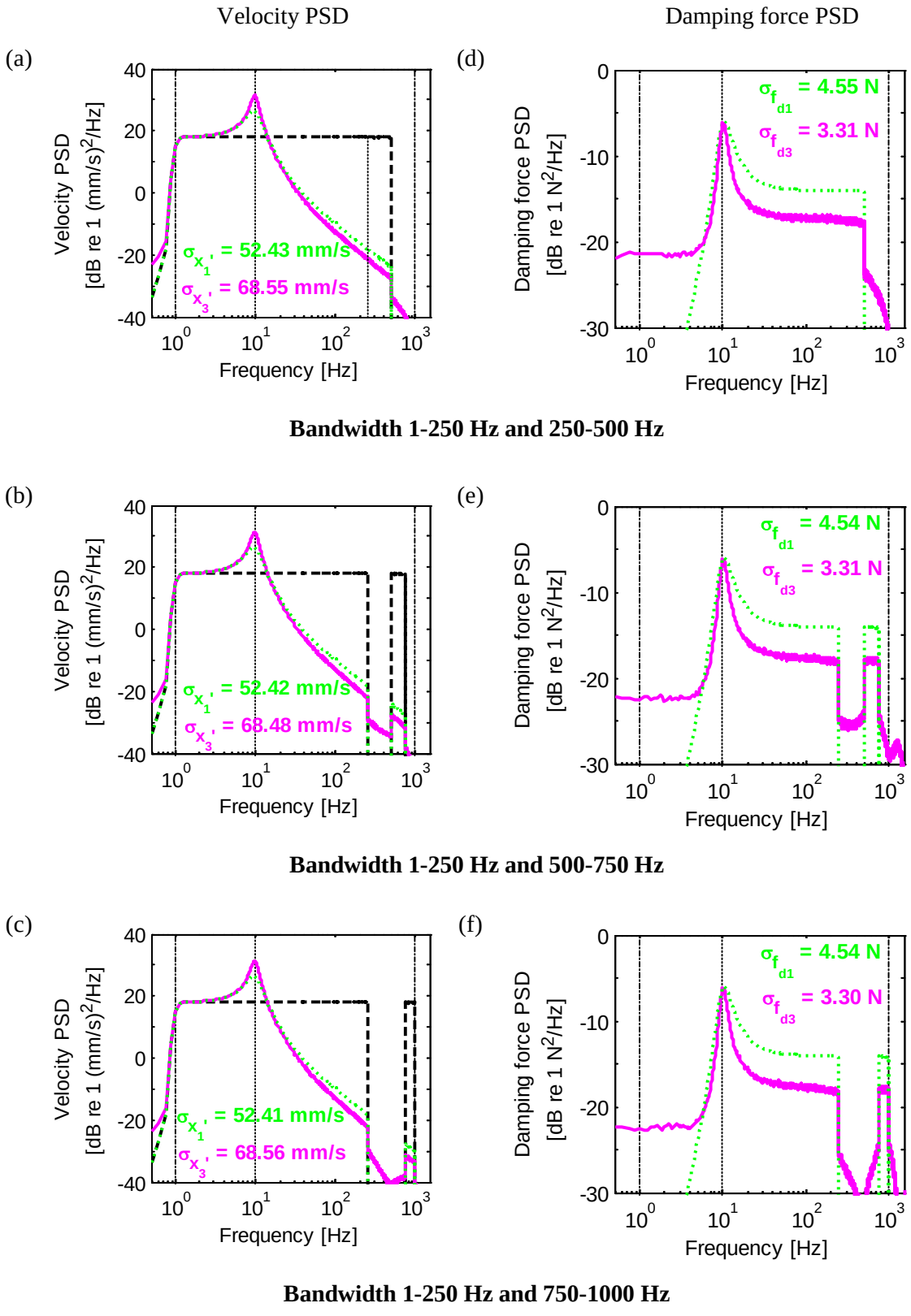

Figure 5.11 Responses for linear viscous damping and cubic damping subject to two pass-band random excitation having a constant velocity amplitude.

- Linearly damped response
- Cubically damped response
- Displacement excitation
- Excitation bandwidth of 1-1000 Hz

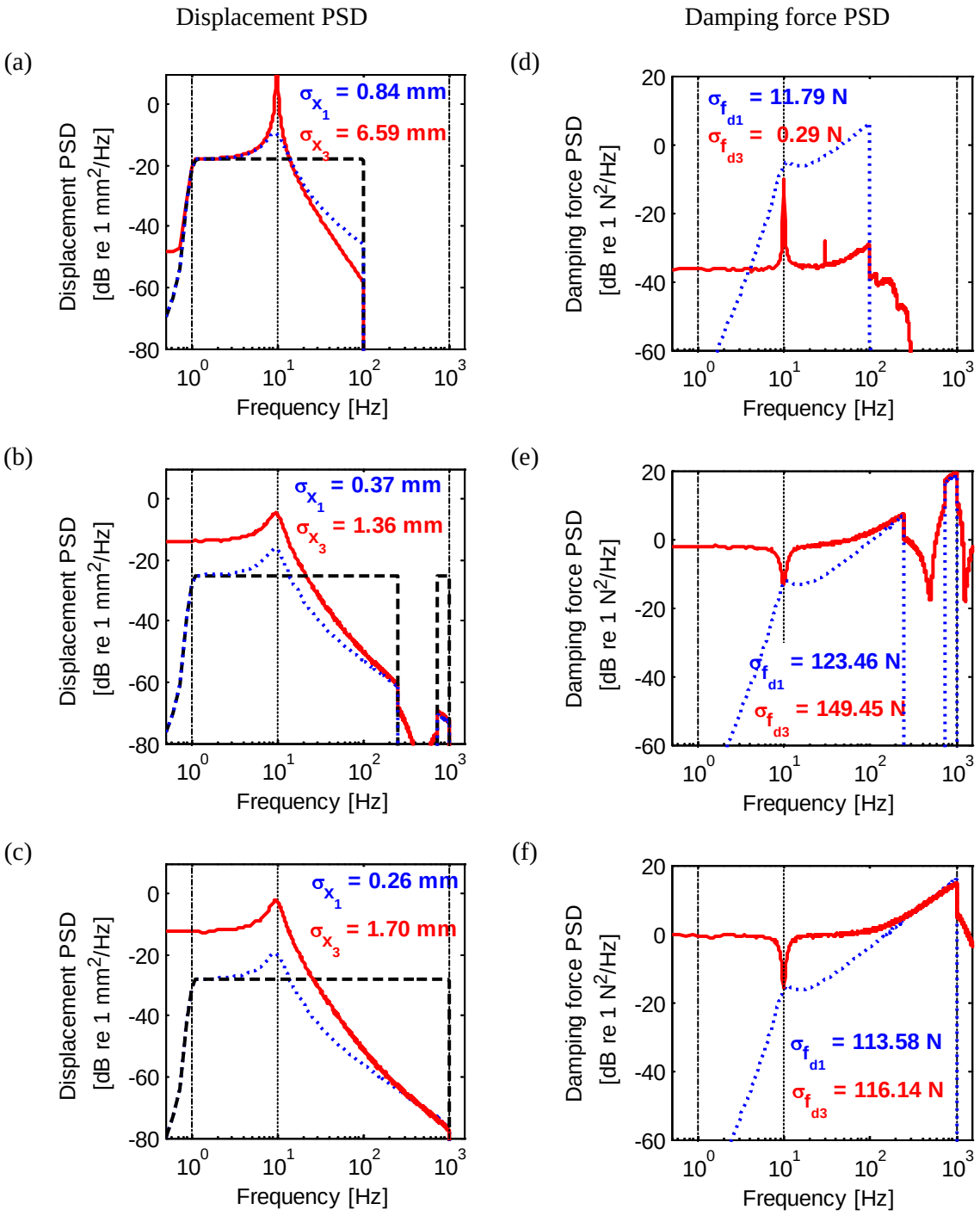

Figure 5.12 Estimate displacement PSD and damping force PSD for the constant displacement amplitude random excitation having the RMS value equals 1.25 mm
(a) and (d) excitation bandwidth of 1-100 Hz
(b) and (e) excitation bandwidth of 1-250 Hz plus 750-1000 Hz
(c) and (f) excitation bandwidth of 1-1000 Hz
Linearly damped response
Cubically damped response
Displacement excitation
Excitation bandwidth of 1-1000 Hz

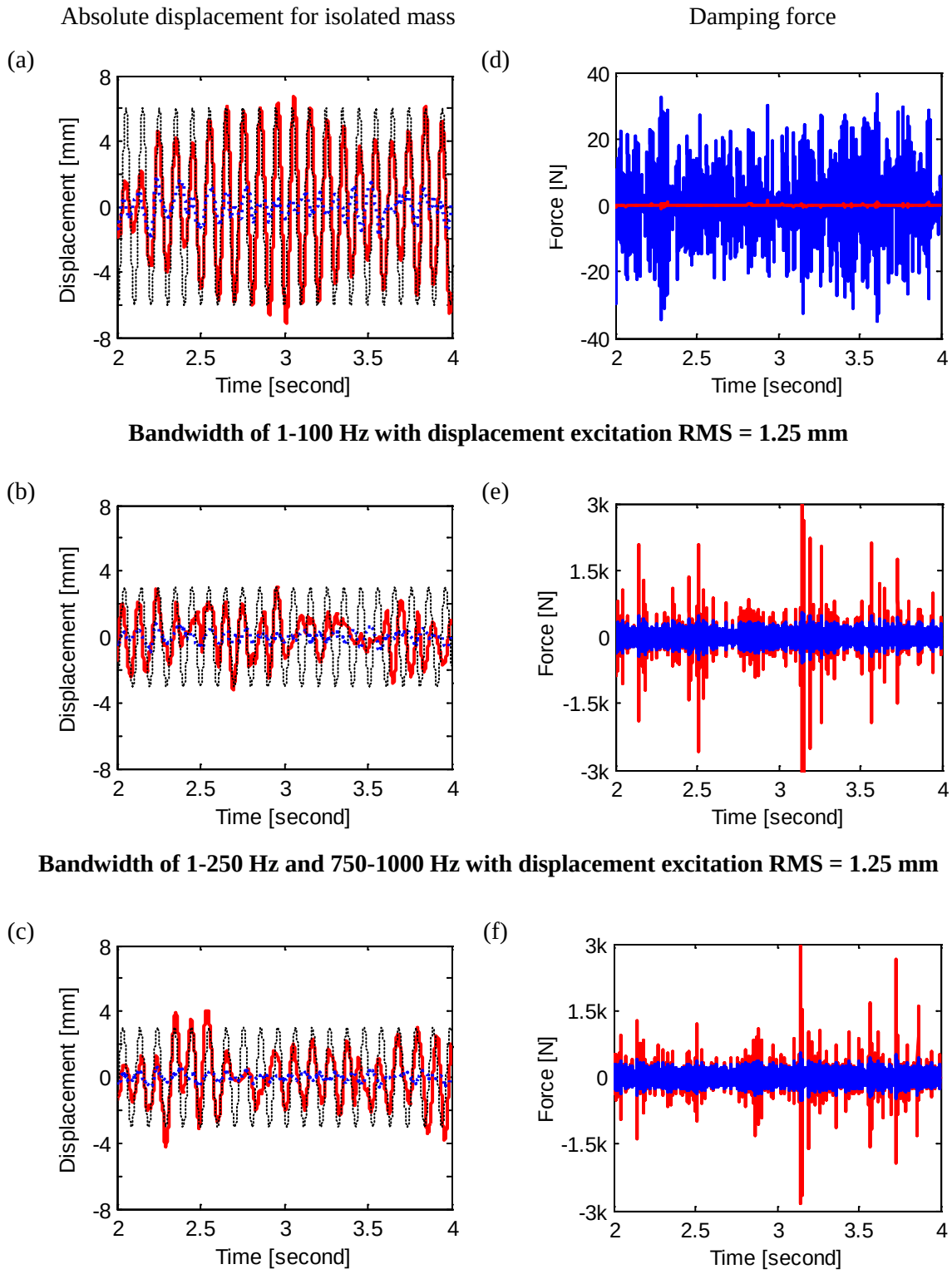

Figure 5.13 Time histories of the broadband responses due to constant displacement amplitude random excitations (CDR).
..... Linearly damped response
——— Cubically damped response
- - - - - Sinusoidal at 10 Hz (resonance frequency)

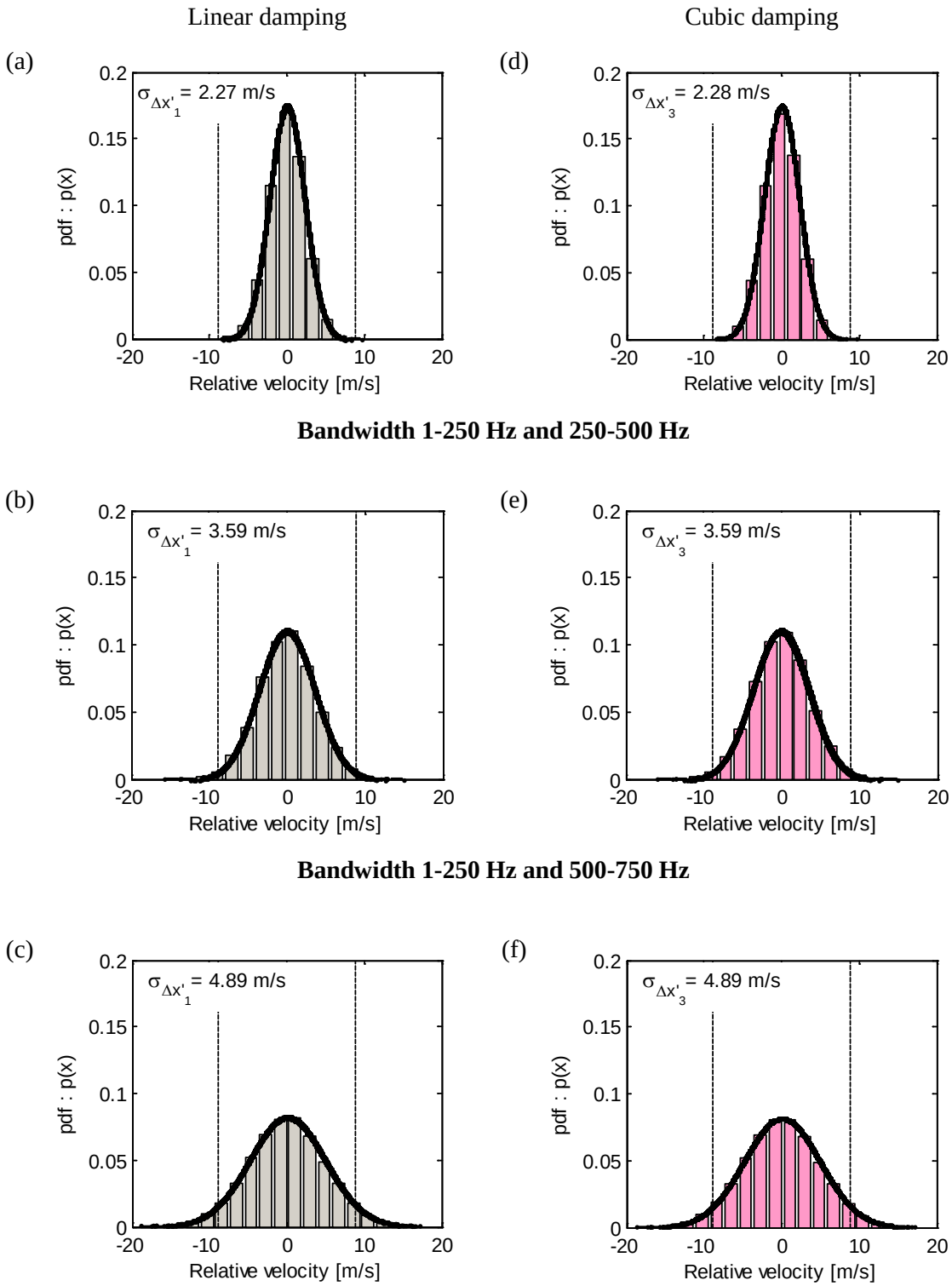

Figure 5.14 Probability density function of the relative velocity for the responses subject to two pass-band random excitations having constant displacement amplitude with the RMS displacement excitation of around 1.25 mm.
—— Gaussian distribution
The vertical dashed lines represent the relative velocity where linear and cubic damping forces are equal, i.e. $\Delta\dot{x}$ = 8.785 m/s for the case of CDR excitation.

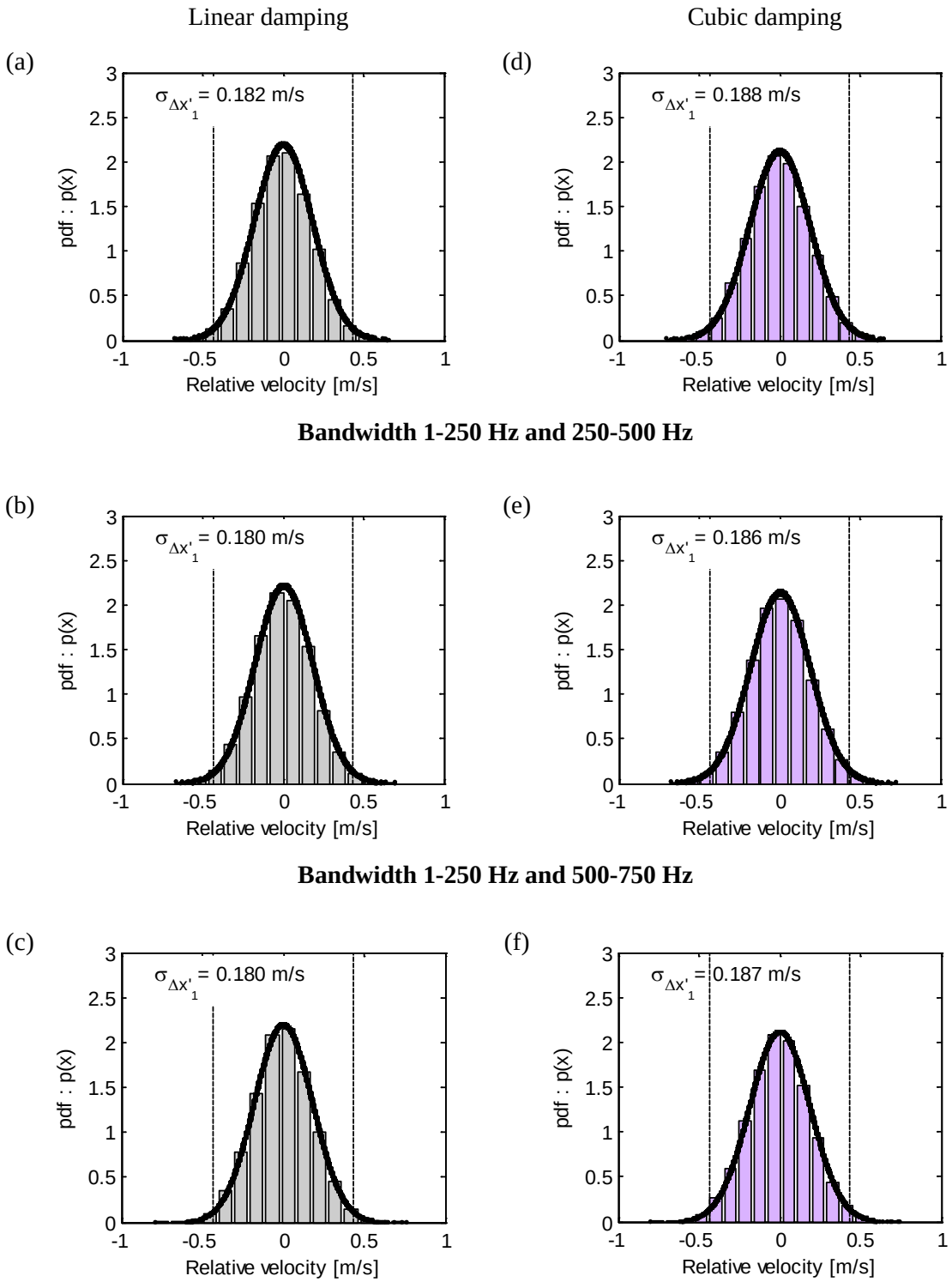

Figure 5.15 Probability density function of the relative velocity for the responses subject to two pass-band random excitations having constant velocity amplitude with the RMS displacement excitation of around 1.25 mm.
—— Gaussian distribution
The vertical dashed lines represent the relative velocity where the linear and cubic damping forces are equal, i.e. $\Delta\dot{x}$ = 0.435 m/s for the case of CVR excitation.

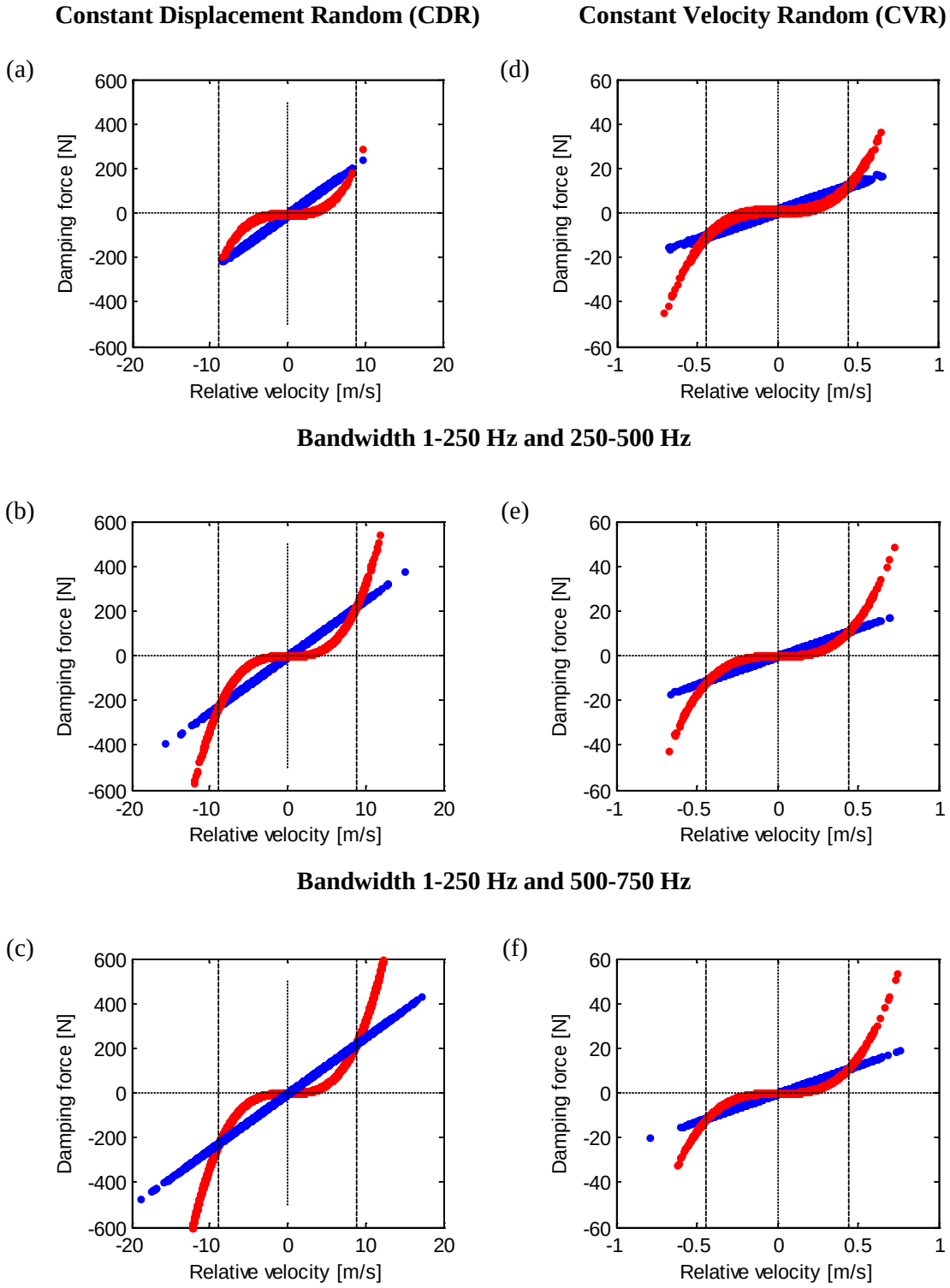

Figure 5.16 Force-velocity characteristic for the linear and cubic damping system subject to two pass-band excitation frequency for both CDR and CVR excitations.

- Linear damping force
- Cubic damping force

Vertical dashed lines represent the relative velocity which the amplitudes of linear and cubic damping forces are equal, i.e. $\Delta\dot{x}$ = 8.785 m/s for the case of CDR excitation and $\Delta\dot{x}$ = 0.435 m/s for the case of CVR excitation.

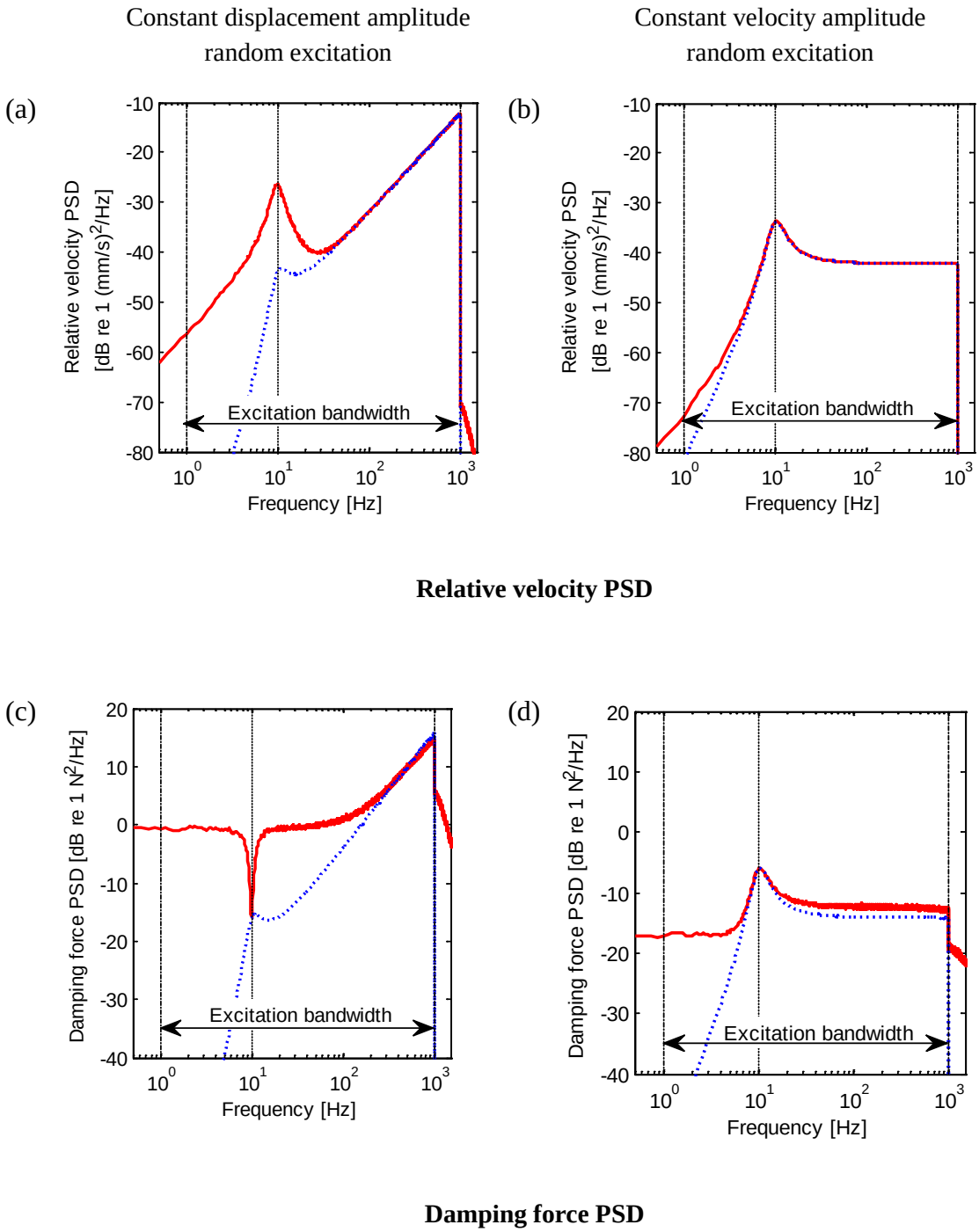

Figure 5.17 Plots of the PSD of the relative velocity and damping force in comparison for the response subject to a constant displacement amplitude and constant velocity amplitude random excitation.
(a) and (b) Estimate PSDs for the relative velocity
(c) and (d) Estimate PSDs for the damping force
..... Linearly damped response
——— Cubically damped response
–·–·– Excitation bandwidth
- - - - - Excitation frequency at around resonance

Chapter 6 Experimental validation and analysis

6.1 Introduction

From the preceding chapters, the degree to which cubic damping influences the level of effective damping of the system was found to be dependent upon both the amplitude and bandwidth of the excitation. It proved to be detrimental for a constant displacement amplitude harmonic base excitation where an increased response occurred in the isolation region. It is also detrimental for broadband excitation for which high response was witnessed at low frequencies even outside the excitation bandwidth. These cubic damping effects are examined experimentally here.

The experimental study was implemented using an electrodynamic shaker. The rig was designed to exhibit a SDOF response characteristic under base excitation. Cubic damping was implemented using active damping with a simple velocity feedback. Two base excitation characteristics namely harmonic and broadband excitation were employed. The focus of this chapter is to examine and report the effects of cubic damping in comparison to the theoretical results. The responses for system with cubic damping are also examined in comparison to that with linear damping.

The experimental results obtained confirm the detrimental effects of cubic damping on a base excited SDOF isolation system. They are consistent with those reported theoretically. The physical reasons for the detrimental effect due to the presence of cubic damping for base isolation are also reported. These results show significant contribution of cubic damping to the detrimental effects.

6.2 Design and considerations of experimental rig

The key design parameters were the natural frequency and mode of vibration of an experimental rig. The experimental rig should exhibit an obvious single resonance frequency as assumed theoretically. In addition, there should be sufficient frequency separation of the first resonance frequency and subsequent modes. According to the theoretical approximation for harmonic excitation, the detrimental effect for a particular

value of cubic damping can be seen at a frequency around ten times higher than the fundamental resonance frequency. So, higher modes should be at frequencies higher than this. For practical instrumentation reasons the natural frequency of the rig should not be too low due to the ability of the available exciters and instrumentation.

A vertical realisation was chosen, to possess only a vertical vibration mode. The occurrence of other possible modes, for example rotating or pitching modes, should be eliminated or minimised. The components used in the experiment should also be consistent with the theoretical assumptions, for example the assumptions of linear massless springs and massless damping. These basic requirements led to the design of the rig which is described in detail in the following section.

6.2.1 Rig design and set up

The design of the rig was based on an assumption of a SDOF simple mass, spring and damper system. The damping component in the isolation was implemented using an electrodynamic shaker which also formed part of the isolated mass. A drawing of the experimental rig is given in figure 6.1. An active damper was introduced using an LDS electrodynamic shaker (model V101). It has a mass of 0.91 kg with an axial suspension stiffness of 3.15 kN/m as informed in technical specification. The shaker was mounted on an aluminium plate of mass 0.5 kg and led to a total mass of 1.41 kg. The combined unit of shaker, aluminium plate and force transducers A and B formed the isolated mass which was supported by two helical springs.

Since the system mass was supported by two helical springs, an existence of a pitching mode of the rig rotating about its centre can be anticipated. To reduce the effect of any pitching mode, the pitching frequency was designed to be lower than the bounce mode frequency and this was achieved by reducing the distance between the two isolator springs. The rig natural frequency was initially chosen to be close to 10 Hz. A pitching frequency was initially set at 4 Hz. This yielded the distance between two helical springs to be 93 mm, symmetrically positioned about the centre of the plate. Later for manufacturing convenience, this distance was simplified to 80 mm as shown in figure 6.1 and resulted in a new calculated pitching frequency of about 3.45 Hz.

As the rig natural frequency of 10 Hz was chosen, a total value of the corresponding vertical stiffness should be 5.53 kN/m. Therefore the total stiffness of

two the helical springs should be equal to 2.42 kN/m or 1.21 kN/m each. It is assumed that the properties and geometry of these two helical springs were identical. However, the practical value of the total stiffness of the two helical springs was measured. The measured data are plotted as the load-deflection characteristic shown in figure 6.2 using circle markers. The method of linear regression was applied to the measured data and the total stiffness was found to be 1.94 kN/m. Thus the total vertical stiffness of the isolation was 5.09 kN/m. Hence the natural frequency of the bounce mode should presumably be 9.56 Hz.

After manufacturing and assembly, the actual isolated mass was found to be 1.50 kg approximately. Thus the undamped natural frequency of the system becomes 9.27 Hz. This also resulted in a static deflection of the two helical springs, with no stinger connection, of 7.6 mm. The static deflection was greater than the displacement limitation of the shaker, which is 2.5 mm. Therefore the springs are always in compression. The stinger was then inserted to connect the shaker and the base at this static equilibrium position. Thus the shaker does not have to take the static load.

Figure 6.3 shows a schematic physical model. The schematic illustrates that the isolated mass is physically supported by the two helical springs and the passive suspension of the shaker. The damping force was obtained from the electromagnetic force, F_d, which was acting between the permanent magnetic (shaker body) and the armature. The armature was considered very light compared to the isolated mass and was connected to the force transducer C by a stinger. This connection was assumed infinitely stiff in the vertical direction compared to the axial suspension stiffness. Thus one might anticipate the damping force F_d transmitted to the force transducer C is not affected by the armature mass.

6.2.2 Experimental rig characterisation

The experimental rig, with no active damping implementation, was initially tested under white noise random base excitation. The excitation signal was generated using the B&K Noise Generator type 1405 with a 20 kHz frequency bandwidth. Both excitation and response signals were acquired and processed using a DataPhysics Dynamic Signal Analyser. The upper frequency of the analyser was set to 400 Hz with a sampling frequency of 1024 Hz automatically chosen by the analyser (2.56 times of the

upper frequency). A frequency resolution was set to 0.25 Hz, corresponding to a record length of 4 s. A Hanning window was applied to the acquired signals with 75% overlap and 300 averages for the spectral estimates.

The acceleration responses of both the base and the isolated mass were captured using the B&K charge type piezoelectric accelerometers model 4375 and B&K Charge Amplifiers Type 2635. A transmissibility function for the system is shown in figure 6.4. It appears to resemble fairly well a SDOF system over a frequency range of 7–100 Hz, shown by the dashed lines in figure 6.4 (a), with an obvious resonance peak around 11 Hz. Figure 6.4 (b) shows the comparison of the phase between the base excitation and the isolated mass. The theoretical prediction fits fairly well in the frequency region below and around the resonance frequency. The prediction tends to $-\pi/2$ radians at higher frequencies whereas that for experimental data is constant at around $-\pi$ radians. This may be a result of hysteretic damping of the passive system. The coherence function shown in figure 6.4 (c) also appears reasonably acceptable for this frequency range.

Other resonances appear at frequencies approximately equal to 211, 222, 300 and 340 Hz. The first two frequencies were identifiable as the internal resonances of the isolator springs, the detail of which is given in section 6.2.4. The latter two frequencies could be the higher modes of the rig. Hence a suitable frequency range for investigating the effect of cubic damping on this rig was about 7–100 Hz.

The bounce mode natural frequency and damping ratio were estimated from the measured transfer functions. These parameters were calculated and compared using two different tools, i.e. a circle fit method [74] and a MATLAB function ‘invfreqs’ [75,76]. In order to do the modal fit, the measured motion transmissibility was rearranged to form the receptance of the system when it is clamped to the base, i.e.

$$H(\omega)=\frac{1}{\omega^2}\left[\frac{X(\omega)}{X_0(\omega)}-1\right] \tag{6.1}$$

where ω is an excitation frequency, $X(\omega)$ and $X_0(\omega)$ are the measured displacement amplitude of the isolated mass and the base excitation respectively. Equation (6.1) has the form of the receptance scaled by the system mass.

Details of the circle fit method and the MATLAB function ‘invfreqs’ are described in Appendix D. The estimated results from these two techniques appeared similar and consistent. A natural frequency of 11 Hz and the corresponding passive linear viscous damping ratio of 0.04 were obtained. A plot shown by a dashed line in figure 6.4 (a) reveals that the estimated linear lightly damped SDOF system fits the experimental data reasonably well.

6.2.3 Implementation of active damping

The active damping was implemented using an electrodynamic shaker with a simple velocity feedback. Note that, the active damper in this study was only implemented to represent a linear or nonlinear damping characteristic. The implemented active damper was not intended to act as a control strategy.

The vertical damping force was produced as a result of the feedback signal to the shaker and the desired level was achieved by adjusting the shaker amplifier gain. The role of the variable gain of the shaker amplifier is to adjust the damping coefficient. It is a factor multiplying the amplitude of a processed signal (relative velocity or relative velocity cubed). The processed signal was obtained by processing the acquired velocity of the base and isolated mass with the control schematic shown in figure 6.5.

The velocity was obtained by integrating the measured acceleration using the charge amplifiers where the low cut-off frequency was set at 1 Hz. The data processing unit produced the relative velocity determined from the difference in the velocities. Any arbitrary damping configuration, for this instance, the linear and cubic damping configurations can be reproduced. The processed signal was fed to the shaker amplifier to produce the desired damping force level by the shaker.

6.2.4 Internal resonance of helical spring

Theoretically, the isolator was assumed to comprise a massless spring. Also, the geometry of the spring was not considered. However, practically the mass of the spring cannot be neglected and the geometry of the spring is important. One possible behaviour of the actual helical spring is the internal resonance of the spring itself which is dependent on its physical mass and geometry. The h^{th} internal axial resonance frequency

of a spring, placed between two flat and parallel surfaces, can be determined from [77,78]

$$f_h = \frac{h}{2}\sqrt{\frac{k_{hs}}{m_{hs}}} \qquad h = 1, 2, \ldots \tag{6.2}$$

where k_{hs} and m_{hs} are the stiffness and the mass of the helical spring respectively. The stiffness and the mass of the spring can be determined from its geometrical and material properties which are respectively given by

$$k_{hs} = \frac{Gd^4}{8D^3 N_a} \tag{6.3}$$

$$m_{hs} = \frac{\pi^2 \rho N_t D d^2}{4} \tag{6.4}$$

where G is the shear modulus, d is the wire diameter, D is the outer diameter of the spring, N_a and N_t are the number of active and total coils respectively. ρ is the density of the spring material. The predicted internal resonance frequency for the helical springs used was about 206 Hz. Therefore the appearance of two resonance peaks around 211 and 222 Hz were identifiable as a result of internal resonances of the springs, assuming a slight variation between them.

6.2.5 Spectral analysis of the experimental results

The experimental results for the two excitations under study, i.e. harmonic and broadband excitation, are analysed by means of spectral analysis. For the case of harmonic responses, the Fourier coefficients at the fundamental frequencies were determined from the time histories of both the base excitation and the isolated mass response. Then these quantities were employed to construct the amplitude ratio. The methodology to obtain the Fourier coefficients was given in section 2.4.3.

For the case of broadband excitation, the amplitude spectrum and hence the power spectral density (PSD) were obtained from the analyser. Then the estimated transfer function can be obtained. In this study, the experimental data was acquired only

in the form of auto-PSDs then the estimated transfer function H_0 was applied which is given by

$$\left|H_0\right|^2 = \frac{S_{yy}}{S_{xx}} \tag{6.5}$$

where S_{yy} and S_{xx} are the averaged auto-PSDs for the response and excitation respectively. In addition, the estimated transfer function H_1 and H_2 are not considered here. This is because they are suitable to estimate a transfer function for the system which the output and input are linearly related. This is because the estimator H_1 disregards the effects of nonlinearity present in the output. Similarly, the estimator H_2 disregards the input which is not linearly related to the output.

6.3 Harmonic excitation

The experiment covered the frequency range of 7-100 Hz. A sampling frequency of 1024 Hz was chosen to avoid aliasing from higher odd harmonics in the response due to the non-linearity.

6.3.1 Choice of amplitude for harmonic base excitation

The level of excitation amplitude was chosen considering the relative displacement between the isolated mass and the base for which was limited to 1.25 mm peak due to the 2.5 mm stroke of the shaker.

The amplitude of the relative displacement between the isolated mass and the base input can be calculated from

$$Z = \sqrt{X^2 - 2XX_0\cos(\phi) + X_0^2} \tag{6.6}$$

where Z is the amplitude of the relative displacement, X and X_0 are the displacement amplitude of the isolated mass and base excitation respectively. ϕ is the phase lag between the isolated mass and the base which was assumed to be 90° for the response around the resonance frequency. Therefore equation (6.6) is simplified to

$$Z^2 = X^2 + X_0^2 \tag{6.7}$$

The amplitude of base excitation was initially considered using the response of the passive system as shown in figure 6.4 (a). The peak amplitude of the transmissibility is about 20 dB ($X = 10X_0$). The peak amplitude of 20 dB was assumed as the worst case scenario for the passive system (without active damping configuration). The peak amplitude was lower when the active damping was applied. The relative displacement, Z = 0.625 mm ,was also chosen initially to determine the excitation amplitude. Hence an amplitude of the base excitation, X_0 = 0.062 mm, was obtained from equation (6.7).

For simplicity, the desired levels of the constant displacement excitation were assigned to be 0.060 mm and 0.040 mm for high and low excitation amplitude. The relative displacements around the resonance frequency for these excitation levels were expected to be about 0.603 mm and 0.402 mm respectively. In order to achieve these excitation levels, the amplifier gain for base excitation was manually adjusted until the desired excitation level was obtained. Also to minimise the effect of transient response, the system was allowed to be excited around 60 seconds before the start of signal acquiring process.

In addition, the relative displacement for the system was expected to be lower when the active damping was applied. However, the input displacement with constant amplitude of 0.060 mm could not be achieved for the excitation frequencies above 80 Hz. This was limited by the shaker capability. So the maximum excitation frequency for the harmonic base excitation with amplitude of 0.060 mm was set to 80 Hz.

The other scenario considered for harmonic excitation was to apply a constant velocity amplitude excitation. The amplitude of excitation velocity at 11 Hz (the resonance frequency) corresponding to the displacement excitation of 0.060 mm was considered. It was about 4.147 mm/s or 4 mm/s for simplicity. This excitation amplitude was assigned to be the low excitation amplitude. The high excitation amplitude was set to have velocity amplitude of 6 mm/s.

The experimental responses for harmonic excitation were carried out with linear and cubic damping implementations. There were two scenarios applied for either damping case. The first scenario was to excite the system with different excitation levels

for a fixed feedback gain. The second scenario was to fix the excitation amplitude whilst different levels of damping were applied.

6.3.2 Implementation of linear damping

The experiment on the linear damping configuration was carried out to ensure consistency of the experimental and theoretical results. It could also show reliability of the experimental rig. For the first scenario, the excitation amplitude of 0.04 mm was initially applied. The level of feedback gain was adjusted to result in a peak amplitude ratio of about 10 dB and was kept at this position. Then the excitation amplitudes of 0.06 mm, 4 mm/s and 6 mm/s were applied sequentially for which the results are shown using an amplitude response in figure 6.6.

Theoretically, the amplitude ratio for a particular linear system should be identical and independent of the excitation characteristics. Consistently, figure 6.7 shows that the corresponding amplitude ratios for the four excitations are in excellent agreement with the theoretical linear transmissibility (solid lines). Note that, the theoretical plot was calculated using the estimated value of the damping ratio, $\zeta_1 = 0.17$, and natural frequency, 11 Hz. These values were also obtained by applying either the circle fit method or Matlab function ‘invfreq’ to the measured data when active damping with linear damping configuration was applied.

The second experiment for linear damping implementation was carried out by exciting the system only with the displacement excitation amplitude of 0.04 mm. The level of feedback gain was adjusted to result in an amplification peak amplitude of 15 dB and 10 dB respectively. The resulting amplitude ratios in figure 6.8 are consistent with the theoretical transmissibility for a linear system. These results reveal that the different levels of damping did not affect the linearity of the experimental rig.

Note that, the experimental responses for the linear damping configuration shown in figures 6.6 to 6.8 show amplitude variation at the excitation frequency around 20 Hz. These occurrences were identified to be a result of system asymmetry. An investigation showed that the translation of the isolated mass was not perfectly vertical. Such behaviour occurred between the excitation frequencies of around 14 to 24 Hz. It was possible to minimise this behaviour by adding the counter mass or by adjusting the

location of an accelerometer. However, this behaviour was found not to affect the response at high frequencies as shown in the figures.

To this end, for the linear damping configuration, changing either the level of the input excitation or value of damping did not cause any significant difference between the experimental and theoretical results. There was no nonlinear characteristic within the frequency range of interest when the linear damping configuration was assigned. Therefore, the experimental rig had an acceptable performance to continue the experiment on cubic damping implementation with some confidence.

6.4 The cubic damping implementation for harmonic excitation

The theoretical approximations for harmonic excitation in Chapter 3 showed that the value of non-dimensional cubic damping term is dependent upon the excitation amplitude squared. Higher excitation amplitude results in a greater value for the non-dimensional cubic damping. The higher cubic damping causes the response amplitude in the isolation region to rise up towards the excitation amplitude at lower frequencies. In contrast, theoretically, the presence of cubic damping proved more beneficial when the input is a constant velocity amplitude. Thus there were three main issues to be validated regarding the effects of cubic damping for harmonic excitation:

i) the excitation amplitude dependence property of cubic damping,

ii) the occurrence of a high response level in the isolation region for constant displacement amplitude excitation and

iii) the beneficial effect of cubic damping for a constant velocity amplitude excitation.

The experimental investigation was conducted into two base excitation scenarios, the same as those applied for linear damping implementation. The cubic damping configuration was implemented by taking the relative velocity to the power of three which was accomplished by the data processing unit.

6.4.1 Influence of excitation amplitude on the effect of cubic damping (fixed feedback gain and different excitation levels)

The four different excitations previously mentioned were sequentially applied with a fixed level of feedback gain for cubic damping. The level of feedback gain was

initially chosen to achieve a 15 dB peak amplitude ratio for the excitation amplitude of 0.04 mm. Later, the level of feedback gain was kept at this position for the other excitation levels and characteristics.

The amplitude response for the inputs shown by solid lines in figure 6.9 are seen to produce different response characteristics. It is more noticeable for the responses due to a constant displacement amplitude excitation. This is unlike the linear damping case where the response characteristics are similar and only different in terms of level, figures 6.6 (a) and (b). It is more convenient to present these responses using an amplitude ratio as shown in figure 6.10 where the displacement of the isolated mass is normalised by that of the input.

The amplitude ratios reveal that the change in either the level or the characteristic of the input influences the level of effective cubic damping and hence the response characteristic. The corresponding amplitude ratios show an agreement with the definition of non-dimensional cubic damping given in equation (3.5) and given here again, i.e.

$$\zeta_3 = \frac{c_3}{m}\omega_n X^2 \tag{6.8}$$

This shows that the level of non-dimensional cubic damping is directly proportional to the excitation amplitude squared. It appears in figure 6.10 that the level of the resonance peak is lower when higher excitation amplitude was applied. An interpretation of a lower level of peak response can be referred to as a higher level of damping. Thus the experimental appearances are consistent with the theoretical definition given in equation (6.8).

In addition, the amplitude ratios for the cubically damped responses due to different constant velocity excitation amplitude are shown in figure 6.10 (b). These are unlike the linearly damped response which is independent of excitation characteristic. Different excitation level produces different cubic damping responses around the resonance frequency whereas the amplitude ratio at high excitation frequencies appears to be independent of excitation amplitude. This is because the corresponding displacement amplitude, for a constant amplitude velocity input, drops with increasing frequency by 20 dB per decade, a lower level of damping results, given by equation

(6.8) and hence a lower cubic damping force. This is also in agreement to the HBM conclusions presented in Chapter 3.

6.4.2 Response for different cubic damping levels (fixed excitation level and different feedback gains)

For this scenario, the system was excited only by a displacement amplitude of 0.04 mm. The feedback gain was adjusted to achieve the peak response as in the linear case, i.e. around 15 dB and 10 dB for low and high level of damping respectively. By doing this, the effect of cubic damping for the frequencies above resonance could be distinguished from the linear case.

The comparison of the amplitude ratios for these experiments and theory (HBM) are shown in figure 6.11. It is seen that the theoretical approximations (using dotted line) appear similar to the experiment results, especially the increasing response at high frequencies. When a higher level of damping was applied the frequency at which the amplitude ratio increases is lower. The appearance of such behaviour is consistent with the theoretical approximation for excitation frequencies much higher than resonance, i.e. $\Omega \gg 1$, as given in table 3.2 and here again by

$$W \approx \sqrt{1-\left(\frac{4}{3\zeta_3\Omega}\right)^{\frac{2}{3}}} \tag{6.9}$$

The theoretical approximation shows that a greater value of non-dimensional cubic damping results in a lower frequency for the turning point.

The appearance of the higher response level, when $\Omega \gg 1$ for the constant displacement excitation was described theoretically in terms of a damping force given by equation (3.44), i.e.

$$F_{d3} \approx \Omega^2 \tag{6.10}$$

This damping force increases proportionally to the excitation frequency squared and supported using numerical simulations shown in figure 3.6.

The consideration of the cubic damping force was also investigated experimentally. The experimental rig was designed to capture the isolation force acting on the isolated mass. Force transducers A and B, figure 6.1, captured the restoring

forces which were a result of the helical springs. The force transducer C in the middle captured the force produced from the active damper. The force acquired from transducer C was the summation of the internal passive actuator restoring force and the active damping force and is given by

$$f_T = c_s\left(\dot{x}-\dot{x}_0\right)+k_s\left(x-x_0\right)+f_a \tag{6.11}$$

where f_T is a summation of the forces produced by the active damper or the shaker. c_s and k_s are the passive damping coefficient and stiffness of the shaker suspension. f_a is the additional damping force.

For this instance, the mass of the force transducers are not negligible with respect to the mass of the system. So an inertia force resulting from the transducers must be considered. This means that the force acquired from the transducer C included the inertia force resulting from its own mass. The measured forces for the case of linear and cubic damping obtained from the transducer C are shown in figure 6.12. This figure shows that the force in the isolation region for the case of cubic damping increases at a more rapid rate compared to that for the linear case. This is in accordance with the theoretical approximation.

The level of damping force increases to higher levels for high frequency excitation. From these experimental results, the results using the HBM approximation made in Chapter 3 are reasonably acceptable and validated. The detrimental effect of cubic damping for base excitation is considered physically as the result of the high level of damping force being produced at high excitation frequencies. One can conclude that the theoretical results showing the effect of cubic damping are validated experimentally.

6.5 Experimental setup for random broadband excitation

6.5.1 Time and frequency resolution

The experiment on broadband excitation was also conducted using a sampling frequency of 1024 Hz and a frequency resolution of 0.125 Hz. A corresponding Fourier transform of 8 s of data was a result. The Hanning window with 75% overlap and 300 averages were applied to the recorded data in order to minimise the leakage and recover the data lost after the application of the Hanning window. A total recording time of

600 seconds was obtained as a result of these configurations. The corresponding BT product was equal to $(1.44/8)(600)$ = 108 which is considerably larger than unity. Therefore, the statistical deviation in either the estimated power spectral density (PSD) or the amplitude spectrum is expected to be minimal.

6.5.2 Interpretation of the broadband random excitation

The base excitation was defined to be random broadband with the frequency bandwidth of 7-100 Hz. The random broadband excitation was implemented and controlled using the LMS Test.Lab (12A) Random Control workbook where the excitation profiles were assigned. The closed-loop control using acceleration feedback was applied to control the level and profile of base excitation. Two excitation characteristics were considered following the theoretical investigation given in Chapter 5, i.e. the constant displacement amplitude random (CDR) and constant velocity amplitude random (CVR) excitations. The linear and cubic damping characteristics were implemented using the same conditions as those applied for the experiment on harmonic excitation.

The broadband excitation amplitude was set in accordance to the displacement excitation RMS value for the case of harmonic excitation for which the maximum displacement amplitude was equal to 0.060 mm. The displacement RMS value for such excitation was about 0.042 mm. Thus the displacement RMS value for the random excitation with the bandwidth of 7-100 Hz was chosen initially to be about 0.042 mm for both CDR and CVR excitations.

However, the practical values for the excitation RMS values were about 0.044 mm for CDR and 0.046 mm for CVR excitations. The displacement amplitude spectra for these excitations are plotted using the solid lines in figures 6.13 (a) and (b) respectively for CDR and CVR. The displacement spectrum level for the CDR excitation appears to be about -50 dB re 1 mm (0.003 mm). The amplitude spectrum for the CVR is also presented using the displacement amplitude spectrum which can be converted to the velocity amplitude spectrum. The corresponding velocity amplitude for the displacement RMS value of 0.046 mm is about -7 dB re 1 mm/s (0.45 mm/s). The excitations at these levels were assigned to be the reference levels for each excitation scenario.

Three investigation scenarios were conducted regarding the theoretical study reported in Chapter 5 and are given as follows.

Case (i) Two additional amplitude levels of excitation, i.e. 3 dB higher and lower than the reference levels, were applied in order to examine the influence of excitation amplitude on the effect of cubic damping. These excitation levels are shown in figures 6.13 (a) and (b) using dotted lines.

Case (ii) The excitation bandwidth was reduced to 7-75 Hz, 7-50 Hz and 7-25 Hz as shown using dotted lines in figures 6.14 (a) and (b) for the CDR and CVR excitations respectively. This excitation scenario was performed in order to determine the influence of the frequency content. The excitations with the bandwidth of 7-100 Hz defined as the reference level in case (i) are also displayed by the solid lines.

Case (iii) Additional high frequency contents with the bandwidth of 25 Hz were added to the excitation frequency of 7-25 Hz as shown in figure 6.15. The additional bandwidths were 50-75 Hz and 75-100 Hz. These excitation characteristics were introduced in order to examine the influence of the high frequencies. The responses for these excitation bandwidths are examined in comparison to those for the excitation bandwidth of 7-50 Hz (which consists of two consecutive bandwidths, i.e.7-25 Hz and 25-50 Hz). These excitations share the similar displacement excitation RMS value of about 0.031 mm for CDR excitation and 0.042 mm for CVR excitation.

Note that, in figure 6.15, a noticeable spike appears at 50 Hz for the figures for excitation bandwidth of 7-25 Hz plus 75-100 Hz. This spike can be identified as the effect of interfere from electric power supply which has the frequency at 50 Hz. As a result, there appears a second harmonic at 100 Hz in the figures for excitation bandwidth less than 100 Hz. However the amplitudes at these frequencies due to interfere were very small compared to the amplitude of the excitation signal. Therefore, there would not be any significant effect to the characteristic of the responses.

6.6 Broadband responses and discussions

The experiment on random broadband excitation was conducted in order to confirm the theoretical findings, i.e.

i) the occurrence of high response level at low frequencies outside excitation bandwidth,

ii) the excitation amplitude dependence and

iii) the influence of excitation on the level of effective cubic damping.

The broadband responses due to four experimental scenarios were carried out. The first scenario involved exciting the system using a fixed excitation amplitude and is reported in section 6.6.1. The other three scenarios were to maintain the level of the damping coefficient (feedback gain) at a certain level whilst the different excitations mentioned in section 6.5.2 were applied. The broadband responses for these excitations are reported in sections 6.6.2 to 6.6.4.

6.6.1 The influence of feedback gain on the level of effective damping

The linear and cubic damping responses reported in this section were obtained from the application of the CDR excitation with a RMS value of 0.044 mm and bandwidth of 7-100 Hz. The feedback gain, which represented the physical damping coefficient, was adjusted to produce a peak amplitude of H_0 around 15 dB and 10 dB for low and high damping levels respectively. Note that, the feedback gain is referred to hereafter as the damping coefficient.

The linearly and cubically damped responses for different damping coefficients are shown in figure 6.16 using the amplitude spectra. The corresponding estimated transfer functions are also shown in the figure. It is apparent that the response characteristics for both linear and cubic damping are similar. There is no significant difference within the excitation bandwidth. The level of response spectra at high frequencies does not increase as for harmonic excitation. One can also see that increasing the value of either the linear or cubic damping coefficient reduces the response around the resonance frequency.

However, the difference between linearly and cubically damped responses is noticeable at low frequencies outside the excitation bandwidth. The level of cubically

damped response in this frequency region is higher compared to the linear damping case and seems to be dependent upon the value of cubic damping coefficient. This characteristic appeared consistently in the results obtained from numerical simulation shown in Chapter 5 and is identifiable as a result of raising the relative velocity to the power of three. Therefore, the theoretical numerical results obtained in Chapter 5 are experimentally validated where cubic damping produces response at low frequencies outside the excitation bandwidth. Thus, one should be aware of such detrimental behaviour for the practical systems where the value of damping nonlinearity could not be identified.

6.6.2 The effect of the excitation level on the effective damping

The numerical simulations in Chapter 5 showed that the level of excitation resulted in different levels of effective damping. It was concluded that the effect of cubic damping is mostly contributed to by the amplitude of displacement excitation. Therefore, the investigation into the influence of excitation level was then implemented.

Three excitation amplitudes given in section 6.5.2 case (i) were applied. Only the high level of damping coefficient was applied for this experimental scenario. By considering the response for the CDR excitation, shown in figure 6.17, one can see the difference in the levels of the peak between the linear (dotted line) and cubic (solid line) responses. It is shown in the graphs of H_0 that the peak amplitude for the linearly damped responses are almost at the desired amplitude of 10 dB. In contrast, the peak amplitude for the cubically damped response appears inversely related to the excitation level. A higher peak amplitude occurs for a lower excitation level and vice versa for a higher excitation level.

The responses for the CVR excitation are shown in figure 6.18. Similar to the case of CDR, the peak amplitude in the graphs of H_0 for the system with cubic damping due to excitation with RMS displacement of 0.046 mm was tuned to be around 10 dB. Then the level of cubic damping coefficient was kept fixed for the other excitation amplitudes which were ±3 dB from the reference level.

It was observed for the cubically damped system that to obtain the peak response around 10 dB, the cubic damping coefficient was increased by orders of magnitude

compared to the case of CDR. This is different to linear damping where the damping coefficient is unaltered. This is also consistent with numerical simulations in Chapter 5, where the values of c_3 for CDR and CVR to produce the same level of resonance peak are very different.

To recap, the response for this experimental scenario appeared as expected. There should be a higher peak ratio for the lower excitation level and a lower peak ratio for higher excitation level. This is consistent with the theoretical results interpreted in Chapter 5.

6.6.3 The effect of the excitation bandwidth on the effective damping

Chapter 5 showed that the presence or absence of displacement input at high frequencies contributed to the level of effective cubic damping. Four excitation bandwidths mentioned in section 6.5.2 case (ii) were applied. Similarly to before, where only a single high damping level was applied, the peak amplitude in H_0 for the excitation at a reference level, i.e. excitation with bandwidth of 7-100 Hz, was chosen to be around 10 dB.

The results for the CDR excitations are shown in figure 6.19. It is seen that the response for the narrower bandwidth excitation exhibits a higher peak level. This indicates a lightly damped response. This is due to the absence of displacement excitation at high frequencies which is also consistent to comments in Chapter 5.

The results for the CVR excitations are shown in figure 6.20. The narrower excitation bandwidth, i.e. 7-25 Hz, also resulted in a higher peak response level. A broader excitation bandwidth produced a higher level of effective damping. However, in this case (CVR compared to CDR) the excitation at high frequencies is less significant.

When the amplitude spectra for the CDR excitation, figure 6.19, and CVR excitation, figure 6.20, are compared the differences at low frequencies outside the excitation bandwidth are noticeable. Considering for the same excitation bandwidth, those for the CDR excitation are considerably higher than those for the CVR excitation. Hence the presence or absence of displacement excitation at high frequencies not only contributes to the peak response level, but also the response at low frequencies. These results also validate the numerical simulations presented in Chapter 5.

6.6.4 The effect of the displacement excitation at high frequencies

The excitations given in section 6.5.2 case (iii) were applied. The obtained results are shown in figure 6.21 for the CDR excitation. It is seen in figure 6.21 (c) that the level of peak response for the excitation with higher frequencies is lower (the levels are indicated by horizontal dashed lines). In contrast, for the CVR excitation, as shown in figure 6.22, the peak amplitudes are almost at the same level. This is because the amplitudes of the high frequency displacement content included in the excitation are relatively small compared to those at low frequencies. This is also shown by the standard deviation for the displacement, σ_{x_0}, and velocity, $\sigma_{x_0'}$, annotated in the figures. The values of standard deviation for both the displacement and velocity are not significantly different amongst the cases.

To this end, it could be concluded for this experimental scenario that the presence of the high displacement amplitude at high frequencies has a strong contribution to the level of effective cubic damping. A low displacement amplitude at high frequencies does not influence the level of effective cubic damping very much.

6.6.5 General discussion and conclusion on the effect of cubic damping for random excitation

The experiment on broadband base excitation revealed that the effect of cubic damping is mostly a result of the magnitude of the base displacement amplitude at high frequencies. The presence or absence of the displacement input at high frequencies governs the peak response level and also the occurrence of the response at low frequencies outside the excitation bandwidth. For the case of the CVR excitation, where the displacement amplitude is inversely proportional to the excitation frequency, the influence of the displacement amplitude at high frequencies is limited. This is because the input displacement amplitudes at high frequencies for the CVR excitation are relatively small compared to those at low frequencies. Thus the effect of nonlinearity is minimised and a lightly damped response can be expected. Therefore to maintain a level of peak response one needs to increase the value of c_3.

In conclusion, one should be aware that the effect of cubic damping is dependent on the excitation amplitude. Damping can be reduced when the displacement excitation

contains less significant amplitude at high frequency and that can cause a high response amplitude around resonance. On the other hand, the response at low frequency outside the bandwidth can occur due to the presence of the relatively high displacement amplitude at high frequencies. This occurrence can result in excessive vibration at low frequencies, although a lower peak response can be obtained.

6.7 General conclusions

The experimental study was implemented to investigate the effect of cubic damping on the SDOF base excited vibration isolation system. The effect of cubic damping was observed to be consistent with the results obtained from the theoretical analyses. Under harmonic excitation, cubic damping can cause the response of the isolated mass to increase at high excitation frequencies, tending towards the amplitude of the excitation. This behaviour is identifiable as a result of a high level of the cubic damping force. It is also found that the effect of cubic damping is controlled directly by the excitation amplitude. A higher excitation amplitude produces a stronger effect of cubic damping.

The effect of cubic damping on the responses due to the random broadband excitation also appeared to be excitation dependent. It is slightly different from that for the harmonic case as the excitation dependence for the broadband response can be defined by either the excitation amplitude or excitation bandwidth. However, both theoretical and experimental results showed that the main contribution of the effect of cubic damping comes from the displacement amplitude at high frequencies. The high displacement amplitude at high frequencies, provided by either the excitation amplitude or the excitation bandwidth, can result in a greater effect of cubic damping especially at resonance. Therefore, cubic damping on the system with unknown excitation amplitude can cause the detrimental effects to the response.

The greater effect of cubic damping for the broadband excitation can cause the occurrence of the response at low frequencies outside the excitation bandwidth. That can result in a large amplitude low frequency response. The effect of cubic damping can be reduced by reducing the significant displacement amplitude at high frequencies. However, by doing so the isolated mass might experience high vibration amplitude around resonance.

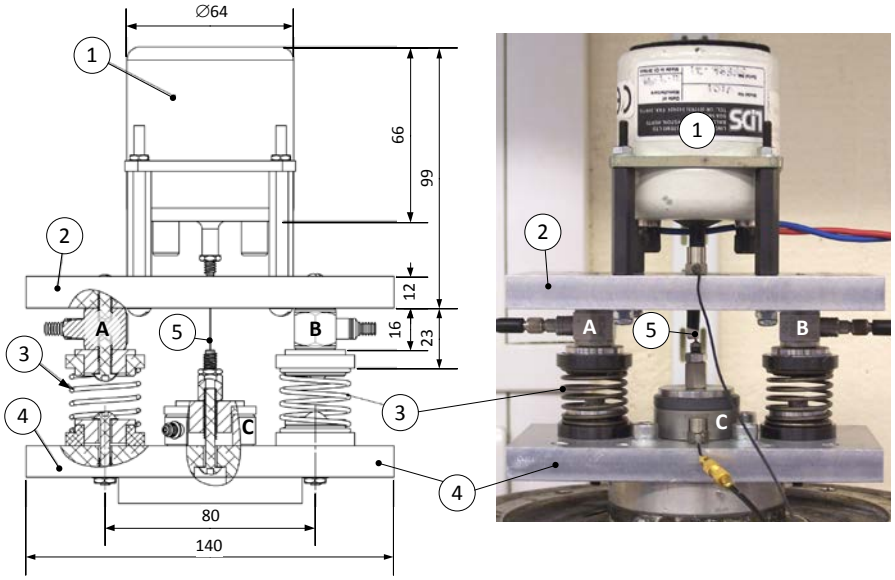

Drawing of the experimental rig Photo of the experimental rig

Figure 6.1 Experimental rig for a SDOF base excited vibration isolation

① LDS Shaker model V101 (active damper)	② Aluminium plate to fit the shaker
③ Helical isolator springs	④ Aluminium plate to fit the excitation unit
⑤ Stinger	A, B and C the force transducers

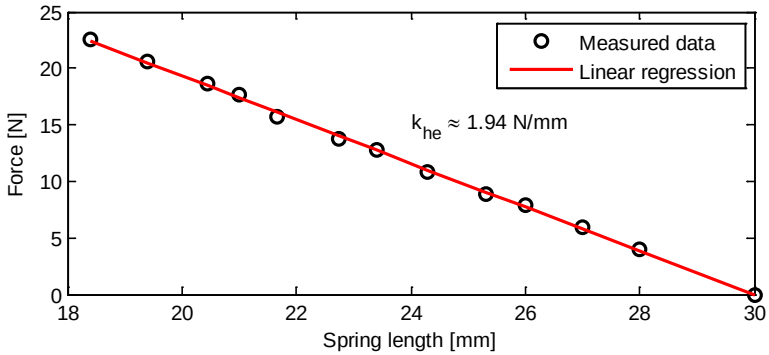

Figure 6.2 Load-deflection characteristic for the measured data and the estimation of the total stiffness for the two helical spring, k_{he} using linear regression.

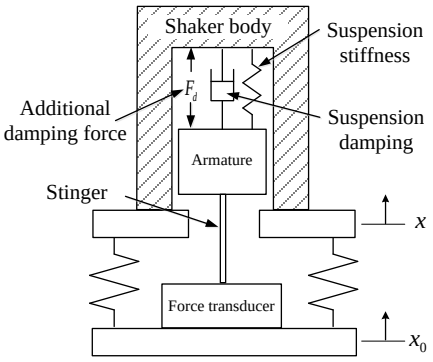

Figure 6.3 The physical representation for mass, spring and damper model for the experimental rig

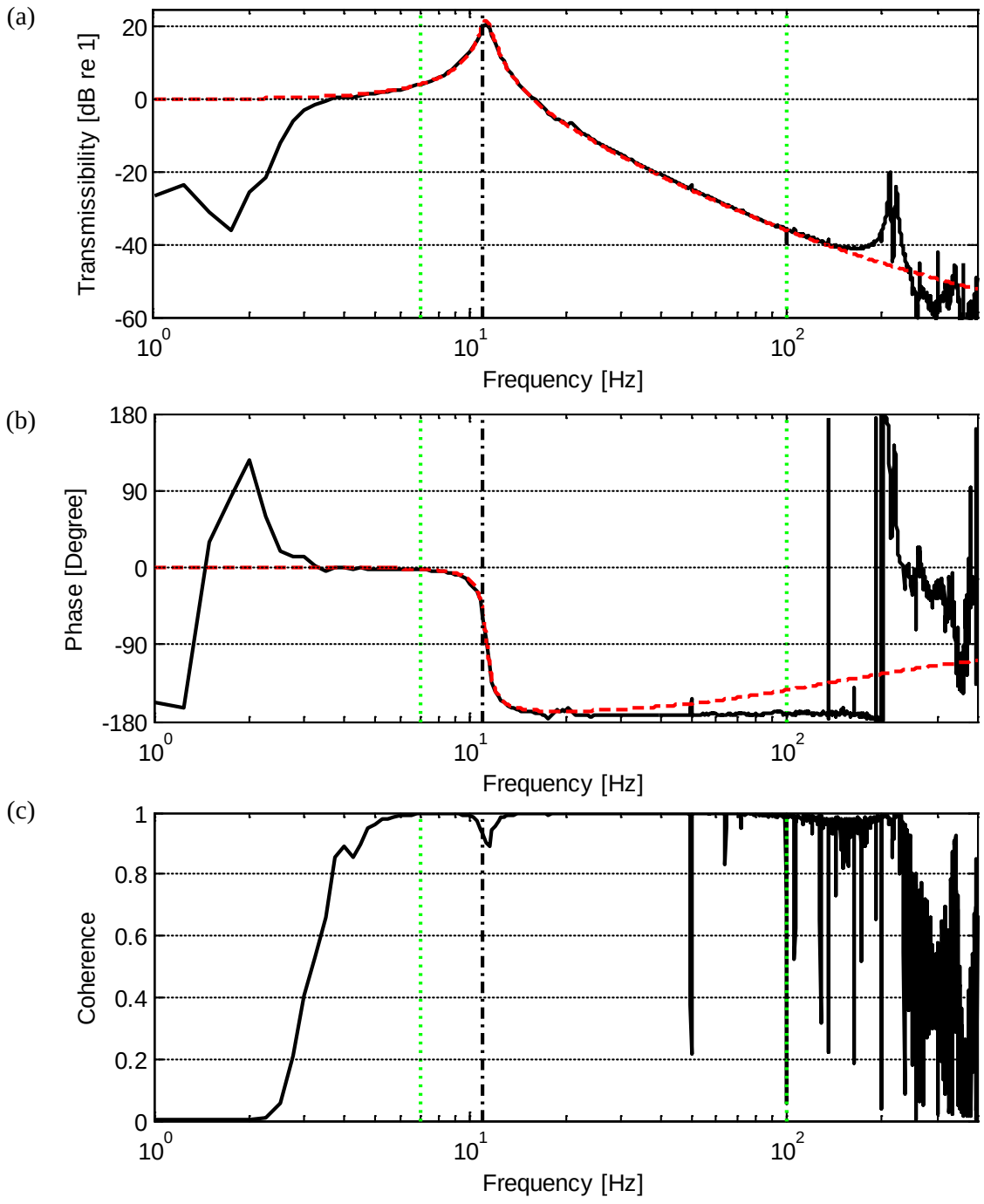

Figure 6.4 Transmissibility of the SDOF base excited isolation system for 20 kHz bandwidth white noise with no damping control
(a) Magnitude
(b) Phase
(c) Coherence function
—— Experimental results
- - - - A fit to the data using a SDOF linearly damped model
····· Frequency range of 7-100 Hz
– · – Resonance frequency (around 11 Hz)

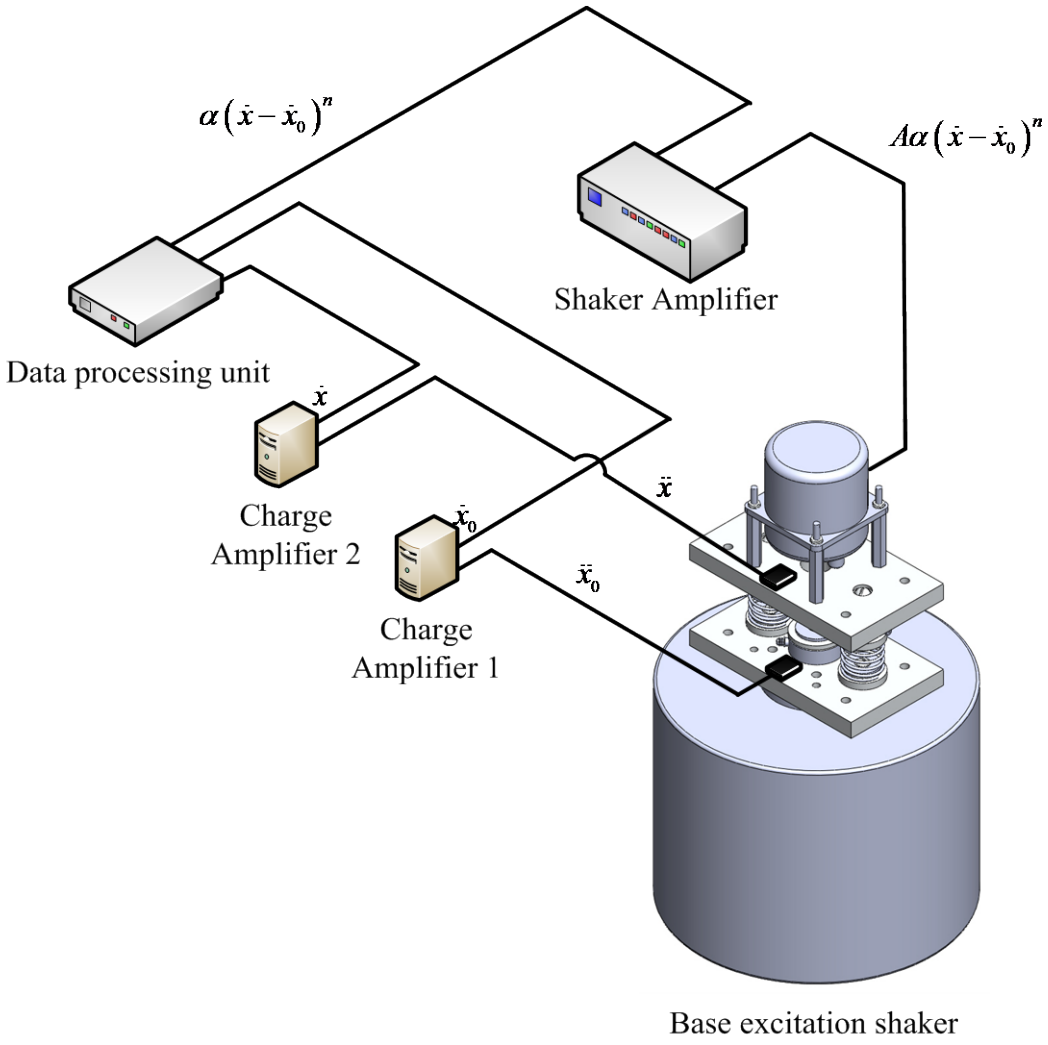

Figure 6.5 Schematic diagram of the feedback loop with lines representing the signal paths

$\ddot{x}$ and $\ddot{x}_0$ are the accelerations of the isolated mass and the base input

$\dot{x}$ and $\dot{x}_0$ are the velocities of the isolated mass and the base input

α is the gain from the charge amplifier

A is the feedback gain from the amplifier for controlling the shaker

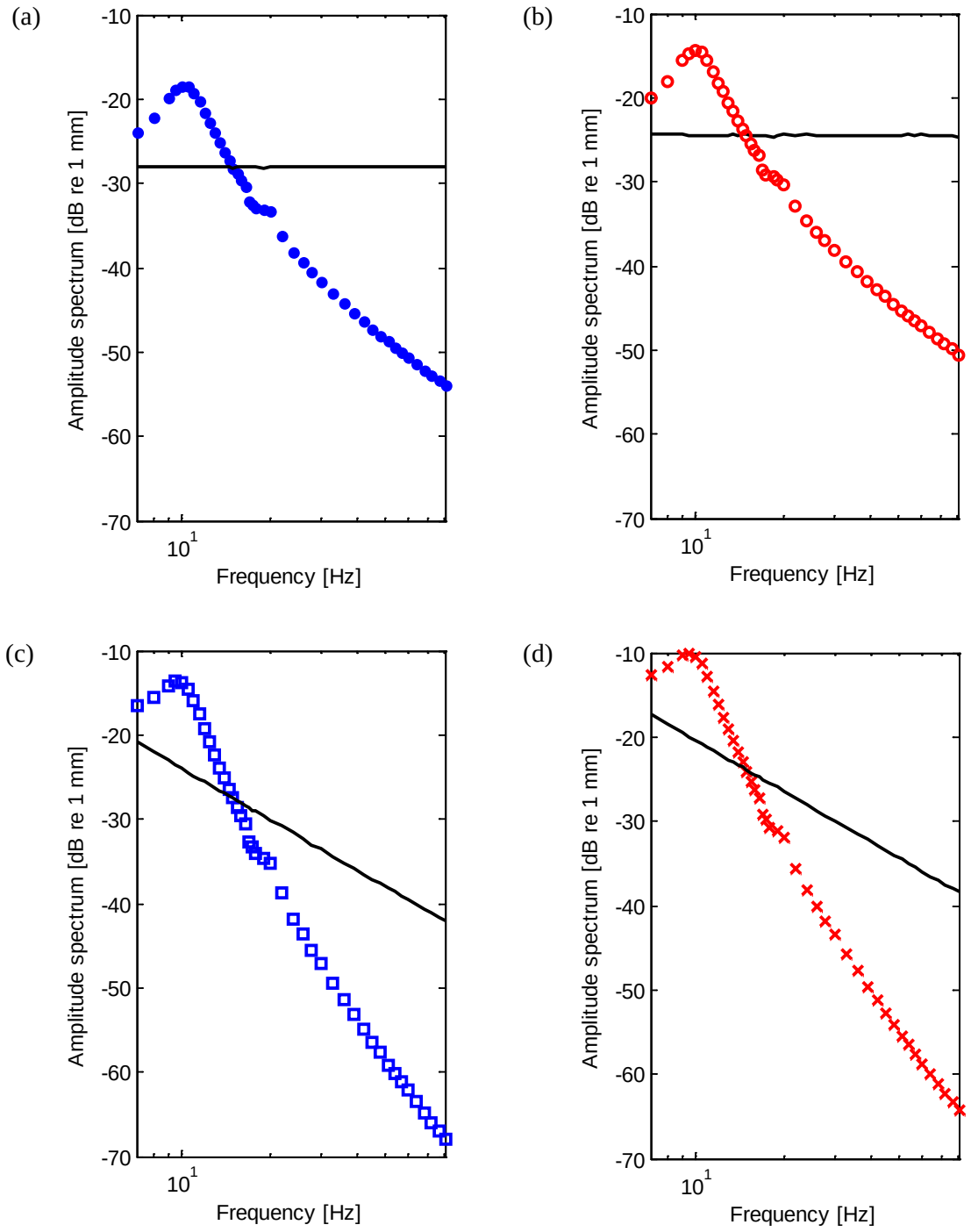

Figure 6.6 Displacement amplitude for response and harmonic base excitations with a fixed feedback gain for linear damping.
(a) 0.04 mm constant displacement input
(b) 0.06 mm constant displacement input
(c) 4 mm/s constant velocity input
(d) 6 mm/s constant velocity input
—— Amplitude of base excitation
Markers represent the amplitude of isolated mass responses

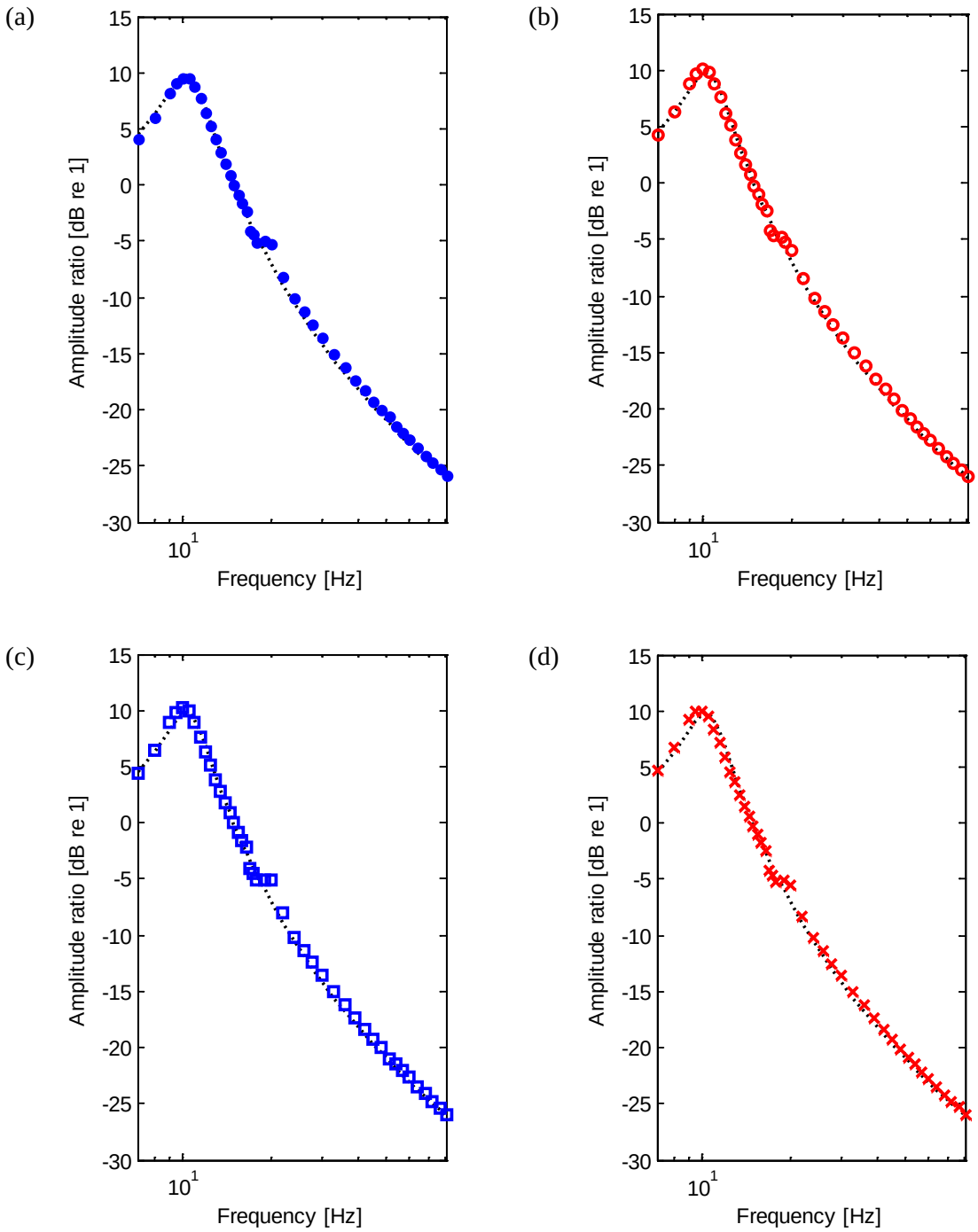

Figure 6.7 Displacement amplitude ratios for a fixed level of feedback gain for linear damping under different harmonic base excitation characteristics (corresponding to the responses and excitation in figure 6.6).
(a) 0.04 mm constant displacement input
(b) 0.06 mm constant displacement input
(c) 4 mm/s constant velocity input
(d) 6 mm/s constant velocity input
Markers represent the ratios of measured data
····· Theoretical transmissibility for linear damping system

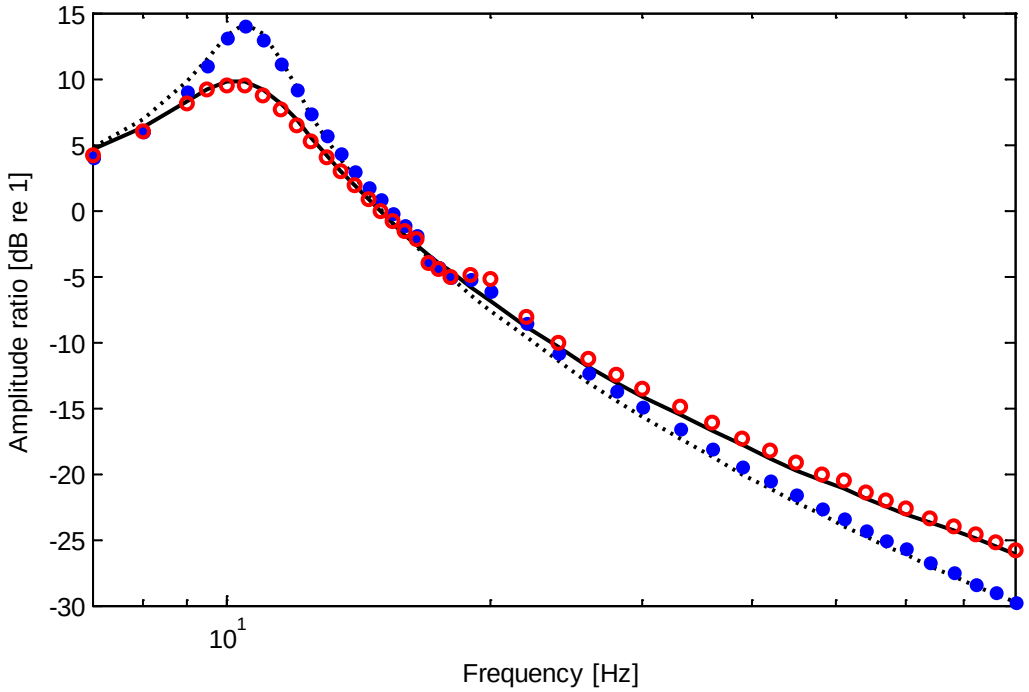

Figure 6.8 Displacement amplitude ratio for linear damping with a constant displacement harmonic base excitation of 0.04 mm

- the experimental data for lower damping
- the linear system estimation for lower damping
- the experimental data for higher damping
- the linear system estimation for higher damping

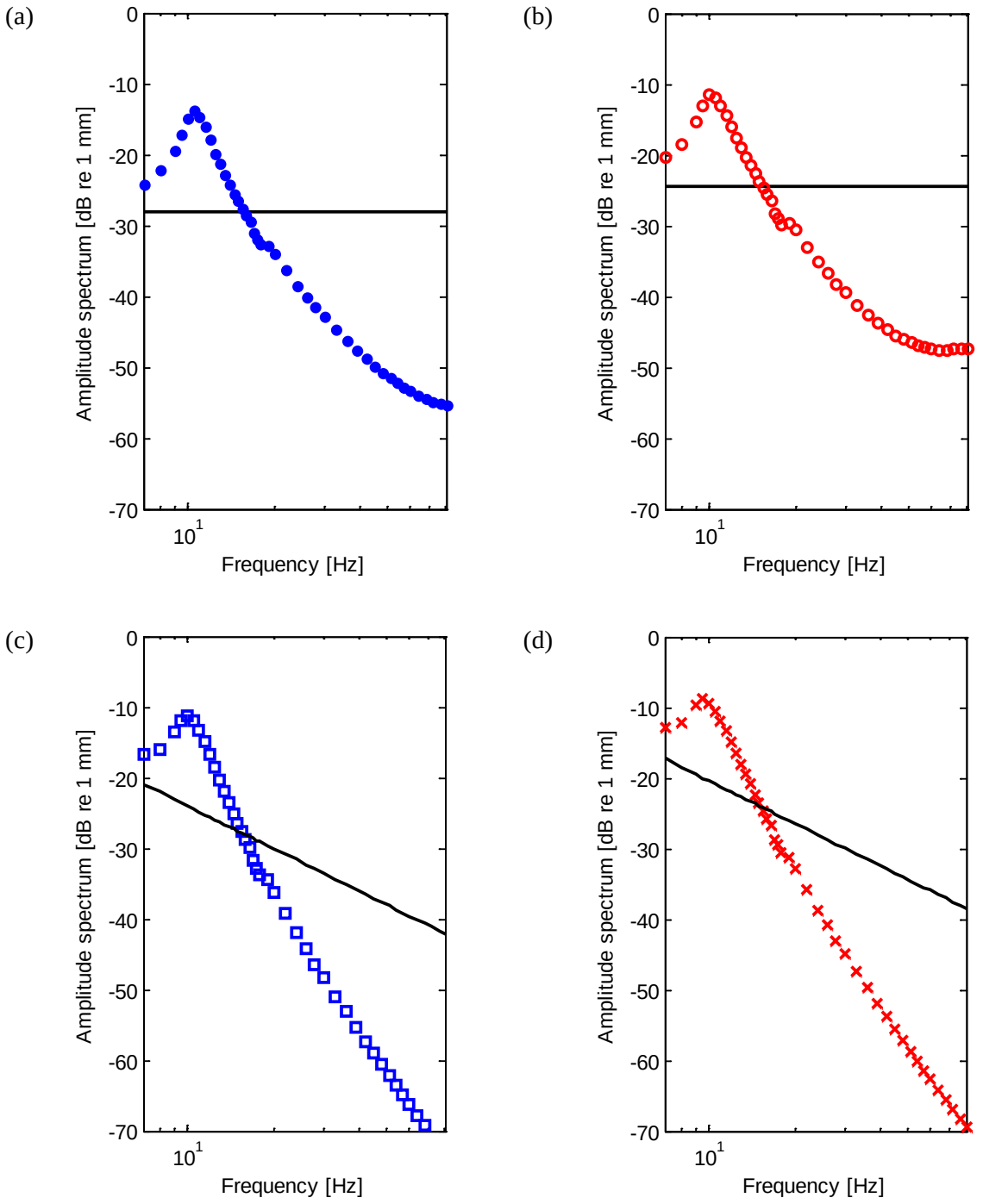

Figure 6.9 Displacement amplitude for response and harmonic base excitation characteristics with fixed feedback gain for cubic damping.
(a) 0.04 mm constant displacement input
(b) 0.06 mm constant displacement input
(c) 4 mm/s constant velocity input
(d) 6 mm/s constant velocity input
—— Amplitude of base excitations
Markers represent the experimental data for the isolated mass responses

(a)

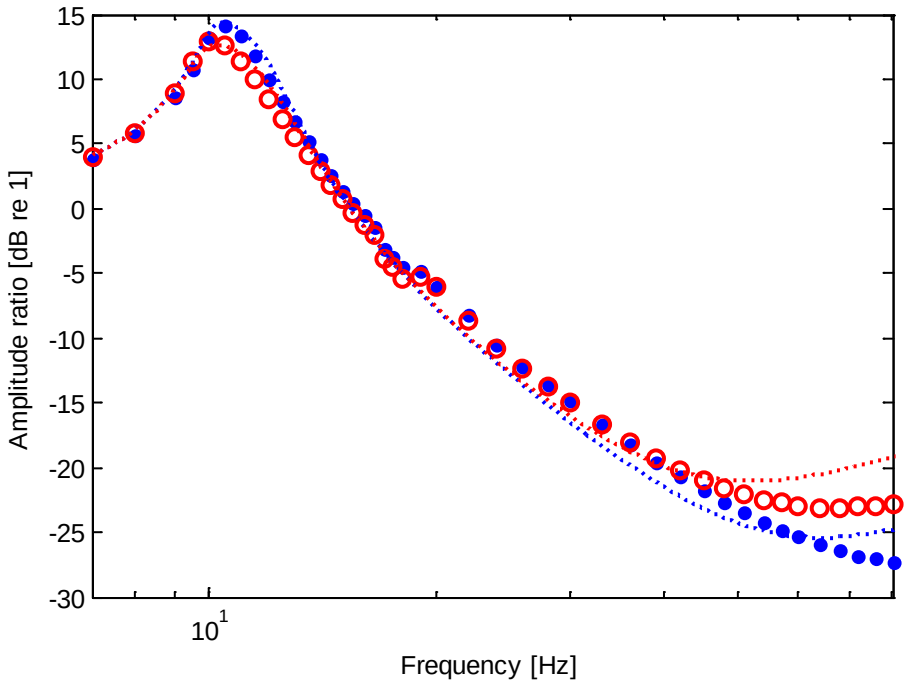

(b)

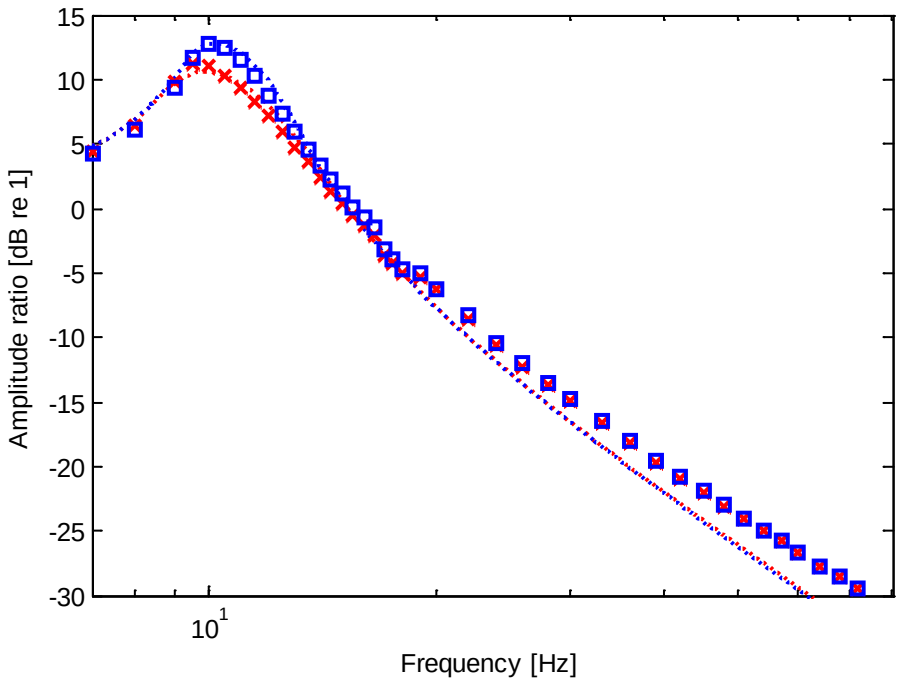

Figure 6.10 Amplitude ratios for a fixed feedback gain for cubic damping under different harmonic excitation characteristics (corresponding to the responses and excitation in figure 6.9).
(a) constant displacement amplitude base excitation
(b) constant velocity amplitude base excitation
- ● constant displacement of 0.04 mm
- ○ constant displacement of 0.06 mm
- □ constant velocity of 4 mm/s
- × constant velocity of 6 mm/s

Dotted lines represent predicted results obtained using HBM approximation.

(a)

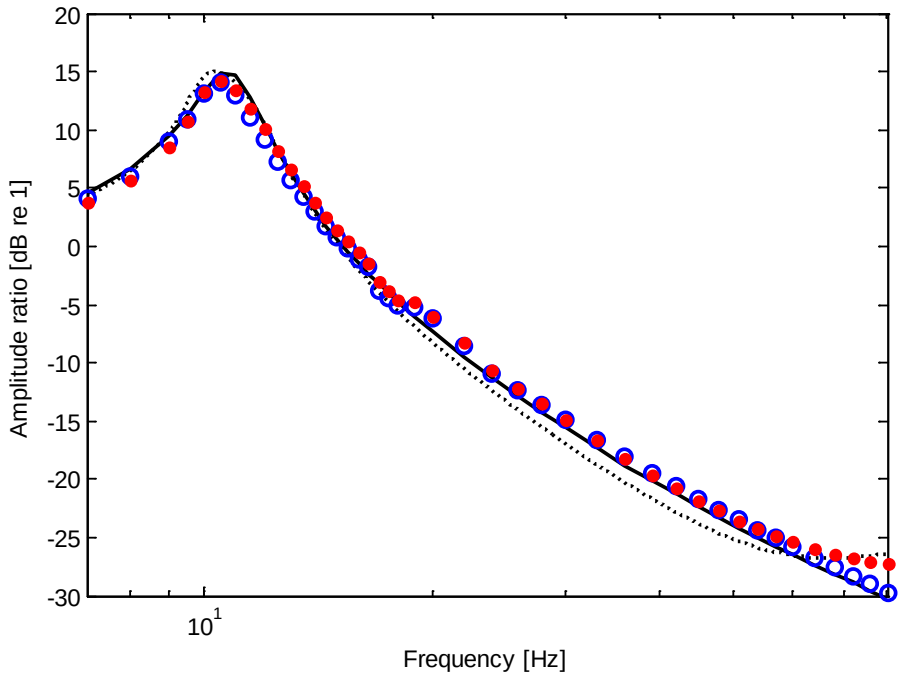

(b)

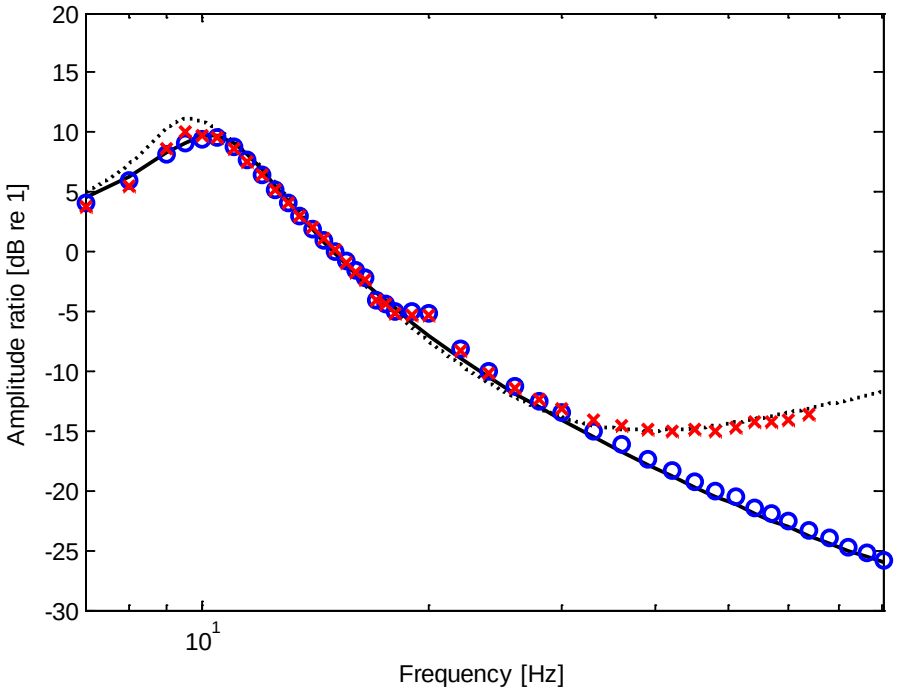

Figure 6.11 Measured and predicted amplitude ratios for the harmonic responses for different damping levels (linear and cubic) under a constant displacement amplitude harmonic base excitation of 0.04 mm.
(a) Lower value of cubic damping
(b) Higher value of cubic damping
○ Experimental data for linear damping configuration
● Experimental data for lower cubic damping configuration
× Experimental data for higher cubic damping configuration
—— Theoretical transmissibility for linear damping system
····· Predicted results obtained using HBM approximation for cubic damping

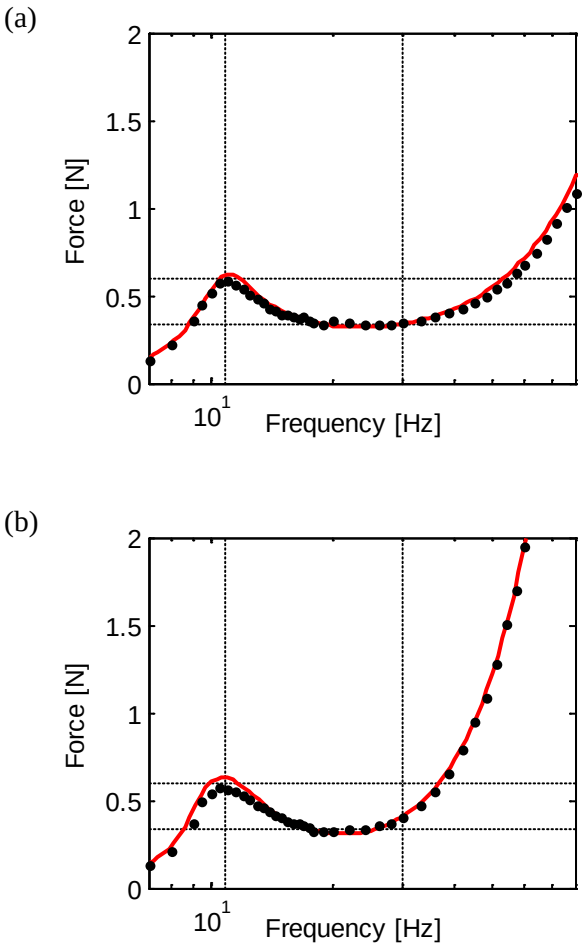

Figure 6.12 The measured secondary actuator force for isolation due to harmonic base excitation with an approximate peak displacement amplitude ratio of about 10 dB.
(a) Linear damping
(b) Cubic damping
- The measured forces

—— The theoretical force f_T evaluated using equation (6.11)

(a)

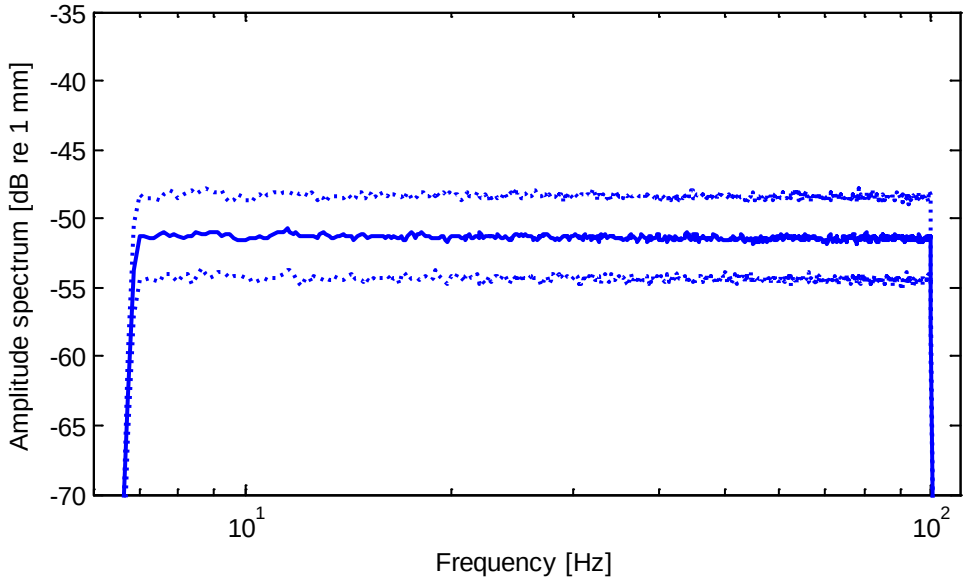

(b)

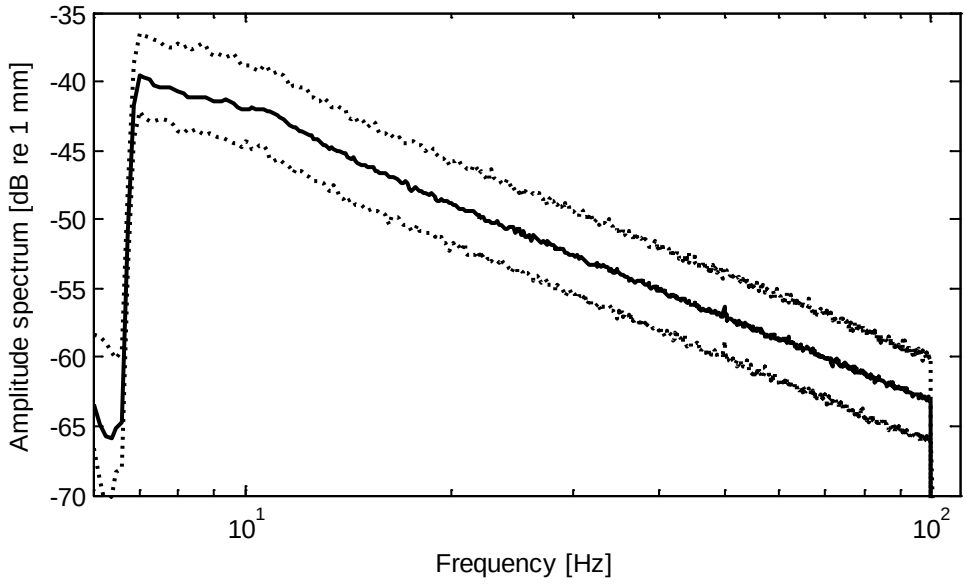

Figure 6.13 Displacement amplitude spectra for broadband excitation with different excitation levels
(a) Constant displacement amplitude random excitation
(b) Constant velocity amplitude random excitation
—— Excitations defined as the reference level
····· Excitations with the amplitude of ±3 dB from the reference level

(a)

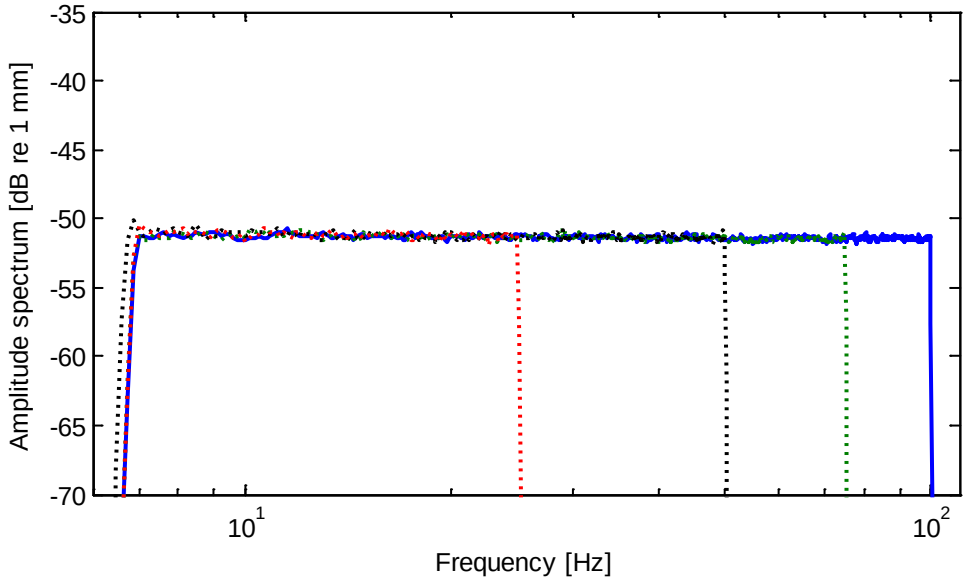

(b)

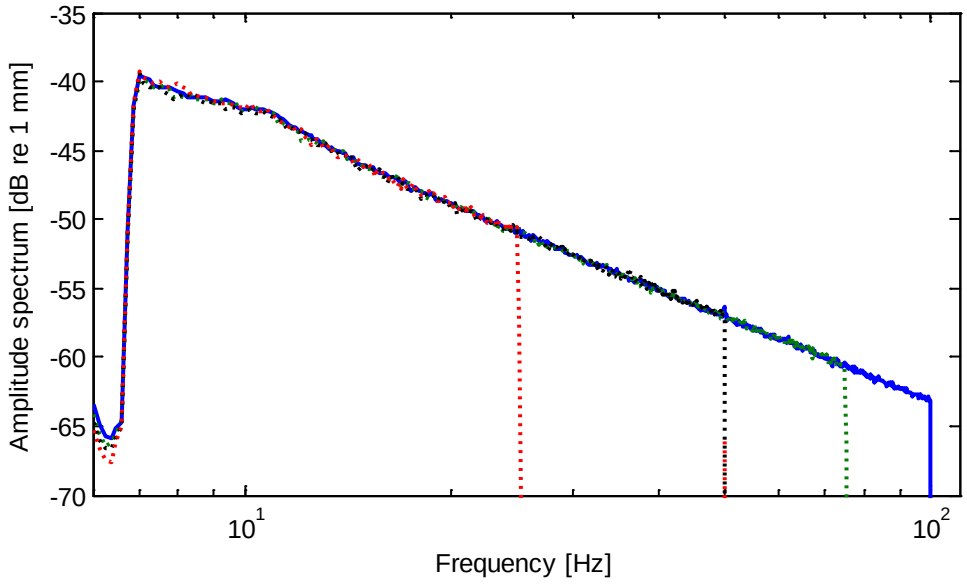

Figure 6.14 Displacement amplitude spectra for broadband excitation with different excitation bandwidths
(a) Constant displacement amplitude random excitation
(b) Constant velocity amplitude random excitation
——— Excitations defined as the reference level
····· Excitations with the bandwidth of 7-25 Hz, 7-50 Hz and 7-75 Hz.

Constant displacement amplitude random

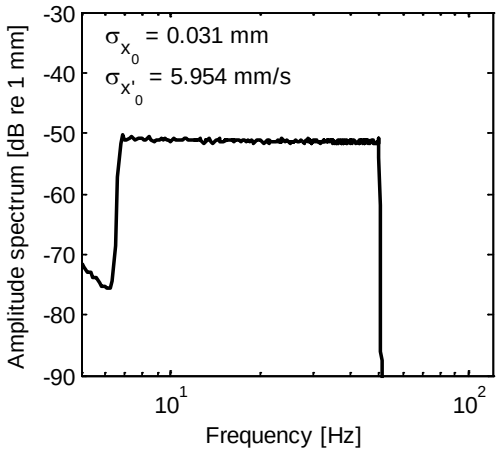

Constant velocity amplitude random

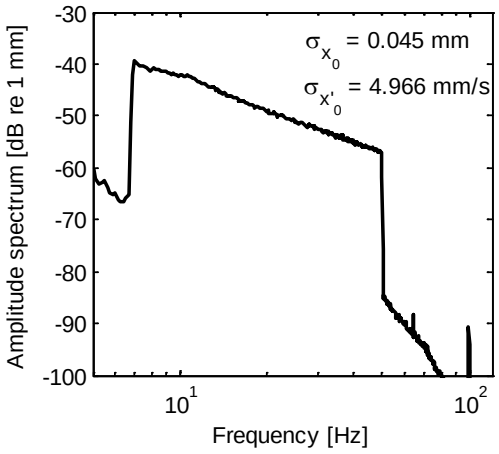

Bandwidth of 7-50 Hz

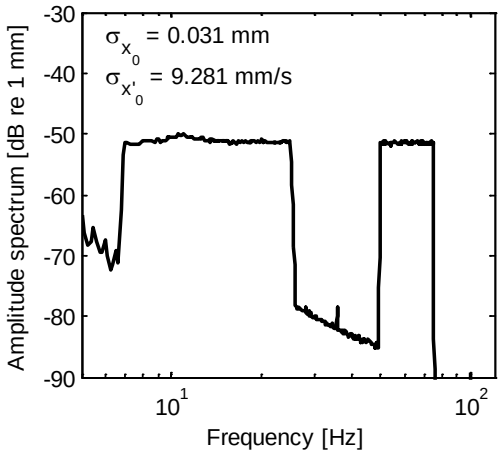

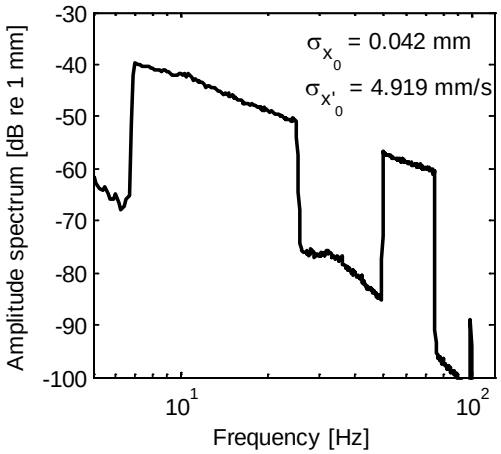

Bandwidth of 7-25 Hz and 50-75 Hz

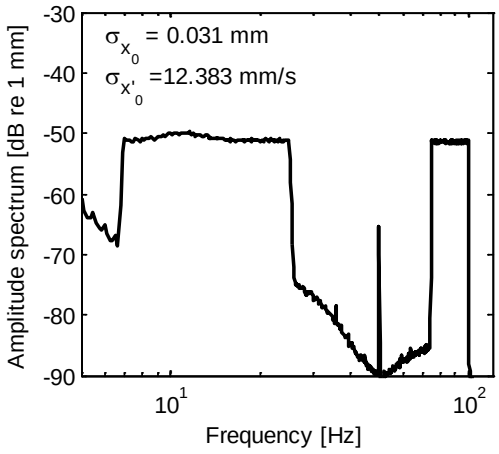

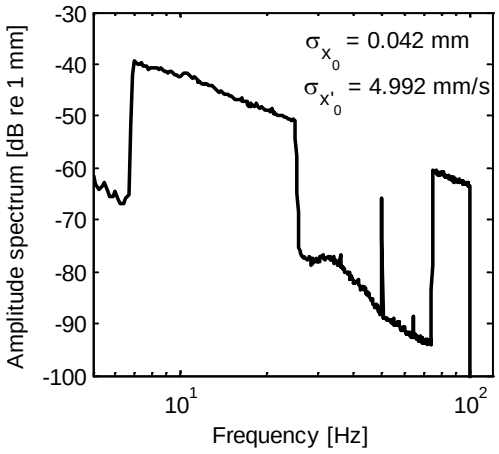

Bandwidth of 7-25 Hz and 75-100 Hz

Figure 6.15 Displacement amplitude spectra for two pass-band broadband random excitation.

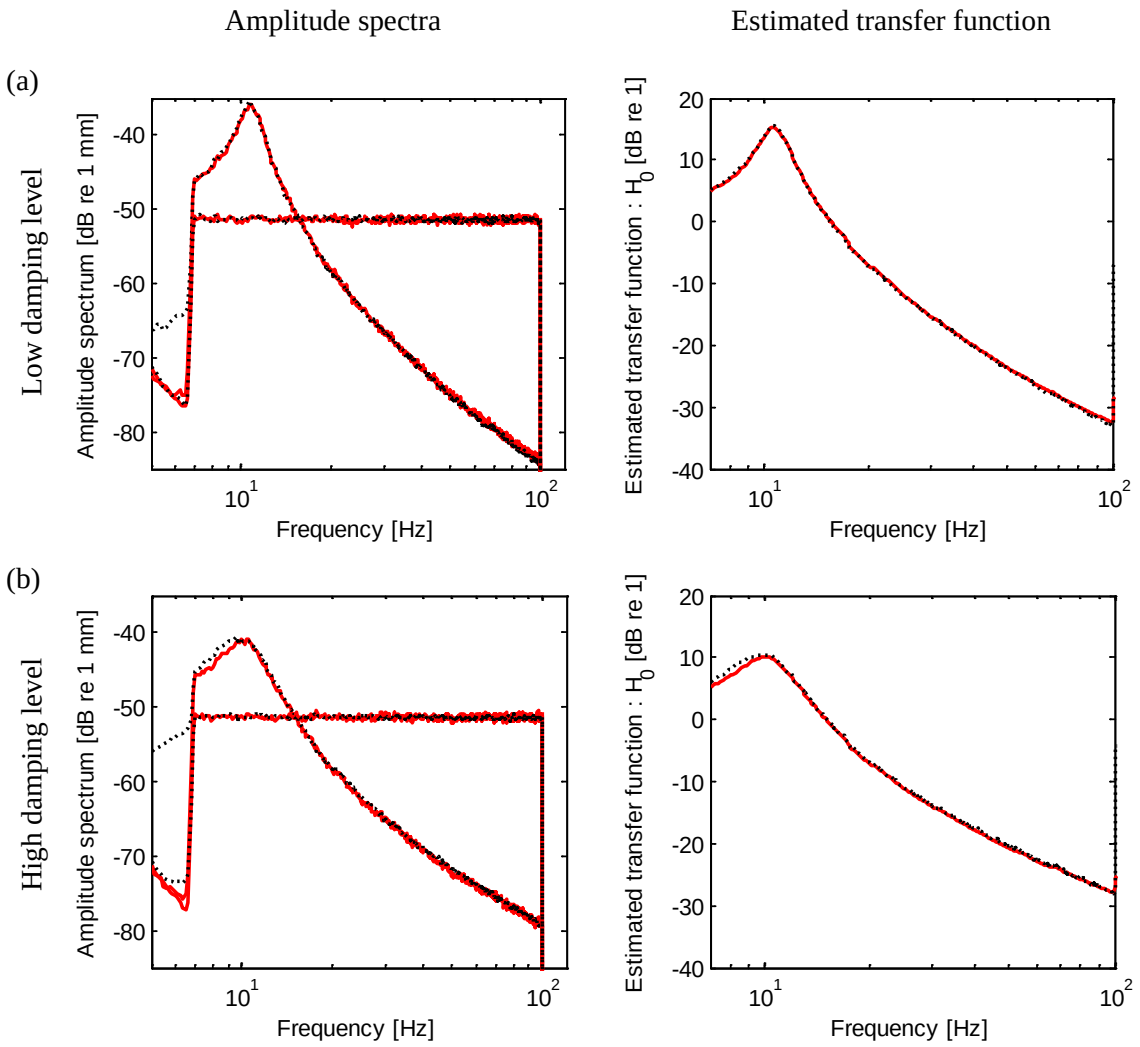

Figure 6.16 Displacement amplitude spectra and estimated transfer function H_0 for the linearly damped and cubically damped responses subject to a constant <u>displacement</u> RMS amplitude random excitation of 0.04 mm

Linearly damped response

Cubically damped response

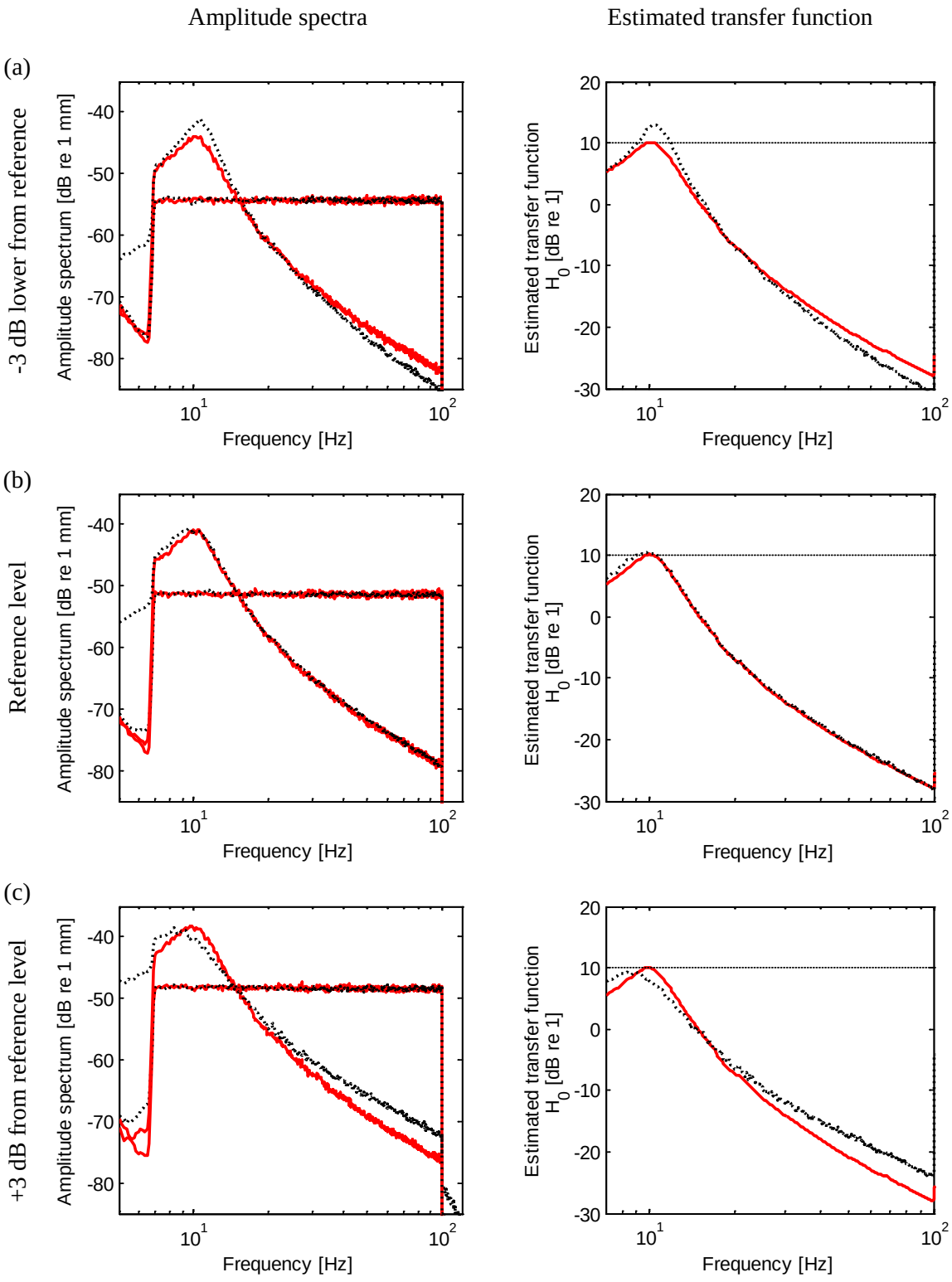

Figure 6.17 Displacement amplitude spectra and estimated transfer function H_0 for the linearly damped and cubically damped responses subject to a constant displacement amplitude random excitation at three different amplitudes and fixed c_3.

Linearly damped response
Cubically damped response
Peak amplitude ratio for linearly damped system

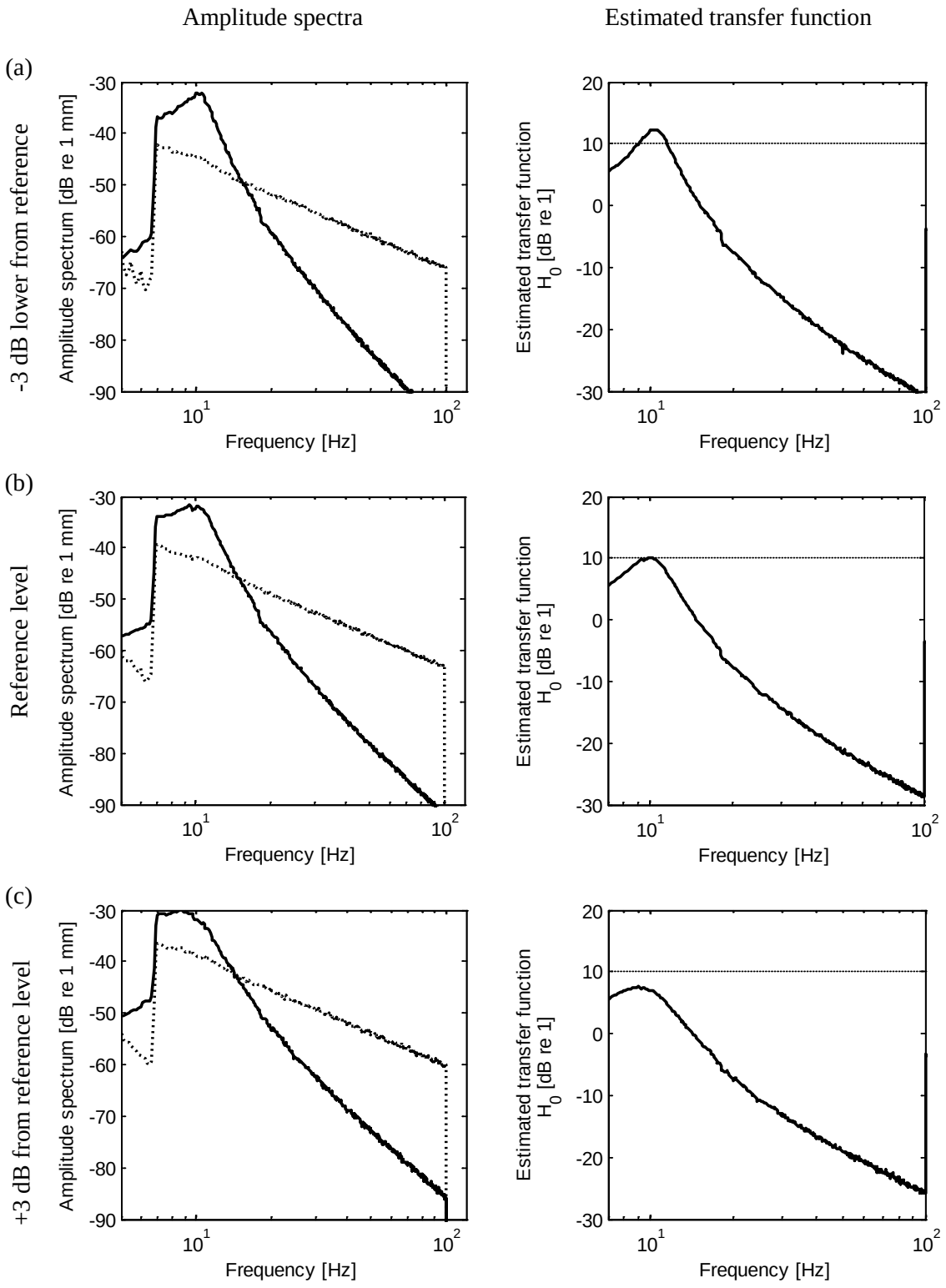

Figure 6.18 Displacement amplitude spectra and estimated transfer function H_0 for the cubically damped responses subject to a constant velocity amplitude random excitation at three different excitation amplitudes and fixed c_3.

——— Cubically damped response
····· Base excitation
····· Peak amplitude ratio for linearly damped system

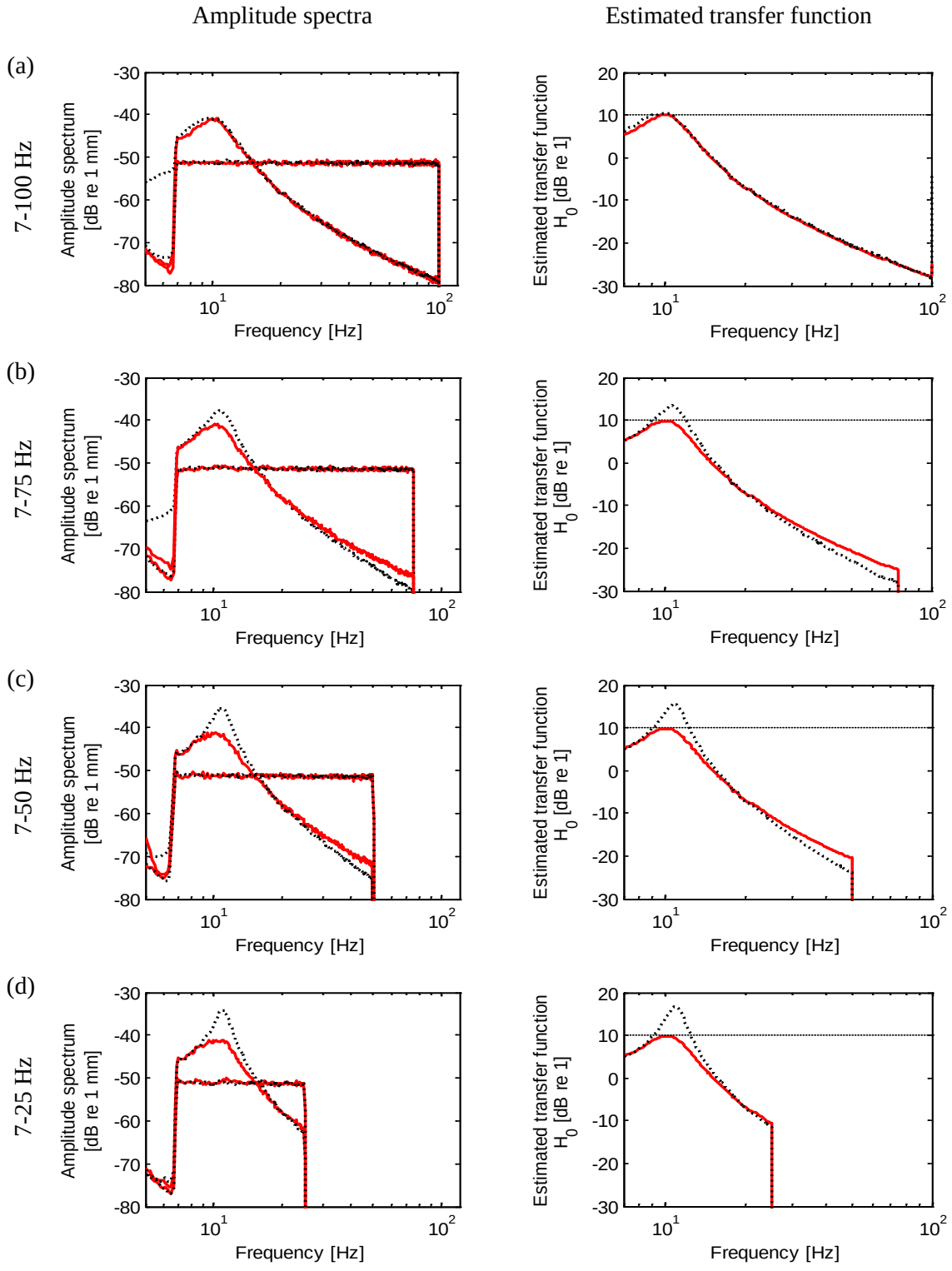

Figure 6.19 Displacement amplitude spectra and estimated transfer function H_0 for the linearly damped and cubically damped responses subject to a constant displacement amplitude random excitation at four different excitation bandwidths and fixed c_3.

Linearly damped response
Cubically damped response
Peak amplitude ratio for linearly damped system

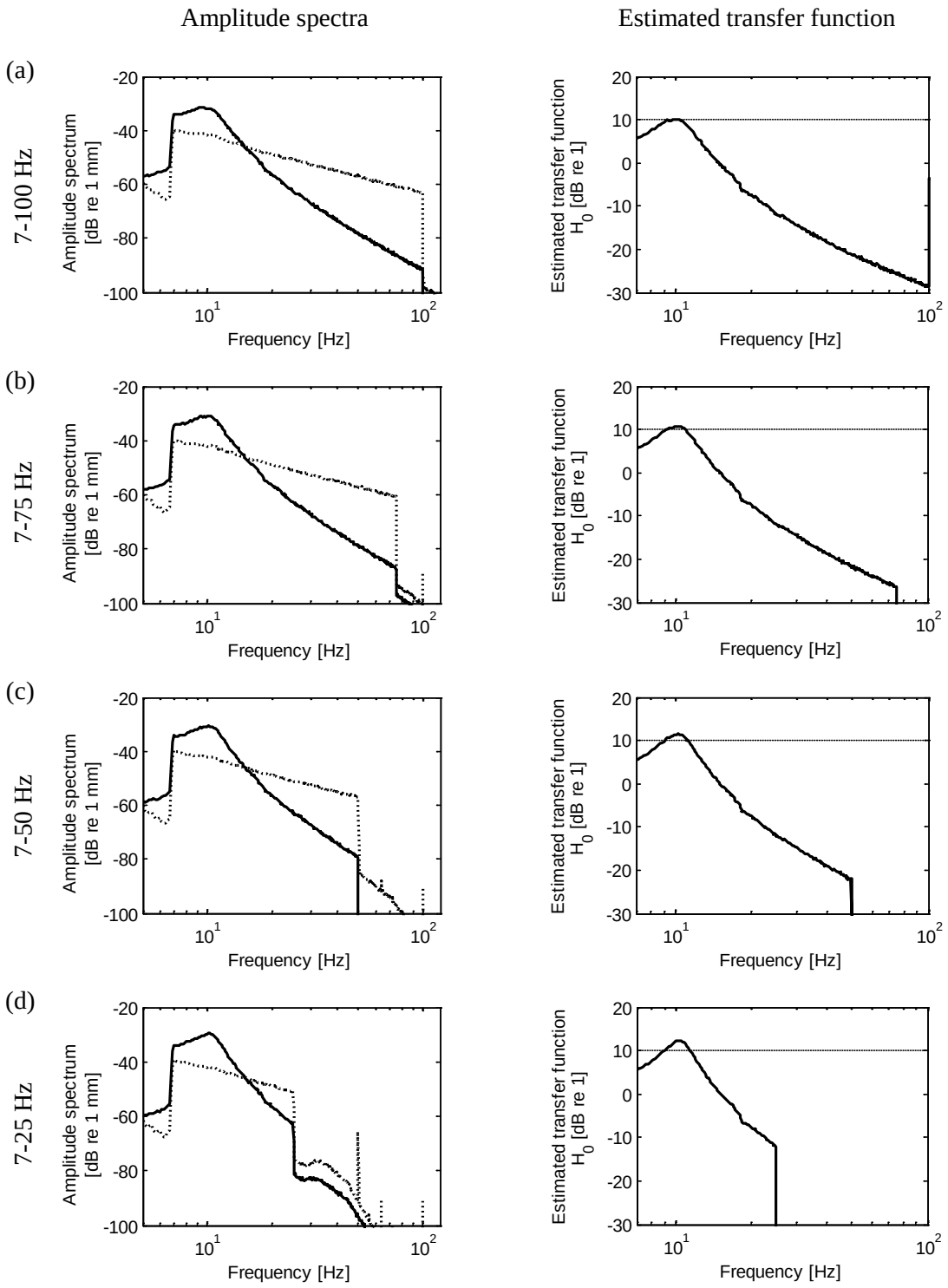

Figure 6.20 Displacement amplitude spectra and estimated transfer function H_0 for the cubically damped responses subject to a constant velocity amplitude random excitation at four different excitation bandwidths and fixed c_3.

——— Cubically damped response
····· Base excitation
····· Peak amplitude ratio for linearly damped system

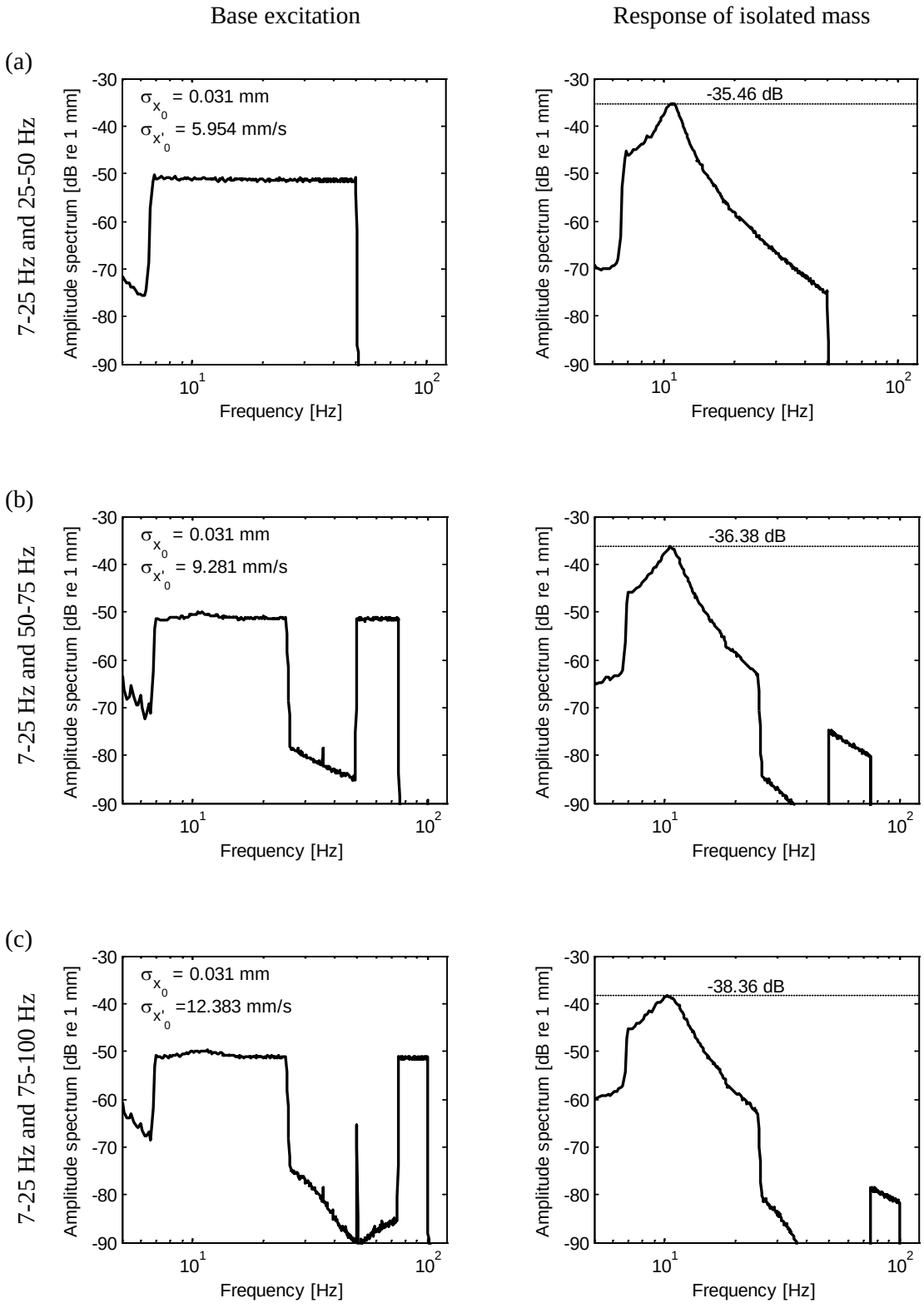

Figure 6.21 Displacement amplitude spectra and estimated transfer function H_0 for the cubically damped responses subject to two pass-band random excitation having a constant <u>displacement</u> amplitude with fixed c_3.

—— Cubically damped response

····· Peak amplitude ratio for linearly damped system

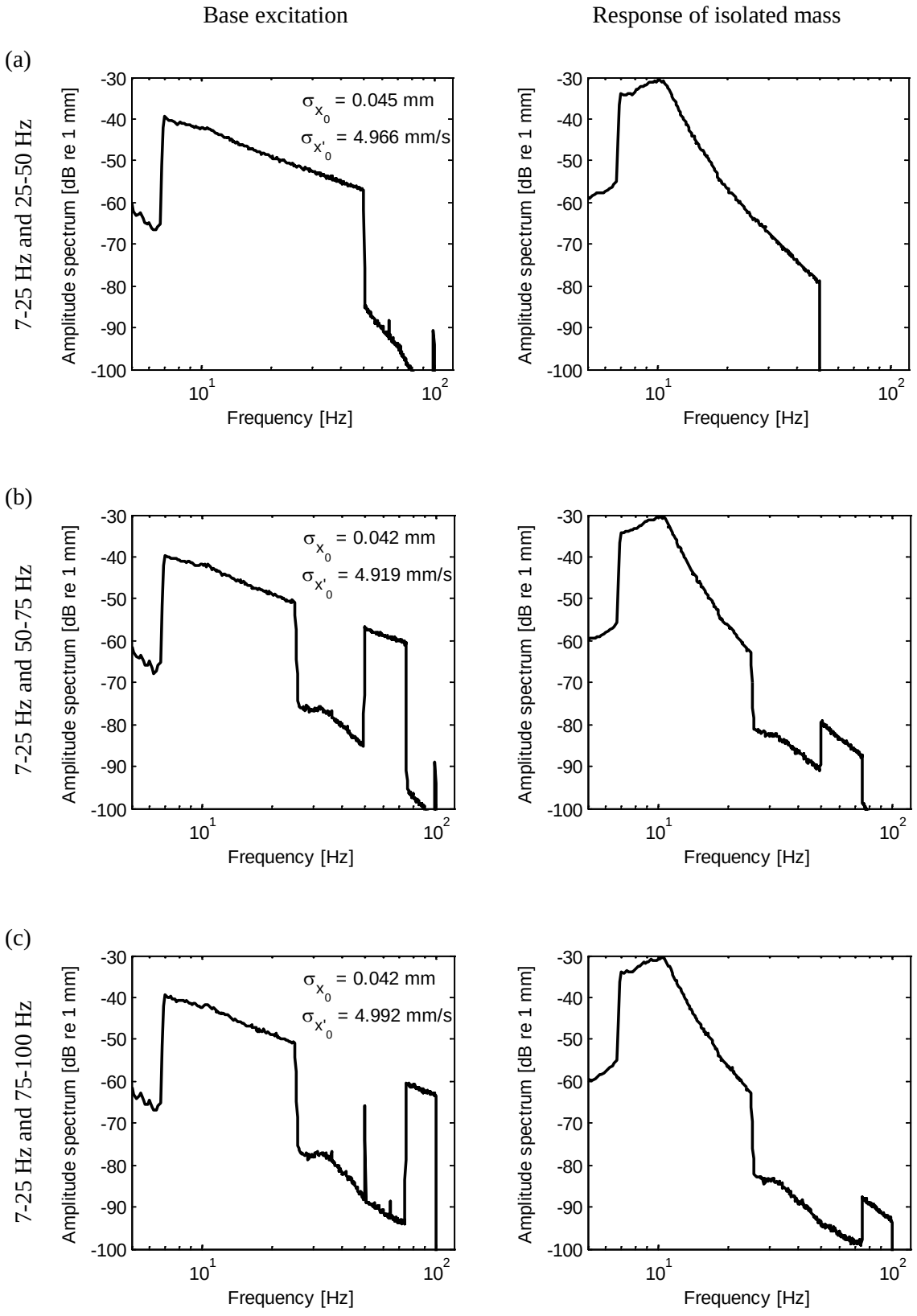

Figure 6.22 Displacement amplitude spectra and estimated transfer function H_0 for the cubically damped responses subject to two pass-band random excitation having a constant <u>velocity</u> amplitude with fixed c_3.

Chapter 7 Conclusions and future work

7.1 General conclusions

The aim of this study was to investigate the effects of power law damping on vibration isolation. The effects of such nonlinear damping were examined here in comparison to that for the linear isolation system. For the latter the force and motion transmissibility are identical. This is not the case for nonlinear systems.

In the literature, the advantages and disadvantages for the application of power law damping on the isolation system were reported. The presence of power law damping is beneficial for the case of force excitation whereas it is detrimental for the case of base excitation. A particular case was investigated in this study, where cubic damping was chosen as an example to replace the linear viscous damping. The focus of the examination was on the base isolation possessing cubic damping for different excitation, namely harmonic and broadband.

For the case of harmonic excitation, the cubically damped responses due to force excitation were carried out for comparison with the case of base excitation. Consideration focused on the responses at the excitation frequencies well above resonance frequency where cubic damping exhibited different effects. On one hand for force excitation, the presence of cubic damping produced a transmitted force which follows the mass line of the undamped linear system. On the other hand for base excitation, it caused a higher transmitted motion for a constant displacement amplitude base excitation. At frequencies well above the resonance frequency, the isolated mass is moving almost in-phase with the base and at a similar amplitude.

The study reveals that the damping force is a key factor for this phenomenon. For the case of force excitation, the cubic damping force in the high frequency region was found to decrease at a rate approximately proportional to the excitation frequency cubed. In contrast, the damping force was found to increase at a rate proportional to the excitation frequency squared for base excitation and this was validated experimentally. The experimental damping implementation was achieved using a simple velocity feedback and electrodynamic shaker (active damping). The acquired cubic damping

force was found to be in agreement with the theoretical conclusions that the level of the cubic damping force at excitation frequencies well above the resonance frequency is much higher than that for linear viscous damping.

This disadvantage of cubic damping for base isolation was overcome using higher order isolation models namely the Zener and two-stage isolation systems. The application of Zener base isolation, for which a relaxation spring was inserted, proved to reduce the absolute displacement of the isolated mass compared to that for the cubically damped SDOF system. The high level of cubic damping force produced an absolute displacement amplitude ratio which followed the mass line of the undamped system. Thus one might consider supporting the cubic damping element elastically to reduce the disadvantageous effects that occur at high frequencies.

The application of the two-stage isolation possessing cubic damping produces an even better response compared to that with the same two-stage model possessing linear damping. The response for the system with cubic damping at high excitation frequencies decreased at 80 dB per decade whereas that with linear damping produces a roll off rate at 60 dB per decade. It is also much better compared to that for the SDOF cubic damping. Note that, this beneficial effect of cubic damping shown in this study is valid when the optimum value of stiffness ratio is considered.

For broadband excitation, the effect of cubic damping under base excitation was investigated using numerical and experimental results. The response due to a constant displacement PSD showed that the level of effective damping is dependent upon the excitation amplitude and bandwidth. Higher damping is produced for larger excitation amplitude or broader excitation bandwidth. The investigation revealed that the main contribution to the level of damping is due to the presence or absence of the excitation content at high frequencies. The excitation at high frequencies also results in a high response level at low frequencies outside the excitation bandwidth. This was identifiable as a result of the power law, i.e. relative velocity cubed, which yields a cubic damping force. It was found that taking the relative velocity cubed produces responses at other than the pre-defined frequencies, both inside and outside the excitation bandwidth, which also contribute to the damping force.

Overall, it is concluded that the introduction of cubic damping into SDOF isolation for harmonic base excitation produces a detrimental high level damping force

at high excitation frequencies well above the resonance frequency. This negative effect can be eliminated by the application of the Zener model where the damping component is elastically supported. Cubic damping turns out to be more beneficial when a two-stage isolation configuration is chosen. The detrimental effect is also revealed for a constant displacement PSD broadband excitation but at low frequencies.

The given information shows that the presence of cubic damping is problematic for the base excited isolation system. The response for the base isolation system with cubic damping is sensitive to the excitation amplitude. One should be reminded that only known excitation amplitudes were applied. For practical situations, it might not be convenient to identify the excitation amplitude and specification. One should also consider that knowing the value or the characteristic of damping might not be practical. The response may vary depending on the excitation amplitude. The application of cubic damping might not be always applicable for some cases. This study provides information for the resulting effects of cubic damping. Therefore, one needs to be selective when dealing with base excited isolation possessing cubic damping.

7.2 Future work

The inclusion of nonlinear damping in an isolation system results in force and absolute displacement amplitude ratios in the isolation region that are not only quantitatively but sometimes qualitatively very different. Also, the absolute displacement amplitude ratios for harmonic and broadband base excitation are not comparable unlike the case of linear viscous damping. Moreover, the theoretical assumption made here is that the isolated mass and the base are rigid. Therefore, there are interesting points for future work contributed from this study which can be listed as follows.

- The application of the Zener and two-stage isolation showed theoretically the possibility of reducing the detrimental effect of cubic damping for harmonic excited base isolation. It might be very useful to explore such behaviour experimentally and validate these findings. It would also be very interesting to extend the study of such the models for broadband random base excitation.

- The case of broadband force excited vibration isolation possessing cubic damping is also interesting to be examined. High vibration amplitude at low frequencies

outside the excitation bandwidth similar to the case of base excitation can be expected in the response. This can be a result of the spike of the very high damping forces resulting from taking relative velocity cubed. Thus higher transmitted forces at frequencies below the resonance frequency are anticipated.

- The simplified SDOF rigid body might not be valid to represent the effects of cubic damping on a highly flexible isolated mass or base excitation system, for which multi-resonance frequencies occur [79][80]. This is because the detrimental effects of cubic damping on a SDOF base excitation are apparent at frequencies well above the fundamental resonance frequency. The system which exhibits multi-resonance frequencies can be undergoing such detrimental effects. This would result in higher response amplitude at higher frequencies where multi-resonance frequencies occur.

Appendices

Appendix A Example of MATLAB routine to solve an ODE problem

The first step for solving ODE problem is to create an ODE function in script or m file.

```
function yp = isolatorb(tspan,y,t,Y0,V0,damp)
% A function for linear base excited isolator
% tspan is a time step used by thee ODE solver.
% y is time dependent being solved.
% t is a desired time step for interpolation.
% Y0 is displacement excitation as a function of tspan.
% V0 is corresponding velocity excitation as a function of tspan.

yp = zeros(2,1);

y0 = interp1(t,Y0,tspan);
% y0 is displacement excitation interpolated to the step of tspan.

v0 = interp1(t,V0,tspan);
% v0 is velocity excitation interpolated to the step of tspan.

yp(1) = y(2);
yp(2) = -(2*damp*(y(2)-v0)+(y(1)-y0));

yp = yp(:);
% To assure that the answer is in the form of column vector.
```

Then call the ODE solver, for example here is ODE45. The command is for solving the ODE function created previously.

```
[~,ytmp] = ode45(@(tm,x) isolatorb(tspan,y,t,Y0,V0,damp),t,[0 0]);
% where [0 0] at the end are the initial conditions.
x = ytmp(:,1); % Vector of resulting displacement at desired time
step, t.
v = ytmp(:,2); % Vector of resulting velocity at desired time step, t.
```

Appendix B Nature of roots for cubic polynomial

The general form of cubic polynomial is given by

$$a_3x^3 + a_2x^2 + a_1x + a_0 = f(x) \tag{B.1}$$

where a_3, a_2, a_1 and a_0 are the real coefficients with $a_3 \neq 0$. For $f(x) = 0$, the roots of equation (B.1) can be determined. There are definitely three roots for as for the cubic polynomial. The possible roots can be considered either; three distinct real roots, real multiple roots or a real and two complex conjugate roots. The way of checking whether the roots are real or complex, the so-called discriminant of the polynomial is applied. The discriminant of the polynomial is a function of the coefficients. The nature of the roots of the polynomials is revealed by this function. The discriminant of the polynomial is given by

$$\Delta = \prod_{i<j}^{n} (r_i - r_j)^2 \tag{B.2}$$

where r_i and r_j are known roots of the polynomial. For the cubic polynomial, equation (B.2) can be written as

$$\Delta = (r_1 - r_2)^2 (r_1 - r_3)^2 (r_2 - r_3)^2 \tag{B.3}$$

By having the known roots of the polynomial, the discriminant can be identified. One can summarise the nature of the roots as follows [81],

$\Delta > 0$: All roots are real and distinct

$\Delta = 0$: All roots are real and at least two roots are equal

$\Delta < 0$: There are one real and two complex conjugate roots

However, without the knowledge of the roots, one can determine the discriminant of the polynomial by using the coefficients of the polynomial. The discriminant of the generic cubic polynomial can be determined alternatively [82] by

$$\Delta = a_2^2a_1^2 - 4a_3a_1^3 - 4a_2^3a_0 - 27a_3^2a_0^2 + 18a_3a_2a_1a_0 \tag{B.4}$$

For the cubic polynomial equation having $a_2 \equiv 0$, equation (B.4) is reduced to

$$\Delta = -\left(4a_3a_1^3 + 27a_3^2a_0^2\right) \tag{B.5}$$

For the assumptions of $a_0 > 0$, $a_1 > 0$ and $a_3 > 0$, one obtains the discriminant which is always less than zero. Thus the solution for equation (B.1) with $a_2 \equiv 0$ consists of one real and two complex conjugates.

Appendix C Simplified expressions for the Harmonic Balance approximations

The simplified expressions reported in this appendix are obtained from the application of the Harmonic Balance approximation. Only the simplified expressions for the case of cubic damping are presented here, i.e. the dependence $B = 0$ is applied for every case. There are four vibration isolation models considered in this appendix, i.e. the SDOF force excited, the SDOF base excited, the Zener base excited and the two-stage base excited vibration isolation. The simplified expressions are presented for four excitation frequency regions. Note that, the frequency regions for the SDOF systems, the Zener model and the two-stage model are slightly different. The dependence A and C for the first three models are given here again by

$$A = 1 - \Omega^2 \text{ and } C = \frac{3}{4}\zeta_3 \Omega^3$$

C.1 The SDOF force excited vibration isolation system

The expansion of the Harmonic Balance approximation for the case of force excitation can be obtained by employing equations (3.25) and (3.31) which are respectively given by

$$C^2U^6 + A^2U^2 = 1 \tag{C.1}$$

$$F_t^2 = C^2U^6 + U^2 \tag{C.2}$$

The simplification of equations (C.1) and (C.2) for the four frequency region are given as follows.

a) For $\Omega \ll 1$ yields $A \approx 1$. Then equations (C.1) and (C.2) are identical. This leads to

$$F_t^2 \approx 1 \tag{C.3}$$

b) For $\Omega \approx 1$, one has $A \approx 0$ and $C \approx \frac{3}{4}\zeta_3$. This leads to equation (C.1) becomes

$$C^2U^6 \approx 1$$

Substitute $U^2 = 1/C^{\frac{2}{3}}$ into equation (C.2), one obtains

$$F_t^2 \approx 1 + \frac{1}{C^{\frac{2}{3}}} \tag{C.4}$$

c) For $\Omega \approx \sqrt{2}$, yields $A \approx -1$. This condition is the same as that for the case of $\Omega \ll 1$. Thus equations (C.1) and (C.2) are equal. That results in

$$F_t^2 \approx 1 \tag{C.5}$$

d) For $\Omega \gg 1$ leads to $A \approx -\Omega^2$ and $C \gg 1$ when $0 \ll \zeta_3 < 1$. These approximations lead to equation (C.1) becomes

$$\tilde{C}^2\Omega^2U^6 + U^2 \approx 0 \tag{C.6}$$

with $\tilde{C} = \frac{3}{4}\tilde{\zeta}_3$. Substituting this into equation (C.2) results in

$$F_t^2 \approx \frac{1}{\Omega^4} \tag{C.7}$$

C.2 The SDOF base excited vibration isolation system

Equations (3.35) and (3.41) are employed here for the Harmonic Balance approximation for the case of base excitation. The equation (3.41) is given by

$$C^2U^6 + A^2U^2 = \Omega^4 \tag{C.8}$$

and equation (3.35) is given by

$$W^2 = U^2 + 2U\cos(\phi_u) + 1 \tag{C.9}$$

The algebraic manipulation yields the simplification of $\cos(\phi_u)$, i.e.

$$\cos(\phi_u) = \frac{A}{\sqrt{C^2U^4 + A^2}} \tag{C.10}$$

The phase lag between the isolated mass and base excitation is given by

$$\phi_w = \tan^{-1}\left(\frac{CU^3}{UA + \sqrt{C^2U^4 + A^2}}\right) \tag{C.11}$$

The simplification expressions for four frequency regions are obtained by the approximation of equations (C.8) to (C.11) which are given as follows.

a) For $\Omega \ll 1$, yields $A \approx 1$ and $C \ll 1$. The resulted approximation of equation (C.8) for this frequency region is obtained by

$$U^2 \approx 0 \tag{C.12}$$

which yields equation (C.9) becomes

$$W^2 \approx 1 \tag{C.13}$$

b) For $\Omega \approx 1$ leads to $A \approx 0$ and $C \approx \frac{3}{4}\zeta_3$. Then equation (C.8) becomes

$$\left(\frac{3}{4}\zeta_3\right)^2 U^6 \approx 1 \tag{C.14}$$

Substituting equation (C.14) into equation (C.9), one obtains

$$W^2 \approx 1 + \left(\frac{4}{3\zeta_3}\right)^{\frac{2}{3}} \tag{C.15}$$

c) For $\Omega \approx \sqrt{2}$, A and C can be approximated as $A \approx -1$ and $C \approx \frac{3}{2}\sqrt{2}\zeta_3$.

Thus equation (C.8) becomes

$$C^2U^6 + U^2 = 4 \tag{C.16}$$

To simplify equation (C.16), the value of cubic damping is assumed to be $\zeta_3 \ll 1$. The assumption yields the equation (C.16) can be simplified as

$$U^2 \approx 0 \tag{C.17}$$

which yields the amplitude of the isolated mass in equation (C.9) becomes

$$W^2 \approx 1 \tag{C.18}$$

d) For $\Omega \gg 1$, the further assumptions made are $A \approx -\Omega^2$. Equation (C.8) becomes

$$\tilde{C}^2 \Omega^2 U^6 + U^2 = 1 \tag{C.19}$$

with $\tilde{C} = \frac{3}{4}\zeta_3$. The further simplification of equation (C.19) yields

$$U^2 \approx \frac{1}{\left(\Omega \tilde{C}\right)^{\frac{2}{3}}} \tag{C.20}$$

Substituting equation (C.20) into equation (C.9) yields

$$W^2 \approx 1 - \frac{1}{\left(\Omega \tilde{C}\right)^{\frac{2}{3}}} \tag{C.21}$$

The simplification of the phase angle is given by

$$\phi_w \approx -\tan^{-1}\left(\frac{1}{\Omega \tilde{C}}\right)^{\frac{1}{3}} \tag{C.22}$$

For the case that amplitude of displacement excitation drops as the excitation frequency increases or the constant velocity amplitude harmonic excitation, the displacement amplitude of the isolated mass is different from that given in equation (C.21). The cubic damping given in equation (3.54) is inversely proportional to the excitation frequency squared. This can be alternatively written as

$$\zeta_3(\Omega) = \frac{\tilde{\zeta}_3}{\Omega^2} \tag{C.23}$$

where $\tilde{\zeta}_3 = \frac{c_3}{\sqrt{km}}\left|\dot{x}_0\right|^2$. Replacing equation (C.23) into the variable C, one can have $C = \frac{3}{4}\tilde{\zeta}_3\Omega$ or $C = \tilde{C}\Omega$. Thus equation (C.8) becomes

$$\tilde{C}^2U^6 + \Omega^2U^2 = \Omega^2 \tag{C.24}$$

As the excitation frequency tends to infinity and $\tilde{C} < 1$, the approximated relative displacement is given by

$$U^2 \approx 1 \tag{C.25}$$

Thus the displacement of the isolated mass can be obtained from the Taylor's series of the resulted expression of equation (C.9) which yields approximation as

$$W \approx \frac{3}{4}\frac{\tilde{\zeta}_3}{\Omega} \tag{C.26}$$

C.3 The Zener base excited vibration isolation system

The expansion of Harmonic Balance approximation for the Zener base excited vibration isolation model can be obtained by using the equations (4.23) and (4.25). These are respectively given here again by

$$\left(\kappa_z + A\right)^2 C^2\tilde{U}^6 + \left(\kappa_z A\right)^2 \tilde{U}^2 = \kappa_z^2\Omega^4 \tag{C.27}$$

and

$$W^2 = \frac{\kappa_z^2 + \left(\kappa_z + 1\right)^2 C^2\tilde{U}^4}{\kappa_z^2A^2 + \left(A + \kappa_z\right)^2 C^2\tilde{U}^4} \tag{C.28}$$

The four excitation frequency regions for the Zener model are $\Omega \ll 1$, $\Omega \approx \sqrt{\kappa + 1}$ and $\Omega \gg 1$ where κ_z is the stiffness ratio between the primary stiffness and the relaxation spring.

a) For $\Omega \ll 1$, the dependences A and C become $A \approx 1$ and $C \approx 0$. The simplified relative displacement and the absolute displacement can be obtained by

$$\tilde{U}^2 \approx \Omega^2 \tag{C.29}$$

and $$W^2 \approx 1 \tag{C.30}$$

b) For $\Omega \approx \sqrt{\kappa_z + 1}$, the dependences A and C become $A \approx -\kappa_z$ and $C = \frac{3}{4}\zeta_3 \left(\kappa_z + 1\right)^{\frac{3}{2}}$. The simplified relative displacement and the absolute displacement can be obtained by

$$\tilde{U}^2 \approx \frac{\left(\kappa_z + 1\right)^2}{\kappa_z^2} \tag{C.31}$$

and $$W^2 \approx \tilde{C}^2 \frac{\left(\kappa_z + 1\right)^9}{\kappa_z^8} \tag{C.32}$$

where $\tilde{C} = \frac{3}{4}\zeta_3$.

c) For $\Omega \gg 1$, the dependences A and C become $A \approx -\Omega^2$ and $C \approx \tilde{C}\Omega^3$. By assuming additionally that $\Omega \gg \kappa_z$, the simplified relative displacement and the absolute displacement can be obtained by

$$\tilde{U}^2 \approx \left(\frac{\kappa_z}{\tilde{C}}\right)^{\frac{2}{3}} \frac{1}{\Omega^2} \tag{C.33}$$

and

$$W^2 \approx \frac{\left(\kappa_z + 1\right)^2}{\Omega^4} \tag{C.34}$$

C.4 The two-stage base excited vibration isolation system

The simplified expressions for the two-stage base excited vibration isolation system obtained from the approximate closed form solution using Harmonic Balance are achieved by employing equations (4.49) and (4.50) which are given by

$$C^2\tilde{U}^6 + \tilde{U}^2 = \Omega^4 W^2 \tag{C.35}$$

$$\left(A - \Omega^2\right)^2 C^2\tilde{U}^6 + \left(A - \Omega^2 D\right)^2 \tilde{U}^2 = \kappa_t^2\Omega^4 \tag{C.36}$$

The four excitation frequency regions for the two-stage vibration isolation are $\Omega \ll 1$ and $\Omega \gg 1$. The equations (C.35) and (C.36) can be simplified for these frequency regions regarding the assumptions of ζ_3 and μ_t, i.e. $0 < \zeta_3 < 1$ and $0 < \mu_t$. The dependences A, C and D are given here again, i.e. $A = \left(1-\Omega^2\right)\mu_t + 1$, $C = \frac{3}{4}\zeta_3\Omega^3$ and $D = \left(1-\Omega^2\right)\mu_t + 2$.

a) For $\Omega \ll 1$, the dependences A, C and D become $A \approx \mu_t + 1 \approx \kappa_t$, $C \approx 0$ and $D \approx \mu_t + 2$. The simplified relative displacement can be obtained from equation (C.36) , i.e.

$$\tilde{U}^2 \approx \Omega^4 \tag{C.37}$$

Then one obtains the simplified absolute displacement W, i.e.

$$W^2 \approx 1 \tag{C.38}$$

b) For $\Omega \gg 1$, the dependence A, C and D become $A \approx -\Omega^2\mu_t$, $C \gg 1$ and $D \approx -\Omega^2\mu_t \approx A$. Equation (C.36) can be reduced to

$$\tilde{U}^2 \approx \frac{\kappa_t^2}{\mu_t^2\Omega^4} \tag{C.39}$$

Thus the resulted simplified expression for the absolute displacement can be given by

$$W^2 \approx \frac{\kappa_t^2}{\mu_t^2\Omega^8} \tag{C.40}$$

Appendix D Modal parameters estimation methods

The modal parameters are the parameters which represent the physical characteristic of the system. The modal parameters are usually considered as the natural frequency and damping ratio. These parameters for the experimental data are obtained in two ways, i.e. using a circle fit method and a MatLab function 'invfreqs'.

D.1 Circle fit method

The circle fit method is based on a Nyquist plot of frequency response for a SDOF system. The real and imaginary terms of the responses around resonance frequency are plotted in a complex plane which should be a circle-like. The plot is fitted with the calculated circle which the diameter and location of centre are known. The modal parameters are determined from this circle. The principle of the circle fit method can be found in reference [74], for example. However a brief explanation can be made by considering an equation of motion for a SDOF subject to the force excitation which is given by

$$m\ddot{x} + c\dot{x} + kx = f(t) \tag{D.1}$$

The frequency response function (FRF) for equation (D.1) can be written as

$$H(\omega) = \frac{X(\omega)}{F(\omega)} = \frac{1}{k - m\omega^2 + jc\omega} \tag{D.2}$$

Equation (D.2) forms a receptance of a system when it is clamped to the base. One can produce the Nyquist plot by extracting the real and imaginary of $H(\omega)$. Then estimate a circle plot to fit the data. The natural frequency can be obtained by the intersection of the line from origin as shown in figure D.1. The damping ratio is estimated by

$$\eta = \frac{\omega_a^2 - \omega_b^2}{\omega_r^2} \cdot \frac{1}{\tan\left(\frac{\theta_a}{2}\right) + \tan\left(\frac{\theta_b}{2}\right)} \tag{D.3}$$

where η is the structural damping loss factor and is given by $\eta = 2\zeta$. ω_a and ω_b are the known frequency above and below the resonance respectively. ω_r is the frequency

of resonance. θ_a and θ_b are the corresponding angles of the known frequencies with respect to the frequency of resonance.

D.2 MatLab function 'invfreqs'

The MatLab function 'invfreqs' is an analogue filter which returns the numerator and denominator of the polynomial for the frequency response. The parameters obtained are used in the mathematical model of the frequency response. The example of using this function can be found in references [75] and [76], for example. The simple syntax of the function is

```
[b,a] = invfreqs(H,w,n,m)
```

where b is the vector of numerator, a is the vector of denominator, H is the vector of frequency response from the experimental data, w is the vector of corresponding frequency, n and m are the desired order of numerator and denominator respectively.

After getting the numerator and denominator are obtained, one can construct the transfer function as

$$H(s) = \frac{b_1 s^n + b_2 s^{n-1} + \cdots + b_{n+1}}{a_1 s^m + a_2 s^{m-1} + \cdots + a_{m+1}} \tag{D.4}$$

To determine the modal parameters using ''invfreqs', the value of numerator, n, and denominator, m, need to be 0 and 2 respectively. Equation (D.4) becomes

$$H(s) = \frac{b_1}{a_1 s^2 + a_2 s + a_3} \tag{D.5}$$

By doing this, the modal parameters can be determined from coefficients a_1, a_2 and a_3.

D.3 Transfer function for the base excited isolation

Thus, to determine the modal parameters for the case of base exited isolation using both methods mentioned, the FRF is needed to be rearranged. The relative response between the base excitation and the isolated mass is considered. The equation of motion for the relative motion is given by

$$m\ddot{z} + c\dot{z} + kz = -m\ddot{x}_0 \tag{D.6}$$

where z is the relative motion and is given by $z = x - x_0$, x and x_0 are the displacement of the isolated mass and base excitation

The frequency response frunction for equation (D.6) can be written as

$$\frac{Z(\omega)}{X_0(\omega)} = \frac{m\omega^2}{\left(k - m\omega^2\right) + jc\omega} \tag{D.7}$$

One can consider equation (D.7) as

$$\frac{X(\omega) - X_0(\omega)}{\omega^2 X_0(\omega)} = \frac{m}{\left(k - m\omega^2\right) + jc\omega} \tag{D.8}$$

Equation (D.8) can be written alternatively as

$$\frac{1}{\omega^2}\left[\frac{X(\omega)}{X_0(\omega)} - 1\right] = \frac{m}{\left(k - m\omega^2\right) + jc\omega} \tag{D.9}$$

Equation (D.9) can be inferred as a scaled receptance of a system which is clamped to the base. Then, the frequency response function obtained from the experimental data which is suitable for both method should be in the form as

$$H(\omega) = \frac{1}{\omega^2}\left[\frac{X(\omega)}{X_0(\omega)} - 1\right] \tag{D.10}$$

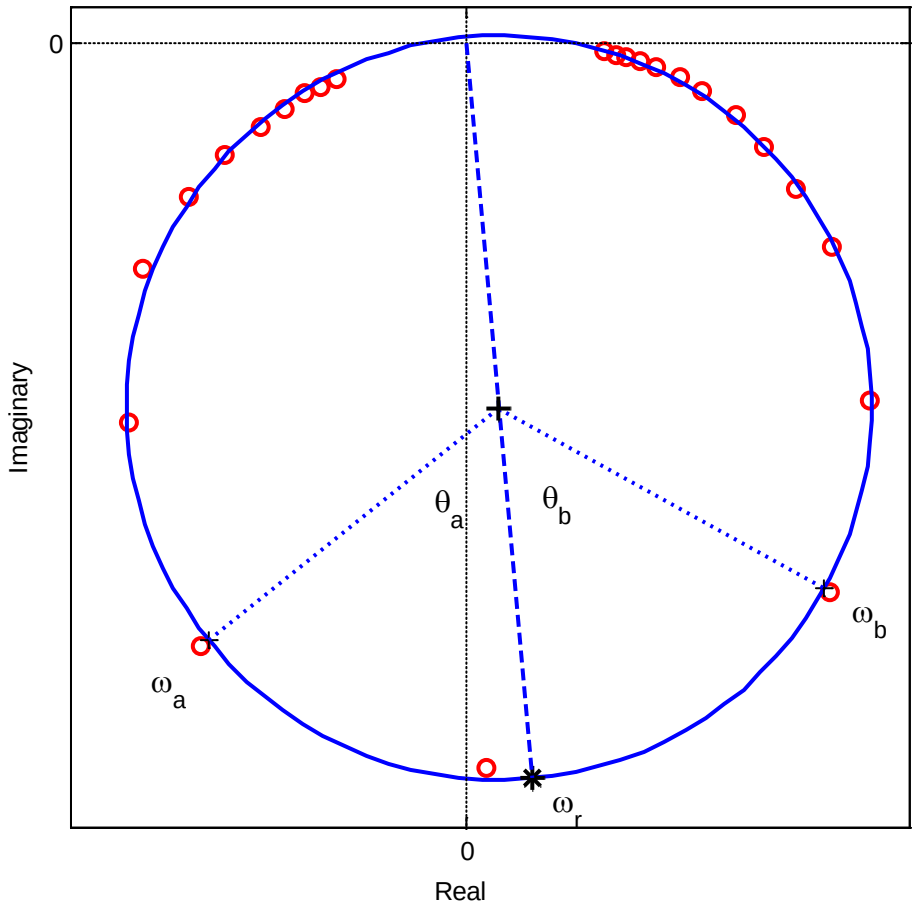

Figure D.1 The Circle fit illustration obtained from the Nyquist plot of the experimental data with lines and marks represent

- Experimental data
- Estimated circle to fit the experimental data
- Diameter drawn from the origin
- Angles of ω_a and ω_b with respect to ω_r
- \+ Centre of the circle
- * Location of resonance frequency

List of references

[1] Dixon, J. C., and Society of Automotive Engineers., 1999, *The shock absorber handbook*, Society of Automotive Engineers, Warrendale, Pa.

[2] Bruns, J. U., Lindner, M., and Popp, K., 2003, Identification of the nonlinear restoring force characteristic of a rubber mounting, *Proceeding in Applied Mathematics and Mechanics*, **2**(1), pp. 270-271.

[3] Brennan, M. J., Kovacic, I., Carrella, A., and Waters, T. P., 2008, On the jump-up and jump-down frequencies of the Duffing oscillator, *Journal of Sound and Vibration*, **318**(4–5), pp. 1250-1261.

[4] Malatkar, P., and Nayfeh, A. H., 2002, Calculation of the jump frequencies in the response of s.d.o.f non-linear systems, *Journal of Sound and Vibration*, **254**(5), pp. 1005-1011.

[5] Nayfeh, A. H., and Mook, D. T., 1979, *Nonlinear oscillations*, Wiley, New York.

[6] Meirovitch, L., 2001, *Fundamentals of vibrations*, International Edition 2001 Edition, McGraw-Hill Book Co, Singapore.

[7] Rao, S. S., 2004, *Mechanical vibrations*, 4th Edition, Pearson Prentice Hall, Upper Saddle River, N.J.

[8] Worden, K., 1996, Letter to the editor: On jump frequencies in the response of the Duffing oscillator, *Journal of Sound and Vibration*, **198**(4), pp. 522-525.

[9] Friswell, M. I., and Penny, J. E. T., 1994, The Accuracy of Jump Frequencies in Series Solutions of the Response of a Duffing Oscillator, *Journal of Sound and Vibration*, **169**(2), pp. 261-269.

[10] Peng, Z. K., Lang, Z. Q., Billings, S. A., and Tomlinson, G. R., 2008, Comparisons between harmonic balance and nonlinear output frequency response function in nonlinear system analysis, *Journal of Sound and Vibration*, **311**(1-2), pp. 56-73.

[11] Carrella, A., Brennan, M. J., and Waters, T. P., Force transmissibility of a nonlinear vibration isolator with high-static-low-dynamic stiffness, *In Proceedings of the Euromech Conference on Nonlinear Vibration (ENOC)*, St. Petersburg, Russia, pp. 242-247.

[12] Verros, G., and Natsiavas, S., 2002, Ride Dynamics of Nonlinear Vehicle Models Using Component Mode Synthesis, *Journal of Vibration and Acoustics*, **124**(3), pp. 427-434.

[13] Litak, G., and Borowiec, M., 2008, Nonlinear vibration of a quarter-car model excited by the road surface profile, *Proceeding in Applied Mathematics and Mechanics*, **8**(1), pp. 10893-10894.

[14] Klein, G. H., 1964, Random Excitation of a Nonlinear System with Tangent Elasticity Characteristics, *Journal of the Acoustical Society of America*, **36**(11), pp. 2095 - 2105.

[15] Kirk, C. L., 1988, Non-linear random vibration isolators, *Journal of Sound and Vibration*, **124**(1), pp. 157-182.

[16] Milliken, W. F., and Milliken, D. L., 1995, *Race car vehicle dynamics*, SAE International, Warrendale, PA, U.S.A.

[17] Wallaschek, J., 1990, Dynamics of non-linear automobile shock-absorbers, *International Journal of Non-Linear Mechanics*, **25**(2-3), pp. 299-308.

[18] Surace, C., Worden, K., and Tomlinson, G. R., 1992, On the non-linear characteristics of automotive shock absorbers, *ARCHIVE: Proceedings of the Institution of Mechanical Engineers, Part D: Journal of Automobile Engineering 1989-1996 (vols 203-210)*, **206**(14), pp. 3-16.

[19] Rajalingham, C., and Rakheja, S., 2003, Influence of suspension damper asymmetry on vehicle vibration response to ground excitation, *Journal of Sound and Vibration*, **266**(5), pp. 1117-1129.

[20] Natsiavas, S., and Verros, G., 1999, Dynamics of Oscillators with Strongly Nonlinear Asymmetric Damping, *Nonlinear Dynamics*, **20**(3), pp. 221-246.

[21] Levitan, E. S., 1960, Forced Oscillation of a Spring-Mass System having Combined Coulomb and Viscous Damping, *The Journal of the Acoustical Society of America*, **32**(10), pp. 1265-1269.

[22] Schlesinger, A., 1979, Vibration Isolation in the Presence of Coulomb Friction, *Journal of Sound and Vibration*, **63**(2), pp. 213-224.

[23] Crede, C. E., and Ruzicka, J. E., 2002, Theory of vibration isolation, Chapter 30 in *Harris' Shock and Vibration Handbook*, eds. C. M. Harris, and A. G. Piersol, McGraw-Hill, New York, USA.

[24] Ravindra, B., and Mallik, A. K., 1994, Performance of Non-linear Vibration Isolators Under Harmonic Excitation, *Journal of Sound and Vibration*, **170**(3), pp. 325-337.

[25] Ho, C., Zi-qiang, L., and Billings, S. A., The benefits of nonlinear cubic viscous damping on the force transmissibility of a Duffing-type vibration isolator, *In Proceedings of the Control (CONTROL), 2012 UKACC International Conference on*, pp. 479-484.

[26] Jing, X., and Lang, Z., 2009, Frequency domain analysis of a dimensionless cubic nonlinear damping system subject to harmonic input, *Nonlinear Dynamics*, **58**(3), pp. 469-485.

[27] Peng, Z. K., Lang, Z. Q., Jing, X. J., Billings, S. A., Tomlinson, G. R., and Guo, L. Z., 2010, The transmissibility of vibration isolators with a nonlinear antisymmetric damping characteristic, *Journal of Vibration and Acoustics*, **132**(1), pp. 1-7.

[28] Laalej, H., Lang, Z. Q., Daley, S., Zazas, I., Billings, S. A., and Tomlinson, G. R., 2012, Application of non-linear damping to vibration isolation: an experimental study, *Nonlinear Dynamics*, **69**(1-2), pp. 409-421.

[29] Hanieh, A. A., 2003, *Active isolation and damping of vibrations via Stewart platform*, Ph.D. Thesis, Mechanical Engineering and Robotics, Université Libre de Bruxelles, Brussels, Belgium.

[30] Laalej, H., Lang, Z. Q., Sapinski, B., and Martynowicz, P., 2012, MR damper based implementation of nonlinear damping for a pitch plane suspension system, *Smart Materials and Structures*, **21**(4), pp. 045006 : 1 - 14.

[31] Guo, P. F., Lang, Z. Q., and Peng, Z. K., 2012, Analysis and design of the force and displacement transmissibility of nonlinear viscous damper based vibration isolation systems, *Nonlinear Dynamics*, **67**(4), pp. 2671-2687.

[32] Shekhar, C. N., Hatwal, H., and Mallik, A. K., 1999, Performance of non-linear isolators and absorbers to shock excitations, *Journal of Sound and Vibration*, **227**(2), pp. 293-307.

[33] Kovačić, I., Milovanović, Z., and Brennan, M. J., 2008, On the relative and absolute transmissibility of a vibration isolation system subjected to base exctation, *FACTA UNIVERSITATIS Series: Working and Living Environmental Protection*, **5**(1), pp. 39 - 48.

[34] Milovanović, Z., Kovačić, I., and Brennan, M. J., 2009, On the displacement transmissibility of a base excited viscously damped nonlinear vibration isolator, *Journal of Vibration and Acoustics*, **131**, pp. 1-7.

[35] Peng, Z. K., Meng, G., Lang, Z. Q., Zhang, W. M., and Chu, F. L., 2012, Study of the effects of cubic nonlinear damping on vibration isolations using Harmonic Balance Method, *International Journal of Non-Linear Mechanics*, **47**(10), pp. 1073-1080.

[36] Balachandran, B., and Magrab, E. B., 2009, *Vibrations*, Second Edition, Cengage Learning, Toronto, Canada.

[37] Ruzicka, J. E., 1957, *Forced vibration in systems with elastically supported dampers*, M.S. Thesis, Mechanical Engineering, Massachusetts Institute of Technology, USA.

[38] Tse, F. S., Morse, I. E., and Hinkle, R. T., 1963, *Mechanical Vibrations*, Prentice-Hall International, London, UK.

[39] Snowdon, J. C., 1963, Steady-state and transient behavior of two- and three-element isolation mountings, *The Journal of the Acoustical Society of America*, **35**(3), pp. 397-403.

[40] Snowdon, J. C., 1979, Vibration isolation - Use and Characterization, *Journal of the Acoustical Society of America*, **66**(5), pp. 1245-1274.

[41] Derby, T. F., and Calcaterra, P. C., 1970, Response and optimization of an isolation system with relaxation type damping, National Aeronautics and Space Administration.

[42] Ledezma-Ramirez, D. F., Ferguson, N. S., and Brennan, M. J., 2005, An overview of the single degree of freedom system and Zener model for passive shock isolation, *ISVR Technical Memorandum No.947*, ISVR, University of Southampton, Southampton.

[43] Brennan, M. J., Carrella, A., Waters, T. P., and Lopes Jr, V., 2008, On the dynamic behaviour of a mass supported by a parallel combination of a spring and an elastically connected damper, *Journal of Sound and Vibration*, **309**(3–5), pp. 823-837.

[44] Brennan, M. J., and Ferguson, N. S., 2004, Vibration control, Chapter 12 in *Advanced Applications in Acoustics, Noise and Vibration*, eds. F. J. Fahy, and J. G. Walker, Spon Press, London, UK.

[45] Fu, W., Qian, Z. C., Huang, X. H., and Tan, F., 2009, Analysis of Two-stage Passive Vibration Isolation System for Crystal Oscillator at High-frequency Vibration*2009 Joint Meeting of the European Frequency and Time Forum and the IEEE International Frequency Control Symposium, Vols 1 and 2*, IEEE, New York, pp. 501-504.

[46] Tang, B., and Brennan, M. J., 2012, A comparison of the effects of nonlinear damping on the free vibration of a single-degree-of-freedom system, *Journal of Vibration and Acoustics*, **134**(2), pp. 1-5.

[47] Tang, B., and Brennan, M. J., 2013, A comparison of two nonlinear damping mechanisms in a vibration isolator, *Journal of Sound and Vibration*, **332**(3), pp. 510-520.

[48] Sun, J., Huang, X., Liu, X., Xiao, F., and Hua, H., 2013, Study on the force transmissibility of vibration isolators with geometric nonlinear damping, *Nonlinear Dynamics*, **74**(4), pp. 1103-1112.

[49] Xiao, Z., Jing, X., and Cheng, L., 2013, The transmissibility of vibration isolators with cubic nonlinear damping under both force and base excitations, *Journal of Sound and Vibration*, **332**(5), pp. 1335-1354.

[50] Lu, Z., Brennan, M. J., Yang, T., Li, X., and Liu, Z., 2013, An investigation of a two-stage nonlinear vibration isolation system, *Journal of Sound and Vibration*, **332**(6), pp. 1456-1464.

[51] Yang, P., Yang, J., and Ding, J., 2006, Dynamic Transmissibility of a Complex Nonlinear Coupling Isolator, *Tsinghua Science & Technology*, **11**(5), pp. 538-542.

[52] Yang, P., 2007, Numerical analysis for dynamic transmissibility of a mixed nonlinear shock absorber, *Communications in Numerical Methods in Engineering*, **23**(12), pp. 1121-1130.

[53] Yang, P., 2008, A systematic approach on computational analysis and optimization design: for a nonlinear coupling shock absorber, *Engineering with Computers*, **24**(1), pp. 87-96.

[54] Gerald, C. F., and Wheatley, P. O., 1999, *Applied Numerical Analysis*, 6th Edition, Addison Wesley Longman, Inc.

[55] Yang, W. Y., Cao, W., Chung, T.-S., and Morris, J., 2005, *Applied numerical methods using MATLAB®*, John Wiley & Sons, Inc., New Jersey, USA.

[56] MathWorks, 2012, "How do I use a fixed step size with ODE23 and ODE45 in MATLAB," http://www.mathworks.com/matlabcentral/answers/92961-how-do-i-use-a-fixed-step-size-with-ode23-and-ode45-in-matlab, Date accessed: 27 May 2014.

[57] Espíndola, J. J., and Bavastri, C. A., An efficient definition of transmissibility for a general equipment isolation system, *In Proceedings of the ASME Design Engineering Technical Conferences (DETC'97)*, Sacramento, California, USA.

[58] Blake, R. E., 2002, Basic vibration theory, Chapter 2 in *Shock and Vibration Handbook*, eds. C. M. Harris, and A. G. Piersol, 5th Edition, McGraw-Hill, U.S.A.

[59] Shin, K., and Hammond, J. K., 2008, *Fundamentals of signal processing for sound and vibration engineers*, John Wiley & Sons Ltd., England.

[60] Cerdeira, A., Alemán, M. A., Estrada, M., and Flandre, D., 2004, Integral function method for determination of nonlinear harmonic distortion, *Solid-State Electronics*, **48**(12), pp. 2225-2234.

[61] Kovačić, I., Brennan, M. J., and Lineton, B., 2009, Effect of a static force on the dynamic behaviour of a harmonically excited quasi-zero stiffness system, *Journal of Sound and Vibration*, **325**(4–5), pp. 870-883.

[62] Lang, Z. Q., Billings, S. A., Tomlinson, G. R., and Yue, R., 2006, Analytical description of the effects of system nonlinearities on output frequency responses: A case study, *Journal of Sound and Vibration*, **295**(3–5), pp. 584-601.

[63] Lang, Z. Q., Jing, X. J., Billings, S. A., Tomlinson, G. R., and Peng, Z. K., 2009, Theoretical study of the effects of nonlinear viscous damping on vibration isolation of sdof systems, *Journal of Sound and Vibration*, **323**(1–2), pp. 352-365.

[64] Worden, K., and Tomlinson, G. R., 2001, *Nonlinearity in structural dynamics : detection, indentification, and modelling*, Institute of Physics, London, UK.

[65] Mickens, R. E., 1984, Comments on the method of harmonic balance, *Journal of Sound and Vibration*, **94**(3), pp. 456 - 460.

[66] Hanselman, D., and Littlefield, B., 1995, *The student edition of MATLAB : version 4*, Prentice-Hall, Inc., New Jersey, U.S.A.

[67] Wei, F., Zhichao, Q., Xianhe, H., and Feng, T., Analysis of two-stage passive vibration isolation system for crystal oscillator at high-frequency vibration, *In Proceedings of the Frequency Control Symposium, Joint with the 22nd European Frequency and Time forum. IEEE International*, pp. 501-504.

[68] Newland, D. E., 1975, *An introduction to random vibrations and spectral analysis*, Longman, London ; New York.

[69] Broch, J. T., 1980, *Mechanical Vibration and Shock Measurements*, Brüel & Kjær Denmark.

[70] Welch, P. D., 1967, The use of fast Fourier transform for the estimation of power spectra: A method based on time averaging over short, modified periodograms, *Audio and Electroacoustics, IEEE Transactions on*, **15**(2), pp. 70-73.

[71] Schiehlen, W., 2006, White noise excitation of road vehicle structures, *Sãdhanã*, **31**, pp. 487-503.

[72] Cuong, H. T., Troesch, A. W., and Birdsall, T. G., 1982, The generation of digital random time histories, *Ocean Engineering*, **9**(6), pp. 581-588.

[73] Mishra, S., and Mishra, S., 2009, Wavelet based identification of dominant scales for self-affine road roughness in context of riding comfort in vehicles, *Geotechnical and Geological Engineering*, **27**(4), pp. 473-484.

[74] Ewins, D. J., 2000, *Modal testing : theory, practice and application*, 2nd Edition, Research studies press Ltd., Hertfordshire, England.

[75] Dinz, P. S. R., Silva, E. A. B. d., and Netto, S. L., 2002, *Digital signal processing : system analysis and design*, Cambridge University Press, Cambridge, UK.

[76] Monje, C. A., Chen, Y., Vinagre, B. M., Xue, D., and Feliu, V., 2010, *Fractional-order Systems and Controls*, Springer-Verlag London Limited London, UK.

[77] Shigley, J., Mischke, C., and Brown, T., 2004, Springs, Chapter 6 in *Standard Handbook of Machine Design*, ed. R. E. Joerres, 3rd Edition, McGraw-Hill, U.S.A.

[78] Yan, B., Brennan, M. J., Elliott, S. J., and Ferguson, N. S., 2009, Characteristics of distributed parameter isolators, *Journal of Sound and Vibration*, **320**(3), pp. 516-526.

[79] Tu, Y. Q., and Zheng, G. T., 2006, On the Vibration Isolation of Flexible Structures, *Journal of Applied Mechanics*, **74**(3), pp. 415-420.

[80] Zheng, G. T., and Tu, Y. Q., 2009, Analytical Study of Vibration Isolation Between a Pair of Flexible Structures, *Journal of Vibration and Acoustics*, **131**(2), pp. 1-11.

[81] Irving, R. S., 2004, *Integers, Polynomials, and Rings : a course in algegra*, Springer-Verlag New-York, Inc., New York.

[82] Vinberg, E. B., 2003, *A course in algebra*, The American Mathematical Society, Rhode Island, USA.